Deciphering the metabolic interactions between mucus associated *Ruminococcus gnavus* and *Limosilactobacillus reuteri* strains

Raven Sinèad Reynolds

A thesis submitted for the degree of Doctor of Philosophy (PhD) To the University of East Anglia

Quadram Institute Bioscience

Food, Microbiome and Health

Norwich Research Park

Norwich

NR4 7UQ

June 2024

Abstract

Cross-feeding between gut microbiota members is crucial for maintaining gut homeostasis. Cobamides, the vitamin B12 family of enzyme cofactors, are synthesised by approximately 25% of gut microbes while 80% rely on cobamides to conduct enzymatic reactions such as methionine (Met) synthesis through cobamide-dependent enzymes. To gain insights into the mechanisms underpinning cobamide cross-feeding in the gut, we focused on two human gut symbionts, *Ruminococcus gnavus* and *Limosilactobacillus reuteri*.

R. gnavus is a prevalent member of the healthy gut microbiota and its disproportionate abundance has been associated with a growing number of diseases. There is therefore great interest in understanding *R. gnavus* adaptation to the gut. *L. reuteri* is a known cobamide producer, with our bioinformatics analyses revealing that 50% of genome-sequenced strains contained a pseudocobalamin (PsCbl) biosynthetic pathway. We demonstrated that *L. reuteri* MM4-1A produces PsCbl extracellularly. In contrast, we showed that *R. gnavus* is auxotrophic for cobamides with 98% of genome-sequenced *R. gnavus* strains encoding cobamide-dependent proteins.

In anaerobic growth assays, *R. gnavus* utilised exogenous cobamides and PsCbl produced by *L. reuteri* MM4-1A. Transcriptomics of *R. gnavus* revealed upregulation of a putative cobamide transporter and cobamide-dependent protein genes in response to cyanopseudocobalamin (CNPsCbl) and PsCbl-producing *L. reuteri*, suggesting cobamide cross-feeding to support cobamide-dependent reactions. This effect was reduced with Met supplementation. Additionally, *R. gnavus* cobamide biosynthetic genes were upregulated upon porphobilinogen (PBG) supplementation in Met-supplemented conditions, suggesting potential PBG salvaging for cobamide production, consistent with the partial cobamide biosynthetic pathway found in 94% of *R. gnavus* strains. In the human gut microbiota, *R. gnavus* exhibited improved fitness with high doses of CNPsCbl and PBG while supplementation had no major impact on the whole microbial community.

This study provides insights into cobamide metabolic interactions occurring between human gut symbionts opening the door for novel strategies to modulate human gut bacteria.

Acknowledgements

This PhD was funded by the BBSRC Norwich Research Park Doctoral Training Programme.

I would like to thank Prof. Arjan Narbad and Dr. Luciana Hannibal for taking their time to read and discuss this PhD thesis.

My sincere thanks go to Prof. Nathalie Juge for her scientific guidance and ongoing support throughout the project and particularly during the writing process.

I would also like to extend my gratitude to all members of my supervisory team, Prof. Martin Warren, Dr. Andrew Bell, Dr. Dimitris Latousakis and Dr. Emmanuelle Crost.

During my time at QIB, I have had the privilege of working closely with several inspiring scientists. I acknowledge the support of all QIB staff and students, past and present, who have assisted me in my work, trained me in various techniques, or shared their expertise. I'd like to give a special thanks to Dr. Sree Gowrinadh Javvadi and Dr. Shikha Saha.

I am particularly grateful for the continued emotional support of Dr Ezgi Özkurt, Manasik Ali, Aryana Zardkoohi-Burgos, Sian Seaman, Jade Davies, Barbora Peck and Aleks Teriosina who have been pivotal to my completion of this PhD journey.

Finally, a special thank you to my close family and friends for their encouragement, counsel and being a source of peace when I needed it most.

Table of Contents

List of Abbreviations

5MB	Cob-cyano-(5-methylbenzimidazolyl)-cobamide
ABC	ATP-binding cassette
AD	Alzheimer's disease
ADHD	Attention-deficit/hyperactivity disorder
AdoCbl	Adenosylcobalamin
AIM	Auto induction media
ANOVA	Analysis of Variance
ASD	Autism spectrum disorder
BHI-YH	Brain Heart Infusion broth with yeast extract and hemin
BLAST	Basic Local Alignment Search Tool
Cbl	Cobalamin
CD	Crohn's disease
CFU	Colony forming unit
CNCbl	Cyanocobalamin
CNPsCbl	Cyanoseudocobalamin
CRC	Colorectal cancer
CRP	C-reactive protein
CSV	Comma-separated files
CVD	Cardiovascular diseases
DMB	Dimethylbenzamidazole
Factor A	Cob-cyano-(2-methyladeninyl)-cobamide
Factor III	Cob-cyano-(5-hydroxybenzimidazolyl)-cobamide
Factor IIIm	Cob-cyano-(5-methoxybenzimidazolyl)-cobamide
FC	Fold change
FNA	Fasta nucleic acid
FPLC	Fast protein liquid chromatography
Gal	Galactose
gDNA	Genomic DNA
GF	Germ-free
GH	Glycoside hydrolase

GI	Gastrointestinal
Glc	Glucose
GlcNAc	N-acetylglucosamine
HMP	Human Microbiome Project
HPLC	High performance liquid chromatography
IBD	Inflammatory bowel disease
IPTG	Isopropyl β- d-1-thiogalactopyranoside
L2FC	Log2 fold change
LAB	Lactic acid bacteria medium
LB	Luria Bertani
LDMII	Lactobacillus defined media type II
LPS	Lipopolysaccharide
MAM	Mucosa-associated microbiota
MAMPs	Microbe-associated molecular patterns
MAPK	Mitogen-activated protein kinase
MCM	MethylmalonylCoA mutase
MeCbl	Methylcobalamin
Met	Methionine
MetaHIT	Metagenomes of the Human Intestinal Tract
MTF	Methyltetrahydrofolate
NCBI	National Center for Biotechnology Information
NLR	NOD-like receptors
OHCbl	Hydroxocobalamin
PBG	Porphobilinogen
PCA	Principle component analysis
PD	Parkinson's disease
PRRs	Pattern recognition receptors
PsCbl	Pseudocobalamin
qPCR	Quantitative polymerase chain reaction
RNASeq	Ribonucleic acid sequencing
RNI	Recommended nutrient intake
rRNA	ribosomal RNA
S. Typhimurium	Salmonella enterica serovar Typhimurium
SAM	S-adenosylmethionine

SCFA	Short chain fatty acids
T2D	Type 2 diabetes
TBLASTN	Protein-nucleotide 6-frame translation
THF	Tetrahydrofolate
TLR	Toll-like receptors
TMA	Trimethylamine
TMAO	Trimethylamine-N-oxide
UC	Ulcerative colitis
UPLC–MS/MS	Ultraperformance liquid chromatography tandem mass spectrometry
UV-DAD	Ultraviolet diode array detector
VitB12	Vitamin B12

List of Figures

List of Tables

List of Appendices

Appendix 1. Supplementary Figures

Appendix 2. Supplementary Tables

Chapter 1

Introduction

1.1 Structure and function of GI tract

1.1.1 Overview of the GI tract

The human gastrointestinal (GI) tract comprises multiple organs and can be divided into upper and lower anatomical regions. The upper GI tract encompasses the mouth, oesophagus, stomach, duodenum, jejunum, and ileum, whilst lower GI tract covers the colon, rectum and anus (Figure 1). The oesophagus functions as a passage of material from the mouth to the stomach, where food bolus mixes with gastric acid and digestive enzymes to form the chyme, a semi-fluid mass of partly digested food. This mass then passes through the pyloric sphincter into the small intestine (duodenum, jejunum, and ileum) where proteins, fats, and carbohydrates are further digested, and nutrients absorbed. The luminal contents then reach the large intestine where they are prepared for excretion via the rectum and anal canal.

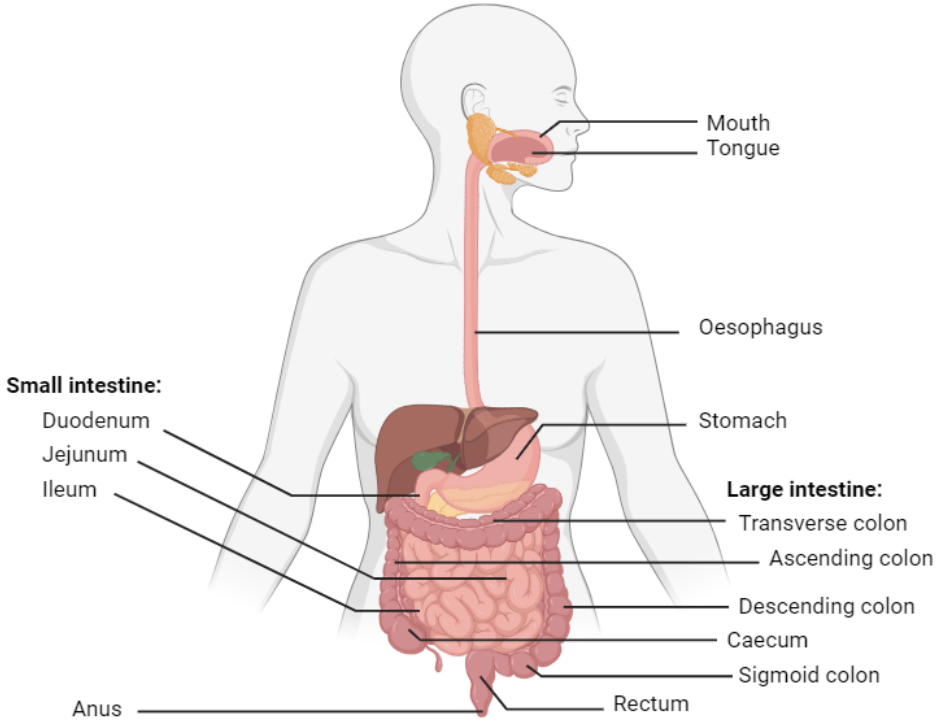

Figure 1 Anatomy of the human gastrointestinal (GI) tract. Human GI tract encompassing mouth, tongue, oesophagus, stomach, small intestine, large intestine, rectum, and anus. Created with BioRender.com

The GI tract is composed of a series of functional layers to allow these digestive processes to occur in a coordinated manner. The mucosa refers to the innermost layer which lines the lumen of the GI tract and consists of the epithelium, lamina propria, and muscularis mucosa (Figure 2).

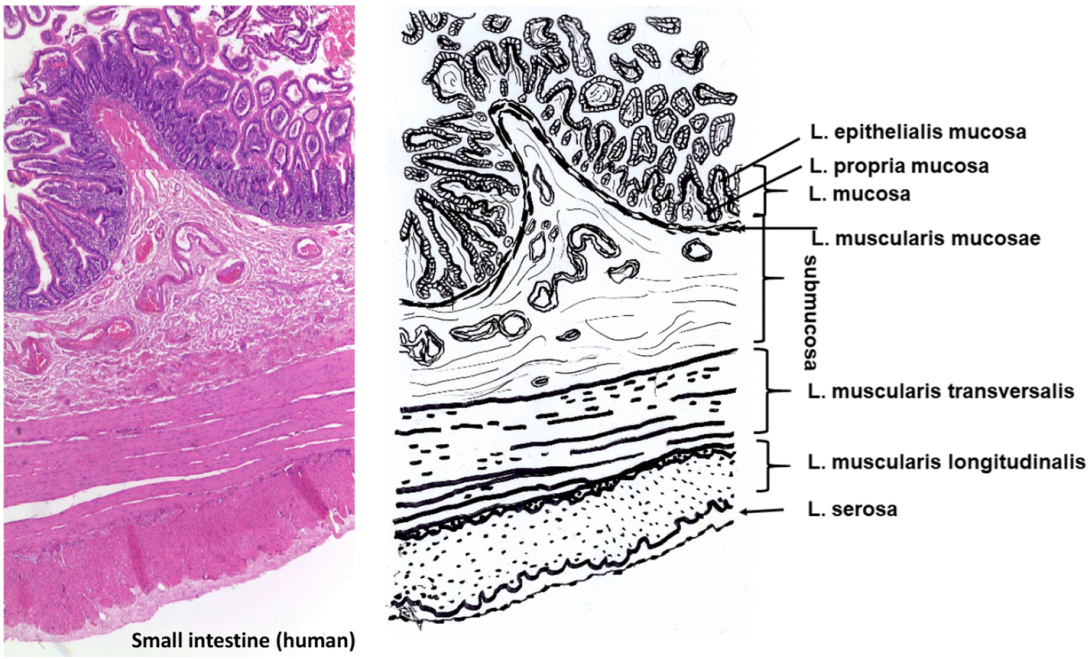

Figure 2 Functional layers of the small intestine. Histological slice of human small intestine alongside corresponding drawing depicting arrangement of Lamina epithelliaslis mucosa, Lamina propria mucosa, Lamina mucosa, Lamina muscularis mucosae, Submucosa, Lamina muscularis transversalis, Lamina muscularis longitudinalis and Lamina serosa. Taken from Meyer, 2019.

The epithelial layer is differentiated along the GI tract with this tissue specialisation corresponding to the regional function. In the upper and lower regions of the GI tract (the mouth, oesophagus and anal canal), the epithelium acts as a protective layer and is composed of stratified squamous epithelial cells, whilst the epithelial layer of the stomach, small intestine and colon are composed of glandular or simple columnal epithelial cells (Thompson, DeLaForest and Battle, 2018). The small intestinal epithelium is made up largely of enterocytes with this cell type representing 80% of all intestinal epithelial cells (Van Der Flier and Clevers, 2009). Enterocytes serve the function of absorbing nutrients. Additionally, finger-like projections protruding from the lumen, known as villi, confers the small intestinal epithelium a large surface area for maximised uptake of nutrients. At the base of the villus are invaginations called crypts which are lined with adult stem cells that constantly proliferate under homeostatic conditions (Figure 3). Villi are long and thin in the proximal region of the small intestine where most of the digestion takes place as the cell surface is in closest contact with nutrients in the lumen. Paneth cells are located at the base of the crypt in the small intestine with the highest

proportion of these cells identified in the jejunum (Cheng and Leblond, 1974). Paneth cells have a life span of approximately 3-6 weeks, and they function to secrete antimicrobial peptides, protecting the epithelial layer from pathogens and keeping the crypts sterile (Gassler, 2017), ultimately contributing to the intestinal innate host defence (Figure 3). Additionally, the small intestinal epithelium contains Peyer's patches which are covered in specialised M cells involved in the initiation of immune response (Kobayashi *et al.*, 2019).

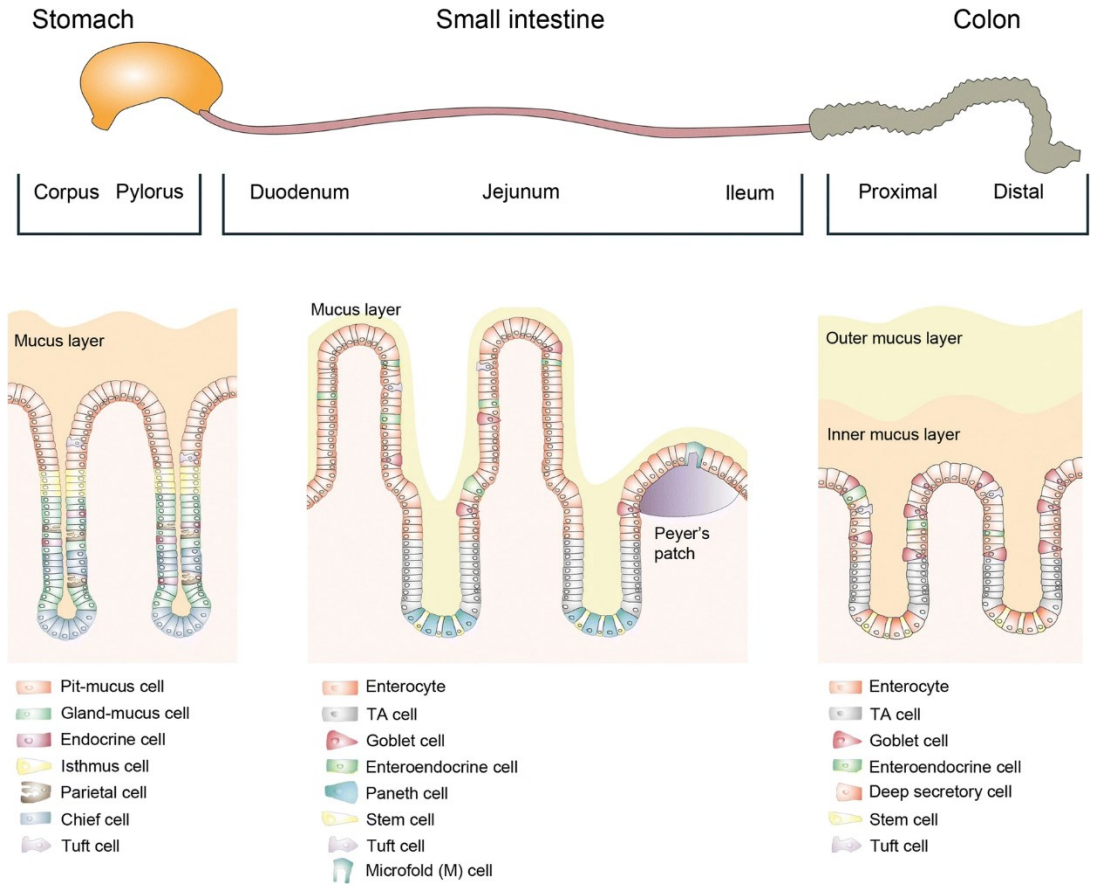

Figure 3 Overview of the GI tract epithelium from stomach to colon. Depiction of the GI tract epithelial layer, including the different cell types located across the stomach, small intestine and colon along with the changing thickness and structure of the mucus layer. Taken from Reyman *et al.*, 2022.

Towards the ileum, the villi shorten in length and broaden in width, where the mucus becomes one of the main lines of defence (Walton *et al.*, 2016). In the colon, there are no villi or Paneth cells, and the crypts are smaller compared to what is seen in the small intestine (Figure 3).

The lamina propria is made up primarily of connective tissue as well as lymphatic and blood vessels that function in transporting hormones, delivering nutrients to the mucosal epithelium and absorbing end products of digestion from the intestinal lumen. In addition, the lamina propria comprises a network of lymphatic and connective tissue which collectively function to protect the GI tract from the infiltration of ingested pathogenic but also commensal microorganisms inhabiting the gut lumen and outer mucus layer (Bruellman and Llorente, 2021). The third sub-layer of the mucosa separates the lamina propria from the submucosa and is a thin layer of smooth muscle referred to as the muscularis mucosa. The outermost layer, the serosa, is made up of connective tissue and has a mesothelium surface composed of simple squamous epithelial cells (Reed and Wickham, 2009).

1.1.2 The mucus layer

The mucus layer is an essential component of the GI tract's defence mechanism, serving as the primary barrier against the entry of pathogenic microorganisms, digestive enzymes and acids, partially digested food particles, microbial metabolites, and dietary toxins, making it integral to the maintenance of intestinal homeostasis (Song *et al.*, 2023). This layer envelops the inner surface of the GI tract, facilitating the lubrication of luminal contents. The organisation of the mucus layer varies along the GI tract: in the stomach and the colon, the mucus layer is double layered with the inner mucus layer adherent to the epithelium and impermeable to bacteria (Hansson, 2012), whilst in the small intestine the mucus layer is single layered and loosely attached, penetrable by microorganisms. Within the large intestine, where most of the gut microbiota is present, the inner mucus layer functions as a protective barrier, effectively partitioning commensal bacteria from direct contact with the host epithelium while the outer colonic mucus layer provides more porous environment densely colonised by commensal bacterial populations (Johansson *et al.*, 2008; Johansson, Holmén Larsson and Hansson, 2011).

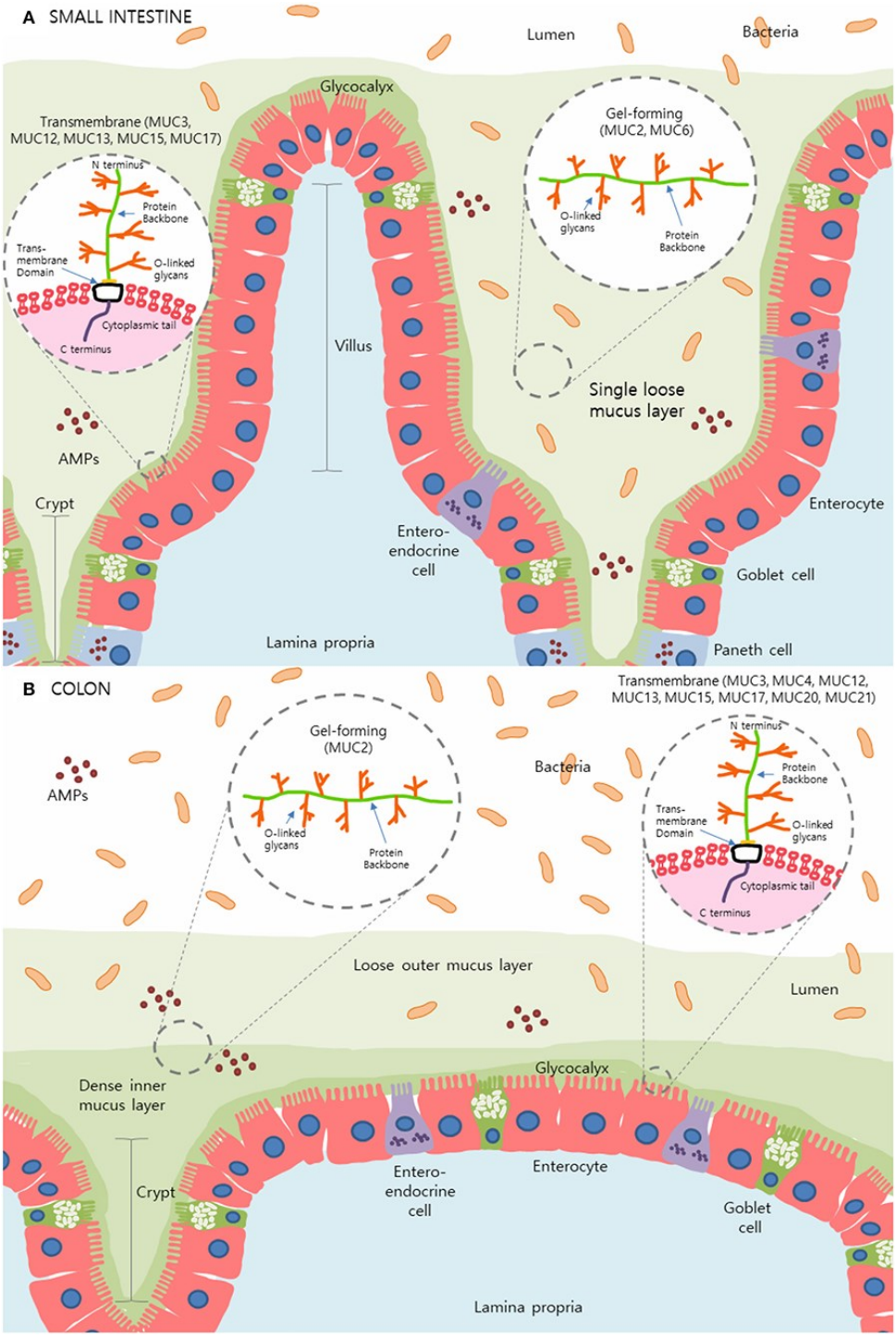

Figure 4 Depiction of the mucus layer within the small intestine and the colon. A) The loosely attached single layer of mucus in the small intestine. Mucus layer made up of transmembrane mucins (MUC3, 12, 13, 15 and 17) as well as gel forming MUC2 and 6. B) Double layered mucus predominantly made up of gel forming MUC2. Transmembrane mucins present in this region include MUC3, 4, 12, 13, 15, 17, 20 and 21). Taken from Grondin *et al.*, 2020.

The main structural components of mucus are large glycoproteins called mucins. Thus far, the identification of 21 mucins have been documented, named from MUC1 to MUC21 in accordance with their sequential discovery (Song *et al.*, 2023). These mucins are further distinguished into two main categories based on their structural attributes and biological roles: membrane-associated mucins and secretory mucins. The membrane-associated mucins encompass MUC1, MUC3A/B, MUC4, MUC12, MUC13, MUC15, MUC17, MUC20, and MUC21 (Song *et al.*, 2023). Conversely, secretory mucins are divided into two subclasses: gel-forming and non-gel-forming mucins. Gel-forming mucins, such as MUC2, MUC5AC, MUC5B, MUC6, and MUC19, contribute to protective, transport, lubrication, and hydration functions. MUC7, MUC8, and MUC9 are categorised as non-gel forming mucins (Song *et al.*, 2023). Under healthy physiological circumstances, goblet cells undergo continuous synthesis and secretion of mucins, thereby facilitating the ongoing replenishment and preservation of the mucus layer's thickness (Song *et al.*, 2023).

MUC2 secreted by goblets cells is the main gel-forming mucin constituting the mucus layers of the small and large intestines. In addition to MUC2, goblet cells also secrete CLCA1, FCGBP, AGR2, ZG16, and TFF3 (Johansson, Thomsson and Hansson, 2009; Rodríguez-Piñeiro *et al.*, 2013). FCGBP and TFF3 collaborate synergistically to strengthen the mucus barrier and stimulate antibacterial activity, whereas CLCA1, a metalloenzyme, primarily contributes to the stratification and expansion of mucus (Johansson, Thomsson and Hansson, 2009; Albert *et al.*, 2010). Additionally, ZG16, RELMβ, Lypd8, secretory immunoglobulin A (sIgA), and antimicrobial peptides (AMPs) present in mucus exhibit bacteriostatic or bactericidal capabilities under varied physiological conditions (Bergstrom and Xia, 2022) (Figure 4).

Mucins are characterised by differences in their oligosaccharide structure, with these structures demonstrating high complexity and diversity. Mucins are characterised by a proline-threonine-serine (PTS) domain which is the primary site of glycosylation. O-glycans constitute a substantial portion (up to 80%) of the total mucin mass with over 100 distinct glycan structures identified in MUC2 (Larsson *et al.*, 2009). These PTS domains, characterised by variable numbers of tandem repeat (VNTR) domains, contribute to the heterogeneity across mucins, owing to variations

in both mucin length and the degree of glycan attachment at these sites (Ambort *et al.*, 2012). This distinctive filamentous protein structure, with outwardly projecting oligosaccharides, gives rise to the characteristic "bottle-brush" morphology of mucins as seen in Figure 4.

Mucin glycosylation is initiated by the covalent bonding of a N-acetylgalactosamine (GalNAc) moiety to the hydroxyl group of serine and threonine, forming the Tn antigen (Figure 5). Glycosyltransferases sequentially add sugars to the GalNAc moiety of the Tn antigen giving rise to 8 core structures (Figure 5). The addition of galactose (Gal) to the Tn antigen forms core 1, Galβ1-3GalNAcα-Ser/Thr, whilst the addition of N-acetylglucosamine (GlcNAc), forms core 3, GlcNAc-β1-3GalNAcα-Ser/Thr. Further extension of core 1 and core 3 with the addition of GlcNAc produces core 2 (Galβ1,3(GlcNAcβ1,6)GalNAcα1-Ser/Thr) and core 4 (GlcNAcβ1,6(GlcNAcβ1,3)GalNAcαSer/Thr), respectively. Distribution of these core structures vary across the GI tract, and is reflected by differing expression patterns of core glycosyltransferases (Larsson *et al.*, 2013). For example, core structures 1 and 2 are common across gastric and duodenal mucins whilst core structures 3 and 4 are typical of colonic mucins (Robbe *et al.*, 2004; Bansil and Turner, 2006; Larsson *et al.*, 2013) (Figure 5). Under healthy conditions in the gut, monosaccharides are added to the core structures for further elongation with these glycan chains often terminated by sulphate, sialic acid or fucose residues (Thomsson *et al.*, 2012; Bergstrom and Xia, 2013; Schroeder, 2019) (Figure 5). Mucin glycosylation varies along the GI tract, with increased levels of sialic acid terminal epitopes from the ileum to the colon and decreased levels of terminal fucose in adult humans (Robbe *et al.*, 2003) and reverse gradients in mice (Larsson *et al.*, 2013) (Figure 5).

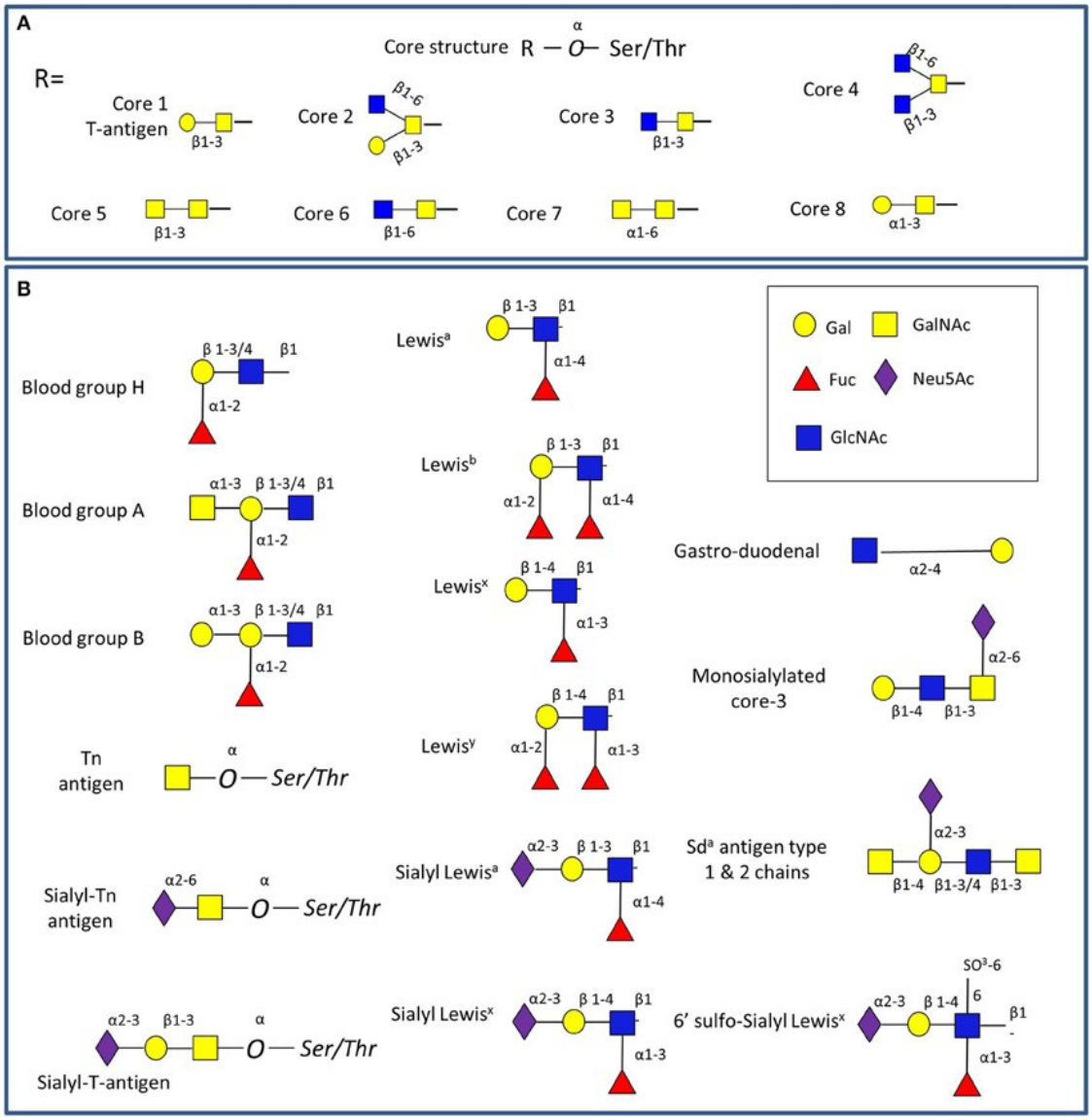

Figure 5 Depiction of GI mucin glycans. A) Core mucin O-glycan structures. B) Mucin glycan epitopes found across GI tract. Taken from Tailford *et al.*, 2015.

These mucin glycans serve as a binding site and carbon source for intestinal bacteria inhabiting the mucus niche (Tailford et al., 2015; Juge 2012). The mucin glycosylation profile therefore influences the microbial composition of mucus-associated microbiota and in turn this selectivity of inhabiting species supports homeostasis between the host and the intestinal microbes (Yamaguchi and Yamamoto, 2023).

1.2 The human gut microbiota

1.2.1 Composition and structure of the human gut microbiota

The human GI tract is home to a dynamic and diverse microbial ecosystem inhabited by bacteria, archaea, viruses, bacteriophages, and eukaryotic microorganisms, interacting with each other and the human host (Ursell *et al.*, 2012). This collection of intestinal microbes, referred to as the human gut microbiota, is considered an essential organ (O'Hara and Shanahan, 2006). The connection between these microorganisms and human health has been recognised since the 1880's following the investigations of Theodore Escherich, who acknowledged their effect on host physiology and digestion in infants (Escherich, 1886). It is estimated that over 10^{13} microorganisms inhabit the GI tract, with the number of bacterial cells to human cells, in the colon, estimated to be close to a 1:1 ratio, making the colon the most densely colonised microbial habitat on earth (Jandhyala *et al.*, 2015; Sender, Fuchs and Milo, 2016).

The characterisation of the human gut microbiome has been significantly advanced by culture-independent techniques based on samples collected from faecal samples and mucosal biopsies (Rao Jala *et al.*, 2020). Primarily, profiling involves the targeted sequencing of the bacterial 16S ribosomal RNA (rRNA) gene, a method allowing species-level bacterial community profiling, while shotgun metagenomic sequencing uses untargeted sequencing of all microbial genomes in a sample and allows strain level identification and information on genes and metabolic pathways (Durazzi *et al.*, 2021).

Seminal population-scale metagenomic projects such as the Human Microbiome Project (HMP) (Hugon *et al.*, 2015) and the Metagenomes of the Human Intestinal Tract (MetaHIT) (Li *et al.*, 2014) have been critical in establishing the first human gene catalogues of the gut microbiome in adults. Together these studies identified 2,172 microbial species derived from 12 distinct bacterial phyla and one archaeal taxon (Euryarchaeota). The majority of species isolated in humans (~90%) were affiliated to four bacterial phyla: Bacteroidetes (also named Bacteroidota) Firmicutes (synonym Bacillota), Proteobacteria (also named Pseudomonadota), Actinobacteria (also named Actinomycetota), with Bacteroidetes and Firmicutes making up the largest proportion (Hugon *et al.*, 2015; Aggarwal *et al.*, 2023). Since then, several large scale metagenomic studies have been conducted. Notably the PREDICT 1

study, one of the largest nutritional study's examining the relationships between diet, the microbiome, and cardiometabolic health markers and included over 1,100 participants from the U.K. and U.S from which 660 were either identical and non-identical twins (Berry *et al.*, 2020). From this study stemmed PREDICT 2 and 3 which had an integrated focus on the impact of ethnicity on microbe-host interactions. Following completion of PREDICT 1 and 2, PREDICT 3 launched in July 2020 and is still ongoing with over 45,000 enrolled participants (Berry, Spector and Wolf, 2023).

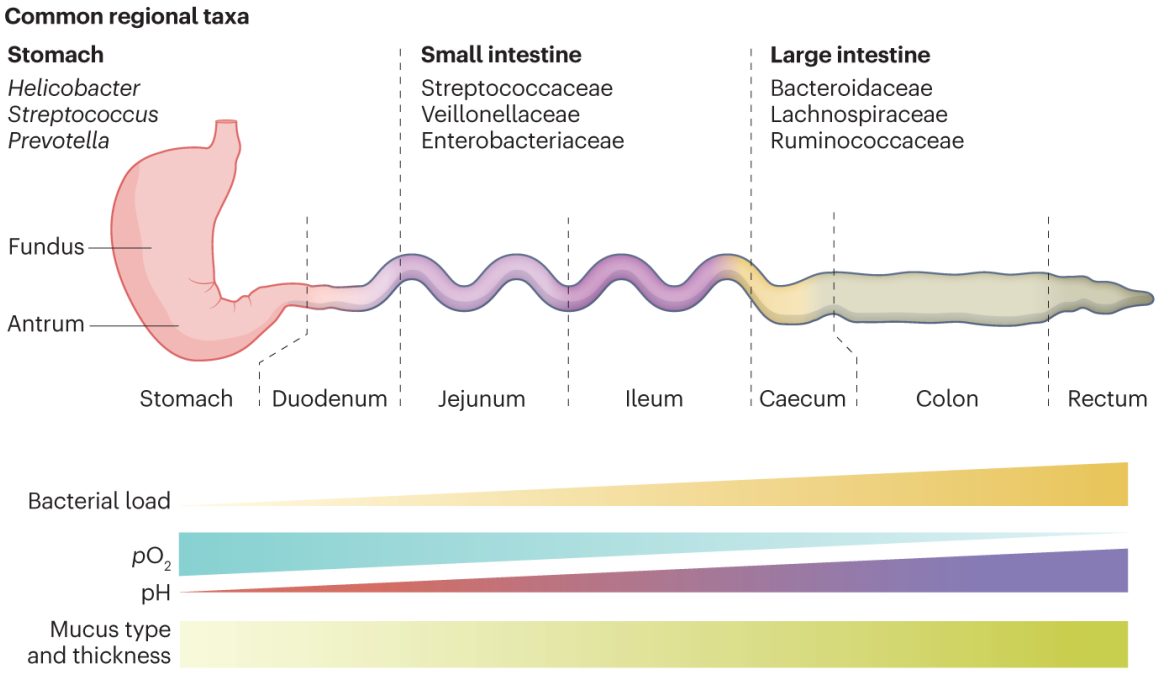

Figure 6 Geographical characteristics specific to different regions of the GI tract. Demonstration of the longitudinal variations environmental conditions and bacterial composition along the axis of the gut. The parameter pO_2 denotes the partial pressure of oxygen. Taken from McCallum and Tropini, 2023.

The gut microbiota composition varies along and across the GI tract, from the stomach to the colon (Figure 6). The stomach is the most acidic environment, reducing the prevalence of bacterial colonisation in this region. The mucus layer lining the stomach blocks direct contact between the tissue and the highly acidic gastric fluid. In addition, the stomach is highly aerobic, has a fast transit time in comparison to the rest of the digestive tract and produces antimicrobial peptides. These conditions are highly unfavourable for microbial growth, resulting in an absolute bacterial abundance of ~10^1–10^3 colony forming units (CFU) ml^{-1} in healthy

humans, making the stomach the region of the GI with the lowest bacterial load (Figure 6) (O'Hara and Shanahan, 2006; McCallum and Tropini, 2023). Human gastric biopsies and fluid samples have revealed the presence of bacteria belonging to the Firmicutes, Bacteroidetes and Proteobacteria phyla within the stomach, through use of amplicon sequencing and 16S rDNA clone libraries (McCallum and Tropini, 2023).

Bacterial load increases moving from the stomach to the small intestine, which is composed of the duodenum, jejunum and ileum (Figure 6). Compared to the stomach, this region of the GI tract has a higher pH (Figure 6), making it a less hostile environment, however not highly favourable due to the high concentration of antimicrobial peptides present here, reducing the type and number of bacteria that possess the ability to colonise. Upon entry into the duodenum, the pH of the luminal contents is still low and partial pressure of oxygen (pO_2) is still high resulting in low bacterial colonisation (~10^1–10^3 CFU ml^{-1}) within humans and, in this region (Figure 6), bacterial diversity remains similar to that which is seen for the stomach (McCallum and Tropini, 2023).

Between the duodenum and the ileum, the pH gradually increases, and the pO_2 gradually decreases, promoting higher bacterial growth in the jejunum and ileum (Figure 6). This reduction in acidity and oxygen is also accompanied with a faster transit time of 2-6 h in humans, and is thought to be a favourable growth environment for fast-growing facultative anaerobes and bacteria that possess the ability to adhere to the epithelium or mucus layer such as segmented filamentous bacteria (Lee, Erdogan and Rao, 2014; Donaldson, Melanie Lee and Mazmanian, 2015; McCallum and Tropini, 2023). Consequently, these more favourable conditions support the growth of an estimated ~10^4–10^7 CFU ml^{-1} bacteria in the healthy human gut (O'Hara and Shanahan, 2006; McCallum and Tropini, 2023). However, it is important to note that although bacterial abundance is increased in this region of the GI tract, the microbial diversity remains equal to or lower than that seen in the upper small intestine and stomach (Jones *et al.*, 2022; McCallum and Tropini, 2023). In humans, bacteria from the Streptococcaceae, Veillonellaceae and Enterobacteriaceae family are amongst the most prominent taxa between these regions (Seekatz *et al.*, 2019; McCallum and Tropini, 2023).

Within the large intestine, there is a slight decrease in pH due to increased short chain fatty acid (SCFA) production from fermented dietary fibres which become the main source of nutrients for microbes in this region. The lumen environment becomes highly anaerobic, transit time is slower and the mucus layer increases in thickness, with all of these preferable factors contributing to an increased microbial abundance, making the colon the most densely populated and diverse region of the GI tract with an estimated ~10^{11}–10^{12} CFU ml^{-1} organisms inhabiting this environment (O'Hara and Shanahan, 2006).

Interestingly, gut microbes have an influence on the glycosylation patterns of mucins through the expression of glycosyltransferases including host ppGalNAcT, core 1 β1,3-galactosyltransferase (C1GALT1), and fucosyltransferase (FUT2) which aid in mucin O-glycosylation (Arike, Holmén-Larsson and Hansson, 2017). Mucin glycosylation also plays a key role in shaping the gut microbiota along the GI tract with mucin glycosylation profiles shown to be region specific (Robbe *et al.*, 2004; Larsson *et al.*, 2013).

The gut microbiota composition also varies across the GI tract, from the lumen to the mucosa (Donaldson, Melanie Lee and Mazmanian, 2015). Here, mucin glycans, O_2 and pH gradients all contribute to shaping the mucosa-associated microbiota (MAM) (Juge, 2022). Differences in pH are observed across the mucus layer, which sequesters hydrogen and bicarbonate ions, thereby protecting the epithelium from fluctuations in luminal pH. Additionally, the concentration of O_2 undergoes alterations along the transverse axes of the GI tract with a diminishing transversal O_2 gradient present from the highly vascularised intestinal mucosa towards the gut lumen (Albenberg *et al.*, 2014). These shifts in pH and O_2 concentration establish localised microenvironments that significantly influence the structure and function of the MAM throughout the GI tract (Friedman *et al.*, 2018).

Within the mucus niche, the presence of mucin glycans are a source of nutrients to mucin glycan foragers including species from the Bacteroidetes, Actinobacteria, Firmicutes, and Verrucomicrobia phyla (Tailford *et al.*, 2015; González-Morelo, Vega-Sagardía and Garrido, 2020). Mucin glycan foragers release mono- and oligosaccharides into the mucus niche that can be used by themselves or by other organisms through cross-feeding (Bell and Juge, 2021). The ability of specific bacteria to utilise mucin glycans as a sustainable nutrient source provides a

competitive advantage for their colonisation of the mucus layer (Yamaguchi and Yamamoto, 2023). *Akkermansia muciniphila*, the sole representative of the Verrucomicrobia phyla within the human gut microbiota, is a mucin-degrading specialist and keystone member of the MAM, playing an active role in modulating immune response, promoting gut barrier integrity and anti-inflammatory effects (Macchione *et al.*, 2019). Owing to their expansive repertoire of carbohydrate-active enzymes, bacteria belonging to the phylum Bacteroidetes exhibit broad glycan degradation capabilities towards host-derived and dietary glycans, enabling them to adapt to luminal and mucosal niches (Ndeh and Gilbert, 2018). Actinobacteria, predominantly characterised by bifidobacteria, are well-suited for the degradation of low molecular weight mucin glycans (resembling human milk oligosaccharides) with a metabolic profile akin to that observed in members of the phylum Firmicutes (Ndeh and Gilbert, 2018). Further cross-feeding activities of released mucin-glycan degradation products and metabolites from these species is an integral part of shaping the MAM (Berkhout, Plugge and Belzer, 2022).

1.2.2 Establishment and modulation of the human gut microbiota

It has been widely documented that the human infant intestine is rapidly colonised following birth. The infant gut is first colonised by facultative anaerobes, specifically those belonging to the *Enterobacteriaceae* family (Notarbartolo *et al.*, 2023).The human infant gut it also characterised by the preponderance of *Actinobacteria* and *Bifidobacteria* (Milani *et al.*, 2017). This initial colonisation reduces the O_2 within the environment to create more favourable conditions to allow for colonisation of anaerobic bacteria, largely those belonging to *Bacteroidaceae* families. These organisms stimulate the production of mucin, reinforcing the gut microbiota-mucus barrier (Notarbartolo *et al.*, 2023). The *Enterobacteriaceae*/*Bacteroidaceae* ratio decreases over time, however the lack of reduction in this ratio is linked to delayed maturation of the gut microbiome (Notarbartolo *et al.*, 2023). In neonates, the intestinal microbiota is characterised by low diversity, however, in the first few weeks after birth microbial diversity and abundance increases and a dominance of Bacteroides and Firmicutes is observed (Suárez-Martínez *et al.*, 2023). By the end of the first year of life, infants exhibit a distinctive microbial composition which by

the ages of 2 and 5, closely mirrors that of adults in terms of both composition and diversity (Rodríguez *et al.*, 2015). This transition is marked by the dominance of three bacterial phyla: Firmicutes (specifically Lachnospiraceae and Ruminococcaceae), Bacteroidetes (including Bacteroidaceae, Prevotellaceae, and Rikenellaceae), and Actinobacteria (encompassing Bifidobacteriaceae and Coriobacteriaceae) (Suárez-Martínez *et al.*, 2023).

The mode of delivery is a major factor in the establishment of this initial colonisation with vaginally-delivered neonates shown to have intestinal microbiomes dominated by *Bacteroides, Bifidobacterium, Parabacteroides, Lactobacillus* and *Escherichia*, whilst caesarean-delivered neonates harbour more species of *Staphylococcus, Enterococcus and Klebsiella*, resembling that of the maternal skin (Dominguez-Bello *et al.*, 2016; Dos Santos *et al.*, 2023; Notarbartolo *et al.*, 2023; Xiao and Zhao, 2023). Another contributor shaping the infant gut microbiota is breast or formula feeding. Exclusively breastfed infants have been shown to have a higher microbial diversity within the gut and increased IgA levels compared to formula-fed infants and combined breast and formula-fed infants. This is proposed to be due to colostrum from the mother, provided to the infant, being rich in maternal antibodies and consequently enhancing immunity (Martínez-Martínez *et al.*, 2024).

As previously mentioned, in adults, the gut is dominated by Firmicutes, Bacteroidetes and Actinobacteria. Bioinformatics analysis of sequenced faecal samples from individuals in Europe and the United States revealed the presence of three distinct clusters of microbial communities, referred to as enterotypes, characterised by differences in abundance and composition of microbial species (Arumugam *et al.*, 2011). This clustering was found to be independent of age, gender, cultural background and geography. These enterotypes were distinguished by the prevalence of specific bacterial genera, namely *Bacteroides* in enterotype 1, *Prevotella* in enterotype 2, and *Ruminococcus* in enterotype 3 (Arumugam *et al.*, 2011; Koren *et al.*, 2013). However, this earlier concept faces limitations as the clustering suggests microbial stability over time, while it is now well established that that the gut microbiome is dynamic and can undergo fluctuations in response to various factors such as diet, lifestyle, and disease (Costea *et al.*, 2017; Frioux *et al.*, 2023). Indeed, the microbial composition within the human gut can be

modulated by both exogenous and endogenous factors including host genetics (Lopera-Maya *et al.*, 2022; Xu *et al.*, 2020; Qin *et al.*, 2022), ethnicity (Mallott *et al.*, 2023), dietary habits (Jardon *et al.*, 2022), lifestyle (Donoso *et al.*, 2022), administration of drugs including antibiotics (Reyman *et al.*, 2022) and environmental exposure to toxicants and pollutants (Giambò *et al.*, 2022), promoting vast inter- and intra-individual variability (Kerimi *et al.*, 2020).

More recently the concept of "enterosignatures" has been introduced, resulting in the stratification of microbial gut communities into five groups dominated by *Bacteroides*, Firmicutes, *Prevotella*, *Bifidobacterium*, or *Escherichia* (Frioux *et al.*, 2023). Unlike the seminal enterotype classification system, the enterosignature grouping takes into account changes and perturbations in the microbial composition, metabolic activity and functional potential within the human gut over a lifetime (Frioux *et al.*, 2023).

With ageing, there is a decrease in the diversity of microbiota in individuals aged 70 and above, as a result of changes in digestion and nutrient absorption, as well as a weakening of immune activity (Hou *et al.*, 2022; Ren *et al.*, 2023). Shifts in dietary habits in elderly, such as increased monotonous diet, can also contribute to a reduction in gut microbiota diversity (Odamaki *et al.*, 2016). These changes are characterised by a decline in anaerobic bacteria like *Bifidobacteria* and *Firmicutes* with anti-inflammatory properties and an increase in proinflammatory microbiota, specifically *Clostridium* and *Proteobacteria*. This shift contributes to exacerbation of inflammation, compromising the duodenal microbiome and leading to a reduction in overall microbial diversity (Leite *et al.*, 2021). The decrease in Bifidobacterium spp., known for its role in stimulating the immune system and metabolic processes, may partly account for the lower systemic inflammatory status and malnutrition observed in older adults (Hou *et al.*, 2022; Ren *et al.*, 2023).

1.2.3 Function of the human gut microbiota

Intestinal bacteria predominantly aid in carbohydrate fermentation, production of metabolites, synthesis of vitamins, maintenance of gut integrity, maturation of the immune system, pathogen defence and detoxification as recently reviewed (Colella *et al.*, 2023) and further detailed in the sections below. As a result, the interplay

between the host and the gut microbiota plays a crucial role in both maintaining health and contributing to disease.

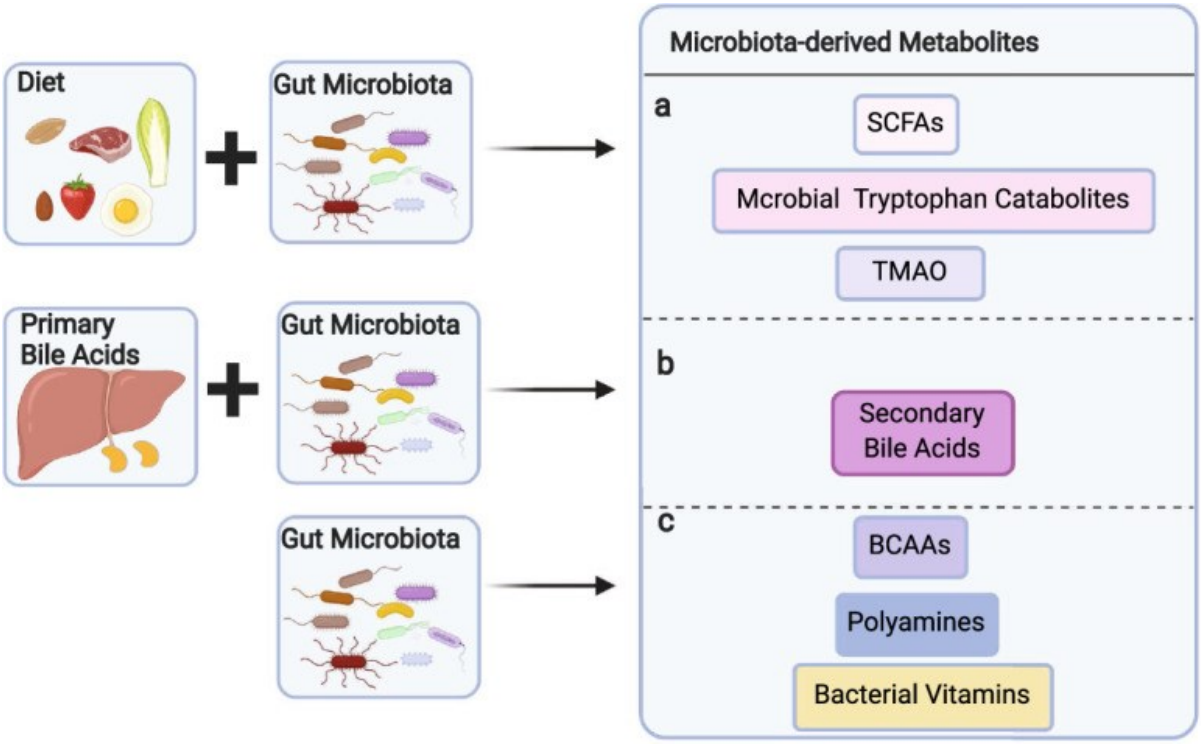

Figure 7 Gut microbiota-derived metabolites. Figure illustrates the production of microbiota-derived metabolites from (A) diet, resulting in the production of SCFA's, microbial derived tryptophan catabolites and TMAO, (B) primary bile acids, which are converted into secondary bile acids and (C) the synthesis of branched-chain amino acids (BCAAs), polyamines and vitamins from gut microbiota. Taken from Yang and Cong, 2021.

1.2.3.1 Carbohydrate fermentation and SCFA production

Complex carbohydrates from the diet reach the colon undigested where they can be metabolised by the gut microbiota. Certain bacterial species, particularly within the Bacteroidetes and Firmicutes phyla, possess the ability to ferment fibres, indigestible carbohydrates, resulting in the production of branched-chain and short-chain fatty acids (SCFAs), lactate, ethanol, hydrogen, and carbon dioxide. These by-products are either utilised by the host or excreted (Rahman *et al.*, 2023). The main SCFAs in humans include acetate, propionate, and butyrate, each serving crucial functions in the human body (Rahman *et al.*, 2023). Of these, butyrate stands out as a key SCFA for human health, acting as the primary energy source for human colonocytes (Cheng and Zhou, 2024). Butyrate has been shown to increase mucin

production by goblet cells, support mucosal integrity and stimulates oxygen consumption in the gut contributing to a highly anaerobic luminal environment (Rahman *et al.*, 2023). Its potential as an anti-carcinogen is reflected by its ability to induce apoptosis in colon cancer cells and regulate gene expression by inhibiting histone deacetylase (Hajjar, Richard and Santos, 2021; Rahman *et al.*, 2023). Propionate, another essential SCFA, serves as a vital energy source for epithelial cells in the liver and plays a crucial role in gluconeogenesis (Beam, Clinger and Hao, 2021). Acetate facilitates the growth of other bacteria by acting as an essential co-factor; for instance, *Faecalibacterium prausnitzii* is unable to grow in pure culture in the absence of acetate (Ahrodia *et al.*, 2022).

1.2.3.2 Production of other metabolites

Tryptophan is an essential aromatic amino acid and is predominantly derived from dietary protein sources. Its absorption mainly takes place in the small intestine where it is used for protein synthesis. However, in the colon, a diverse array of bacteria possesses enzymes that can metabolise tryptophan into various compounds including indole, indole ethanol (IE), indolepropionic acid (IPA), indole lactic acid (ILA), indoleacetic acid (IAA), indolealdehyde (IAld), indoleacrylic acid (IA), skatole, and tryptamine (M. Liu *et al.*, 2022). The composition and levels of these microbial tryptophan metabolites are therefore largely influenced by the gut microbiota.

Indole, for instance, is produced from tryptophan by *Escherichia coli* (Smith, 1897) and *Proteus vulgaris* through the action of a tryptophanase (Hickman *et al.*, 1982; Lee and Lee, 2010). Different metabolic pathways in various bacterial species result in the production of other tryptophan metabolites. For example, *Clostridium sporogenes* and *Ruminococcus gnavus* can synthesise tryptamine via tryptophan decarboxylation, while *Clostridium sporogenes* and *Peptostreptococcus* spp. are known to produce IA (Dodd *et al.*, 2017; Wlodarska *et al.*, 2017). *Clostridium* spp., including *Clostridium botulinum*, *Clostridium caloritolerans*, and *Clostridium sporogenes*, have the ability to convert tryptophan into IPA (Dodd *et al.*, 2017).

These gut microbiota-derived tryptophan catabolites play crucial roles in regulating local intestinal immune responses and influencing host physiology systemically via

the bloodstream. They achieve this by activating receptors such as the pregnane X receptor (PXR) and/or the aryl hydrocarbon receptor (AhR), thereby exerting significant effects on host health and homeostasis (Zelante *et al.*, 2013; Hubbard *et al.*, 2015).

Trimethylamine (TMA) is a metabolite produced by the gut microbiota through the breakdown of dietary carnitine, choline, or choline-containing compounds (Zeisel and Warrier, 2017). The synthesis of TMA is dependent upon the composition and diversity of the gut microbiota. Certain bacteria, such as *Desulfovibrio alaskensis* and *Desulfovibrio desulfuricans*, equipped with the choline-utilisation gene cluster (Cut), have the ability to convert choline into TMA within the gut (Craciun and Balskus, 2012). Similarly, genera like *Acinetobacter* and *Serratia*, which encode CntA and CntB enzymes, facilitating the conversion of L-carnitine into TMA (Koeth *et al.*, 2014; Zhu *et al.*, 2014). Additionally, another gene pair, YeaW/YeaX, sharing homology with CntA/B, also contributes to TMA production (Salzman, 2011).

After its formation, TMA can be absorbed in the intestine and transported to the liver, where it undergoes oxidation by flavin monooxygenases (FMOs) to form trimethylamine-N-oxide (TMAO) (Bennett *et al.*, 2013). Interestingly, while TMA selectively activates human trace amine-associated receptors (TAARs), TMAO does not exhibit this activity (Wallrabenstein *et al.*, 2013). Recent findings suggest that TMAO directly binds and activates protein kinase R-like endoplasmic reticulum kinase (PERK), a critical sensor of intracellular stress (Chen *et al.*, 2019).

1.2.3.3 Bile acid metabolism

Within the gut, bile acids synthesised by hepatocytes act as a detergent and support fat absorption through the intestinal membrane, and also function as potent antimicrobials due to their capacity to disrupt bacterial membranes, as recently reviewed (Guzior and Quinn, 2021). The protective effects of bile acids have been demonstrated in *C. difficile* infections where successful faecal microbiota transplants (FMT's) have been associated with increased bile salt hydrolases (bacterial enzymes responsible for the conversion of bile acids) compared to before, suggesting that bacterial modification of primary bile acids aid in maintaining host health through protection against microbial infection (Mullish *et al.*, 2019; Guzior

and Quinn, 2021; Mullish, McDonald and Marchesi, 2022). Gut bacteria can convert primary bile acids such as cholate and chenodeoycholate into the secondary bile acids deoxycholate and lithocholate, respectively (Hofmann, 1999; Monte *et al.*, 2009). It has been estimated that 5% of bile acids absorbed within the intestine are converted to secondary bile acids, with this function restricted to few bacteria including *Firmicutes* species, notably *Clostridium scindens* (Guzior and Quinn, 2021; Yang and Cong, 2021).

1.2.3.4 Synthesis of vitamins

Members of the gut microbiota can synthesise most water-soluble B vitamins, including biotin, folates, cobalamin, riboflavin and pantothenic acid as well as vitamin K2 (Rahman *et al.*, 2023).

Vitamin K producers include *Lactobacillus, Bifidobacterium* and *Bacillus* (Smajdor *et al.*, 2023). Intestinal vitamin K production plays an essential role in meeting the required amounts needed in humans, with vitamin K deficiency leading to clinically significant coagulopathy, a bleeding disorder affecting how blood clots (Smajdor *et al.*, 2023). For vitamin B12, please see section 1.3.

Vitamins are required by gut bacteria for growth and consequently play a crucial role in shaping microbial richness and diversity within the gut (Hossain, Amarasena and Mayengbam, 2022). Genomic analysis of Bacteroidetes and Fusobacteria have detected the presence of a riboflavin operon across all strains, with this operon also being present in 92% of Proteobacteria (Magnúsdóttir *et al.*, 2015). Riboflavin is required for the postnatal development of the GI tract with riboflavin deficiency shown to be associated with irreversible interruptions in crypt bifurcation and crypt hypertrophy in rats (Yates *et al.*, 2003; Hossain, Amarasena and Mayengbam, 2022). In humans, riboflavin deficiency has been associated with low duodenal cell proliferation and shorter duodenal crypts (Nakano *et al.*, 2011; Hossain, Amarasena and Mayengbam, 2022). In contrast, riboflavin supplementation has been associated with increased the abundance of non-riboflavin producers including *Faecalibacterium prausnitzii* and *Roseburia* spp. as well as *Prevotella* spp. (Carrothers *et al.*, 2015; Steinert *et al.*, 2016; Hossain, Amarasena and Mayengbam, 2022).

1.2.3.5 Maturation of the innate immune system

There is strong evidence demonstrating that the human gut microbiome, an especially early microbiome colonisation, plays a critical role in the maturation of the immune system. For example, home-birth faecal supernatant has been shown to enhance epithelial barrier function and intestinal maturation in *in vitro* models of the intestinal epithelium, resulting in a stronger immunological response when compared to caesarean section born faecal supernatants (Selma-Royo *et al.*, 2020). *Lactobacillus*, *Bifidobacterium*, *Enterococcus* and *Bacteroides* are amongst the genera dominating the neonatal gut microbiome with these organisms playing crucial roles in the innate immune system development (Milani *et al.*, 2017). Breast-feeding facilitates the establishment of *Lactobacillus* in the early microbiome (Witkowska-Zimny and Kaminska-El-Hassan, 2017). Species of *Lactobacillus* have been shown to stimulate dendritic cell differentiation, in turn promoting the secretion of cytokines IL-6, IL-10, IL-12, IL-15, and IL-23 (Haileselassie *et al.*, 2016). This contributes to the activation of immune pathways, specifically the activation of natural killer cells and the synthesis and secretion of granulocyte-macrophage colony-stimulating factor, IL2, interferon-gamma, tumour necrosis factor-alpha, providing a robust defence mechanism against pathogen invasion (Fink *et al.*, 2007; Ferlazzo *et al.*, 2011).

Human milk oligosaccharides (HMOs) derived from breast milk, stimulates the growth of *Bifidobacterium* (Thomson, Medina and Garrido, 2018). *Bifidobacterium* is able to metabolise these HMOs to produce SCFAs which have anti-inflammatory properties (Henrick *et al.*, 2021). Specifically, butyrate has been shown to reduce intestinal inflammation in mouse models with necrotising enterocolitis (Sun *et al.*, 2021). The absence of *Bifidobacterium* and the loss of genes required for utilisation of HMOs has been linked to systemic inflammation and immune imbalance in early life (Henrick *et al.*, 2021).

Enterococcus faecalis, dominating the total lactic acid bacteria identified in neonatal stool, effectively initiates colonisation and reduces inflammation through suppression of proinflammatory cytokines, particularly IL-8, *in vivo* and *in vitro* (Wang *et al.*, 2014). *E. faecalis* has been shown to modulate and activate peroxisome proliferator-activated receptor-γ (PPARγ) activity, with PPARγ involved in inflammation control, and cell differentiation (Are *et al.*, 2008). The activation of

PPARγ increases transcriptional activation of IL-10, a cytokine involved in the modulation of innate immune function (Are *et al.*, 2008).

Bacteroides species are present in varying amounts in the infant microbiome and have been shown to significantly impact immune regulation (Marcobal *et al.*, 2011). *Bacteroides fragilis* produces an immunomodulatory capsular polysaccharide A (PSA) which has been shown to effectively prevent colitis and experimental allergic encephalomyelitis (EAE) in mouse models (Mazmanian, Round and Kasper, 2008; Chang *et al.*, 2017; Ramakrishna *et al.*, 2019).The immunomodulatory properties of PSA stimulate the production of regulatory T cells that secrete IL-10, an anti-inflammatory cytokine that reduces pathogenic inflammation in the gut (Ochoa-Repáraz *et al.*, 2009).

In the adult gut microbiota, microbe-associated molecular patterns (MAMPs) such as cell surface polysaccharides have been shown to interact with receptors of the epithelium and immune system through their interaction with pattern recognition receptors (PRRs) like toll-like receptors (TLR) and NOD-like receptors (NLR) (Oviedo-Boyso, Bravo-Patiño and Baizabal-Aguirre, 2014). This interaction allows the modulation of immunity through the regulation of the cytokines, chemokines but also IgAs produced by the host. Germ-free (GF) mice have decreased levels of secretory IgA and less IELs which play a vital role in defence during inflammation (Round & Mazmanian, 2009). These immunity-associated molecules are important in the maintaining of gut microbiota homeostasis (Pabst et al., 2016).

1.2.3.6 Pathogen defence

The gut microbiome plays a crucial role in pathogen defence by utilising nutrient competition and other mechanisms to prevent pathogen colonisation, as recently reviewed (Horrocks *et al.*, (2023)). The diverse microbial community within the gut competes for essential nutrients, thereby limiting the resources available to pathogenic organisms (Caballero-Flores, Pickard and Núñez, 2023). This competition creates an unfavourable environment for pathogens, reducing their ability to establish and proliferate within the intestine (Caballero-Flores, Pickard and Núñez, 2023). Additionally, the SCFAs produced by the gut microbiota through the fermentation of dietary fibres, further inhibit pathogen growth by lowering the

intestinal pH and creating a hostile environment for many pathogens. For example, infants fed *Bifidobacterium longum* subsp. *infantis* displayed low intestinal pH and a reduced abundance of pathogenic and mucin-degrading bacteria in the gut microbiota (Duar, Kyle and Casaburi, 2020). The secondary bile acids produced by the gut microbiota can have direct antimicrobial effects. For example, secondary bile acids have been shown to inhibit *Clostridium difficile* spore formation and outgrowth in the large intestine (Theriot, Bowman and Young, 2016). Disturbances in the gut microbiome, through antibiotic treatment for instance, can disrupt these protective mechanisms by reducing microbial diversity and the availability of competitive commensal bacteria, thereby facilitating pathogen colonisation and infection (Dethlefsen *et al.*, 2008; Panda *et al.*, 2014). Strategies aimed at restoring or maintaining a healthy gut microbiota, such as FMT's or next-generation microbiome therapeutics, show promise in enhancing colonisation resistance and protecting against intestinal infections (Merrick *et al.*, 2023). Currently FMT is a well-established and effective mode of treatment for *C. difficile* infections, resulting in the recovery of SCFAs and bile acids and restoring colonisation resistance (Brown *et al.*, 2018; Seekatz *et al.*, 2018; Jess *et al.*, 2023).

1.2.4 Association between gut microbiota and disease

Imbalances in the composition of the human gut microbiome, a state referred to as dysbiosis, has been documented in numerous diseases including metabolic diseases, (obesity, cardiovascular diseases (CVDs), diabetes), colon cancer, inflammatory bowel disease (IBD) or brain disorders (for a review see Hou *et al.*, 2022). Recent examples are provided below.

1.2.4.1 Inflammatory bowel disease (IBD)

IBD is a term used to refer to Crohn's disease (CD) and ulcerative colitis (UC) characterised by abdominal pain, rectal bleeding, fatigue and weight loss as a result of chronic inflammation, restricted to either the colon in UC or throughout the digestive tract as seen in CD (Abdel-Rahman and Morgan, 2023). IBD is the result of an alteration in the interplay between environmental, genetic, and microbial factors. Increasing evidence suggests a direct correlation between the gut

microbiome and the pathogenesis of IBD, with IBD patients having lower beta diversity and differences in their intestinal taxonomic composition compared to healthy subjects (Neurath, 2020; Clooney *et al.*, 2021; Olaisen *et al.*, 2021; Abdel-Rahman and Morgan, 2023). Recently, a systematic meta-analysis of IBD studies reported that a reduction in alpha diversity was consistent in both CD and UC, however more pronounced in CD (Abdel-Rahman and Morgan, 2023). It was also reported that *Fusobacterium* and *Enterococcus* were most consistently reported as being enriched in CD (Abdel-Rahman and Morgan, 2023). *Fusobacterium* is able to adhere to a wide range of immune cells and is a potent immune stimulator with an ability to invade human epithelial cells, however it is not yet known whether this ability directly contributes to CD pathogenesis or whether enrichment is due to opportunistic growth (Abdel-Rahman and Morgan, 2023). It is suggested that *Enterococci* enrichment in CD may be due to high bile acid tolerance compared to other gut commensals in addition to increased antimicrobial resistance, however, again it remains unclear whether Enterococcus has a causal effect on IBD or whether it is an opportunistic bystander (Abdel-Rahman and Morgan, 2023). In contrast, IBD patients showed reduction of *F. prausnitzii* with similar loads of *A. muciniphila* in colonic biopsies when compared to healthy subjects (Lopez-Siles *et al.*, 2018; Juge, 2022).

1.2.4.2 Colorectal cancer (CRC)

Mounting evidence indicates an association between gut microbiota and the onset and progression of colorectal cancer (CRC). Dysbiosis of the gut microbiota can trigger inflammation and immune responses indirectly linked to carcinogenesis (Cheng, Ling and Li, 2020; Asseri *et al.*, 2023). The impact of gut microbiota on CRC progression is thought to involve modulation of specific signalling pathways, including E-cadherin/β-catenin, TLR4/MYD88/NF-κB, and SMO/RAS/p38 MAPK (Li *et al.*, 2022). Chen et al. proposed that both commensal and pathogenic bacteria contribute to CRC progression by 1) exploiting defects in the tumour surface barrier, 2) invading normal colonic tissue and inducing local inflammation, and 3) producing genotoxic metabolites to induce oncogenic transformation of colonic epithelial cells (Chen, Pitmon and Wang, 2017).

Major bacteria implicated in CRC include *Enterococcus faecalis, Escherichia coli, Bacteroides fragilis, Streptococcus bovis, Fusobacterium nucleatum,* and *Heliobacter pylori* (Dai *et al.*, 2019; Deng *et al.*, 2020; L. Zhang *et al.*, 2023; Lichtenstern and Lamichhane-Khadka, 2023; Martin-Gallausiaux *et al.*, 2024). Some of these bacteria have the capacity to produce genotoxic substances such as colibactin, *B. fragilis* toxin, and typhoid toxin, leading to host DNA damage (Li *et al.*, 2022). In contrast, *Fusobacterium nucleatum* plays a role in the progression of CRC by modulating innate immune cell activity (Kostic *et al.*, 2013; Ye *et al.*, 2017). *F. nucleatum* abundance is significantly higher in mucosal and faecal samples of CRC patients compared to healthy controls (Janati *et al.*, 2020; Shaw *et al.*, 2022; Palmieri *et al.*, 2023) and transmission electron microscopy showed that *F. nucleatum* possesses the ability to invade CRC tumour cells (Bullman *et al.*, 2017; Wang *et al.*, 2021).

1.2.4.3 Metabolic diseases

An altered gut microbial composition is associated with metabolic diseases, including cardiovascular diseases (CVDs), obesity, diabetes, or non-alcoholic fatty liver disease with several metabolites identified as potential mediators of these diseases.

TMAO has been linked with early atherosclerosis and an elevated long-term mortality risk for CVDs (Day-Walsh *et al.*, 2021). Mechanistically, TMAO can activate the mitogen-activated protein kinase (MAPK) and NF-κB signalling pathways in endothelial cells and smooth muscle cells (Roncal *et al.*, 2019; Zheng and He, 2022). The MAPK signalling pathway can be triggered by growth factors, pathogen-associated molecules, and inflammatory cytokines, leading to a MAPKKK-MAPKK-MAPK-TFs signalling cascade and the subsequent expression of inflammatory cytokines IL-6, IL-8, and TNF-α. NF-κB, a well-established inflammation mediator, plays a crucial role in regulating the activation, differentiation, and effector function of inflammatory immune cells. Consequently, the dysregulation of NF-κB may contribute to the pathogenesis of atherosclerosis by promoting monocyte recruitment (Hou *et al.*, 2022).

Propionate and butyrate show a protective effect against hypertensive cardiovascular damage in animal studies (Bartolomaeus *et al.*, 2019; Hou *et al.*, 2022). Propionate is suggested to play a role in regulating the balance between effector T cells and regulatory T cells, a critical aspect in hypertension and hypertension-induced organ damage (Hou *et al.*, 2022). Additionally, propionate has been associated with a reduced lateralisation of the gap junction protein, connexin 43, in cardiomyocytes, consequently lowering susceptibility to ventricular tachycardia (Bartolomaeus *et al.*, 2019; Hou *et al.*, 2022). Studies have also shown that butyrate can modulate blood pressure through partial inhibition of the brain renin–angiotensin system responsible for blood pressure regulation, as shown in animal models (Wang *et al.*, 2017; Hou *et al.*, 2022).

Propionate and butyrate have also been shown to have anti-obesogenic effects through the stimulation of leptin and anorexigenic hormone synthesis whilst acetate has been reported to induce obesogenic action by inducing secretion of the "hunger hormone", ghrelin and promoting fat storage (Crudele *et al.*, 2023). Increasing evidence in animal models and human studies showed the reduction of butyrate-producing species, including *Faecalibacterium prausnitzii* and *Roseburia intestinalis* as one of the predominant features associated with the onset and development of type-2-diabetes and obesity (Crudele *et al.*, 2023; Peng *et al.*, 2023). Supplementation of butyrate-producing bacteria has been shown to ameliorate weight gain and insulin resistance, however the specific mechanisms between butyrate availability and type-2-diabetes and obesity remain unclear (Li *et al.*, 2020; Gart *et al.*, 2021; Peng *et al.*, 2023). In addition, the administration of tributyrin, a butyrate precursor drug, showed protection from liver stenosis, insulin resistance and obesity in mouse models whilst obese subjects undergoing treatment with vancomycin, an antibiotic known to inhibit the growth of butyrate producers, showed steady development of insulin resistance (Vrieze *et al.*, 2014; Crudele *et al.*, 2023).

1.2.4.4 Neurological disorders

Recently, an increasing body of evidence from diverse studies underscores the significance of the gut microbiota in the progression of various neurological disorders, including Alzheimer's disease (AD), Parkinson's disease (PD) and autism

spectrum disorder (ASD) (Mitrea *et al.*, 2022; Taniya *et al.*, 2022; Bicknell *et al.*, 2023; Gulrandhe *et al.*, 2023). This interplay between the GI tract and the central nervous system is referred to as the gut-brain axis and it is described as a dynamic and bidirectional signalling pathway comprising the immune system, tryptophan metabolism, vagus nerve activity, the enteric nervous system, as well as bioactives (microbial by-products or metabolites) produced by the gut microbiome (Cryan *et al.*, 2019; Gulrandhe *et al.*, 2023).

Pathological features of AD are characterised by the presence of amyloid-β plaques (Masters *et al.*, 1985) and intracellular tau-based neurofibrillary tangles (Grundke-Iqbal *et al.*, 1986). During dysbiosis, the microbial abundance of *E. coli, Shigella* increases whilst the abundance of *E. rectale, B. fragilis, Lactobacilli* and *Bifidiobacteria* decreases. This alteration in microbial composition results in an increase in bacterial amyloid and lipopolysaccharide (LPS) secretion. LPS is an endotoxin and with its pro-inflammatory effects demonstrated in mouse models (Skrzypczak-Wiercioch and Sałat, 2022). Increased bacterial secretion of LPS therefore results in impaired gut permeability and increased release of inflammatory cytokines, IL-6, IL-17A, IL-1β, IL-22 and calprotectin (Kesika *et al.*, 2021). In addition, the increase in bacterial-derived amyloids activates the immune system through interaction with toll-like receptor TLR2 and inducing a proinflammatory signalling cascade, provoking neuronal amyloid production in the brain (W. Zhang *et al.*, 2023). These secretions alter the inflammatory signalling system and trigger neuronal inflammation and damage which eventually leads to neuronal death (Kesika *et al.*, 2021).

PD refers to a chronic neurodegenerative disease characterised by an accumulation of misfolded α-synuclein aggregates, also referred to as Lewy bodies, in dopaminergic neurons within the region of the brain responsible for dopamine production, the *substantia nigra,* as well as in other related circuitry (Zhang, Tang and Guo, 2023). This contributes to the progressive loss of motor function with extensive evidence showing an association between compositional changes in the gut microbiota and the pathogenesis and evolution of PD (Klann *et al.*, 2021; Romano *et al.*, 2021; Gulrandhe *et al.*, 2023; Kleine Bardenhorst *et al.*, 2023; Zhang, Tang and Guo, 2023). It has been widely documented that there is an observed increased in the relative abundance of species from the *Akkermansia*, *Lactobacillus*,

Verrucomicrobia and *Bifidobacterium* genera in PD compared to controls, whilst the relative abundance of *Prevotella*, *Faecalibacterium*, *Bacteroidetes*, and *Blautia* genera is reduced in PD compared to controls. However, despite these associations the underlying molecular mechanisms remain unclear (Romano *et al.*, 2021; Zhu *et al.*, 2022; Z. Li *et al.*, 2023). Studies investigating gut permeability in PD patients showed a decrease in the expression of tight junction proteins occludin and ZO-1 in sigmoid biopsies compared to non-PD controls, indicating impaired barrier function within the GI tract (Clairembault *et al.*, 2015). Notably, it has also been shown that intestinal permeability significantly correlates with expression of α-synuclein within the intestine, increased levels of serum LPS-binding proteins and *E. coli* presence in the gut (Forsyth *et al.*, 2011).

ASD is a neurological and developmental disorder characterised by impairments in cognition, behaviour and communication. ASD is also linked with GI symptoms including constipation, abdominal bloating and diarrhoea with disruptions in the gut-brain axis widely reported in ASD subjects (Davies *et al.*, 2021; Li *et al.*, 2021; Mohammad *et al.*, 2022; Wong *et al.*, 2022; Morton *et al.*, 2023). The relative abundance of organisms associated with ASD compared to controls are inconsistent across studies. However, a cross-cohort multi-level analysis of taxonomic, metabolomic, RNA, immune and dietary data identified a functional architecture along the gut-brain axis correlating with heterogeneity within ASD phenotypes (Morton *et al.*, 2023). Clear differentiation was evident between children with ASD and age- and sex-matched neurotypical controls. A total of 591 ASD-associated taxa were identified, with *Faecalibacterium prausnitzii, Ruminococcus bicirculans* and *Alistipes finegoldii* among the top 25% exhibiting notable increases correlated with elevated IL-6 levels, with this being an indicator of compromised gut permeability. Reduction of 57% of ASD-associated taxa led to reported behavioural and cognitive enhancements, suggesting their potential role in influencing ASD symptoms, although this requires further confirmation (Morton *et al.*, 2023).

1.2.5 *Ruminococcus gnavus* in health and disease

1.2.5.1 *R. gnavus* colonisation of the human gut

R. gnavus was first isolated from human faeces and GI content in 1974 (Moore and Holdeman, 1974a) where it was defined as a novel species and described to have a

highly fermentative nature, with the Latin word *gnavus* meaning busy or active (Moore, Johnson and Holdeman, 1976). Members of the genus *Ruminococcus* have been classified into three genera and families based on 16S rRNA sequencing: *Blautia* (Lachnospiraceae), *Ruminococcus* (Ruminococcaceae) and *Clostridium* (Clostridiaceae) (Liu et al., 2008; Lawson and Finegold, 2015). More recently, Ruminococcus species underwent phylogenetic and genomic scrutiny, and a new genus was proposed; Mediterraneibacter, to which 4 Ruminococcus species now belong to, including *R. gnavus*, with this species belonging to the Lachnospiraceae family (Togo et al., 2018).

R. gnavus is an early coloniser of the human gut (Sagheddu *et al.*, 2016). A 2014 study carried out on infants and children in Bangladesh showed *R. gnavus* to be one of the 24 "age-discriminatory" taxa whose changes in relative abundance over time defined normal microbial maturation (Subramanian *et al.*, 2014). A randomised controlled trial showed a substantial increase in the abundance of *R. gnavus* over time in the faecal microbiota of infants fed an isocaloric extensive protein hydrolysate formula (EHF) compared to cows' milk formula (CMF). *R. gnavus* was also shown to be the most prominent signature, distinguishing the microbial composition of the EHF fed group compared to the CMF fed group (Mennella *et al.*, 2022). These studies suggest that *R. gnavus* play an integral role in priming the microbial composition in the human gut in association with normative weight status and weight gain velocity in infants.

In adults, *R. gnavus* is one of the top 57 species detected in over 90% of human faecal samples from adults as shown by metagenomic sequencing (Qin *et al.*, 2010). A recent metagenomic analysis of the human gut microbiota of healthy individuals revealed the presence of *R. gnavus* in 65% of adults from Ethiopia, China, USA, Spain and Sweden, at an average abundance of 0.3% (Candeliere *et al.*, 2022).

R. gnavus shows strain-specific strategies to survive and persist in the gut microbiota, for example through the production of bacteriocins targeting competitors or through the enzymatic processing of carbohydrates and cross-feeding mechanisms (Crost *et al.*, 2018, 2023).

Bacteriocin production in *R. gnavus* was first documented in *R. gnavus* E1, a strain previously characterised for its anti-*C. perfringens* activity (Ramare *et al.*, 1993). Following this discovery, the production of ruminococcins, a type of bacteriocin, was confirmed to be responsible for the antimicrobial activity of this strain (Dabard *et al.*, 2001). *R. gnavus* strain E1 has the ability to synthesise both ruminococcin A (RumA) and ruminococcin C (RumC) , with RumA being the first of the antimicrobial peptides to be characterised (Dabard *et al.*, 2001) and displaying bactericidal activity against pathogenic *Clostridum* species (Ramare *et al.*, 1993; Dabard *et al.*, 2001). RumC1 is effective against *Clostridium difficile, Clostridium perfringens, Clostridium botulinum, Listeria monocytogenes, Bacillus cereus,* vancomycin-resistant *Enterococcus faecalis,* methicillin-resistant *staphylococcus aureus and* nisin-resistant *Bacillus subtilis* (Balty *et al.*, 2019; Chiumento *et al.*, 2019; Roblin *et al.*, 2020). In recent years, RumC1 has been shown to be effective against *C. perfringens* in a complex community, resulting in reduced abundance of strains in the *Clostridium* cluster XIVa (Roblin *et al.*, 2021). This reduction of *C. perfringens* strains by RumC1 also influenced SCFA production in the gut with an observed increase of acetate and butyrate and a decrease in ammonia and propionate. These results suggest a beneficial influence of *R. gnavus* E1 on gut homeostasis (Roblin *et al.*, 2021).

R. gnavus is particularly adept at persisting in the gut due to its ability to grow on a variety of carbohydrates. The use of complex carbohydrates by *R. gnavus* has been demonstrated in relation to host glycans, including mucin glycans and HMOs with *R. gnavus* ATCC 29149, ATCC 35913 but not E1 having the capacity to forage on mucin glycan epitopes (sialic acid , fucose, blood group antigens) within the intestinal mucus layer (Crost *et al.*, 2013, 2016; Bell *et al.*, 2019; Wu, Crost, *et al.*, 2021; Wu, Rebello, *et al.*, 2021). The ability of these strains to utilise mucin glycans as nutrient source is associated with their expression of glycoside hydrolases (GHs) needed to break the glycosidic bonds at the terminal end of mucin glycan chains such as GH29 and GH95 fucosidases (Wu, Rebello, *et al.*, 2021), GH98 galactosidase (Wu, Crost, *et al.*, 2021) and GH33 intramolecular *trans*-sialidase (IT-sialidase) (Tailford et al., 2015; Owen *et al.*, 2017; Bell *et al.*, 2019). More specifically, *R. gnavus* ATCC 29149 IT-sialidase leads to the release of 2,7-anhydro-Neu5Ac instead of Neu5Ac from mucins, with Neu5Ac being the most common form of sialic acid in humans (Tailford *et al.*, 2015; Bell *et al.*, 2019; Crost *et al.*,

2023). *R. gnavus* is then able to uptake and metabolise 2,7-anhydro-Neu5Ac via a *nan* operon, dedicated to 2,7-anhydro-Neu5Ac catabolism (Bell *et al.*, 2019). This unique sialic acid metabolism pathway serves as a competitive advantage for *R. gnavus* strains to colonise the mucus layer (Bell *et al.*, 2019). *R. gnavus* ATCC 29149 has also been shown to produce propanol and propionate when grown on mucin, fucose and fucosylated glycans (Crost *et al.*, 2013).

R. gnavus E1 has been studied for its capacity to utilise dietary carbohydrates such as legume-derived raffinose family oligosaccharides owing to its panel of GH36 enzymes (Cervera-Tison *et al.*, 2012). In addition, while *R. gnavus* ATCC 29149 is not able to degrade starch, it can utilise starch degradation products released by *R. bromii* L2-63 in co-cultures (Crost *et al.*, 2018). This study also suggested that *R. gnavus* ATCC 29149 is able to utilise vitB12 as *R. bromii* L2-63 showed a down-regulation in vitB12-dependent methionine biosynthesis when grown in co-culture with *R. gnavus*, compared to the growth of *R. bromii* in monoculture, suggesting that vitB12 availability decreases in the presence of *R. gnavus* ATCC 29149 (Crost *et al.*, 2018). When grown in monoculture on glucose and in co-culture with *R. bromii* on starch, *R. gnavus* ATCC 29149 produces propanediol as main end-fermentation product (Crost *et al.*, 2018).

1.2.5.2 Association between *R. gnavus* and diseases

Although *R. gnavus* is part of the healthy human gut microbiota, it shows disproportionate representation in GI- and non-GI related disorders including IBD, metabolic diseases and neurological disorders, as recently reviewed (Crost *et al.*, 2023). Some of the metabolites and molecules produced by *R. gnavus* strains have been identified and may be implicated in the onset or progression of these diseases as illustrated in Figure 8. However, it remains unclear as to whether *R. gnavus* plays a direct role in the development of disease or whether it benefits from the microbial and environmental changes brought about during disease. A recent comparative genomic study showed that only 3.74% of the 28,072 predicted genes represented the core genes shared amongst *R. gnavus* 152 strains, highlighting the vast phylogenomic divergence across *R. gnavus* strains and likely an explanation to the diverse effects on host health. In addition, genomic evidence highlighted both host beneficial and detrimental properties of *R. gnavus* with the presence of coding

sequences for vitamin production, arsenic detoxification as well as antibiotic-resistance and virulence (Abdugheni *et al.*, 2023).

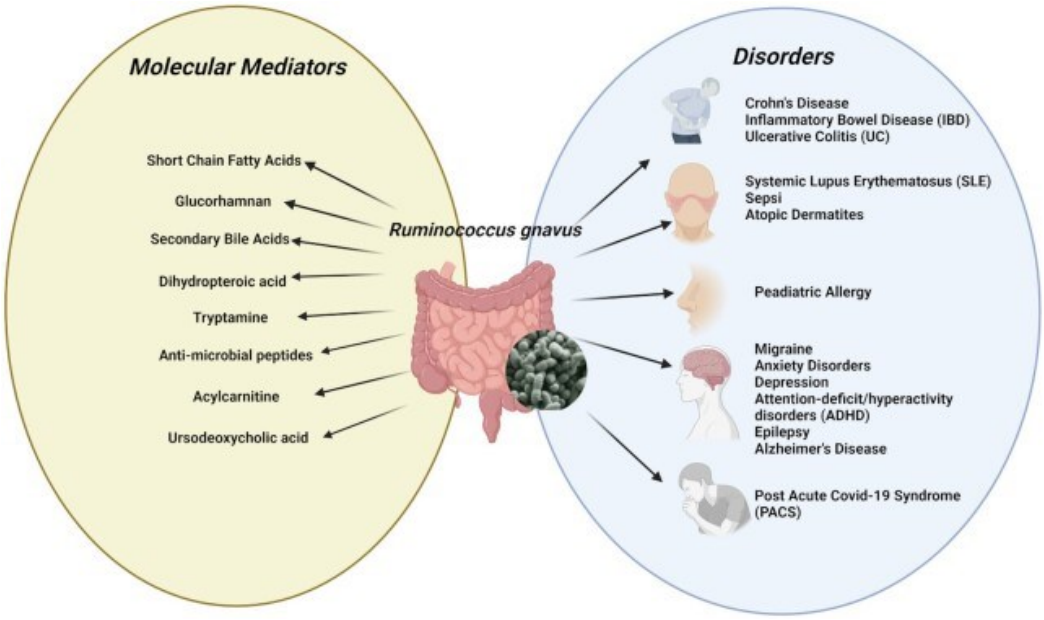

Figure 8 Illustration of *R. gnavus* associated diseases. The figure highlights disorders associated with *R. gnavus* including inflammatory bowel disease, systemic lupus erythematous, sepsis, atopic dermatites, paediatric allergy, migrane, anxiety disorder, depression, attention deficit/hyperactivity disorder (ADHD) and post acute covid 19 syndrome . The Figure aslo highlights molecular mediators of disease including short chain fatty acids, glucorhamnan, secondary bile acids, dihydropteroic acid, tryptamine, anti-microbial peptides, acylcarnitine and ursodeoxycholic acid. Taken from Crost *et al.*, 2023.

1.2.5.2.1 *R. gnavus* and IBD

The association between *R. gnavus* and IBD has been widely documented, with a consistent increase in *R. gnavus* abundance being positively associated with disease activity, however a causal effect is yet to be demonstrated (Hall *et al.*, 2017; Henke *et al.*, 2019; Wu *et al.*, 2024). This correlation has been shown to be strain-dependent with a pangenome analysis of *R. gnavus* revealing a distinct functional repertoire in strains differentially abundant in IBD (Hall *et al.*, 2017). IBD-associated *R. gnavus* strains possess genes involved in oxidative stress responses, adhesion and iron-acquisition suggesting a potential adaptive mechanism allowing persistence in the IBD gut (Hall *et al.*, 2017). A human study investigating the effects of FMT on disease remission in UC found a positive correlation between patients who relapsed and donor microbiota containing high levels (2%) of *R. gnavus*. *R. gnavus* was identified in concentrations 3.8-fold greater than that which

was seen in donor samples from patients in sustained remission, suggesting a causal role in IBD (Fuentes *et al.*, 2017). Recently, *R. gnavus* has been proposed as a potential risk factor for UC as network analyses revealed it as one of the top two critical UC-associated species due to it showing significantly high abundance across two enterotypes (Wu *et al.*, 2024).

Contrastingly, mouse models have shown that *R. gnavus* ATCC 29149 supplementation enhanced Reg3γ expression, an important antimicrobial peptide, produced in gut epithelial Paneth cells, that helps maintain spatial segregation between the epithelium and the microbiota and promotes gut homeostasis (Surana and Kasper, 2017). This study showed that *R. gnavus* reduced induced colitis in gnotobiotic mice due to its interaction with immune and gut epithelial cells (Surana and Kasper, 2017). A further study supported these findings by showing that *R. gnavus* ATCC 29149 led to a decrease in the severity of inflammation in mouse models of colitis (Grabinger *et al.*, 2019).

At the molecular level, *R. gnavus* ATCC 29149 is able to synthesise and secrete a TLR4-dependent, inflammatory glucorhamnan polysaccharide which has been shown to stimulate dendritic cell production of inflammatory cytokines which may contribute to CD pathology (Henke *et al.*, 2019). However, a follow up study showed that some *R. gnavus* strains including ATCC 29149 possess a large capsular polysaccharide conferring tolerogenic properties *in vitro* and in mouse models (Henke et al., 2021), which may explain the discrepancies between *in vitro* and *in vivo* findings.

1.2.5.2.2 *R. gnavus* and metabolic diseases

R. gnavus is linked to factors associated with metabolic syndrome, including increased body fat percentage, visceral adipose tissue, serum triglycerides, C-reactive protein (CRP), HbA1c (Mineharu *et al.*, 2022; Yan *et al.*, 2022). *R. gnavus* has been found to be amongst the intestinal bacteria highly enriched in patients with high visceral fat area as well as being positively correlated with inflammatory and metabolic indicators, specifically white blood cell and blood neutrophil count (Yan *et al.*, 2022).

However, in mice, *R. gnavus* TS8243C strain was shown to ameliorate growth and metabolic abnormalities when added to the microbiota from undernourished donors

in recipient animals by modulating acylcarnitine metabolites, revealing *R. gnavus* as a potential therapeutic target (Blanton *et al.*, 2016).

R. gnavus abundance was proposed as an effective determinant in distinguishing the rare cerebrovascular condition, moyamoya disease, against controls with *R. gnavus* enrichment positively correlated with this disease and *R. gnavus* involvement suggested to be linked to its pro-inflammatory properties (Mineharu *et al.*, 2022). Additionally, *R. gnavus* has been reported in association with systemic lupus erythematosus (Azzouz *et al.*, 2019) and Kawasaki disease (Morimoto *et al.*, 2016), two risk factors of moyamoya syndrome. However, observations in differential abundance are inconsistent across metabolic disease studies with a reduction in the relative abundance of *R. gnavus* seen in patients with coronary heart disease complicated with non-alcoholic fatty liver disease (Y. Zhang *et al.*, 2019).

Recently, levels of *R. gnavus*, tryptamine, and phenethylamine have been shown to be positively associated with insulin resistance in type 2 diabetes (T2D) patients and patients with irritable bowel syndrome (IBS) (Zhai *et al.*, 2023). Monoassociation of *R. gnavus* ATCC 29149 in germ free mice resulted in reduced insulin sensitivity and glucose control. Mechanistically, administration of *R. gnavus*-derived metabolites tryptamine and phenethylamine was shown to weaken insulin signalling, with this signalling mediated by the trace amine-associated receptor 1 (TAAR1)-extracellular signal-regulated kinase (ERK) signaling axis (Zhai *et al.*, 2023). These findings therefore suggest a causal role of *R. gnavus* in the pathogenesis of metabolic disorders through disruption of insulin signalling pathways.

1.2.5.2.3 *R. gnavus* and neurological diseases

Altered levels of *R. gnavus* is commonly reported in patients with neurological disorders (Wan *et al.*, 2020; Nishiwaki, Ito, *et al.*, 2022; Nishiwaki, Ueyama, *et al.*, 2022). *R. gnavus* has been shown to be one of the species significantly reduced in the faecal samples of children with attention-deficit/hyperactivity disorder (ADHD) in a case-control study (Wan *et al.*, 2020). This alteration was associated with differences in the metabolic pathways of neurotransmitters (e.g. serotonin and dopamine) and may contribute to ADHD symptoms (Wan *et al.*, 2020). A recent study identified *R. gnavus* as being increased in faecal samples of patients with PD (Nishiwaki, Ito, *et al.*, 2022). *R. gnavus* has also been shown to be associated in

dementia where relative abundance has been found to be significantly enriched in sufferers compared to healthy controls (Lubomski *et al.*, 2022; Nishiwaki, Ueyama, *et al.*, 2022). Similarly, patients with post-stroke cognitive impairment also displayed *R. gnavus* enrichment in faecal samples compared with healthy subjects (Feng *et al.*, 2021). At the mechanics level, gnotobiotic mouse studies investigating the role of *R. gnavus* in gut-brain axis identified changes in metabolites associated with brain function such as tryptamine, indolacetate, and trimethylamine N-oxide (Coletto et al., 2023).

These studies underscore the need to investigate the mechanisms of *R. gnavus* adaptation to the gut at the strain level for the development of strategies to target and modulate *R. gnavus* strains in humans.

1.3 Cobamides, the vitamin B12 family of cofactors

1.3.1 Role of vitamin B12 (vitB12) on human health

The discovery of vitB12 arose from studies investigating the cause of pernicious anaemia, a condition first described by Thomas Addison in 1849 (Thomas, 1849). Initially recognised as an extrinsic factor, vitB12 was discovered in the 1920s by Minot, Murphy, and Whipple (Robscheit-Robbins and Whipple, 1925; Minot and Murphy, 1926). Their research demonstrated that the addition of liver to the diet alleviated the symptoms of pernicious anaemia (Robscheit-Robbins and Whipple, 1925; Minot and Murphy, 1926). The vitamin was then isolated from liver samples, revealing a deep-red pigment (Lester Smith, 1948; Rickes *et al.*, 1948). Dorothy Hodgkin's groundbreaking work using X-ray crystallography later revealed the compound's structure, unveiling it as a cyanolated, cobalt-containing, amidated tetrapyrrole (Hodgkin *et al.*, 1956). Consequently, it was named cyanocobalamin (CNCbl), and technically, vitB12 specifically refers to cyanocobalamin.

Humans have an auxotrophic requirement for vitB12, with the UK stipulating that the recommended nutrient intake (RNI) for vitB12 in adults is 1.5 µg per day ('Government Dietary Recommendations Government recommendations for energy and nutrients for males and females aged 1-18 years and 19+ years', 2016). In humans, vitB12 is required as a co-factor of two enzymes, methionine synthase (MetH) and methylmalonylCoA mutase (MCM) which are essential for the synthesis

of deoxyribonucleic acid (DNA), myelin, fatty acids and red blood cells (Ankar and Bhimji, 2021).

VitB12 is synthesised exclusively by few bacteria and archaea whilst plants and animals cannot make their own (Roth, Lawrence and Bobik, 1996). In humans, diet is the main source of vitB12, particularly, the milk and meat of herbivorous ruminant animals such as sheep and cattle. Ruminants acquire vitB12 from vitB12-producing bacteria within the forestomach. Subsequently, it is transferred and accumulates in the tissues of these animals (Watanabe and Bito, 2018).

Within the human gut, a large proportion of these vitB12 synthesising organisms are found in the large intestine. Until recently, it was widely accepted that endogenous vitB12 produced by bacteria within the colon was not bioavailable due to the receptors required for absorption of this vitamin being located in the small intestine, upstream of the local corrinoid (cofactor structurally similar to vitB12) production (Seetharam and Alpers, 1982). However, a recent study using [13C]-CNCbl presented direct evidence of colonic absorption (Kurpad *et al.*, 2023). In this study a 7% uptake of cyanocobalamin from a 5 µg dose of [13C]-cyanocobalamin administered directly into the ascending colon was observed in plasma (Kurpad *et al.*, 2023). This colonic absorption of vitB12 suggests a potential role for the gut microbiota in supporting the vitB12 requirements of the host and the development of gut microbiota targeted strategies for the treatment of vitB12 deficiencies.

VitB12 deficiency is a global public health concern and is associated with nervous system diseases, pernicious anaemia, neuropathy and disturbances in cell division (Issac *et al.*, 2015; Xu *et al.*, 2018). Worldwide, malabsorption due to ageing, poor nutrition, and acquired defects in vitB12 metabolism are primary causes of deficiency with inborn errors of vitB12 metabolism considered rare (Elangovan and Baruteau, 2022). VitB12 deficiency is often under-diagnosed during pregnancy and in infants born to mothers with insufficient micronutrient levels (Wheeler, 2008; Sarafoglou *et al.*, 2011). Adequate vitB12 intake is strongly recommended during pre-conception, pregnancy, and post-partum (Monsen *et al.*, 2001; Rasmussen, Fernhoff and Scanlon, 2001; Bjørke-Monsen *et al.*, 2008; Hinton *et al.*, 2010). Other at-risk populations include the elderly, vegetarians, vegans, recipients of bariatric surgery (Majumder *et al.*, 2013; Kwon *et al.*, 2014), and individuals with GI diseases featuring ileal resections >20 cm (Battat *et al.*, 2014). Certain medications, such as

metformin (Greibe *et al.*, 2013; Aroda *et al.*, 2016) and proton-pump inhibitors (Howden, 2000; Wilhelm, Rjater and Kale-Pradhan, 2013) may transiently induce cobalamin deficiency, which can be reversible with the completion of treatment and/or oral vitB12 supplementation.

Inadequate vitB12 supply and genetic defects affecting cellular processing and trafficking of the vitamin result in the accumulation of homocysteine (Hcy) and methylmalonic acid (MMA). These compounds enter circulation, leading to hyperhomocystinemia, associated with increased cardiovascular, cerebrovascular, and thromboembolic diseases (Chrysant and Chrysant, 2018) and methylmalonic acidemia, an inherited disorder in which the body is unable to process certain proteins and fats (lipids) (Zhou, Cui and Han, 2018).

1.3.2 Vitamin B12 biosynthesis

The biosynthesis of cobalamin (Figure 9) involves up to 30 enzyme-mediated steps. At the core, it possesses a corrin ring, in the form of cobyric acid with a central cobalt ion (Figure 9). Typically, a 5,6-dimethylbenzimidazole (DMB) can be found covalently bonded to the central cobalt ion in the lower ligands of the vitB12 structure, whilst a cyano, methyl, hydroxy or 5′-deoxyadenosyl group as seen in Figure 9, can be attached to the cobalt ion in the upper ligand, with the functional group being critical to the function of the coenzyme (Costa *et al.*, 2020).

Methylcobalamin (MeCbl) and adenosylcobalamin (AdoCbl) are the only biologically active forms of cobalamin with MeCbl utilised in the last stage of methionine biosynthesis and AdoCbl required for radical-based reactions, including dehydrations, reductive dehalogenations and deaminations (Cauthen, Foster and Woods, 1966; Banerjee and Ragsdale, 2003).

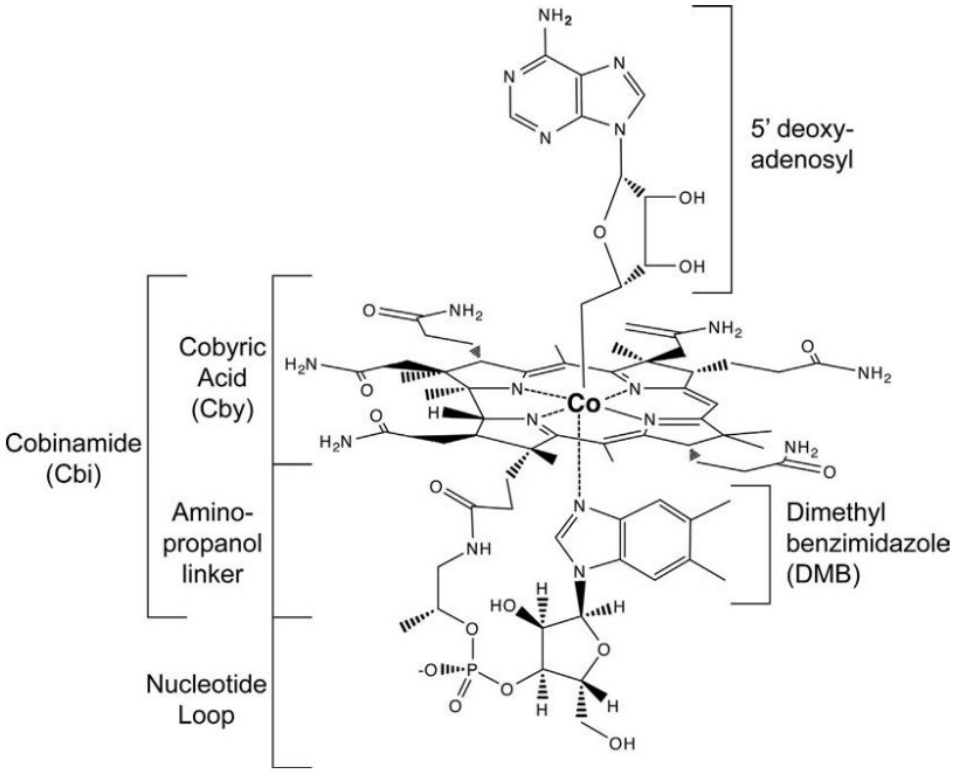

Figure 9 Structure of Adenosylcobalamin. Figure depicts amidated corrin ring and central cobalt ion. A covalent organometallic bond can be seen between 5' deoxyadenosine and the central cobalt ion. An aminopropanol linker connects the nucleotide loop structure to the corrin ring. 5,6-dimethylbenzimidazole (DMB) is located at the base of the AdoCbl structure. Taken from Costa et al., 2020.

The biosynthesis of vitB12 is typically divided into three parts: 1) The synthesis of uroporphyrinogen III from either glycine and succinyl-CoA or glutamyl-tRNA; 2) The corrin ring synthesis, which occurs via two alternative pathways: the anaerobic or aerobic pathway (as presented in Figure 10); and 3) the corrin ring adenosylation, attachment on the amino-propanol linker and the assembly of the nucleotide loop, bridging the lower ligand to the central cobalt ion of the corrin ring. Some microorganisms are also able to synthesise vitB12 through the salvage pathway by absorbing corrinoids (Fang, Kang and Zhang, 2017) (Figure 10).

1.3.2.1 Synthesis of uroporphyrinogen III

Briefly, δ-Aminolevulinate (ALA) is the first precursor of the vitB12 biosynthesis pathway and is synthesised through either the C_4 or C_5 pathway. In the C_4 pathway, ALA synthase (HemA) catalyses the formation of ALA from glycine or succinlyl-CoA whilst, in the C_5 pathway, ALA is formed from glutamate through three enzymatic

reactions. Glutamate-tRNA ligase (GltX) catalyses the conversion of glutamate to L-glutamyl-tRNA in a two-step reaction. This is followed by the catalysis of L-glutamyl-tRNA(Glu) to glutamate 1-semialdehyde (GSA) by Glutamyl-tRNA reductase (HemA) and GSA is then converted to ALA by glutamate-1-semialdehyde 2,1-aminomutase (HemL) (Figure 10) (Avissar, Ormerod and Beale, 1989).

Following this, two molecules of ALA are condensed, forming porphobilinogen (PBG) through porphobilinogen synthase (HemB) and four molecules of PBG are then polymerised and cyclised to form the macrocyclic uroporphyrinogen III, catalysed by PBG deaminase (HemC) and uroporphyrinogen-III synthase (HemD) (Figure 10) (Costa *et al.*, 2020).

1.3.2.2 Synthesis of corrin ring

Uroporphyrinogen-III is methylated to form precorrin-2 by Uroporphyrinogen-III C-methyltransferase (CysG/CobA/MET_{1p}), a two-step reaction involving the donation of two S-adenosyl-L-methionine (SAM)-derived methyl groups (Figure 10) (Martens *et al.*, 2002; Zappa, Li and Bauer, 2010). In *E. coli* and *S.* Typhimurium, two organisms that synthesise vitB12 anaerobically, this reaction is catalysed by the fusion enzyme, CysG, within the anaerobic pathway (Warren *et al.*, 1990), whilst in *Pseudomonas denitrificans*, an organism that synthesises vitB12 aerobically, CobA is the responsible enzyme used in the aerobic pathway (Raux *et al.*, 1996; Warren and Escalante-Semerena, 2008; Moore and Warren, 2012; Fang, Kang and Zhang, 2017). MET_{1p} acts as a uroporphyrinogen III methyltransferase in *Saccharomyces cerevisiae* (Raux *et al.*, 1999).

At this point, the pathway diverges into its anaerobic and aerobic branches, reconverging at the production of coby(II)rinic acid a, c-diamide, where CbiA/CobB, belonging to the family of glutamine amidotransferases, amidates the a and c side chains (Costa *et al.*, 2020). The anaerobic pathway involves mostly cbi genes, whilst the aerobic pathway mostly involves cob genes (Figure 10).

1.3.2.3 Corrin ring adenosylation, attachment of the amino-propanol linker and the assembly of the nucleotide loop

Coby(II)rinic acid a, c-diamide is adenosylated to yield adenosylcobyrinic acid a,c-diamide by CobA/CobO (Crouzet *et al.*, 1991). The second of the amidotransferases involved in the vitB12 biosynthesis pathway, CobQ/CbiP, amidate the b, d, e and g

side chains, sequentially to form adenosylcobyric acid (Figure 10) (Williams *et al.*, 2007).

In the attachment of the amino-propanol linker, PduX, the threonine kinase, phosphorylates L-threonine to produce L-threonine phosphate and CobD converts this to aminopropanol-P. This aminopropanol group is then attached to the f side chain of the adenosylcobyric acid molecule by CbiB to form adenosylcobinamide phosphate (Figure 10) (Costa *et al.*, 2020).

The nucleotide loop connects the lower ligand to the corrin ring through activation of adenosylcobinamide phosphate by CobU to form adenosylcobinamide-GDP. The lower base also requires activation, and this is carried out through two enzymatic reactions, yielding α-ribazole from 5,6- dimethylbenzimidazole (Figure 10) (Costa *et al.*, 2020).

The activated adenosylcobinamide-GDP and α-ribazole are then assembled by CobS, finally yielding Adenosylcobalamin from adenosylcobalamin 5'-phosphate by CobC (Figure 10) (Costa *et al.*, 2020).

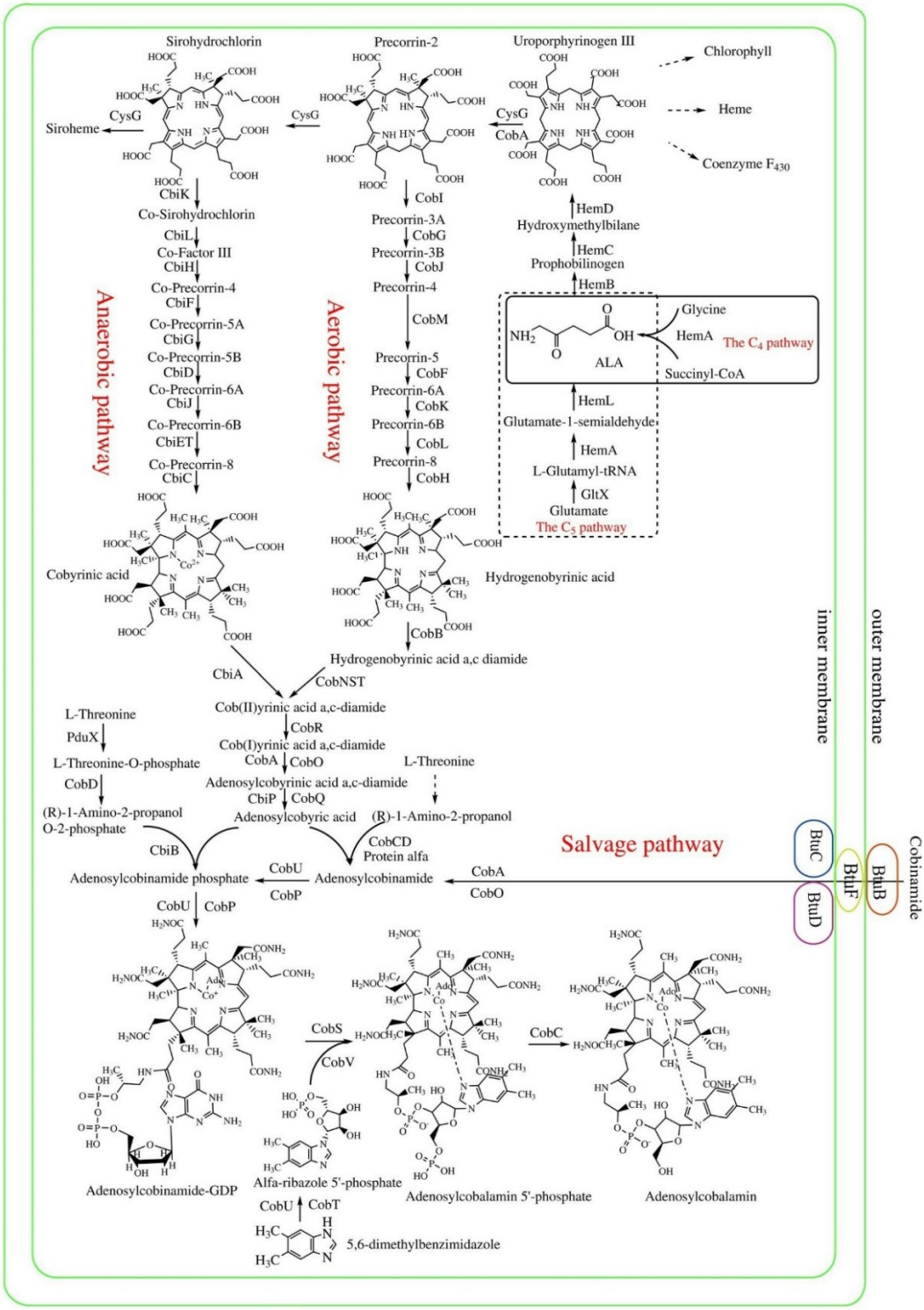

Figure 10 Biosynthesis pathway of Adenosylcobalamin. Biosynthesis of adenosylcobalamin from aminolevulinic acid (ALA) and including both the aerobic and anaerobic pathway along with the salvage pathway. This figure is based on the anaerobic and aerobic vitB12 biosynthesis pathways best studied in Salmonella Typhimurium and Pseudomonas denitrificans, respectively. Taken from Fang, Kang and Zhang, 2017.

In gram-negative bacteria, the ATP-binding cassette (ABC) transport system, made up of BtuF, BtuC and BtuD is used to transport exogenous corrinoids into the cells for vitB12 synthesis, through the salvage pathway (Figure 10) (Seetharam and Alpers, 1982; DeVeaux and Kadner, 1985). The salvage pathway starts with the tonB-dependent transport of corrinoids across the outer membrane via recognition by BtuB, an outer membrane binding protein, delivering them to BtuF, the periplasmic corrinoid-binding protein (Kadner and McElhaney, 1978). BtuF then delivers the corrinoid molecule to the BtuCD complex of the inner membrane (Figure 10) where it is later adenosylated by CobA and CobO to form adenosylcobinamide, which then undergoes several enzymatic reactions to form adenosylcobalamin (Martens *et al.*, 2002).

1.3.3 Cobamide production and metabolism by the human gut microbiota

1.3.3.1 Cobamide modelling and synthesis by gut bacteria

In humans, unabsorbed vit12 from the diet reaches the large intestine, where gut bacteria metabolise ~80% of it, converting the compound into other cobamide analogues as described below (Brandt, Bernstein and Wagle, 1977; Allen and Stabler, 2008).

In 1977, Brandt et al., identified the bacterial conversion of orally-administered cyanocobalamin into other cobamide analogues in patients with bacterial overgrowth in the small intestine. Radioactivity and bioautographic evidence revealed the presence of cobamide analogues [Ade]CNCBA, [2-Me Ade] CNCba, [CN]2Cbi and factor E) in jejunal contents, with these analogues representing 25% of the administered cyanocobalamin (Brandt, Bernstein and Wagle, 1977).

Complete identification and quantification of cobalamin and individual cobalamin analogues from human faecal samples was first carried out in 2008 (Allen and Stabler, 2008). Using liquid chromatography–mass spectrometry (LC-MS), cobalamin, cobinamide and 6 cobalamin analogues containing bases other than 5,6-dimethylbenzimidizidole were identified and quantified in faecal samples from healthy subjects consuming ≤ 25 µg cobalamin supplements (Allen and Stabler, 2008). These 6 analogues were identified to possess, 2-methyladenine, p-cresol, adenine, 2-(methylthio)adenine, 5-hydroxybenzimidazole or phenol in the lower ligand in replacement of 5,6-dimethylbenzimidizidole (Figure 11).

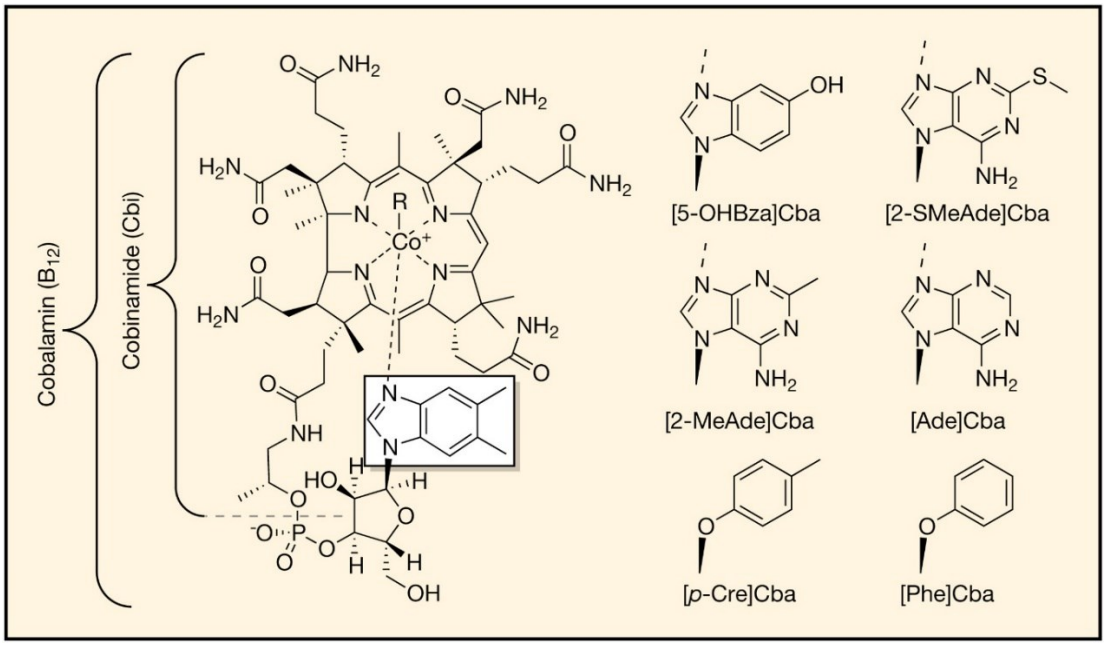

Figure 11Structures of cobamides. Figure illustrates the heterogeneity of the lower ligand of vitB12 with alternative bases displayed in replacement of 5,6-dimethylbenzimidizidole including 2-methyladenine, p-cresol, adenine, 2-(methylthio)adenine, 5-hydroxybenzimidazole or phenol. Taken from Degnan, Taga and Goodman, 2014.

The vitB12 analogue containing 2-methyladenine in the lower ligand made up on average 60.6% of total vitB12 extracted from samples with cobalamin representing only a small proportion (1.4%) (Allen and Stabler, 2008). In this study, it was also revealed that healthy subjects ingesting 1–2 mg cyanocobalamin on a one-time or daily basis demonstrated an overall increased faecal content of analogues containing either 2-methyladenine, p-cresol, adenine, or 2-(methylthio)adenine in their lower ligand compared to subjects on a lower supplement dosage (Allen and Stabler, 2008). The presence and increase of cobalamin analogues following cobalamin supplementation is strongly indicative of cobamide remodelling in the gut.

The mechanisms underpinning corrinoid remodelling in bacteria were first described in *Rhodobacter sphaeroides*, where the process is initiated by CbiZ which functions to remove the aminopropanol linker and nucleotide loop during remodelling, allowing the replacement of an alternative lower ligand (Gray, Tavares and Escalante-Semerena, 2008; Gray and Escalante-Semerena, 2009).

Akkermansia muciniphila strain Muc^T is an example of a human gut symbiont that does not possess the genetic machinery to be able to synthesis corrinoids *de novo*

but encodes four cobamide-dependent enzymes: MetH, MCM, ribonucleotide reductase NrdJ, and epoxyqueuosine reductase QueG (Kirmiz *et al.*, 2020). Notably, *A. muciniphila* strain Muc^T has been shown to be able to remodel cobamides for its use (Mok *et al.*, 2020). *A. muciniphila* displayed similar growth rates when grown on seven different cobamides, showing little to no selectivity (Mok *et al.*, 2020) and further investigation demonstrated the capacity of *A. muciniphila* strain Muc^T to convert supplemented cobamide into pseudocobalamin by cleaving the lower ligand of available cobamide and replacing it with an adenine base (Mok *et al.*, 2020). However, genomic analysis of the *A. muciniphila* strain Muc^T could not identify CbiZ in its genome. Instead a novel enzyme was identified, CbiR, capable of hydrolysing the phosphoribosyl bond within the nucleotide loop of cobamide, subsequently remodelling the initial structure (Mok *et al.*, 2020). Comparative genomic analyses revealed the presence of the CbiR gene in 75 *A. muciniphila* strains of human and mouse intestinal origin (Mok *et al.*, 2020). Additionally, homologs of the CbiR gene have been identified in approximately 276 other microbial taxa across 22 phyla. These results strongly indicate the potential of other bacteria in utilising a diverse range of cobamide in the environment due to the lack of selectivity demonstrated in the CbiR-initiated remodelling mechanism (Mok *et al.*, 2020).

Few gut bacteria have the capacity to *de novo* synthesise cobamides. *Enterococcus* is an ubiquitous member of the GI tract in both humans and animals with significant influence in environmental, food, and clinical microbiology (Li *et al.*, 2017). Strains of *Enterococcus faecalis* (LZ32 and LZ83) and *faecium* (LZ86, LZ18, and LZ85), isolated from infant faeces, have been documented as vitB12-producers with strains synthesising this compound in varying quantities (Li *et al.*, 2017). *E. faecalis* LZ83 and *E. faecium* LZ86 strains were shown to produce the highest quantities of vitB12 across the five isolates with intracellular production quantified at 338.1 ± 19.11 and 499.8 ± 83.7 µg/L, respectively. HPLC analysis confirmed the presence of AdoCbl and MeCbl in *E. faecalis* LZ83 cell extracts and the presence of AdoCbl in *E. faecium* LZ86 cell extracts, with both of these forms being biologically active in humans (Li *et al.*, 2017).

More notable is the cobamide-synthesising capacity of *Lactobacillus* strains, including *Lactobacillus reuteri* CRL1098 (Taranto *et al.*, 2003), *Lactobacillus casei* L4 (Giri *et al.*, 2018), *Lactobacillus rossiae* DSM 15814T (De Angelis *et al.*, 2014)

and *Lactobacillus fermentum* CFR 2195 (Basavanna and Prapulla, 2013). Intracellular and extracellular vitB12 production has been documented in *Lactobacillus casei* L4 following 48 h fermentation in coconut water, in efforts to synthesise a functional beverage aimed at targeting vitB12 deficiencies (Giri *et al.*, 2018). Comparative genomic analyses of *L. rossiae* strain DSM 15814T identified a complete *de novo* vitB12 biosynthetic pathway (De Angelis *et al.*, 2014). To confirm the capacity of *L. rossiae* strain DSM 15814T to synthesis vitB12, a vitB12 bioassay was carried out using *Lactobacillus delbrueckii* ATCC 7830 as an indicator strain due to its inability to grow without vitB12 availability. Using this assay vitB12 production from cytoplasmic extract was confirmed in *L. rossiae* strain DSM 15814T (De Angelis *et al.*, 2014). Competitive ELISA techniques using a mutant *E. coli* strain auxotrophic for vitB12 confirmed intracellular vitB12 production by *L. fermentum* CFR 2195, isolated from infant faeces, following a 96 h fermentation, resulting in the synthesis of 29.45 ng vitB12/g dry biomass (Basavanna and Prapulla, 2013).

Based on *in silico* analyses of vitB12 synthesis pathways it is estimated that 25% of gut bacteria possess the genetic capability to synthesise vitB12, providing them a competitive advantage within the intestinal microbial community (Degnan *et al.*, 2014).

1.3.3.2 Cobamides as a co-factor and regulator of bacterial enzymes

Over 80% of sequenced gut-associated microbial species are predicted to require exogenous cobamides which are used as essential co-factors in numerous enzymatic reactions (Degnan *et al.*, 2014). Microorganisms requiring cobamides as a co-factor but lacking the genes for *de novo* synthesis (see section 1.3.2) include *Bacteroides fragilis*, *Bacteroides thetaiotaomicron*, *Bacteroides vulgatus*,*Clostridioides difficile*, *Enterococcus faecalis*, *Escherichia coli*, and *Parabacteroides distasonis* (Mok *et al.*, 2020). Distinct from other co-factors, cobamides are extensively structurally and subsequently functionally diverse. Some cobamide-dependent reactions require specific cobamide binding for metabolism, and so the ability to convert one form of cobamide into the preferred form serves a competitive advantage in microbial communities. *In vitro* studies have demonstrated distinct selectivity in the binding of co-factors to bacterial enzymes

with the uptake or production of less preferable cobamides resulting in inhibited growth (Mok and Taga, 2013; Helliwell *et al.*, 2016; Keller *et al.*, 2018).

Cobamide-dependent MetH and MCM are amongst the most abundant cobamide-dependent enzymes present in the human gut microbiota (Mascarenhas *et al.*, 2022).

MetH is an essential enzyme, catalysing three distinct methyl-transfer reactions for the synthesis of methionine (Figure 12). The synthesis of methionine via MetH is a methylcobalamin-dependent reaction and involves the conversion of methyltetrahydrofolate (MTF) to tetrahydrofolate (THF), in addition to the conversion of homocysteine to methionine. In doing so, MetH recruits "supernucleophile" cobalt (I) to source a methyl group from MTF yielding THF. A methyl group from methylcobalamin is also transferred to homocysteine yielding methionine (Jensen, 2005; Mendoza *et al.*, 2023). It takes approximately 2000 catalytic turnovers for MetH to become inactive, however methylation by S-adenosyl-L-methionine (AdoMet, SAM) restores functionality (Mendoza *et al.*, 2023).

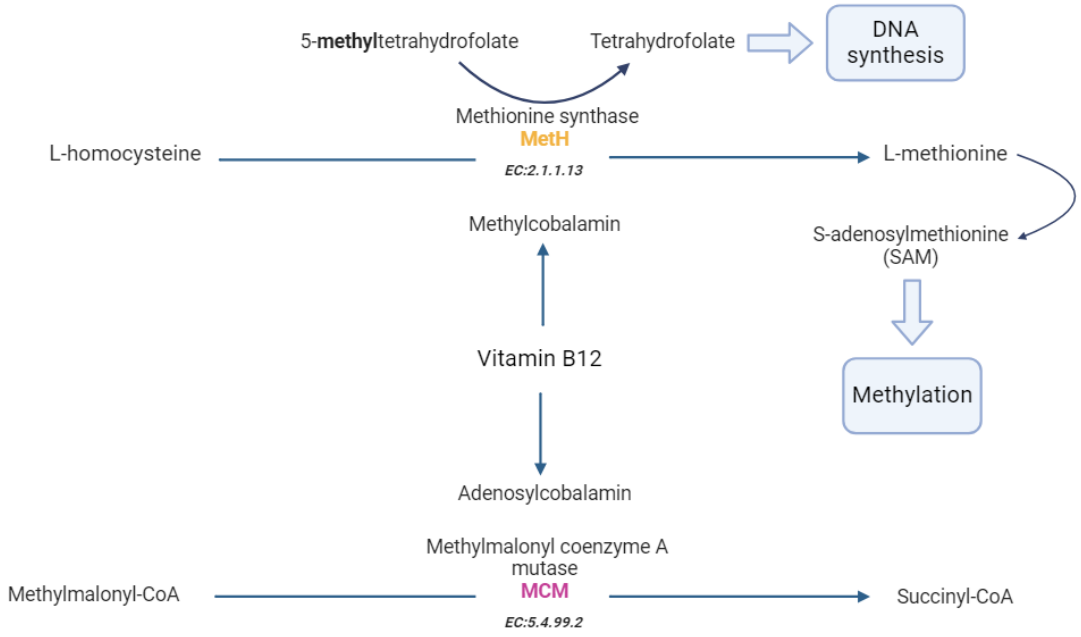

Figure 12 VitB12 as a coenzyme. Active forms of vitB12, Methylcobalamin and Adenosylcobalamin act as coenzymes in the conversion of homocysteine to methionine and the conversion of pyruvate to propionate, respectively. The conversion of homocysteine to methionine is carried out by Methylcobalamin dependent methionine synthase where methionine is then used to make S-adenosylmethionine (SAM), required for the methylation of various biochemical reactions. During the conversion of homocysteine to methionine, tetrahydrofolate is also produced and is required for DNA synthesis. The conversion of methylmalonyl CoA to succinyl CoA is catalysed by Adenosylcobalamin during the multi-step bacterial fermentation of pyruvate to propionate. Created with BioRender.com

MCM is conversion of methylmalonyl CoA to succinyl CoA is catalysed by Adenosylcobalamin during the multi-step bacterial fermentation of pyruvate to propionate (Figure 12) (Evans and Mancia, 2007). In MCM, the presence of an adenosyl group in the upper ligand of a cobamide is required for catalytic activity, where the Co-C bond of adenosylcobalamin is homolytically cleaved upon binding, releasing an adenosyl radical that can be used as a catalyst in downstream reactions (Takahashi-Iñiguez *et al.*, 2012; Kumar, Bucher and Kozlowski, 2019). In addition to the above, cobamide selectivity has also been documented for bacterial MCM. A study comparing cobamide-binding affinity of MCM orthologs from cobamide-producing *Sinorhizobium meliloti, Escherichia coli* and *Veillonella parvula*, showed that the native cobamide synthesised by these microbes bound with the highest affinity to the corresponding bacterial MCM ortholog (Sokolovskaya *et al.*, 2019). In this study, differences in catalytic performance of bacterial MCM were also tested, with little to no difference seen in catalytic turnover when adenosylcobalamin, Ado[5-MeBza]Cba, Ado[Cre]Cba or Ado[Phe]Cba was bound to *S. meliloti's* MCM, demonstrating the limited effects of the lower ligand in contrast to the upper ligand requirement of this enzyme (Sokolovskaya *et al.*, 2019).

AdoCbl is also required for ethanolamine ammonia lyase (EutBC), present in 17% of sequenced human gut commensals. EutBC catalyses the conversion of ethanolamine to acetaldehyde and ammonia which can be used by gut bacteria, with the ammonia serving as a supply of reduced nitrogen and the acetaldehyde available for conversion into acetyl-CoA (Degnan *et al.*, 2014; Kaval and Garsin, 2018) .

Gut bacteria that are dependent on cobamides encode multiple corrinoid riboswitches which can be found upstream of various cobamide-dependent genes (Degnan, Taga and Goodman, 2014b). Corrinoid transport, corrinoid biosynthesis, corrinoid-dependent and independent enzymes make up nearly half of the approximate 4000 genes known to be regulated by corrinoid riboswitches in human gut microbes (Degnan *et al.*, 2014). Consequently, additional genes may be susceptible to expression modulation in environments where corrinoids are readily available. In *Bacteroidetes*, half of the sequenced genomes have been shown contain a multi-subunit carboxylase gene cluster (EC 6.4.1.-) regulated by a corrinoid riboswitch (Rodionov *et al.*, 2003). Additionally, genomic studies of the human gut

microbiome have identified approximately 100 ORFs regulated by corrinoid riboswitches (Degnan *et al.*, 2014). These ORFs encode predicted transcriptional regulators and DNA-binding proteins, suggesting their potential influence on the expression of numerous downstream genes (Degnan *et al.*, 2014).

1.3.3.3 VitB12 as a modulator of the gut microbial ecology

Given the distribution of cobamide auxotrophs (~80%) and cobamide synthesisers (~25%) within the human gut microbiota it is expected that the competition and sharing of cobamides in the gut contributes to shaping the gut microbial community (Degnan *et al.*, 2014). A systematic review on the impact of vitB12 supplementation on the gut microbiome analysed a total of 22 studies including 3 *in vitro,* 8 animal and 11 human observational studies (Guetterman *et al.*, 2022). Studies reported alterations in microbial abundance, α diversity and β-diversity, and SCFA production in response to cobamide intake, status and supplementation, however the influence of cobamides on the gut microbiome's composition and function were heterogenous across studies.

Findings from *in vitro* studies reported increased alpha diversity in response to cobamide supplementation however results varied depending on the cobamide form and dose administered in addition to co-interventions. One study (Zheng *et al.*, 2021) documented increased alpha diversity in response to low dose (0.78 µg/g) CNCbl-enriched spinach, whilst there was no observed change in the control group, in which there was no cobamide supplementation. In addition a significant decrease in alpha diversity in response to high dose (0.94 µg/g) CNCbl-enriched spinach was observed (Zheng *et al.*, 2021). Within this same study principal component analysis (PCA) plots of relative abundance of OTUs revealed the distinct clustering of groups receiving low dose CNCbl-enriched spinach and high dose CNCbl-enriched spinach away from control groups indicating shifts in microbial community composition due to CNCbl supplementation independent of dosage (Zheng *et al.*, 2021). At phylum level the relative abundance of Bacteroidetes increased in response to CNCbl supplementation with this increase demonstrated at a greater extent in groups receiving low dose CNCbl-enriched spinach compared to high dose (Zheng *et al.*, 2021). Numerous studies have demonstrated anti-inflammatory effects of Bacteroidetes (Bloom *et al.*, 2011; Zhou and Zhi, 2016; Bousbaine *et al.*, 2022; L.

Liu *et al.*, 2022; Price *et al.*, 2024), however some studies have reported its increased abundance linked to IBD (Loh and Blaut, 2012; Nomura *et al.*, 2021; Al-Amrah *et al.*, 2023). These differences in health outcomes are likely due to strain specific differences and so without strain level resolution is it unknown as to where CNCbl supplementation are contributing to improved or reduced health status.

When investigating the effect of cobamides on SCFA production it was observed that butyrate and acetate concentrations decreased in groups receiving high dose CNCbl-enriched and control groups over time, contrastingly, groups receiving low dose CNCbl-enriched spinach demonstrated increased butyrate and acetate concentrations over time. Altogether he results of this study demonstrate a beneficial effect of low dose CNCbl supplementation on gut health compared to high dose (Zheng *et al.*, 2021).

Another study observed a decrease in alpha diversity following 7 days of MeCbl supplementation compared to CNCbl and control groups (Xu *et al.*, 2018). In this study PCA plots of relative abundance of OTUs showed the close clustering of CNCbl treated and control groups whilst MeCbl treated samples formed a distinct cluster (Xu *et al.*, 2018), indicating a reduced effect of CNCbl on microbial shifts and a more pronounced effect elicited by MeCbl. Shifts in relative abundance of bacteria were not documented in this study. In terms of metabolic activity it was reported that MeCbl and CNCbl supplementation resulted in an increase in total SCFAs compared to the control group indicating improved gut health as a result of cobamide supplementation (Xu *et al.*, 2018).

Animal studies have reported heterogenous results for alpha diversity with one study using mouse models documenting no significant difference in CNCbl supplemented groups and control groups (Kelly *et al.*, 2019). Another study using mouse models documented no significant effect of increasing CNCbl dosage on alpha diversity (Lurz *et al.*, 2020). A third mouse study reported reduced alpha diversity upon CNCbl and MeCbl supplementation compared to untreated control groups, however statistical significance was not reported (Zhu *et al.*, 2019). In terms of beta diversity investigations in studies using mouse models, Kelly *et al.*, (2019) observed significant differences at the genus level in response to CNCbl (cyanocobalamin) supplementation compared to control groups (Kelly *et al.*, 2019). However other studies reported no difference in cobamide intervention compared

to control groups (Park, Kang and Sol Kim, 2019; Zhu *et al.*, 2019; Lurz *et al.*, 2020). Reports of shifts in bacterial abundances were also inconsistent with Zhu *et al.*, (2019) demonstrating at the phylum level, mice receiving CNCbl showed higher relative abundances of Bacteroidetes and Proteobacteria and lower Firmicutes compared to those receiving MeCbl (Zhu *et al.*, 2019). Proteobacteria has been considered a microbial signature of dysbiosis in the gut (Shin, Whon and Bae, 2015; Litvak *et al.*, 2017; Rizzatti *et al.*, 2017) and is linked to reduced abundance of Firmicutes (Morgan *et al.*, 2012). The Firmicutes/Bacteroidetes (F/B) ratio is widely accepted as an index of gut health with decreases in the F/B ratio observed in incidences of IBD (Stojanov, Berlec and Štrukelj, 2020).

Both cobamide supplementation groups had lower Bacteroidetes and higher Firmicutes compared to the control group (Zhu *et al.*, 2019). Park, Kang and Sol Kim, (2019) did not observe similar changes at phylum level in response to CNCbl supplementation but instead observed an increased abundance of specific classes within the Proteobacteria phylum, Alphaproteobacteria and Gammaproteobacteria in a cobamide deficient group when compared to the control group (Park, Kang and Sol Kim, 2019). In terms of metabolic effect of cobamide availability, Kelly *et al.*, (2019) observed no significant changes in acetate, propionate or butyrate concentrations in response to CNCbl supplementation (Kelly *et al.*, 2019).

Similarly, findings from observation studies conducted in humans were also inconsistent. It was shown in a cohort of lactating women that alpha diversity was significantly greater in women intaking vitB12 at 3.0–6.3 µg/day compared to 0–1.7, 1.6-2.9 and 6.4 to 18.4 µg/day (Carrothers *et al.*, 2015). Another study carried out in men aged 50-75 years observed that higher dietary consumption of vitB12 intake resulted in higher alpha diversity based on shannon index (Gurwara *et al.*, 2019). Contrastingly, it has also been reported that alpha diversity, as measured by the Shannon index, does not significantly differ between vitB12–sufficient (≥150 pmol/L) and vitB12–deficient (<150 pmol/L) infants (Boran *et al.*, 2020). Furthermore, no significant changes in alpha diversity or beta diversity were observed in vitB12–deficient infants before and after intramuscular administration of vitB12 (Boran *et al.*, 2020). The results of this study demonstrate no notable impact of vitB12 on the overall microbial diversity within this population. Similarly a study in children aged 2-9 years including participants of varying ethnicities

including African American, Hispanic, White, Asian, and Pacific Islander, reported no changes in Shannon index, phylogenetic diversity, or richness in response to vitB12 intake (Herman *et al.*, 2020). However, when stratified by age group, it was observed that beta-diversity varied with vitamin B-12 deficiency in infants at 6 months, however this was not observed in groups at 4 or 5 months. Altogether, vitB12 intake did not induce shifts in beta-diversity in infants and children (Boran *et al.*, 2020; Herman *et al.*, 2020) or lactating women (Carrothers *et al.*, 2015) but did however induce shifts in older men (Gurwara *et al.*, 2019).

In relation to shifts in taxonomic abundance induced by cobamides, Gurwara *et al.*, (2019) and Carrothers *et al.*, (2015) demonstrated a reduction in the relative abundance of *Bacteroides* in response to vitB12 intake. When confined to the gut *Bacteroides* typically sustains a beneficial relationship with the host as extensively reviewed by Xu and Gordon, (2003), however migration outside of this environment has been demonstrated to result in significant pathological effects including appendicitis (Bennion *et al.*, 1990), gynaecological infections (Lindner, Plantema and Hoogkamp-Korstanje, 1978), and necrotising soft tissue infections (Elliott, Kufera and Myers, 2000).

Carrothers *et al.*, (2015) also demonstrated an increased abundance of *Prevotella* in lactating women in reponse to vitB12 intake whilst constrastingly Boran *et al.*, (2020) demonstrated lower abundance of *Prevotella* in breastfed infants in reponse to higher vitB12 status (Boran *et al.*, 2020). *Prevotella* species are mostly considered as gut commensals with high abundance frequently associated with positive health indicators, such as lower levels of visceral fat and better glucose metabolism (Kovatcheva-Datchary *et al.*, 2015; Asnicar *et al.*, 2021).

Increased intake of vitB12 in adults (Carrothers *et al.*, 2015; Gurwara *et al.*, 2019) and elevated vitB12 levels in breastfed infants (Boran *et al.*, 2020) have been linked to a higher abundance of *Faecalibacterium*, with species of this genera commonly considered beneficial due to their anti-inflammatory properties and inverse association with numerous diseases including colorectal cancer, dermatitis and depression as recently reviewed by Martín *et al.*, (2023).

The review highlighted that to date, there have been very few human observational studies and no randomised controlled trials conducted in humans to investigate the

effects of cobamides on the human gut microbiome, limiting our current understanding (Guetterman *et al.*, 2022).

Guetterman *et al.*, (2022) concluded that the lack of consistency in current findings may be due to several methodological variations across studies. These include differences in the study design, the specific form and dose of cobamides used, and the presence of co-interventions, all of which may influence outcomes.

Indeed, several studies have revealed the differential impacts elicited by different cobamide analogues on the human gut microbiota highlighting their unique biological effects and therapeutic potentials. Zhu et al. (2019) demonstrated that MeCbl and CNCbl have distinct influences on gut microbial populations and host health, particularly in the context of inflammatory bowel disease (IBD). In mouse models of IBD, supplementation with MeCbl was found to restore microbial dysbiosis and reduce intestinal inflammation by decreasing the fast growth of Enterobacteriaceae, specifically shiga toxin producer *E. coli*, through riboswitch modulation. In contrast shiga toxin release was enhanced in the presence of cyanocobalamin, subsequently aggravating IBD symptoms (Zhu *et al.*, 2019).

More recently it was shown that vitB12 derived from *Blautia producta* DSM 14466, *Marvinbryantia formatexigens* DSM 14469 and *Blautia hydrogenotrophica* DSM 10507 T stimulated succinate conversion to propionate by *A. muciniphila* and *B. thetaiotaomicron.* Additionally, it was observed that high doses of commercially available AdoCbl and OHCbl resulted in complete conversion of succinate to propionate by *A. muciniphila* whilst low doses only allowed for partial conversion. In contrast, little dose impact was observed when monitoring succinate conversion by *A. muciniphila,* with both high and low CNCbl doses promoting complete conversion (Kundra *et al.*, 2024). Kundra *et al.*, 2024 also demonstrated a propiogenic effect of vitB12 analogues on *B. thetaiotaomicron* DSM 2079. With the exception of CNCbl, increased dosage of AdoCbl and OHCbl stimulated increased conversion of succinate to propionate. These data demonstrate that different vitB12 analogues elicit distinct effects on the propionate production in gut commensals and could potentially be used as a modulator to target GI disorders linked to reduced propionate synthesis (Kundra *et al.*, 2024).

Another study investigating the effects of vitB12 supplementation on microbe-host interactions in the gut showed an enhancement of mouse pathogen *Citrobacter rodentium* colonisation following excessive cyanocobalamin supplementation in mouse models (Forgie *et al.*, 2023). This was accompanied by dysbiosis and production of inflammatory cytokines, contributing to a reduction in alpha diversity, reduced abundance of *Clostridia vadin BB60 and Lachnospiraceae NK4A136* group (Forgie *et al.*, 2023).

Together these data suggest that the effects of cobamide supplementation on the gut microbiota are complex and highly dependent on the specific form and dose of cobamide, as well as the existing microbial community. Further research, particularly well-designed randomised controlled trials, is essential to elucidate the precise impacts of cobamides on the gut microbiome and their potential therapeutic applications.

1.3.4 *Limosilactobacillus reuteri* as an example of a cobamide producer

1.3.4.1 *L. reuteri* colonisation in the gut

Limosilactobacillus. reuteri (formerly named *Lactobacillus reuteri)* belongs to the Firmicutes phylum and *Lactobacillus* genus which taxonomy has recently been revised based on the genetic relatedness and phylogeny of the species within the *Lactobacillus* genus (Zheng *et al.*, 2020). *L. reuteri* is a heterofermentative lactic acid bacterium colonising the gut of a range of vertebrates (Walter, Britton and Roos, 2011). *L. reuteri* strains show health-promoting properties such as reducing infections (Sagheddu *et al.*, 2020), enhancing adsorption of minerals, nutrients and vitamins (D'Amelio, 2019; Manoppo *et al.*, 2019), promoting gut mucosal integrity (Wang *et al.*, 2022), reducing bacterial translocation (Zhou *et al.*, 2022), or modulating host immune responses (Lasaviciute *et al.*, 2022).

L. reuteri has been used as a model to study host adaptation of gut symbionts. *L. reuteri* is the only autochthonous Lactobacillus species in the human gut (Walter, 2008a; Walter, Britton and Roos, 2011) and is also found in the vagina (Martin *et al.*, 1999; McLean and Rosenstein, 2000; Gabriel *et al.*, 2018), breast milk (Soto *et al.*, 2014; X. Zhang *et al.*, 2020) and the skin (Delanghe *et al.*, 2021), with its abundance differing among individuals (Mu, Tavella and Luo, 2018). (Walter *et al.*, 2003). It is

also a prevalent microorganism identified in several foods, including sourdoughs (Zheng *et al.*, 2015) and cereals, such as wheat and rye (Meroth *et al.*, 2003).

The ecological strategies of *L. reuteri* gut colonisation are fundamentally different in humans and animals (Walter, 2008a). In rodents, pigs, chickens, and horses, lactobacilli form large populations in proximal regions of the GI tract, and they adhere directly to the stratified squamous epithelium present at these sites (Walter, 2008a). In contrast, stratified squamous epithelia are absent in the human gut, where the lactobacilli population is less important and is restricted to the mucus layers and intestinal crypts (Walter, 2008a). A series of phylogenetic, phylogenomic, and experimental studies in mice have established this species as a paradigm for host adaptation. Genome comparisons of *L. reuteri* strains originating from different hosts identified lineage-specific genomic content that reflects the niche differences in the GI tract of vertebrates (Oh *et al.*, 2010). In support of these findings, core-genome phylogenetic analyses have shown distinct clustering of 25 *L. reuteri* strains into 6 host-defined lineages (Duar *et al.*, 2017) (Figure 13).

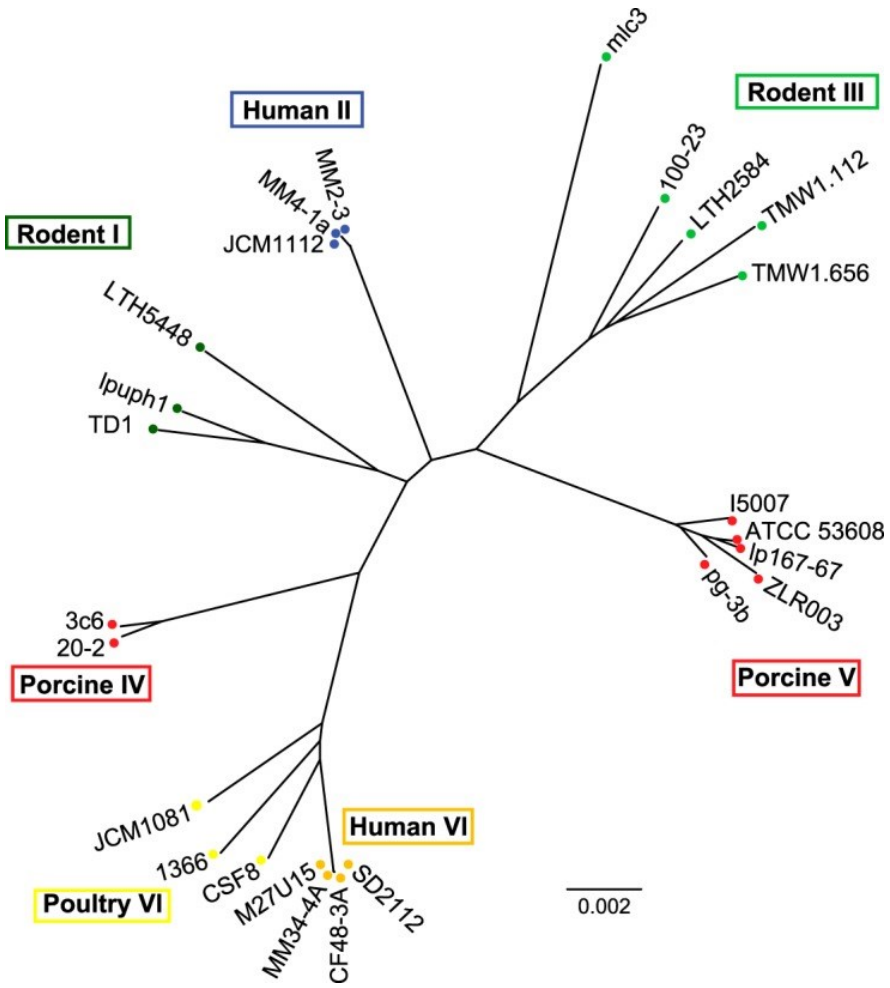

Figure 13 A phylogenetic tree depicting *Lactobacillus reuteri's* evolutionary relationships. Phylogenetic tree comprising 900 genes from 25 strains clustering into 6 host defined lineages with the branches' endpoints colour-coded according to lineage. Taken from Duar *et al.*, (2017).

The analysis also demonstrated the close clustering of a subset of human isolates and poultry isolates into a single lineage (VI), suggesting shared evolutionary history (Duar *et al.*, 2017).

Recent phylogenomic and comparative genomic analyses of *L. reuteri* strains revealed that ancestral lineages primarily constitute isolates from rodents (four lineages) and birds (one lineage) whilst lineages dominated by strains from herbivores, humans, pigs, and primates emerged more recently and displayed reduced host specificity (F. Li *et al.*, 2023). Using host ancestral state analysis and bayesian phylogenetic analysis, rodents were identified as the likely ancestral hosts of *L. reuteri,* with birds, humans, herbivores, primates, non-human primates and pigs, all transitioning from rodents between 7000 and 5000 years ago (F. Li *et al.*,

2023). These phylogenomic analyses showed that human strains cluster tightly with birds (lineage II) and herbivore (lineage VI) strains (F. Li *et al.*, 2023), in line with previous findings (Duar *et al.*, 2017). Further analyses showed that human isolates did not possess genes unique to humans when compared to poultry and herbivore isolates and it was suggested that this is likely due to transmission between hosts as a result of humans historically living in more rural areas such as on farms (F. Li *et al.*, 2023).

Experiments in *Lactobacillus*-free mice measuring the ecological fitness of strains originating from different hosts supported host adaptation. For example, an early study using gnotobiotic mice demonstrated that only rodent-derived strains effectively colonised the mice (Frese *et al.*, 2011). Furthermore, the ability of *L. reuteri* to form epithelial biofilms in the forestomach of mono-associated mice was strictly dependent on the strain's host origin (Frese *et al.*, 2011). Further experimental evaluation of host adaptation of *L. reuteri* strains to different vertebrate species confirmed that rodent strains were best adapted to mouse hosts compared to pig, chicken and human derived strains (Duar *et al.*, 2017). More recently, *L. reuteri* has been found to coexist with species that belong to the *Lactobacillus johnsonii* cluster (*L. johnsonii, L. gasseri,*and *L taiwanensis*) in the gut of wild rodents, with phenotypic analyses of mono- and mixed-species biofilms in the forestomach of mice suggesting the pre-established colonisation of *L. reuteri* facilitates the colonisation of *Lactobacillus taiwanensis* through coaggregation, with this coaggregation allowing *L. taiwanensis* to become integrated in mixed-species biofilms (Lin *et al.*, 2018).

Several genetic features associated with *L. reuteri* ecotypes have been identified that contribute to *L. reuteri* lifestyle in respective hosts (Freese et al., 2011). Easily accessible nutrients are in low supply in the human colon, with most of the absorption taking place in the small intestine. *L. reuteri* strains isolated from human can utilise 1,2-propanediol as an energy source through the *pdu-cbi-cob-hem* cluster (Figure 14) which might therefore constitute an important colonisation factor in the human gut. *L. reuteri* DSM 17938 showed enhanced growth rate in the presence propanediol (Rattanaprasert *et al.*, 2014) while *L. reuteri* ATCC PTA 6475, both of human origin, showed enhanced growth upon cross-feeding of propanediol derived from the *in vitro* fermentation of rhamnose and fucose by *E. coli* and

Bifidobacterium breve, respectively (Cheng *et al.*, 2020). This trophic interaction was dependent upon the *pduCDE* operon in *L. reuteri,* encoding proteins involved in propanediol utilisation (Cheng *et al.*, 2020). The production of reuterin, which is also conferred by this cluster, may also contribute to the fitness of *L. reuteri* in the human gut through inhibition of competitors and remodelling the composition of commensal microbes (Jacobsen *et al.*, 1999; Mu, Tavella and Luo, 2018). Reuterin is produced from the transformation of glycerol, with the genes responsible for this reaction found within the 1,2-propanediol utilization (*pdu)* operon of the *pdu-cbi-cob-hem* cluster (Figure 14) (Frese *et al.*, 2020). Reuterin can function as a precursor of acrolein, an antimicrobial compound, or as an electron acceptor, enhancing the growth of *L. reuteri* (Giuseppe Rizzello *et al.*, 2020). *L. reuteri* DSM 17938 showed enhanced growth, through glycerol utilisation, and greater reuterin production when grown on maltose and glucose as compared to strains from other host-lineages where reuterin production was significantly increased on lactose and raffinose. These results suggested substrate-specific regulation of the *pdu* operon, offering novel insight into the ecological and evolutionary role of *L. reuteri* strains in their respective hosts (Zhang *et al.*, 2020). Enzymes involved in 1,2-propanediol utilisation and reuterin production require vitB12 as a co-factor (Talarico *et al.*, 1990; Sriramulu *et al.*, 2008). The genes required for the synthesis of cobamides are also located within the pdu-cbi-cob-hem cluster, and cobamide production has been suggested to be an important colonisation factor for intestinal bacteria, as shown in *Bacteroides thetaiotaomicron* (Goodman *et al.*, 2009).

1.3.4.2 *L. reuteri* cobamide synthesis

The first report of a lactic acid bacteria synthesising cobamides was from *L. reuteri* CRL1098, a strain isolated from sourdough (Taranto *et al.*, 2003). *L. reuteri* CRL1098 demonstrated the ability to metabolise glycerol in cobamide-free medium, a reaction requiring cobamide as a co-factor (Taranto *et al.*, 2003). This strain was also shown to allow the growth of *E. coli* (MetE) and *S.* Typhimurium (MetE CbiB); two cobamide auxotrophs, in minimal media (Taranto *et al.*, 2003). These observations were the first to suggest that lactic acid bacteria produced cobamides.

L. reuteri CRL1098 was then shown to produce a cobalamin-like compound under anaerobic conditions, as confirmed by chromatography, with a similar absorption spectrum to that of cobalamin, however with a different elution time (Taranto *et al.*,

2003). The compound was identified as cyanocobalamin using various cobamide bioassays alongside reverse-phase high-pressure liquid chromatography (Taranto *et al.*, 2003). In 2008, a study using high performance liquid chromatography (HPLC) with an ultraviolet diode array detector (UV-DAD) coupled with mass spectrometry (MS) and nuclear magnetic resonance (NMR) spectroscopy also identified a cobamide produced by *L. reuteri* CRL1098 under anaerobic conditions, which was identified as pseudocobalamin (PsCbl) (Santos *et al.*, 2007). Interestingly, in the past decade, phylogenetic, genetic, and physiological analyses of several sourdough isolates of *L. reuteri* (*L. reuteri* LTH5448, LTH2584, TWM1.112, TWM1.656, TMW1.106, FUA3400 and FUA340) suggested that these may be of human (*L. reuteri* FUA3400 and FUA340) or rodent (*L. reuteri* LTH5448, LTH2584, TWM1.112, TMW1.106 and TWM1.656) lineage. This mis- identification was thought to result from original microbial contamination (Shu-Wei Su *et al.*, 2012; Zheng *et al.*, 2015). Although *L. reuteri* CRL1098 had not been included in these studies, the findings raise the possibility that this strain is also of human or rodent origin. Since then, cobamide production has been shown in *L. reuteri* DSM 20016 (Sriramulu *et al.*, 2008) and JCM1112 (Santos, Wegkamp, *et al.*, 2008) strains, both isolated from the human gut.

At the genomic level, cobamide biosynthesis in *L. reuteri* strains is carried out by the *cbi-cob-hem* operon within the *pdu-cbi-cob-hem* cluster where genes required for cobamide biosynthesis (*cbi-cob-hem*) are located adjacently to the *pdu* operon, coding for glycerol utilisation, propanediol fermentation, and production of the antimicrobial compound reuterin, as described above (Figure 14) (Talarico *et al.*, 1988, 1990; Morita *et al.*, 2008; Sriramulu *et al.*, 2008).

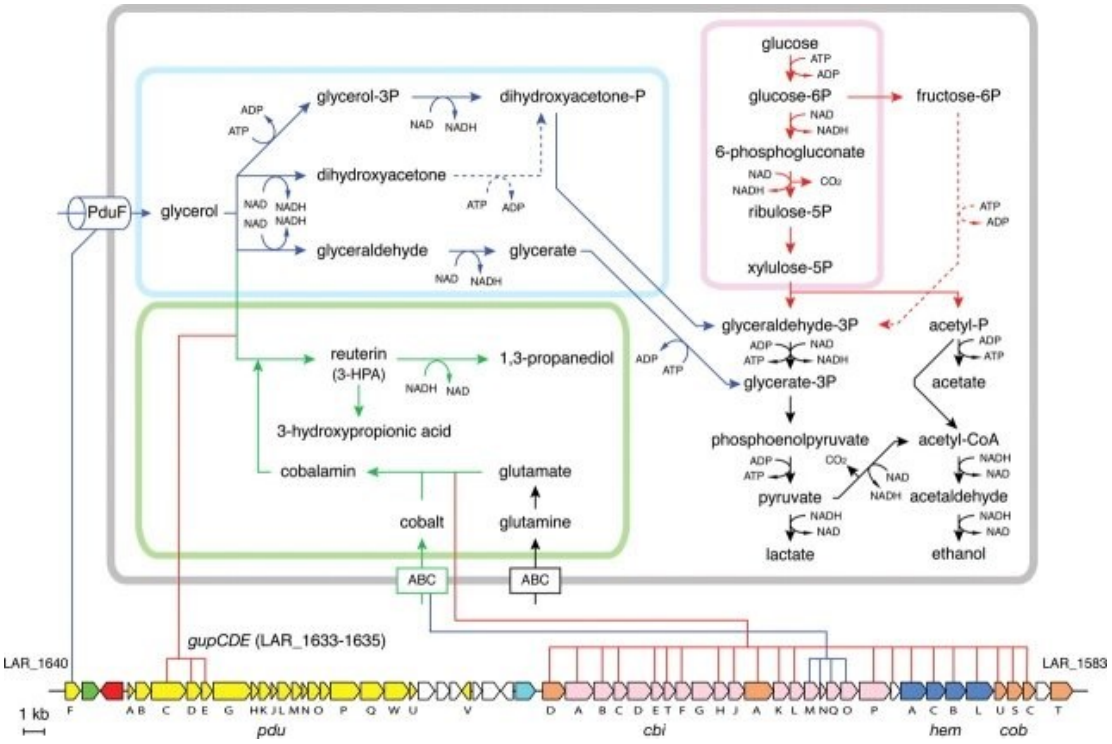

Figure 14 Proposed metabolic pathways for glycerol and glucose in *Lactobacillus reuteri* JCM 1112. Pathways are delineated by colour: blue represents glycerol metabolism, green indicates reuterin biosynthesis, and red denotes glucose metabolism. Dashed lines represent unidentified enzymes specific to *L. reuteri* JCM 1112. The lower section of the figure illustrates the pdu-cbi-cob-hem gene cluster structure in *L. reuteri* JCM 1112. Genes are depicted with arrows indicating transcription direction and color-coded as follows: yellow for pdu (including pduCDE genes), pink for cbi genes, orange for cob genes, blue for hem genes, red for pocR, green for eut, sky blue for transposase genes, and white for other genes. Connecting lines denote corresponding genes between the pathways and the gene cluster, with red lines representing enzymes and blue lines indicating transporters. Taken from Morita *et al.*, 2008.

This organisation represents a close association between the two operons, reflective of the requirement of cobamides as co-factors for glycerol utilisation, production of reuterin and propanediol fermentation (Daniel, Bobik and Gottschalk, 1998; Lawrence, 2003; Morita *et al.*, 2008). This cluster was shown to be conserved across human strains, and its representation in rodent strains is dependent of the rodent sub-lineage (Frese *et al.*, 2011). As seen for rodent strains, the *pdu-cbi-cob-hem* is only present in a subset of pig strains (Frese *et al.*, 2011; Walter, Britton and Roos, 2011). Two out of the four strains from a host-adapted phylogenetic lineage comprised of *L. reuteri* pig isolates (clade V), *L. reuteri* ATCC 53608 and lp167-6, possess this cluster and a further two strains from clade IV (the second lineage of *L. reuteri* pig isolates), *L. reuteri* 20-2 and 3c6, have also been shown to possess this cluster, whilst this genomic island is not conserved in any

other pig strains (found in clade V) (Figure 14) (Frese *et al.*, 2011; Wegmann *et al.*, 2015). This suggests a selective advantage, conferred by the *pdu-cbi-cob-hem* cluster in specific *L. reuteri* strains, potentially contributing to their ecological success and host specificity.

1.4 Aims and Objectives

Cobamides are an example of a shared resource that may play a role in shaping the gut microbial community. The aim of my project is to gain mechanistic insights into the cobamide trophic interactions between the gut symbionts *L. reuteri* and *R. gnavus* strains. Specific objectives include:

1. To investigate cobamide production and metabolism by *L. reuteri* and *R. gnavus* strains

2. To determine the metabolism pathways involved in cobamide synthesis and utilisation by *L. reuteri* and *R. gnavus* strains.

3. To investigate the effect of cobamide cross-feeding on *R. gnavus* growth and modulation of the gut microbiota

Chapter 2

Materials and Methods

2.1 Microbiology

2.1.1 Bacterial strains

Ruminococcus gnavus strain*s* (ATCC 29149 (isolated from a healthy male (Moore and Holdeman, 1974b)), ATCC 35913 (isolated from a healthy subject (Hoskins *et al.*, 1985)), E1 (isolated from a healthy adult man (Ramare *et al.*, 1993)), Finegold#79 (isolated from an autistic male child) , 0_1_58FAA (isolated from a female patient with ulcerative colitis (Peterson *et al.*, 2009)) and CC55_001C (isolated from a colon cancer tumour biopsy from a human subject (Peterson *et al.*, 2009))) and *Limosilactobacillus reuteri* strains (MM4-1A (human origin) , 20-2 (pig origin), ATCC 53608 (pig origin), DSM 20016 (human origin) and L1600-1(mouse origin) were obtained from our in-house collection (Juge Lab, Quadram Institute biosciences, UK).

Salmonella Typhimurium *MetE CbiB* (AR2680) was provided by Martin Warren's Lab (University of Kent, UK).

Escherichia coli BL21 was from New England Biolabs, UK.

2.1.2 Media and cobamide analogues

Brain Heart Infusion with Yeast extract and Haemin (BHI-YH) (Ramare *et al.*, 1993) was used for anaerobic starter cultures of *R. gnavus* strains. BHI-YH contains Brain Heart Infusion (BHI) broth (Oxoid LTD, Basingstoke, UK) supplemented with 5 g/L of Bacto™ yeast extract (Becton, Dickinson and Company, Sparks, MD) and 5 mg/L of haemin (Sigma-Aldrich, USA).

Lactobacillus defined medium type 2 (LDMII) (Kotarski and Savage, 1979) was used as a vitB12-free medium for the anaerobic and aerobic culturing of *L. reuteri* strains for cobamide detection. For composition of LDMII, see Supplementary Table 1.

Lactic acid bacteria medium (LAB) (Tramontano *et al.*, 2018) was used for anaerobic culturing of *R. gnavus and L. reuteri* strains in monoculture and co-culture. For composition of LAB, see Supplementary Table 2. Met-deficient LAB media was

used for anaerobic culturing of *R. gnavus* and *L. reuteri* in monoculture and co-culture. The composition of Met-deficient LAB media is the same as the composition of LAB but lacks methionine.

A modified version of batch culture medium (Parmanand *et al.*, 2019) was used for anaerobic batch fermentations of human stool samples. 1 L batch culture medium, pH 6.5, contained 2 g peptone, 2 g yeast extract, 0.1 g NaCl, 0.01 g MgSO4.6H2O, 0.01 g CaCl2.2H2O, 2 g NaHCO3, 0.5 g cysteine, 0.5 g Bile salts, 2 mL tween 80, 0.02 g haemin and 10 µL 0.5% v/v vitamin K. 10 mL 1 M K2HPO4 and KH2PO4 were added to 1 L batch culture medium to maintain pH of 6.6–7.0.

Luria Bertani (LB) (Bertani, 1951) was used for aerobic culturing of *E. coli* recombinant cells. 1 L LB broth contained 10 g tryptone, 10 g NaCl and 5 g yeast extract. LB agar was prepared by adding 1.5% agar.

Auto-induction media (AIM) (Sivashanmugam *et al.*, 2009) was used for IPTG-inducible BtuG2 expression in *E. coli*. AIM was prepared by Formedium, UK, with the following formula: 12 g/L Tryptone, 24 g/L Yeast extract, 3.3 g/L (NH4)2SO4, 6.8 g/L KH2PO4, 7.1 g/L Na2HPO4, 0.5 g/L Glucose, 2 g/L α-Lactose, 0.15 g/L MgSO4 and 0.03 g/L Trace Elements. 55.85 g powdered medium was dissolved in 1 L Milli-Q® water.

M9 medium (Raux *et al.*, 1996) was used for culturing *S.* Typhimurium MetE minus mutant during cobamide analysis. M9 agar contained 100 mL 10X M9 salts (60 g Na2HPO4, 30 g KH2PO4, 10 g NH4Cl and 5 g NaCl made up to 1L with Milli-Q® water), 20 mL 20% glucose, 2 mL 1M MgSO4, 1 mL 0.1 M CaCl2 and 900 mL H2O (+/- 15 g bacto-agar). M9 + MET agar contained an additional 10 mL L-methionine (5 mg/ml).

The cobamide analogues and derivatives were provided by Martin Warren's Lab (University of Kent, UK). These included analogues cyanocobalamin (CNCbl), methylcobalamin (MeCbl), adenosylcobalamin (AdoCbl) and hydroxocobalamin (OHCbl) and derivatives Coβ-cyano-adeninyl-cobamide (cyanopseudocobalamin), Coβ-cyano-(5-methylbenzimidazolyl)-cobamide (5 MB), Coβ-cyano-(5-

methoxybenzimidazolyl)-cobamide (vitamin B_{12} - Factor IIIm), Coβ-cyano-(2-methyladeninyl)-cobamide (vitamin B_{12} - Factor A) and Coβ-cyano-(5-hydroxybenzimidazolyl)-cobamide (vitamin B_{12} - Factor III).

2.1.3 Mono and co-culture conditions

Starter cultures of *R. gnavus* strains were prepared in BHI-YH from glycerol stocks with a 4% inoculum at 37˚C overnight in an anaerobic cabinet (Don Whitley, Shipley, United Kingdom), with the following conditions 85% N_2, 10% H_2, 5% CO_2. Following overnight growth of *R. gnavus* strains, a 2% inoculum was used from cultures normalised to an OD at 600 nm of 1 for selective *in vitro* growth assays.

L. reuteri MM4-1A was first cultured in 10 mL LDMII at 37˚C overnight in an anaerobic cabinet (Don Whitley, Shipley, United Kingdom), with the following conditions 85% N_2, 10% H_2, 5% CO_2. Following overnight growth of *L. reuteri* MM4-1A, a 2% inoculum was used from cultures normalised to an OD at 600 nm of 1 for selective *in vitro* growth assays.

For selective *in vitro* growth assays, a 2% inoculum from cultures normalised to an OD at 600 nm of 1 was used to inoculate Met-deficient LAB media (LAB (-Met)), LAB media, LAB media supplemented with 0.5% glucose (Glc), LAB (-Met) media supplemented with 0.5% Glc and LAB (-Met) media supplemented with 0.5% Glc and cobamide analogues (CNCbl, MeCbl, AdoCbl, OHCbl, PsCbl, 5 MB, vitamin B_{12} - Factor IIIm, vitamin B_{12} - Factor A or vitamin B_{12} - Factor III) or Porphobilinogen (PBG) at 0.001 mg/mL final concentration and in LAB (-Met) medium or in co-culture with *L. reuteri* MM4-1 first grown in LDMII under anaerobic conditions (Kotarski and Savage, 1979). Cultures were carried out in triplicates or quadruplets with a single negative control for each growth condition 96-well microtiter plates with 200 µL cultures per well or in 14 mL tubes with 8 mL cultures per tube for sampling. Spectrophotometric measurements at 600 nm were taken every h for 24 h when monitoring the effect of cobamide analogues on *R. gnavus* growth and every 2 h for 12 h, when monitoring growth for RNA extraction and sample collection was carried out after 9 and 12 h of growth.

2.2 Batch cultures

Batch cultures were carried out using human stool samples from adult volunteers recruited onto the QIB Colon Model Study (ClinicalTrials.gov ID: NCT02653001, http://www.clinicaltrials.gov). Participants included men and women over the age of 18 living or working within 10 miles of the Norwich Research Park. Participants within this study displayed normal bowel habits (defecation between 3 times a day and 3 times a week), with a Bristol stool chart classification of 3-5 and no prior diagnosis of chronic gastrointestinal health problem, such as irritable bowel syndrome (IBS), inflammatory bowel disease (IBD), or coeliac disease. Individuals were excluded from the study if they had used antibiotics in the past 2 months or had recently taken other medication or food supplements, were pregnant or breastfeeding, recently had any operations or surgeries requiring general anaesthetic or experienced gastrointestinal complications such as vomiting or diarrhoea in the past 72 h.

Stool samples were processed before use by diluting 1:10 with pre-reduced PBS containing 10% glycerol and homogenising in a Stomacher 400 (Seward, UK) at 230 rpm for 45 sec. Processed stool samples were then aliquoted in 1 mL Eppendorf's and stored at -80˚C.

Batch cultures were carried out at 37˚C in an anaerobic cabinet (Don Whitley, Shipley, United Kingdom), with the following conditions 85% N_2, 10% H_2, 5% CO_2. Cultures were prepared in 14 mL tubes containing 10 mL batch culture media per tube for sampling. The medium was supplemented with 0.5% Glc or 0.5% Glc and 5 ng/mL CNPsCbl (low dose of CNPsCbl) or 2500 ng/mL CNPsCbl (high dose of CNPsCbl) or 5 ng/mL PBG or inoculated with 2% *L. reuteri* MM4-1A or L16001strains normalised to an OD at 600 nm of 1 following growth in LDMII.

The CNPsCbl concentrations (low dose of 5 ng/mL or high dose of 2500 ng/mL) reflect those expected under typical dietary conditions and high dose vitamin B12 supplementation (1500 µg/tablet *(NIH Office of Dietary Supplements. Dietary Supplement Label Database (DSLD)*, 2022)). Based on an average dietary intake of 4.5 µg/day of vitB12 in Europe (Dhonukshe-Rutten *et al.*, 2009) and considering daily intestinal absorption rates of 50% for from dietary (*Vitamin B12 - Health Professional Fact Sheet* , 2022) and 1% from high dose supplementation (Shah *et al.*, 2017; *Vitamin B12 - Health Professional Fact Sheet* , 2022), approximately 2.25

µg of vitB12 from a typical diet and 5940 µg from high dose supplementation would reach the proximal colon daily. Given a proximal colon volume of 200 mL (Pritchard *et al.*, 2014) and an 8 h retention time (Kim and Rhee, 2012), this translates to a daily proximal colon volume of 600 mL. Thus, the vitB12 concentration would correspond to approximately 3.75 ng/mL from a typical diet and 2475 ng/mL from the high dose supplementation.

Finally, all tubes were inoculated with 1% thawed faecal suspension. Cultures were carried out in triplicates and 2 mL samples were taken just after inoculation and again at 4 h, 8 h and 24 h of growth and pelleted by centrifugation at 7000 g for 5 min. Supernatants were collected and transferred to a 1.5 mL Eppendorf and both pellets and supernatants were stored at -80˚C until DNA extraction or SFCA analysis.

2.3 Molecular biology

2.3.1 Genomic DNA (gDNA) extraction

For preparation of qPCR standards, gDNA from *R. gnavus* ATCC 29149 and *L. reuteri* MM4-1A strains, cells were harvested by centrifugation (10 min, 8000 x g, 4°C) from a 2 mL overnight culture for *R. gnavus* ATCC 29149 and 48 h culture for *L. reuteri* MM4-1A. DNA extraction was carried out using GeneJET Genomic DNA purification kit (Thermoscientific), following the 'Gram-Positive Bacteria Genomic DNA Purification Protocol', eluting with 400 µL of elution buffer for maximum DNA yield. DNA quality and quantity were determined using both Nanodrop 2000 spectrophotometer (Thermoscientific) and Qubit dsDNA HS assay on Qubit 2.0 fluorometer (Thermoscientific).

For the isolation of gDNA from cultured cells of *R. gnavus* ATCC 29149 and *L. reuteri* MM4-1A or L16001 in monoculture or co-culture, cells were harvested by centrifugation (10 min, 8000 x g, 4°C) from 2 mL cultures collected between 0 and 24 h. DNA extraction was carried out using Maxwell® RSC PureFood GMO and Authentication Kit (Promega) using a modified purification workflow. Briefly, the cell pellet was resuspended in 1 mL hexacetyltrimethylammonium bromide (CTAB) buffer (2% CTAB, 1.4M NaCl, 100mM Tris-HCl, 20mM EDTA pH 8.0) by vortexing for 30 sec. Resuspended samples were then heated to 95°C for 5 min and vortexed

for 1 min post incubation. Samples were then homogenised in the FastPrep-24™ Classic Bead Beating Grinder and Lysis System (MP Biomedicals) for 45 sec at 6.0 speed. Proteinase K (40 µL) and RNase A (20 µL) were added to the suspensions and vortexed to mix followed by a 10 min incubation at 70°C. Samples were finally centrifuged at 14,000 x g for 5 min before adding 300 µL lysate and 300µL of lysis buffer (25-50% Guanidinium chloride, 25-50% Urea, 1-5% Sodium dodecyl sulphate) to well 1 of Maxwell® RSC cartridge. Samples were eluted in 100 µL elution buffer (10 mM Tris, 0.1 mM EDTA, pH 8.0).

For the isolation of total gDNA from batch fermentation cultures, cells were harvested by centrifugation (10 min, 8000 x g, 4°C) from 2 mL cultures taken between 0 and 24 h. DNA extraction was carried out using Maxwell® RSC PureFood GMO and Authentication Kit (Promega).

2.3.2 RNA extraction

RNA from *R. gnavus* ATCC 29149 and *L. reuteri* MM4-1A was extracted from 3 mL of mid- to late exponential phase cultures. RNA stabilisation was carried out following the RNAprotect Bacterial Reagent and RNeasy Protect Bacteria Kits quick start protocol (Qiagen), steps 3-5 and RNA purification were carried out following the Quick Start Protocol RNeasy Mini Kit Part 1 for 1 x 10^8 – 2.5 x 10^8 bacteria, eluting in 50 µL RNase free water. Genomic DNA contamination was reduced using TURBO DNA-free™ DNase Treatment and Removal Reagents (Life Technologies Ltd., Paisley, UK) according to the supplier's recommendations. Quantity, purity and quality of DNase-treated RNA were determined using the NanoDrop 2000 spectrophotometer, Qubit RNA HS assay on Qubit 2.0 fluorometer and with Agilent 2200 TapeStation system following the Agilent High Sensitivity RNA ScreenTape System Quick Guide.

2.3.3 Bacterial quantification by quantitative PCR (qPCR)

16S rRNA standards for bacterial quantification by qPCR were prepared as follows: the 16S rRNA gene was amplified from *R. gnavus* ATCC 29149 and *L. reuteri* MM4-1A gDNA using HotStar Taq master mix (Qiagen, Germany) with the 27F (5"-

AGAGTTTGATCMTGGCTCAG- 3") and RP2 (5"-ACGGCTACCTTGTTACGACT T-3") primers at an annealing temperature of 52°C. The PCR products were purified using QIAquick PCR Purification Kit (Qiagen, Germany), analysed by agarose gel electrophoresis and diluted in RNase-free water to a concentration of 16.4 ng/µL, equal to 10^{10} copies/µL. A series of dilutions was then carried out in RNase-free water containing salmon sperm DNA (5 ng/µL) to obtain 10^7 to 10^2 copies/2 µL of the 16S PCR product used as standards for qPCR.

The qPCR was carried out using a Step One Plus real time PCR system (Applied Biosystems). Briefly, *R. gnavus* specific primers (16SRgF/R) or *L. reuteri* specific primers (LR16SF/R) (Table 1) were added at a final concentration of 0.4 µM to 2 µL of DNA matrix at 1 ng/µL. The qPCR reaction was carried out with an annealing temperature of 60°C for 30 sec using QuantiNova SYBR Green PCR kit, according to supplier's instructions.

Table 1 PCR primers used for amplification of the 16S region of *R. gnavus* and *L. reuteri* strains

Primer name	Sequence	Target (16S rRNA gene)	Reference
16SRgF	TGGCGGCGTGCTTAACA	*R. gnavus*	(Joossens *et al.*, 2011)
16SRgR	TCCGAAGAAATCCGTCA AGGT		
LR16SF	GAAGAAGTGCATCGGA AACC	*L. reuteri*	Designed in-house.
LR16SR	CACCGCTACACATGGA GTTC		

To check the efficiency of the primers a standard curve was produced with the previously prepared serial dilutions of 16S PCR product, and the log of each known concentration was plotted against the Ct value for the corresponding concentration.

2.3.4 Heterologous expression and purification of BtuG2

BtuG2 was recombinantly expressed in *E. coli* BL21 harbouring a HIS-BtuG2-pet14b plasmid (provided by Warren Lab, University of Kent). In this construct, the BtuG2-encoding gene lacks the N-terminal lipobox-lipoprotein export signal peptide and is fused to a N-terminal HIS-tag encoding region. The expression of BtuG2 is controlled by the T7 promoter and lac operon (see Supplementary Figure 1). For production of recombinant BtuG2, *E. coli* recombinant cells were grown in 10 mL LB containing 100 µg/mL carbenicillin at 37˚C overnight with shaking at 200 rpm. The culture was then used to inoculate 1 L of AIM supplemented with 100 µg/mL carbenicillin and incubated at 37˚C with shaking at 180 rpm for 3 h and then transferred to 18˚C for 72 h. Cells were pelleted by centrifugation at 8,000 x g for 20 min at 4˚C and resuspended in 25 mL binding buffer (20 mM TRIS-HCl, 500 mM NaCl, pH 7.9). Lysozyme (1 KU/mL) and benzonase (25 U/mL) were added to the suspension. Following sonication at an amplitude of 35% for 30 sec 'on' and 30 sec 'off' on ice 5 times, the cell debris were pelleted by centrifugation at 18,000 x g for 20 min at 4˚C. The cell lysate was then loaded onto a Nickel charged 5 mL HIS-TRAP column on the AKTA pure FPLC. Non-specific proteins were removed by washing the column with binding buffer containing 40 mM imidazole and eluted using the binding buffer containing 150 mM imidazole. The eluted protein was stored in loops and immediately desalted using a HiPrep 26/10 desalting column into desalting buffer (20 mM TRIS-HCl, 150 mM NaCl, pH 7.9). The eluted BtuG2 protein was analysed by electrophoresis onto a NuPAGE™ 4 to 12% Bis-Tris 1.0–1.5 mm protein gel (Invitrogen™) and protein concentration was determined using a Nanodrop 2000 spectrophotometer (Thermoscientific) by measuring OD at 280 nm.

2.4 Cobamide analysis

2.4.1 Cobamide extraction from bacteria

L. reuteri was grown in 500 mL LDMII, under aerobic conditions, without shaking, at 37˚C for 48 h. Bacterial cultures were centrifuged at 8000 x g for 20 min.

For cobamide extraction from the cells, the pellet was resuspended in 5 mL binding buffer (20 mM Tris pH 7.5, 500 mM NaCl and 5 mM imidazole) and subsequently

boiled for 15 min (99 °C). This suspension was then transferred into 2 mL screw cap tubes containing 25–50 mg acid-washed glass beads and cells were further lysed using the FastPrep-24™ Classic Bead Beating Grinder and Lysis System (MP Biomedicals), for 2x45 sec at 5.0 speed, with 1 min rest in between cycles. Lysed cells were centrifuged at 18,000 x g for 20 min and the soluble extract was further heat-treated at 56˚C for 1 h to denature any remaining proteins and then centrifuged at 8000 x g for 20 min. The soluble fraction was transferred into a centrifugal tube, concentrated using a centrifugal evaporator (Genevac - SP Scientific) and resuspended in 300 µL deionised water. The solution was centrifuged at 14,000 x g for 20 min and the supernatant collected for cobamide detection using cobamide bioassay plates (see section 2.3.2) and UPLC-MS/MS analysis (see section 2.3.3). Work was carried out under a gold light where possible in order to avoid cobamide degradation.

For cobamide extraction from the culture media, the bacterial supernatant was boiled for 15 min (99 °C), debris were pelleted by centrifugation at 8000 x g for 20 min and the supernatant was transferred into a Duran bottle to be filter-sterilised. The filtered supernatant was then loaded onto a HIS-TRAP-BtuG2 column prepared by loading 2 mg BtuG2 protein (from section 2.2.4) onto a 1 mL crude prep HIS-TRAP column in the ÄKTA pure™ FPLC (Cytiva Life Sciences).
The BtuG2 protein in complex with the cobamide was eluted with binding buffer (20 mM TRIS, 500 mM NaCl, pH 7.9) containing 150 mM imidazole. The eluted sample was desalted into Milli-Q® using a 10 kDa MWCO, ultra-centrifugal filter unit and then heated at 70˚C for 20 min to denature the BtuG2 and release cobamides. Debris were pelleted by centrifugation at 13,300 rpm for 20 min and the supernatant transferred into a centrifugal tube, concentrated using a centrifugal evaporator (Genevac - SP Scientific) and resuspended in 300 µL deionised water. The solution was centrifuged at 14,000 x g for 20 min and the supernatant collected for cobamide detection using cobamide bioassay plates (see section 2.3.2) and UPLC-MS/MS analysis (see section 2.3.3).

2.4.2 Cobamide analysis by microbiological plate assay

The method was first described by Raux *et al.*, 1996 using *S.* Typhimurium *MetE CbiB* (AR2680) as an indicator strain. This mutant can only make methionine by its cobamide-dependent methionine synthase MetH, thus, growth of the bacterium is dependent the addition of a cobamide to the medium. In addition, the CbiB mutation blocks the cobamide pathway between cobyric acid and cobinamide, therefore, the first intermediate which can be detected is cobinamide, a late precursor in the biosynthesis of cobalamin. This mutation allows for the detection of cobamide biosynthetic intermediates between cobinamide and cobalamin in the biosynthetic pathway. Briefly, the *S.* Typhimurium MetE minus mutant was streaked onto M9 agar plates and grown overnight at 37˚C. Following overnight incubation, *S.* Typhimurium growth was scraped off the plate and reconstituted into molten M9 agar and poured to form bioassay plates. *L. reuteri* cell and supernatant samples were spotted onto the surface of bioassay plates and the plates were incubated overnight at 37˚C. The amount of growth is proportional to the amount of cobamide that is added to the growth medium. To generate a standard curve, 10 µL of CNPsCbl dilutions at 0.1, 0.01, 0.001, 0.0001 and 0.00001 µg/mL were spotted onto the plates.

2.4.3 Cobamide analysis by ultra-high performance liquid chromatography-MS/MS (UHPLC-MS/MS)

The Agilent® 1290 Infinity LC systems coupled to a 6490 triple quadrupole mass spectrometer with an Agilent® Jet Stream source (Santa Clara, USA) was used to detect and quantify cobamide analogues from bacterial cell extracts and supernatants. The mobile phase A contained 0.1% formic acid in water while mobile phase B consisted of 0.1% formic acid in acetonitrile. The separation was carried out on a Waters Acquity UPLC HSS T3 1.8 µm column. The following gradients were applied to the column: 0.0-2.0 min, 95% A and 5% B; 14 min, 68% A and 32% B; 14.5-17.0 min, 1 % A and 99% B; and 17.1-20.0 min, 95% A and 5% B. The total run time was 20 min, and the flow rate was 300 µL/min. The UPLC-MS/MS system was equipped with an electrospray ionization (ESI) source operated in positive-ion detection mode. Nitrogen gas was used for nebulisation, desolvation,

and collision and the analytes were monitored in multiple-reaction monitoring (MRM) mode.

2.4.4 Short Chain Fatty Acid (SCFA) analysis

All SCFAs authentic standards were reconstituted in acidified Milli-Q® water to prepare 100 mM stock solutions which were kept at -20°C. A standard curve was produced from stock solutions using serial dilutions (10 mM to 0.001 mM). All serial dilutions were prepared fresh prior to each run.

Agilent 6490 Triple Quad MS mass spectrometer equipped with an Agilent 1290 HPLC system (Agilent Technologies, Santa Clara, CA, USA) was used for the analysis of SCFAs. The LC flow rate was 0.15 mL/min. The column used for the analysis was a Thermofisher PGC 3µm (50 x 2.1mm) with guard column. The column temperature and auto sampler were maintained at 40°C and 4°C, respectively. 2 µL was used for the injection volume. Samples were analysed using 0.1% formic acid in water (mobile phase A) and 0.1% formic acid in acetonitrile (mobile phase B). The gradient was started with 0% B, increased 60% B within 4 min, after washing for 2 min using 100% mobile phase B and equilibration was for another 4 min using 100% mobile phase A. The total run was 10 min. The 6490 MS/MS system was equipped with an ES source operated in positive and negative-ion detection mode. Nitrogen gas was used for nebulation, desolvation, and collision. The analytes were monitored in multiple-reaction monitoring (MRM) mode. The MRM precursor, product ions and collision energy were optimized by Agilent optimizer software. The transitions of precursor ions to product ions (m/z) and some optimised MS operating parameters of the analyte are described in Table 2. The source parameters were as follows: gas temperature of 200 ˚C with a gas flow of 16 L/min, a sheath gas temperature of 300 ˚C with a sheath gas flow of 11 L/min, a nebuliser pressure of 50 psi and capillary voltage of 3500 V for positive polarity, Nozzle Voltage 1000 V. The iFunnel parameters were; high pressure radio frequency (RF) of 150 V and low-pressure RF of 60 V. The LC eluent flow was sprayed into the mass spectrometer interface without splitting. Identification was achieved based on retention time of authentic SCFA standards and by product ions monitor.

Table 2 Transitions of precursor ions to product ions (m/z) and optimised MS operating parameters of SCFAs.

Analyte	Retention time (mins)	Precursor ion (*m/z*)	Product ion (*m/z*)	Collision energy	Cell accelerator energy	Polarity
Acetate	1.9	61.1	43.0	16	4	Positive
D4-Acetate	1.9	65.1	47.0	14	4	Positive
Butyrate	4.3	89.1	43.1	14	4	Positive
13C2-Butyrate	4.3	91.1	44.0	14	4	Positive
Isobutyrate	3.4	89.1	43.1	14	4	Positive
D6-Isobutyrate	3.4	95.0	49.0	14	4	Positive
Iso-Valerate	4.7	103.1	43.0	14	4	Positive
D9-Isovalerate	4.7	112.2	50.2	18	4	Positive
Lactate	2.1	89.0	42.9	10	5	Negative
13C3-Lactate	2.1	92.0	46.0	10	4	Negative
Propionate	2.9	75.0	29.0	18	4	Positive
D2-Propionate	2.9	77.0	31.1	14	4	Positive
Valerate	5.1	103.1	75.0	10	4	Positive
D9-Valerate	5.1	112.1	80.0	10	4	Positive

2.5 Sequencing

2.5.1 Prokaryotic RNA sequencing (RNAseq)

RNAseq was carried out by Novogene, Hong Kong. Firstly, ribosomal RNA was removed from total RNA obtained as described in section 2.3.2, followed by ethanol precipitation. Following fragmentation, the first strand cDNA was synthesised using random hexamer primers. During the second strand cDNA synthesis, deoxyuridine triphosphates (dUTPs) were replaced with deoxythymidine triphosphates (dTTPs) in the reaction buffer. The directional library was ready after end repair, A-tailing, adapter ligation, size selection, USER enzyme digestion, amplification, and purification. The library was examined with Qubit and real-time PCR for quantification and bioanalyzer for size distribution detection. Quantified libraries were pooled according to effective library concentration and data amount required. The clustering of the index-coded samples was performed according to the

manufacturer's instructions. After cluster generation, the library preparations were sequenced on an Illumina platform and paired-end reads were generated.

2.5.2 Shotgun metagenomics sequencing

Shotgun metagenomic sequencing was carried out by Novogene, Hong Kong. Firstly, the gDNA (section 2.3.1) was fragmented into short fragments and then end-polished, A-tailed, and ligated with full-length adapters for Illumina sequencing before further size selection. PCR amplification was then conducted. Purification was then carried out using the AM Pure XP system (Beverly). The resulting library was assessed on the 5400 Agilent Fragment Analyzer System (Agilent) and quantified to 1.5 nM through Qubit (Thermo Fisher Scientific) and qPCR. The qualified libraries were pooled and sequenced using the Illumina sequencing system NovaSeq X Plus, according to the effective library concentration and data amount.

2.6 Bioinformatics

2.6.1 Comparative genomics

A screening of *L. reuteri* and *R. gnavus* specific cobamide biosynthetic genes and *R. gnavus* genes encoding cobamide-dependent and transporter genes and their homologs was carried out using the Basic Local Alignment Search Tool (BLAST) (https://blast.ncbi.nlm.nih.gov/Blast.cgi) program (Altschul et al., 1990), specifically tblastn (tblastn search translated nucleotide databases using a protein query.).

Briefly, all publicly available *L. reuteri* (381) (see Supplementary Table 3 for full list of strains) for and *R. gnavus* (162) (see Supplementary Table 6 for full list of strains) genomes were downloaded (*L. reuteri* dataset downloaded 08/02/22 and *R. gnavus* dataset downloaded 28/02/23) as genomic sequences (FASTA) from NCBI Datasets at https://ncbi.nlm.nih.gov/datasets/genome/. FASTA files were concatenated to produce a single FASTA file for *L. reuteri* and *R. gnavus* genomic sequences, respectively.

Protein sequences of cobamide biosynthesis genes (Genes required for cobamide biosynthesis from glutamate to adenosylcobalamin) and genes encoding putative cobamide-dependent proteins and transporters from the UniprotKB repository (https://www.uniprot.org/help/uniprotkb) were downloaded and stored in FASTA format. FASTA files were concatenated to produce a single FASTA file for *L. reuteri* and *R. gnavus* protein sequences, respectively.

Using BLAST command line version 2.9.0, the makeblastdb application was used to create a local BLAST database from the concatenated FASTA files, producing a local BLAST database in FASTA format, along with.nhr, nin, nog , .nsd , .nsi , and .nsq files for *L. reuteri* and *R. gnavus* sequences, respectively.

The newly created local BLAST database containing *L. reuteri* and *R. gnavus* genome sequences, respectively was used as an input database using the –db option.

Local BLAST databases containing cobamide biosynthesis or cobamide-dependent and transporter genes, respectively, were submitted as a protein query using the -query option.

A search was then run against the corresponding *L. reuteri* or *R. gnavus local* genome databases, respectively, with the following parameters: -max_target_seqs 100000 -evalue 0.05 -word_size 3 -outfmt 10. The -out option was used in combination with "[OUTPUT FILENAME].csv" in order to produce an output file in csv format.

The csv file produced from the tblastn run was then imported into BLASTmap, a shiny-based application (Baker *et al.*, 2018), run in R version 4.1.2 (R Core Team, 2021) and percentage identity values were plot (Supplementary Figure 2, 3 and 4).

2.6.2 RNAseq data analysis

RNAseq data analysis was carried out by Novogene, Hong Kong. Raw reads in FASTQ format were first processed through fastp (Chen *et al.*, 2018). In this step,

clean reads were obtained by trimming reads containing adapter and removing poly-N sequences and reads with low quality from raw data. Q20, Q30 and GC content of the clean data were calculated. All the downstream analyses were based on the clean data with high quality. Read mapping to reference genome was carried out using Bowtie2 (Langmead and Salzberg, 2012).

Rockhopper was used to identify novel genes, operon and transcription start sites (McClure *et al.*, 2013).

FeatureCounts was used to quantify the reads mapped to each gene. Then the FPKM of each gene was calculated based on the length of the gene and reads count mapped to this gene. FPKM (Fragments Per Kilobase of transcript per Million mapped reads) of each gene was calculated, taking into account the gene length and the number of reads mapped to it. FPKM normalises read counts by considering both sequencing depth and gene length, providing a more accurate measure of gene expression (Trapnell *et al.*, 2010).

Differential expression analysis of two conditions/groups (two biological replicates per condition) was carried out using the DESeq2 R package (Love, Huber and Anders, 2014).

2.6.3 Shotgun metagenomics analysis

Shotgun metagenomics analysis was carried out by Novogene, Hong Kong. Fastp (https://github.com/OpenGene/fastp) was used for preprocessing raw data from NovaSeq X Plus to obtain clean data for subsequent analysis. Paired reads were discarded in the following situations: one read contains adapter contamination; one read contains more than 10 % uncertain nucleotides or one read contains more than 50 % low quality nucleotides (base quality less than 5).

Bowtie2 software (http://bowtie-bio.sourceforge.net/bowtie2/index.shtml) was used to filter out reads that may come from host origin, with the following parameter settings: --end-to-end, --sensitive, -I 200, and -X 400.

MEGAHIT software (https://github.com/voutcn/megahit/) was used for assembly analysis of clean data, with assembly parameter settings: --presets meta-large (--end-to-end, --sensitive, -l 200, -X 400).

With the default parameters, MetaGeneMark (http://topaz.gatech.edu/GeneMark/) was used to perform ORF prediction for scaftigs (sequences of length >= 500 bp) of each sample and the sequences with lengths less than 100 nucleotides in the prediction results were filtered out.

For the open reading frame (ORF) prediction results, CD-HIT software (http://www.bioinformatics.org/cd-hit/) was used to eliminate redundancy and obtain a non-redundant initial gene catalogue (Zeller G et al., 2014), with parameter settings: -c 0.95,-G 0,-aS 0.9,-g 1,-d 0.

Clean data of each sample were aligned to the initial gene catalogue by using Bowtie2 (Langmead and Salzberg, 2012) to calculate the number of reads of the genes on each sample alignment, with parameter settings: --end-to-end, --sensitive, -l 200, -x 400. Genes with reads <= 2 in each sample were filtered out to finally determine the gene catalogue (Unigenes) for subsequent analysis.

Based on the number of reads aligned and the length of gene, the abundance of each gene in each sample was calculated by the following formula, in which r is the number of gene reads on alignment, and L is the length of gene.

$$G_k = \frac{r_k}{L_k} \cdot \frac{1}{\sum_{i=1}^{n} \frac{r_i}{L_i}}$$

Species annotation was carried out using DIAMOND software (https://github.com/bbuchfink/diamond/) and unigenes sequences were aligned against Micro_NR database, which includes sequences from bacteria, fungi, archaea, and viruses extracted from NCBI's NR database (https://www.ncbi.nlm.nih.gov/). This alignment was performed using the blastp

algorithm with a parameter setting of 1e-5. Functional annotations using KEGG (https://www.genome.jp/kegg/pathway.html), eggNOG (http://eggnog5.embl.de) and CAZy (www.cazy.org) databases were also carried out using DIAMOND software.

Lowest common ancestor (LCA) algorithm (applied to systematic taxonomy of MEGAN software (https://en.wikipedia.org/wiki/Lowest_common_ancestor) was used to determine the species annotation information of the sequence. Out of the results of LCA annotation and gene abundance table, the abundance of each sample at each taxonomy (kingdom, phylum, class, order, family, genus, or species) and the corresponding gene abundance tables were acquired.

2.7 Statistical analyses

2.7.1 Comparative genomics

BLAST alignments (Altschul *et al.*, 1990) were carried out using statistical theory to produce an expect value (e-value) for each pair (query and subject). E-values provide an indication of the statistical significance of a pairwise alignment. The lower the e-value the more significant the hit. The e-value threshold set for the tblastn run was 0.05, indicating that the similarity between a query and subject has a 5 in 100 chance of occurring by chance alone, indicating statistical significance.

2.7.2 Growth assays

Two-way ANOVA (Analysis of Variance) with Bonferroni multiple comparisons was performed to determine the significant differences between treatment conditions and the control at different time points.

2.7.3 RNAseq data analysis

Differential expression analysis was carried out using the DESeq2 R package (Love, Huber and Anders, 2014). The raw p-values resulting from the statistical tests were adjusted to control the False Discovery Rate (FDR). Here, the Benjamini-Hochberg (BH) method was applied, adjusting the p-values to account for multiple comparisons (Benjamini and Hochberg, 1995). Genes with an adjusted p-value <0.05 found by DESeq were assigned as differentially expressed. A log2(Fold Change) threshold of 0 was applied.

2.7.4 Shotgun metagenomics analysis

ANOSIM (Analysis of Similarities) (R vegan package) (https://github.com/vegandevs/vegan) was used as a nonparametric test to statistically determine the beta diversity between groups. A non-parametric Wilcoxon statistical analysis was used to determine the significance in alpha diversity between treated batch cultures. MetaGenomeSeq (Paulson *et al.*, 2013) and linear discriminant analysis (LDA) Effect Size (LEfSe) analysis (Segata *et al.*, 2011) were used to search for species differences between groups. MetaGenomeSeq analysis (Paulson *et al.*, 2013) was used to perform permutation test between groups on each taxonomy level and obtain a p-value. The LEfSe software was used for LEfSe analysis to determine genomic features most likely to explain differences between conditions. LDA scores are a measure used to assess the effect size of features (e.g., taxa, genes, or any other biological unit) effect size, by default LDA score is set to 4.

2.7.5 SCFA analysis

Two-way ANOVA (Analysis of Variance) was performed on individual and total SCFA concentrations across treated conditions and a control condition followed by Bonferroni correction ($P < 0.05$) for *post-hoc* analysis to correct for multiple comparisons.

Chapter 3

Cobamide production in *L. reuteri*

3.1 Introduction

VitB12 belongs to a group of cobalt-containing compounds named cobalamins distinguished by a macrocyclic tetrapyrrole group (corrin ring) linked to a 5,6-dimethylbenzimidazole (5,6-DMB) moiety in the lower ligand (Figure 15). Cobalamins are part of a larger group of compounds called cobamides which are a family of enzyme co-factors (Sokolovskaya, Shelton and Taga, 2020). Over a dozen cobamides are found in nature with cobalamins being one of the most extensively studied (Sokolovskaya, Shelton and Taga, 2020). Cobamides are defined by the presence of a corrin ring and functional upper ligand moiety and distinguished by the heterogeneity of the lower ligand (Figure 15).

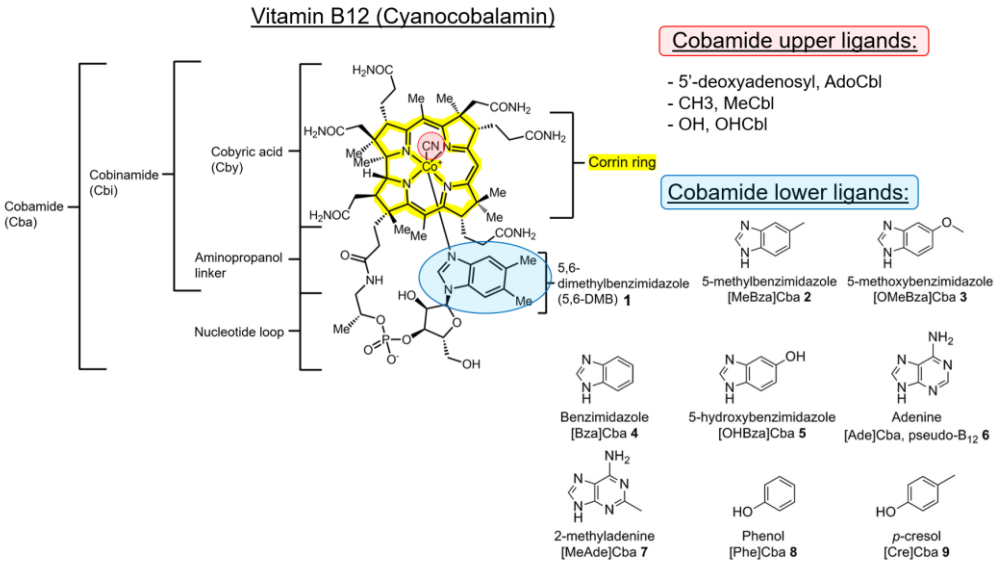

Figure 15 Vitamin B12 structure and diversity of upper and lower ligand. Chemical structure of vitamin B12 (cyanocobalamin) with 5,6-DMB in the lower ligand and a cyano group in the upper ligand. The upper ligand varies and can contain a 5'-deoxyadenosyl, methyl or hydroxy group. The lower ligand also varies with the incorporation of a benzimidazole moiety, purine or phenolic compound. The figure also depicts the corrin ring structure, cobyric acid structure, aminopropanol linker and nucleotide loop. The cobinamide structure encompasses cobyric acid and the aminopropanol linker but unlike the cobamide structure, does not include the nucleotide loop or 5,6-DMB moiety. Adapted from Crofts *et al.*, 2013.

Modifications in the upper ligand of cobalamin give rise to different cobalamin analogues. In naturally occurring cobalamins, the upper ligand can be a cyano (CN)-, hydroxo-, aquo-, methyl-, or ado-group, leading to corresponding chemical forms. VitB12 corresponds to cyanocobalamin (CNCbl), a cobalamin compound with a CN group in the upper ligand and 5,6-dimethylbenzimidazole (5,6-DMB) moiety in the lower ligand (Figure 15).

Methylcobalamin (MeCbl) and AdoCbl serve as coenzymes for metabolic reactions, although they are highly susceptible to light-induced degradation (Neil and Marsh, 1999). The lack of stability of MeCbl and AdoCbl allows easy displacement of Me- and Ado- moieties in the upper ligand resulting in the formation of other analogues such as CNCbl. CNCbl is the most structurally stable compound and is therefore commonly used in therapeutic preparations (Halczuk *et al.*, 2023). Hydroxycobalamin (OHCbl) can act as a precursor molecule from which the body can synthesise both MeCbl and AdoCbl by removal of the OH group in the upper ligand (Fedosov, Nexo and Heegaard, 2024). OHCbl is used therapeutically for the treatment of vitB12 deficiency (Wolffenbuttel *et al.*, 2023) and cyanide poisoning, as it can bind to cyanide ions, aiding in their detoxification (Shepherd and Velez, 2008; Thompson and Marrs, 2012; SG and JM, 2019). Modifications can also occur in the lower ligand giving rise to cobamide analogues with the 5,6-DMB moiety replaced by other structures, typically purines and phenolic compounds (benzimidazoles: 5,6-DMB, 5-methylbenzimidazole, 5-methoxylbenzimidazole, benzimidazole, 5-hydroxybenzimidazole, Purine: adenine, phenolic compounds such as phenol and p-cresol) (Figure 15).

The potential biosynthetic production of cobamides by bacteria was first reported in 1985 when the first genes encoding cobalamin synthesis enzymes were identified in *Escherichia coli* (Heller and Kadner, 1985). Early investigations carried out by researchers at Rhône-Poulenc Santé (now Sanofi), a leading commercial producer of cobalamins, then isolated and expressed cobalamin biosynthetic genes from *Pseudomonas denitrificans*. These genes were designated with the prefix "cob," with the following letter indicating the gene's position within the operon rather than its specific function (Crouzet *et al.*, 1990). Shortly thereafter, cobalamin biosynthesis genes were identified in *S.* Typhimurium strain LT2 (Roth *et al.*, 1993) and *Bacillus megaterium* strains ATCC 10778 and DSM509 (Raux *et al.*, 1996). Characterisation of these genes revealed genetic differences in the biosynthesis of cobalamin by *P. denitrificans* and *S.* Typhimurium and *B. megaterium,* with the pathway utilised by *S.* Typhimurium and *B. megaterium* lacking a monooxygenase. This work led to the description of two separate cobalamin biosynthetic pathways: 1) the aerobic pathway, performed by *P. denitrificans* (Stamford *et al.*, 1997), involving the following genes: CobA, I, G, J, M, F, K, L, H, B and NST; and 2) the

anaerobic pathway performed by *B. megaterium* and *S.* Typhimurium (Moore and Warren, 2012) involving the following genes: CysG, CbiK, L, H, F, G, D, J, ET, C and A (Figure 16). Genes utilised by *S.* Typhimurium and *B. megaterium* strains were designated with the prefix "cbi," reflecting the distinct anaerobic biosynthetic pathway employed by these organisms, in contrast to the aerobic pathway observed in *P. denitrificans*. The cobalamin analogue synthesised by *P. denitrificans*, *S.* Typhimurium and *B. megaterium* strains is adenosylcobalamin (AdoCbl) (Moore and Warren, 2012). The main difference between the two pathways is the requirement for molecular oxygen in the aerobic pathway, rendering it incapable of functioning under anaerobic conditions. Conversely, the anaerobic pathway operates independently of molecular oxygen, but is also operational under aerobic conditions as well (Moore *et al.*, 2013). In 1990, *in vitro* studies on *S.* Typhimurium LT2 revealed the requirement of *cobA* in assimilating exogenous corrinoids into the cobalamin biosynthesis pathway, with this integration of corrinoids now more commonly referred to as the corrinoid salvage pathway (Escalante-Semerena, Suh and Roth, 1990) (Figure 10).

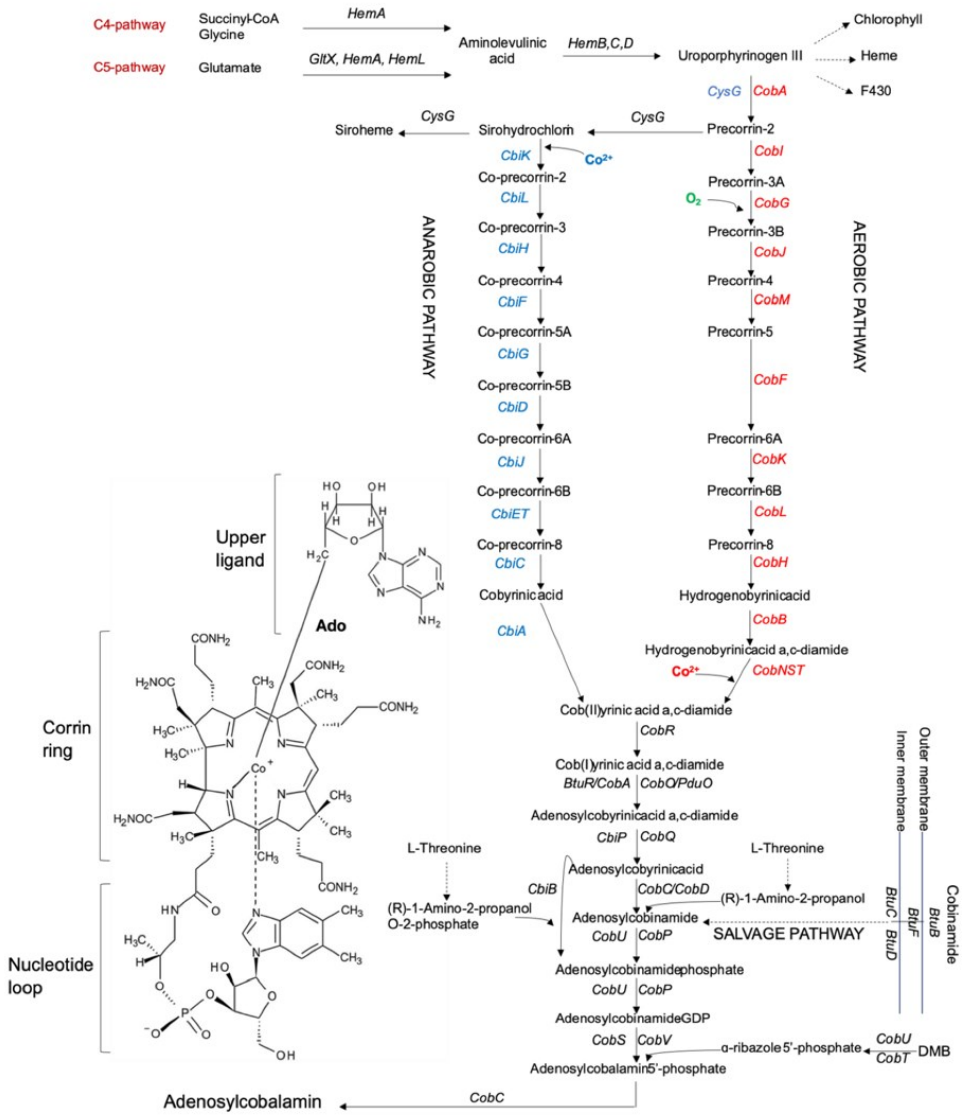

Figure 16 Adenosylcobalamin biosynthesis pathway highlighting aerobic, anaerobic and salvage routes. The aerobic pathway highlighted in red has been characterised in *P. denitrificans* and *Sinorhizobium meliloti.* The anaerobic pathway highlighted in blue has been characterised in *S. Typhimurium, P. shermanii* and *B. megaterium.* Taken from Balabanova *et al.*, 2021.

The diversity in the lower ligand of cobamides is dependent on the cobT gene-encoding enzyme, involved in the attachment of the lower ligand by activation of the lower ligand base (Crofts *et al.*, 2013). This enzyme exhibits substrate specificity, limiting the variety of lower ligands that can be attached (Crofts *et al.*, 2013). *S.* Typhimurium is able to incorporate each of the benzimidazoles as well as adenine into its lower ligand, but demonstrated an inability to incorporate phenolic compounds (Crofts *et al.*, 2013). To confirm that this selectivity was due to the cobT gene-encoding enzyme, homologs of cobT from *S.* Typhimurium were

heterologously expressed in a *Sinorhizobium meliloti BluB cobU* mutant unable to synthesise cobalamin *de novo*. Guided cobamide biosynthesis of *Si. meliloti BluB cobU* expressing *S.* Typhimurium *cobT* homolog (*Sm cobT*$_{Se}^{+}$) demonstrated incorporation of DMB, MeBza, OMeBza, Bza and adenine, confirming the function of *cobT* in lower ligand selectivity (Crofts *et al.*, 2013).

It has previously been reported that *L. reuteri* strains JCM 1112 (Filipe Santos, Wegkamp, et al., 2008), DSM 20016 (Sriramulu et al., 2008) and CRL1098 (Taranto et al., 2003), have the ability to synthesise cobamides *de novo* with CRL1098 reported to exclusively produce the cobamide analogue pseudocobalamin (PsCbl), via the *cbi-cob* operon (*cobD, cbiABCDETFGHJ, cobA/hemD, cbiKLMNQOP, sirA, hemACBL*, and *cobUSC, hemD, cobT*) demonstrated in Figure 17 (Santos et al., 2007).

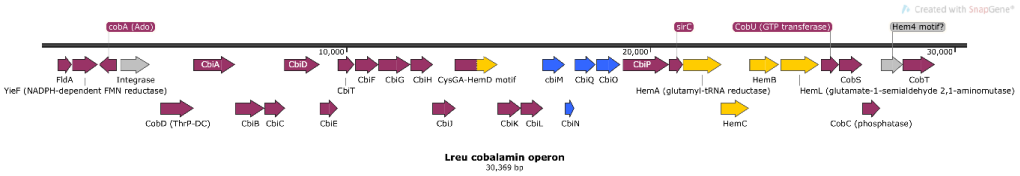

Figure 17 Schematic representation of the cobalamin operon in *L. reuteri.*

Here, we report the predicted *de novo* cobamide synthesis capacity of 191/381 *L. reuteri* strains and confirmed the production of PsCbl by *L. reuteri* 20-2, MM4-1A, and ATCC 53608 strains cultured aerobically using ultra-performance liquid chromatography-mass spectrometry (UPLC-MS/MS).

3.2 Results

3.2.1 *L. reuteri* strains possess a partial cobalamin biosynthetic pathway.

Cobalamin production in *L. reuteri* strains was first analysed by comparative genomic analysis across all publicly available genomes. Using BLAST command line, nucleotide sequences of cobalamin biosynthesis genes were aligned against a database of 381 *L. reuteri* genomes, and the statistical significance of the match was calculated and output as sequence percentage identity (Supplementary Figure 2). Out of the 381 *L. reuteri* genomes analysed (see Supplementary Table 3 for full list of strains included in the analysis), a total of 191 strains (see Supplementary Table 5)

were found to harbour the cobamide biosynthesis pathway (*cbiABCDETFGHJ, cobA/hemD, cbiKLMNQOP, CysG*, *hemACBL*, cobUSC hemD and cobT) originally reported for *L. reuteri* CRL1098 strain (Santos, Vera, *et al.*, 2008), with the addition of genes *cobI, cobL, cobM, cobJ, cobB, cobD, GltX* and *FldA*. A total of 38 cobamide biosynthesis genes were predicted to be present in the genomes of 191 *L. reuteri* strains (see Supplementary Table 4 for full list of cobamide synthesis genes), including genes encoding enzymes required for the synthesis of uroporphyrinogen III and the corrin ring, corrin ring adenosylation, attachment of the amino-propanol linker and the assembly of the nucleotide loop. Amongst the 191 strains predicted positive for cobamide production were the three *L. reuteri* strains previously characterised as cobamide-producers under anaerobic conditions, CRL1098, JCM 1112 and DSM 20016 (Taranto *et al.*, 2003; Santos, Wegkamp, *et al.*, 2008; Sriramulu *et al.*, 2008).

Genes encoding enzymes required for the synthesis of 5,6-DMB in the lower ligand of cobalamin, including *BzaABCDE* and *BluB* were not identified in any of the *L. reuteri* strains analysed, which suggests that *L. reuteri* is not able to synthesise cobalamin in the form of AdoCbl, MeCbl, OHCbl or CNCbl. Together, this *in silico* analysis suggests that *L. reuteri* strains (191/381) could produce a cobamide derivative with a molecule different to 5,6-DMB in its lower ligand, such as the purine adenine, which is found in PsCbl and Coβ-cyano-(2-methyladeninyl)-cobamide (vitB12 - Factor A) (Figure 18).

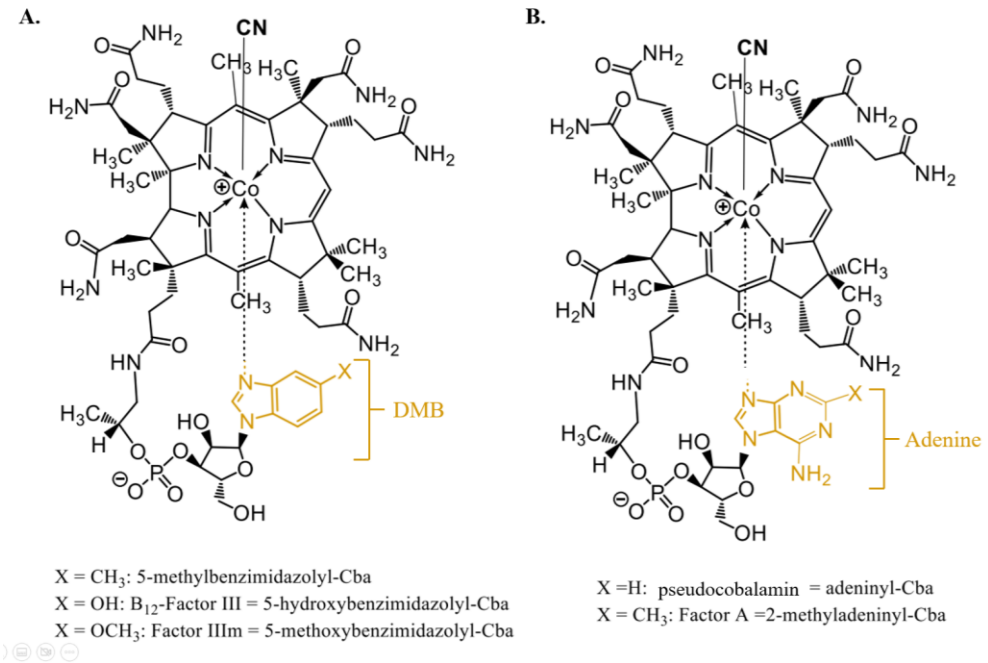

Figure 18 The structure of cobamide derivatives. (A) Structures with DMB in the lower ligand (B) and with adenine in the lower ligand.

3.2.2 *L. reuteri* strains produce pseudocobalamin (PsCbl) aerobically.

In order to validate the results of the *in silico* analysis, cobamide production was determined for *L. reuteri* 20-2, MM4-1A and ATCC 53608 strains predicted to be positive for cobamide production and for *L. reuteri* L1600-1 and 100-23 strains, predicted to be negative for cobamide production. *L. reuteri* 20-2 and 53608 strains were isolated from pigs, L1600-1 and 100-23 from mice and MM4-1A from humans. All strains were grown aerobically in synthetic (LDMII) media. Cobamide production was analysed in both cell extracts and supernatants following cyanide pre-treatment to convert all cobamides into the cyano form for improved analyte stability and accurate quantification.

Out of the strains tested, *L. reuteri* DSM 20016, a strain bioinformatically-predicted to be positive for cobamide production in our analysis, was previously reported to produce cobamide intracellularly when grown anaerobically (Sriramulu *et al.*, 2008). Here, we showed that this strain produced intracellular PsCbl when grown both anaerobically and aerobically using UPLC-MS/MS analysis (Figure 19). These data indicate that the presence of genes *cbiABCDETFGHJ, cobA/hemD, cbiKLMNQOP,*

CysG, hemACBL, cobUSC hemD, cobT, cobI, cobL, cobM, cobJ, cobB, cobD, GltX and FldA confer *L. reuteri* the ability to produce cobamide through both aerobic and anaerobic pathways. These results demonstrate that cobamide-producing *L. reuteri* strains do not rely on molecular oxygen for cobamide production. Based on these results, all *L. reuteri* strains used in this work for cobamide detection were cultured aerobically.

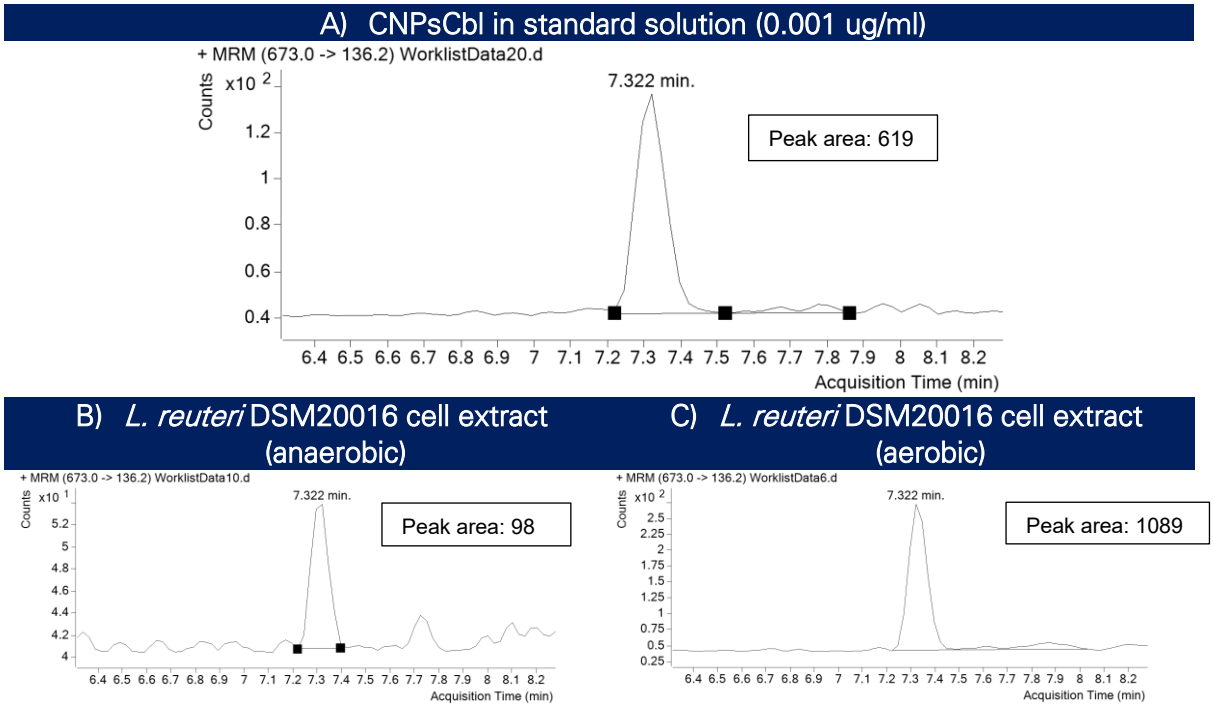

Figure 19 UPLC-MS/MS detection of cobamide in *L. reuteri* DSM20016. Shown are the chromatograms for: A) CNPsCbl standard at 0.001 ug/ml, B) *L. reuteri* DSM20016 cell extract, from an anaerobic culture and C) *L. reuteri* DSM20016 cell extract, from an aerobic culture.

A cobamide plate bioassay was first used for the detection of cobamide production in cell extracts and supernatants of *L. reuteri* MM4-1A, L1600-1, 20-2, ATCC 53608 and 100-23 strains. In this assay, quantification is determined by measuring the halo produced by the cobamide auxotroph *S.* Typhimurium AR2680 (grown on the plate) which is proportional to the amount of cobamide present as shown using a standard curve (Figure 20). The limit of detection for this assay was 100 ng/mL CNPsCbl. Using this approach, intracellular cytosolic cobamide production was demonstrated for *L. reuteri* MM4-1A, 20-2 and ATCC 53608 strains (Figure 20). No extracellular cobamide production by *L. reuteri* MM4-1A, L1600-1, 20-2, ATCC

53608 and 100-23 was detected using this bioassay. The lack of cobamide production by *L. reuteri* 100-23 and L1600-1 strains was in agreement with our bioinformatics analyses.

In order to estimate the cobamide concentrations within the cell extracts of *L. reuteri* MM4-1A, 20-2 and ATCC 53608 strains, the number of *L. reuteri* cells in the growth culture (500 mL) were first determined using optical density (OD) measurements at a wavelength of 600 nm (OD_{600}). Bacterial enumeration was determined using viable cell counts of plated serial dilutions of liquid cultures. An OD_{600} of 1 was found to be equivalent to 10^7 cells/mL for *L. reuteri* MM4-1A, whilst an OD_{600} of 1 was equivalent to 10^8 cells/mL for *L. reuteri* 20-2 and ATCC 53608. At the time of sample collection *L. reuteri* MM4-1A, 20-2 and ATCC 53608 had an OD_{600} of 0.88, 0.62 and 0.47, respectively. Using this approach, it was estimated that 0.02053 ng, 0.00017 ng and 0.00024 ng of cobamide were produced by 10^9 *L. reuteri* MM4-1A, 20-2 and ATCC 53608 cells, respectively.

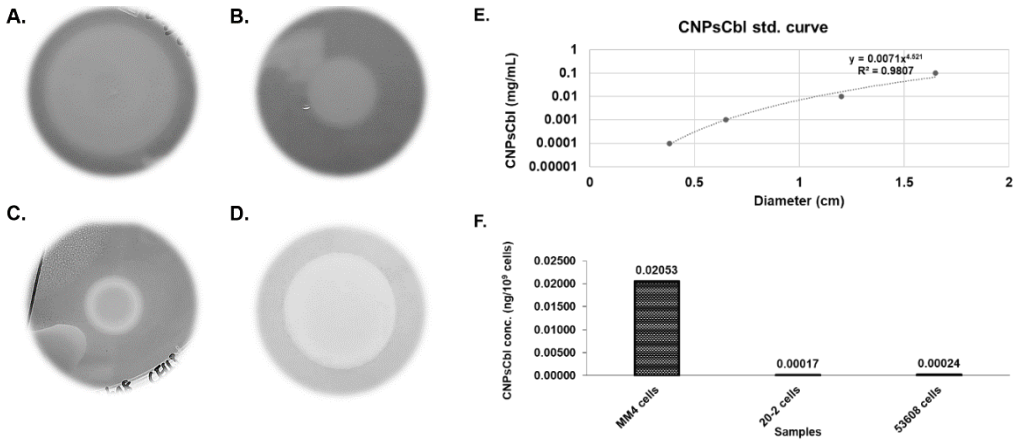

Figure 20 Determination of cobamide production in *L. reuteri* strains using cobamide quantitative bioassay. Growth of cobamide auxotroph *S. Typhimurium* AR2680 upon addition of cobamide extracted from A) *L. reuteri* MM4-1A, B) 20-2 and C) ATCC 53608 compared to D) 0.1 mg/mL CNPsCbl standard. The halo produced by *S. Typhimurium* is proportional to the amount of cobamide present. Halo's A, B, C and D are not to scale. The quantity produced was calculated from a standard curve (E) derived from serially diluting a 1 mg/mL stock solution to form 0.1, 0.01, 0.001, 0.0001, 0.00001 and 0.000001 mg/mL. F) Quantification of CNPsCbl detected in cell extracts expressed as ng/10^9 cells. Cell number was calculated based on optical density (OD) of cultures at the time of sample collection, with absorbance measured at 600 nm. Cultures of MM4-1A, 20-2 and ATCC 53608 had an OD of 0.88, 0.62 and 0.47 at 600nm respectively. An OD of 1 is equivalent to 10^7 cells/mL for *L. reuteri* MM4-1A and 10^8 cells/mL for *L. reuteri* 20-2, ATCC 53608.

Next, UPLC-MS/MS was used as a more sensitive method for cobamide detection and quantification. Here, CNPsCbl limit of detection by UPLC-MS/MS was

estimated to be 0.0001 mg/mL using standard dilutions. This analysis confirmed the production of PsCbl by *L. reuteri* 20-2, MM4-1A, and ATCC 53608 strains in cell extracts and supernatants grown under aerobic conditions. Cyanolated PsCbl was not detected in cell extracts or supernatants of *L. reuteri* strains L16001 or 100-23 under these experimental conditions (Figure 21 and 22), as also shown by the plate assay. However, this more sensitive approach showed PsCbl production by *L. reuteri* MM4-1A in both cytosolic and extracellular whilst in *L. reuteri* 20-2 and ATCC 53608 strains, PsCbl was restricted to cytosolic production (Figure 21 and 22).

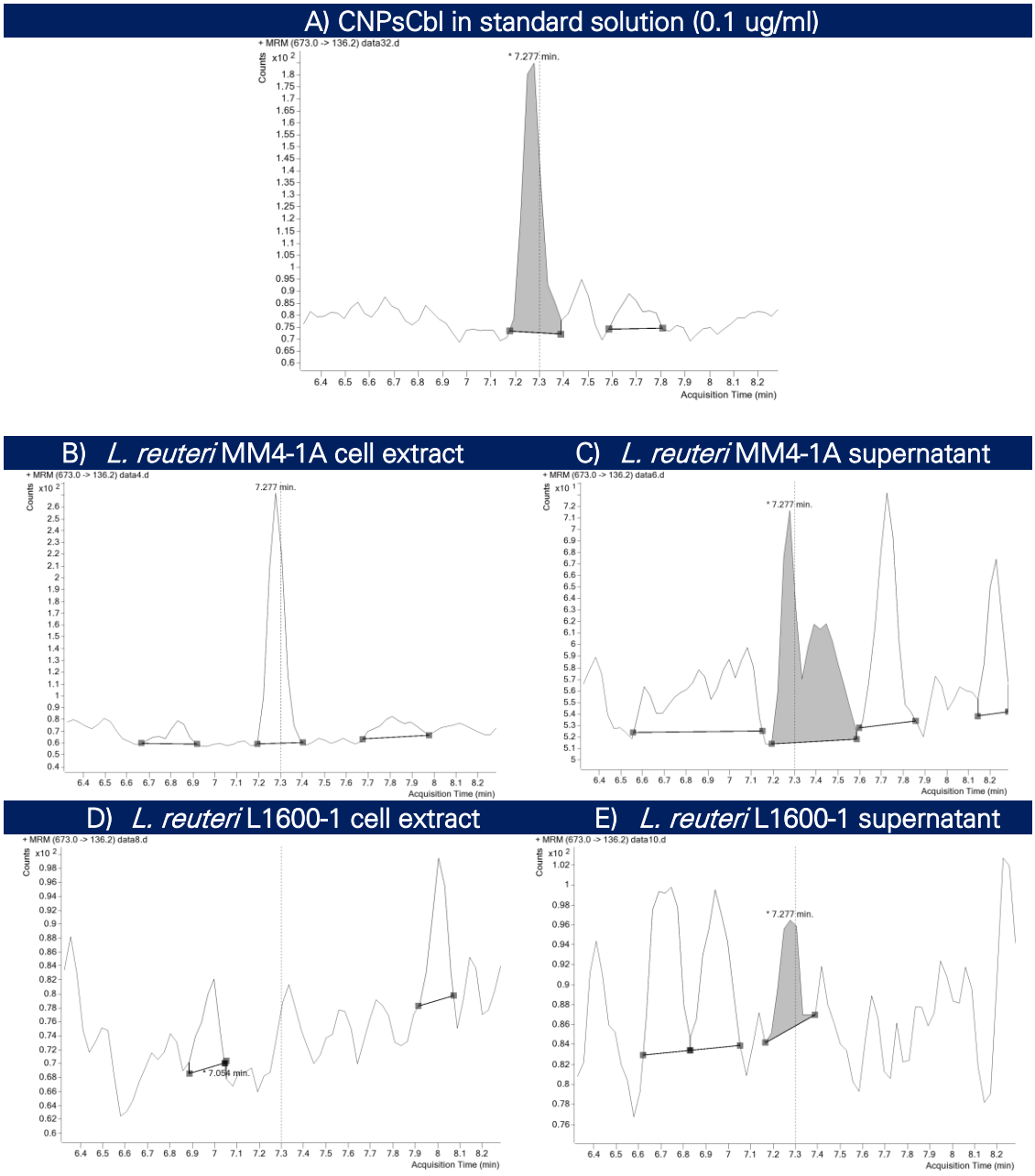

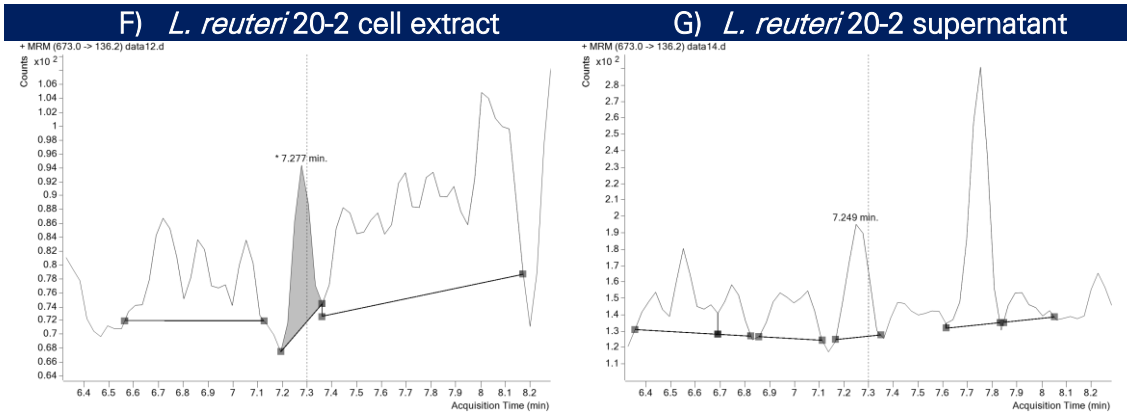

Figure 21 UPLC-MS/MS detection of cobamide in *L. reuteri* MM4-1A, L1600-1 and 20-2. Shown are the chromatograms for: A) CNPsCbl standard at 0.1 ug/ml, B) *L. reuteri* MM4-1A cell extract, C) *L. reuteri* MM4-1A supernatant, D) *L. reuteri* L1600-1 cell extract, E) *L. reuteri* L1600-1 supernatant, F) *L. reuteri* 20-2 cell extract and G) *L. reuteri* 20-2 supernatant.

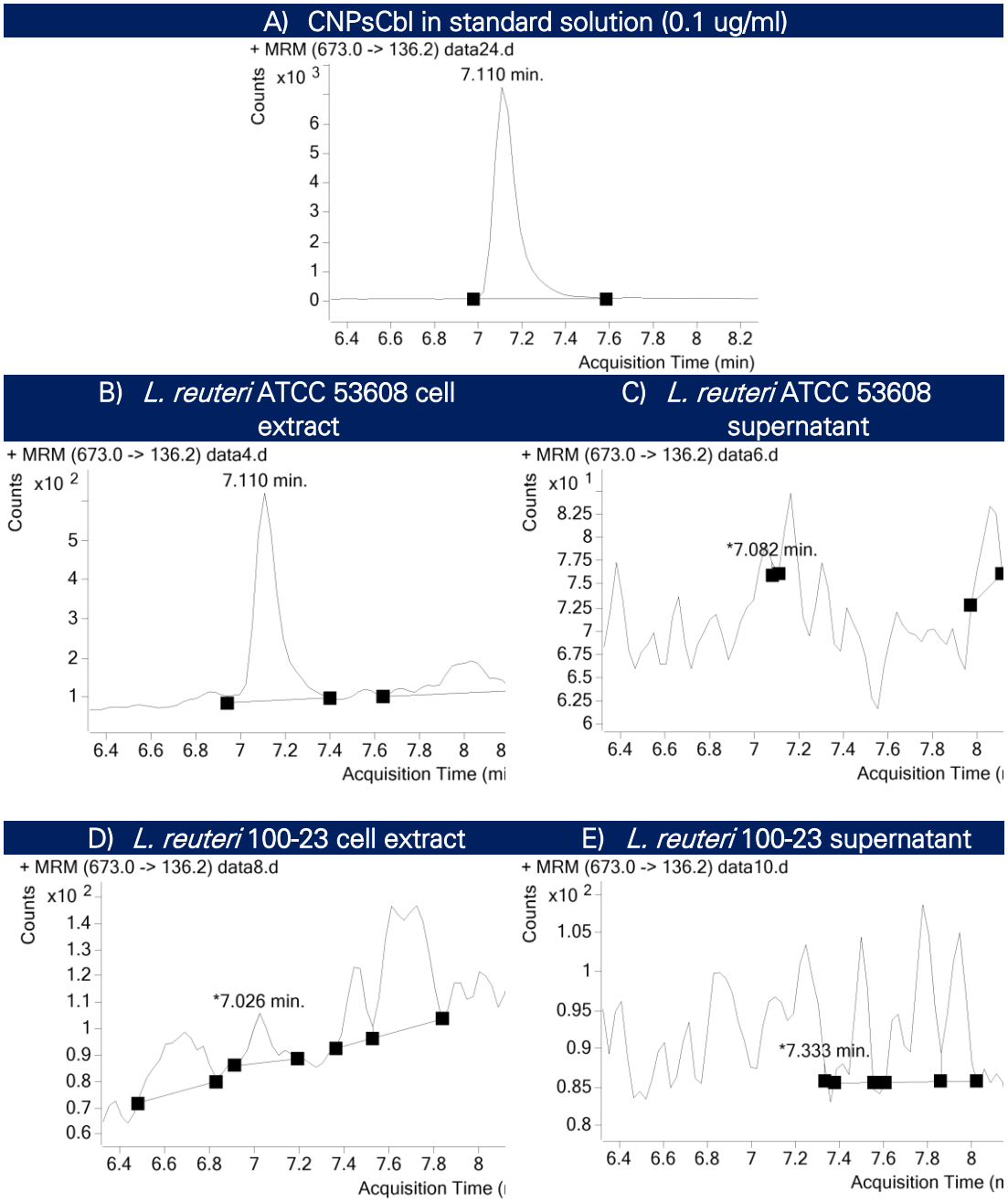

Figure 22 UPLC-MS/MS detection of cobamide in *L. reuteri* ATCC 53608 and 100-23. Shown are the chromatograms for: A) CNPsCbl standard at 0.1 ug/ml, B) *L. reuteri* ATCC 53608 cell extract, C*) L. reuteri* ATCC 53608 supernatant, D) *L. reuteri* 100-23 cell extract and E) *L. reuteri* 100-23 supernatant.

A CNPsCbl calibration curve was then used to quantify cyanolated PsCbl in the cell extracts and supernatants of *L. reuteri* MM4-1A, 20-2 and ATCC 53608 strains (Figure 23A). Using this approach, 0.153 ng, 0.002 ng and 0.207 ng of PsCbl were shown to be produced in cell extracts by 10^9 *L. reuteri* MM4-1A, 20-2 and ATCC 53608 cells, respectively (Figure 23B). This analysis confirmed that *L. reuteri* MM4-

1A was the only strain that demonstrated extracellular production of PsCbl, with 0.013 ng CNPsCbl detected in the supernatant from 10^9 *L. reuteri* MM4-1A cells (Figure 23B).

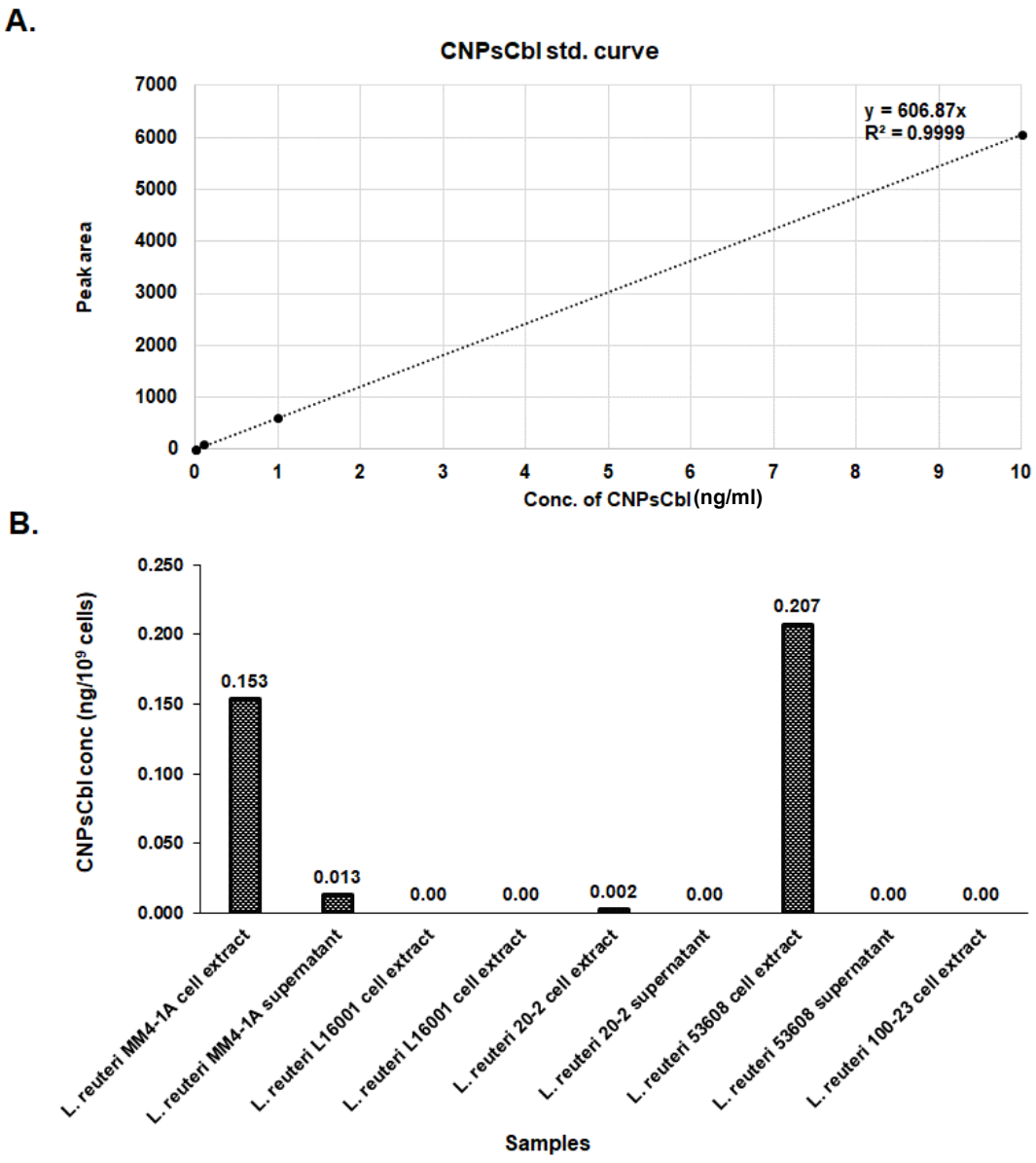

Figure 23 Quantification of cytosolic and extracellular PsCbl production by *L. reuteri* strains using UPLC-MS/MS. A. CNPsCbl standard curve used to calculate concentration from peak area produced by samples. B. Quantification of CNPsCbl detected in cell extracts expressed as ng/10^9 cells. Cell number was calculated based on optical density (OD) of cultures at the time of sample collection, with absorbance measured at 600 nm. Cultures of MM4-1A, 20-2 and ATCC 53608 had an OD of 0.88, 0.62 and 0.47 at 600nm respectively. An OD of 1 is equivalent to 10^7 cells/mL for *L. reuteri* MM4-1A and 10^8 cells/mL for *L. reuteri* 20-2, ATCC 53608.

3.3 Discussion

The biosynthesis of cobamide is confined to a subset of prokaryotes, with approximately 25% of gut bacteria predicted to be able to synthesise cobamides *de novo* while an estimated 80% of gut microbes are auxotrophic for cobamides, namely cobalamins, making cobamide production within the gut a major colonisation factor and a likely modulator of microbial communities (Degnan *et al.*, 2014). *L. reuteri* CRL 1098 was the first lactic acid bacteria shown to produce the cobamide PsCbl, with cobamide production restricted to this form (Taranto *et al.*, 2003; Santos *et al.*, 2007).

Here, a comprehensive *in silico* analysis of all publicly available *L. reuteri* genomes was carried out to determine *L. reuteri* cobamide biosynthesis potential. *L. reuteri* strains that have been characterised as producers of cobamides include JCM 1112 (Santos, Wegkamp, *et al.*, 2008), DSM 20016 (Sriramulu *et al.*, 2008) and CRL1098 (Taranto *et al.*, 2003), with this strain reported to exclusively produce PsCbl (Santos *et al.*, 2007). Previous transcriptomic analyses of *L. reuteri* CRL1098 suggested that *cbiABCDETFGHJ, cobA/hemD, cbiKLMNQOP, sirA*, *hemACBL*, cobUSC, *hemD* and *cobT* genes were required for the *de novo* anaerobic biosynthesis of PsCbl (Santos, Vera, *et al.*, 2008). Here, 191/381 (50.13%) *L. reuteri* strains, including *L. reuteri* CRL1098, JCM 1112 and DSM 20016 were shown to possess this pathway (Supplementary Figure 2). However, genomic analysis alone does not allow to determine the specific cobamide produced by the strains due to the heterogeneity of exogenous compounds that can be incorporated in the lower ligand of cobamides such as 5,6-DMB and other benzimidazoles, purines or phenolic compounds. VitB12 has 5,6-DMB in its lower ligand while PsCbl for example has an adenine group in its lower ligand. Synthesis of 5,6-DMB, can occur via an aerobic or anaerobic pathway with the aerobic pathway utilising 5,6-DMB synthase, *BluB,* involved in the synthesis of 5,6-DMB from flavin mononucleotide (FMN) (Taga *et al.*, 2007) and the anaerobic pathway requiring *bzaABCDE* genes converting 5-aminoimidazole ribotide (AIR) to DMB through a series of enzymatic reactions (Figure 24) (Hazra *et al.*, 2015). Here, the lack of DMB biosynthesis genes (BzaA-E and BluB) in the genomes of the analysed *L. reuteri* strains confirmed the inability of these strains to produce cobalamin whereas their genetic machinery suggested

the synthesis of different cobamide harbouring an alternative lower ligand moiety. These results are in line with previous reports demonstrating cobamide synthesis by *L. reuteri* strains showing the production of PsCbl, a cobamide with the purine adenine in its lower ligand in replacement of the 5,6-DMB moiety present in cobalamin (Santos *et al.*, 2007; Sriramulu *et al.*, 2008; Crofts *et al.*, 2013).

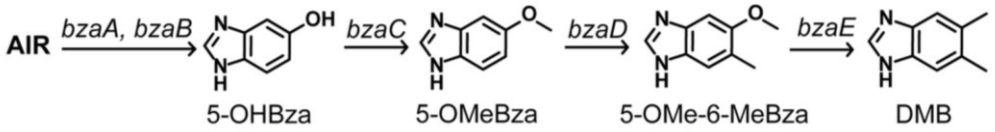

Figure 24 Schematic of anaerobic 5,6-DMB synthesis by bzaABCDE. Function of bzaABCDE genes in the conversion of AIR to 5,6-DMB. 5-OHBza is first synthesised by bzaA and bzaB genes. bzaC methylates 5-OHBza, forming 5-OMeBza. bzaD further methylates 5-OMeBza converting it into 5-OMe-6-MeBza which is then converted to DMB by bzaE. Taken from Hazra *et al.*, 2015.

Experimental validation of both cytosolic and extracellular cobamide production was carried out with five *L. reuteri* strains, MM4-1A, L1600-1, 20-2, 53608 and 100-23. Cytosolic PsCbl production was confirmed for *L. reuteri* strains, MM4-1A, 20-2 and 53608 using UPLC-MS/MS and plate assays while extracellular production was only detected for MM4-1A by LC-MS, likely due to reduced sensitivity of the cobamide plate bioassay. These results are in line with our *in silico* analysis which predicted the production of a cobamide by *L. reuteri* MM4-1A, 20-2 and ATCC 53608 strains due to the presence of a partial cobalamin biosynthesis pathway and predicted the inability to synthesise cobamides by *L. reuteri* L1600-1 and 20-2 which are lacking the genes required for cobamide synthesis.

It is important to note that not all genomes analysed in this study were complete, with approximately 90% in the form of draft or partial genomes (see Supplementary Table 3 for details on assembly level of *L. reuteri strains* included in this study), the *in silico* analysis may therefore be under-representative of the range of *L. reuteri* cobamide-producing strains. In addition, the analytical approach used here for detecting and quantifying cobamides does not allow to differentiate between various forms of PsCbl.

The capacity of *L. reuteri* strains, MM4-1A, 20-2 and 53608 to produce PsCbl is in agreement with the substrate specificity of the *L. reuteri* cobT gene encoding the nicotinate-nucleotide--dimethylbenzimidazole phosphoribosyltransferase enzyme, responsible for the incorporation of compounds into the lower ligand of the cobamide structure (Crofts *et al.*, 2013). In *L. reuteri* DSM 20016, this enzyme has been shown to restrict the incorporation of benzimidazoles and phenolic compounds into the lower ligand, only allowing incorporation of adenine and subsequently limiting *L. reuteri* cobamide production to PsCbl (Crofts *et al.*, 2013).

Characterisation of PsCbl dates back to 1952 (Dion, Calkins and Pfiffner, 1952) although PsCbl has been found to lack functionality in humans and as result of this PsCbl has gained less attention in comparison to the highly studied cobamide, cobalamin. This can be attributed to the inability of PsCbl to act as a cofactor for mammalian cobalamin-dependent methylmalonyl-CoA mutase and methionine synthase (Bito *et al.*, 2020) as well as having significantly low binding affinity to the mammalian cobalamin-binding receptor required for cobalamin uptake, intrinsic factor, which largely reduces its utilisation by humans (Stupperich and Nexø, 1991). However, with regard to the human gut microbial community, PsCbl and its methylated form, Coβ-cyano-(2-methyladeninyl)-cobamide (Factor A) have been shown to make up 12.5% and 60.6% of all cobamide forms present in human faeces, respectively, indicative of microbial production of PsCbl in the human intestine (Allen and Stabler, 2008). Aside from *L. reuteri* strains, PsCbl production has also been documented in *S.* Typhimurium, which can incorporate either adenine or 2-methyl-adenine into the lower ligand of its synthesised corrinoid, producing either PsCbl or factor A under strict anaerobic conditions (Keck and Renz, 2000). Recently, PsCbl production was also demonstrated in *Blautia producta DSM 14466*, *Blautia hydrogenotrophica* DSM 10507 T*, Blautia obeum* DSM 25238, *Marvinbryantia formatexigens* DSM 14469 and *Ruminococcus gauvreauii* DSM 19829 with PsCbl being the primary cobamide produced by *B. producta*, *M. formatexigens* and *R. gauvreauii* and cyanocobalamin in *B. hydrogenotrophica* and *B. obeum* (Kundra *et al.*, 2024)*. Eubacterium hallii* strain L2-7 was also shown to produce PsCbl in a separate study (Belzer *et al.*, 2017).

Very little has been documented about PsCbl biological function in the gut but, in recent years, PsCbl has been shown to promote the growth of and stimulate propionate production in *Akkermansia muciniphila* from PsCbl produced by *E. hallii* (Belzer *et al.*, 2017; Mok *et al.*, 2020)*, B. producta*, *M. formatexigens* and *R. gauvreauii* (Kundra *et al.*, 2024)*. A. muciniphila* represents 3-5% of the human microbiota (Derrien *et al.*, 2004; Belzer and De Vos, 2012) and is largely known for its beneficial effects against diabetes and obesity as well as being inversely correlated with inflammation and metabolic syndrome as reviewed by Zhou, 2017. Increased dietary intake of cobalamin has also been shown to increase the relative abundance of *A. muciniphila* in the gut (Gurwara *et al.*, 2019) with *in vitro* studies demonstrating the ability of *A. muciniphila* to remodel several structurally dissimilar cobamides into PsCbl through use of novel enzyme, cobamide remodelling phosphodiesterase encoded by the *CbiR* gene (Mok *et al.*, 2020)*.* This enzymes initiates the remodelling process through hydrolysis of the phosphoribosyl bond within the nucleotide loop of the cobamide structure (Mok *et al.*, 2020)*.*

The ability of *L. reuteri* strains to be able to synthesise PsCbl and more importantly release the compound into its environment has therefore the potential to influence the composition of the human gut microbiota through cross-feeding interactions with PsCbl-utilising gut commensals such as health-promoting *A. muciniphila*. Since *L. reuteri* is a known GRAS strain, this work will help select strains that could be used as part of probiotic approaches to benefit human health.

Chapter 4

Cobamide metabolism in *R. gnavus* strains

4.1 Introduction

In the human gut, over 80% of bacteria are predicted to utilise cobamides as co-factors in enzymatic reactions to facilitate structural rearrangements, methylations and eliminations of specific groups from compounds, whilst approximately only 20% have been proposed to possess the genetic machinery for cobamide synthesis (Degnan, Taga and Goodman, 2014).

The transport of cobamides from the environment into the cell is a significant determinant of fitness for bacteria within the gut ecosystem (Degnan *et al.*, 2014). Over half of gut microorganisms are bioinformatically predicted to possess cobamide transporters (Shelton *et al.*, 2018).

The mechanisms of cobamide transport by Gram-negative bacteria have mainly been studied in *Escherichia coli*, wherein the outer-membrane β-barrel protein, BtuB, facilitates the translocation of cobamides across the outer membrane into the periplasm (Figure 25) (Roth, Lawrence and Bobik, 1996) and its expression is regulated by a riboswitch that binds adenosylcobalamin (AdoCbl) (Lundrigan *et al.*, 1987). In the periplasm, the cobamide binds to the periplasmic protein BtuF, which then crosses the inner membrane through the ABC-type transporter BtuCD where it enters the cytoplasm (Figure 25) (Roth, Lawrence and Bobik, 1996). These proteins form part of the BtuBCDF system which is encoded by genes within the *btu* operon, characterised in *Synechococcus* sp. strain PCC 7002 (Pérez, Rodionov and Bryant, 2016). A subset of Gram-negative prokaryotes lack the BtuBCDF and instead use BtuM for cobamide transportation as characterised in *Thiobacillus denitrificans* (Figure 25) (Rempel *et al.*, 2018).

In Gram-positive prokaryotes, cobamide transportation is carried out via an energy-coupling factor (ECF)-type ATP-binding cassette (ABC) transporter, CbrT, characterised in *Lactobacillus delbrueckii,* with this system sharing functionality with the BtuBCDF transport system (Figure 25) (Santos *et al.*, 2018).

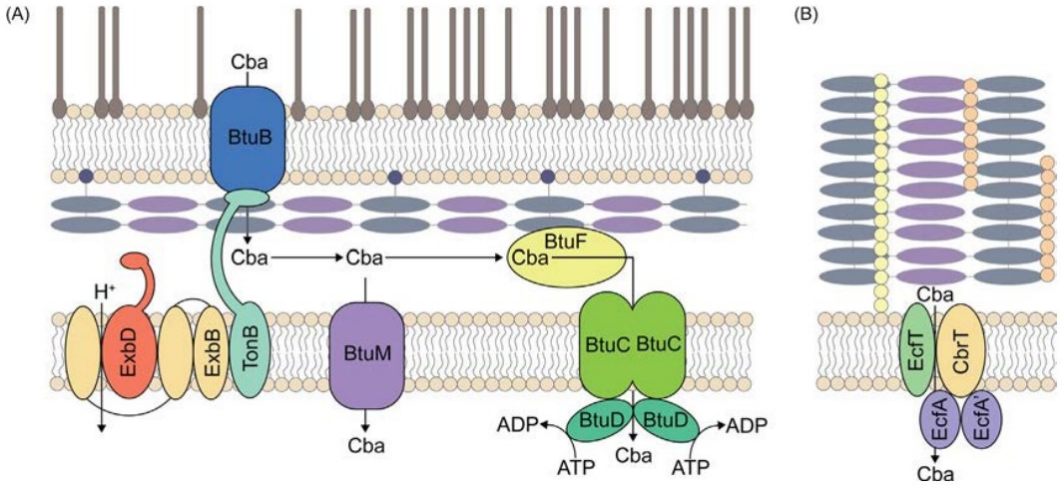

Figure 25 Cobamide uptake and scavenging systems in prokaryotes. (A) Cobamide transport system in Gram-negative prokaryotes. Cobamides are actively transported across the outer membrane by the Ton-dependent transporter BtuB into the periplasmic space. Within the periplasm, the protein BtuF binds cobamides and delivers them to the BtuCD transporter for transport into the cytoplasm. Gram-negative bacteria lacking the BtuCDF system, utilise the BtuM transporter instead which facilitates the direct transport of cobamides into the cytoplasm. (B) Cobamide transport system utilised in Gram-positive prokaryotes. In this system, the energy coupling factor (ECF)-dependent transporter CbrT is responsible for the direct transport of cobamides into the cytoplasm. Taken from (Costa *et al.*, 2020).

Cobalamins are the best studied cobamides for their role in enzymatic mechanisms and include adenosylcobalamin (AdoCbl), methylcobalamin (MeCbl), hydroxycobalamin (OHCbl) and cyanocobalamin (CNCbl), whilst structural differences in the lower ligand of cobalamin compounds give rise to a range of cobamide derivatives (Costa *et al.*, 2020) including pseudocobalamin (PsCbl), Coβ-cyano-(5-methylbenzimidazolyl)-cobamide (vitamin B_{12}- 5 MB), Coβ-cyano-(5-methoxybenzimidazolyl)-cobamide (vitamin B_{12}- Factor IIIm), Coβ-cyano-(2-methyladeninyl)-cobamide (vitamin B_{12}- Factor A), and Coβ-cyano-(5-hydroxybenzimidazolyl)-cobamide (vitamin B_{12}- Factor III).

In bacteria, cobamide-dependent reactions are carried out by two main subfamilies of enzymes, isomerases and methyltransferases (Costa *et al.*, 2020).

Isomerases represent the predominant category of enzymes dependent on cobamides and they function in breaking the cobalt-carbon bond in AdoCbl, to produce an adenosyl radical required for the initiation of several metabolic processes (Banerjee and Ragsdale, 2003). These isomerases include the well-studied methylmalonyl-CoA mutase (MCM), which is involved in the fermentation of pyruvate to propionate in bacteria (graphically represented in Chapter 1, section

1.3.3.2, Figure 12). Other isomerases include ethylmalonyl-CoA mutase (Ecm) and (Glm) involved in the conversion of ethylmalonyl-CoA to methylsuccinyl-CoA and (S)-glutamate to (2S,3S)-3-methylaspartate, respectively (Banerjee and Ragsdale, 2003).

Radical SAM methyltransferases are a large group of enzymes, bioinformatically predicted to encompass thousands of members (Bridwell-Rabb, Grell and Drennan, 2018). These enzymes are responsible for catalysing methylation reactions and have been shown to be involved in the production of antimicrobials (Bridwell-Rabb, Grell and Drennan, 2018) and bacteriochlorophyll in plant symbionts (Gough, Petersen and Duus, 2000). In cobamide-dependent methylation reactions, a methyl group is transferred from a methyl donor to an acceptor using a cobamide carrier which has a methyl group covalently bonded to the central cobalt ion of the corrin ring structure (Costa *et al.*, 2020). These enzymes are involved in a range of essential pathways including CO_2 fixation, amino acid metabolism and one-carbon metabolism (Costa *et al.*, 2020). Amongst the cobamide-dependent methyltransferases, the cobamide-dependent methionine synthase, encoded by the gene *MetH,* is one of the most prominent cobamide-dependent enzymes in bacteria (Shelton *et al.*, 2018). Cobamide-dependent methionine synthase functions in transferring a methyl group from MeCbl to homocysteine to form methionine, an essential amino acid in all organisms (graphically represented in Chapter 1, section 1.3.3.2, Figure 12) (Costa *et al.*, 2020).

Cobamides are an example of shared resources which have been suggested to act as a modulator of the human gut microbiota (Degnan, Taga and Goodman, 2014). Previous work showed that when grown in co-culture with *R. gnavus* ATCC 29149, *MetH* was one of the main genes down-regulated in *R. bromii* L2-63, suggesting that cobamide availability became limited in the presence of *R. gnavus* ATCC 29149 and therefore that *R. gnavus* may be able to utilise cobamide (Crost *et al.*, 2018). This study also demonstrated the ability of *R. gnavus* to utilise starch degradation products released by *R. bromii* L2-63 in co-culture (Crost *et al.*, 2018), demonstrating the ability of *R. gnavus* to cross-feed with other organisms inhabiting the human gut for improved fitness. In addition, *R. gnavus* CC55_001C was proposed as a 'tetrapyrrole precursor salvager' based on *in silico* analyses revealing a partial biosynthetic pathway in its genome (Shelton *et al.*, 2018).

This chapter combined comparative genomics, transcriptomics and *in vitro* growth assays to gain mechanistic insights into (i) *R. gnavus* utilisation of cobamides from both exogenous sources and via cross-feeding with cobamide-producing *L. reuteri* strain and (ii) *R. gnavus* cobamide synthesis capacity.

4.2 Results

4.2.1 *In silico* analysis revealed cobamide-dependent, transporter and biosynthetic genes across *R. gnavus* strains

4.2.1.1 *R. gnavus* strains possess the genetic capacity to utilise cobamides

Cobamide utilisation by *R. gnavus* strains was first investigated by analysing the occurrence of genes encoding cobamide-dependent proteins and putative cobamide transporters across all publicly available genomes using BLAST command line. The statistical significance of the BLAST alignment was calculated and output as sequence percentage identity, visually represented in Supplementary Figure 3. Gene presence (indicated by the red colour) was predicted if percentage identity between the query sequence (cobamide-dependent proteins or putative cobamide transporters) and the target sequence (*R. gnavus* genome) was greater than 80% whereas gene absence (indicated by the blue colour) was predicted if percentage identity between the query sequence and the target was less than 80%.

Out of the 162 *R. gnavus* genomes analysed, over 98% were found to possess genes encoding the following cobamide-dependent or transporter enzymes: cobamide-dependent methionine synthase, *MetH* and a *MetH* subunit *metH2*; methanol:coenzyme M methyltransferase, *MtaB*; a TIGR03960 family cobamide-binding radical SAM protein, RGna_03200; glycerol dehydratase complex, *dhaBCE*; propanediol dehydratase complex, *pduCDE* and a *YgiQ* like, cobamide-dependent radical SAM superfamily protein RGna_12670. In addition, *R. gnavus* strain AF33-12, RTP21484st1_C12_RTP21484_190118, RTP21484st1_E7_RTP21484_190118 and RTP21484st1_H11_RTP21484_190118 were the only strains predicted to possess a *btuF*-like gene, encoding ABC transporter substrate-binding protein involved in cobamide import. All *R. gnavus* strains included in this analysis were predicted to possess at least one gene encoding a cobamide-dependent protein or transporter enzyme, suggesting that *R. gnavus* strains can utilise cobamides.

4.2.1.2 *R. gnavus* strains possess a partial cobamide biosynthetic pathway

The cobamide biosynthesis capacity of *R. gnavus* was examined by analysing the occurrence of genes encoding putative proteins required for cobamide biosynthesis in the genomes of all publicly available *R. gnavus* strains using BLAST command line. The statistical significance of the BLAST alignment was calculated and output as sequence percentage identity. The data are graphically represented in the form of a heat map shown in Supplementary Figure 4. Gene presence (indicated by the red colour) was predicted if percentage identity between the query sequence (cobamide biosynthesis gene) and the target sequence (*R. gnavus* genome) was greater than 80% whereas gene absence (indicated by the blue colour) was predicted if percentage identity between the query sequence (cobamide biosynthesis gene) and the target sequence (*R. gnavus* genome) was less than 80%.

None of the *R. gnavus* strains analysed harboured the complete cobalamin biosynthesis pathway (with the exception of *R. gnavus* isolate B93_003). All strains lacked the genes *HemA, HemL* and *HemB* involved in the synthesis of precursors uroporphyrinogen III from glutamate (Figure 26); *CbiO, CbiT, CbiN, CobR, CobF, CbiE, CbiQ, CbiM, CobG* and *CobN*, involved in the synthesis of the corrin ring, and *CbiZ, CobY* and *PduX* involved in corrin ring adenosylation, attachment of the amino-propanol linker and the assembly of the nucleotide loop (Figure 26). *HemD* was also absent in all strains but identified as a *CysGA-HemD* fusion gene in 159/162 strains. *BluB* and *BzaABCDE* genes, responsible for the synthesis of 5,6-DMB in the lower ligand of the active forms of cobalamin (AdoCbl, MeCbl, OHCbl and CNCbl) were also absent across *R. gnavus* strains, however the closely related gene *ThiC* (Figure 26) (Hazra et al., 2015) was present across all strains.

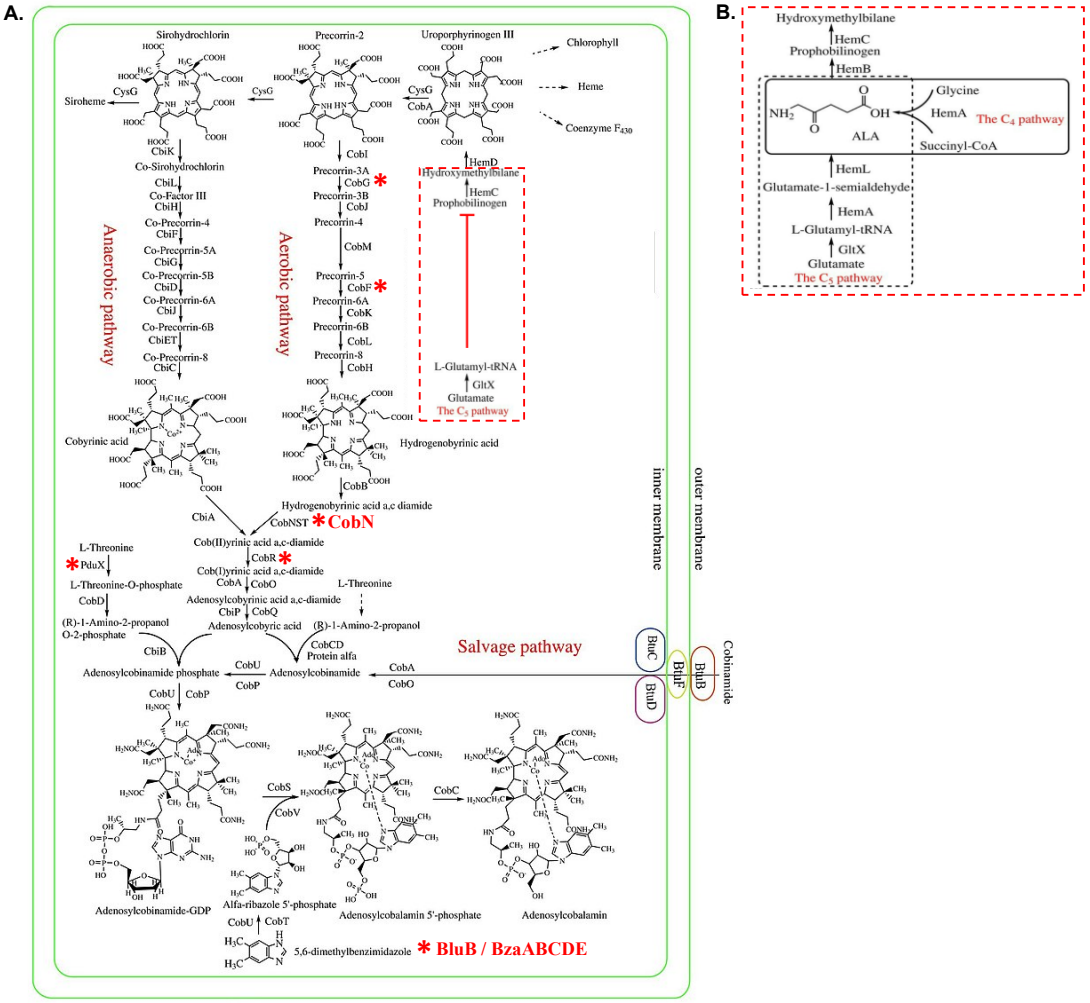

Figure 26 The predicted *R. gnavus* cobamide biosynthetic pathway. A. The red asterisks highlight the absence of a gene from the pathway. Red dashed border highlights disrupted cobalamin biosynthetic pathway, glutamate to hydroxymethylbilane in *R. gnavus*. B. The cobalamin biosynthetic pathway, glutamate to hydroxymethylbilane, with complete set of genes for hydroxymethylbilane biosynthesis.

These findings suggest that *R. gnavus* strains cannot synthesise cobalamin *de novo*, however out of the 162 *R. gnavus* strains analysed, 94% possess a partial cobamide biosynthesis pathway which could support the synthesis of a cobamide derivative from the cobamide precursor porphobilinogen (PBG) (Supplementary Figure 4) (see Supplementary Table 7 for the list of cobalamin biosynthetic genes and Supplementary Table 8 for full list of strains with potential for cobamide biosynthesis from PBG).

4.2.2 *R. gnavus* shows enhanced growth in monoculture in the presence of cobamide analogues and derivatives and in co-culture with PsCbl-producing *L. reuteri* MM4-1A.

Preliminary *in silico* data revealed the presence of a *MetE* gene, across all *R. gnavus* genomes analysed (Supplementary Figure 5), which encodes a cobamide-independent methionine synthase. This enzyme catalyses the transfer of a methyl group from 5-methyltetrahydrofolate to homocysteine to form methionine (Met) (Gonzalez *et al.*, 1992). *MetH*, encoding cobamide-dependent methionine synthase is also present in all *R. gnavus* genomes analysed with exception to *R. gnavus* strain MSK.8.22 and *R. gnavus* strain B636_003 (Supplementary Figure 5). These data suggest that *R. gnavus* ATCC 29149 may be capable of synthesising Met *de novo* (via MetE) and/or via cobamide-dependent pathways (via MetH) depending on the environment/growth conditions and cobamide/Met availability.

In order to validate the *in silico* findings (section 4.2.1) which predicted cobamide utilisation capacity across 163 *R. gnavus* strains, *R. gnavus* ATCC 29149 was first grown under strict anaerobic conditions in monoculture in synthetic medium lacking methionine (LAB(-Met)) with glucose (Glc) as carbon source. LAB(-Met) media was supplemented with exogenous cobalamin analogues (cyanocobalamin (CNCbl), methylcobalamin (MeCbl), adenosylcobalamin (AdoCbl) and hydroxocobalamin (OHCbl)) or cobamide derivatives (cyanopseudocobalamin (CNPsCbl), coβ-cyano-(5-methylbenzimidazolyl)-cobamide (5MB), coβ-cyano-(5-methoxybenzimidazolyl)-cobamide (vitB12 - Factor IIIm), coβ-cyano-(2-methyladeninyl)-cobamide (vit B12 - Factor A), or coβ-cyano-(5-hydroxybenzimidazolyl)-cobamide (vitB12 - Factor III)).

The growth rate was monitored spectrophotometrically at 600 nm over 12 h (Figure 27).

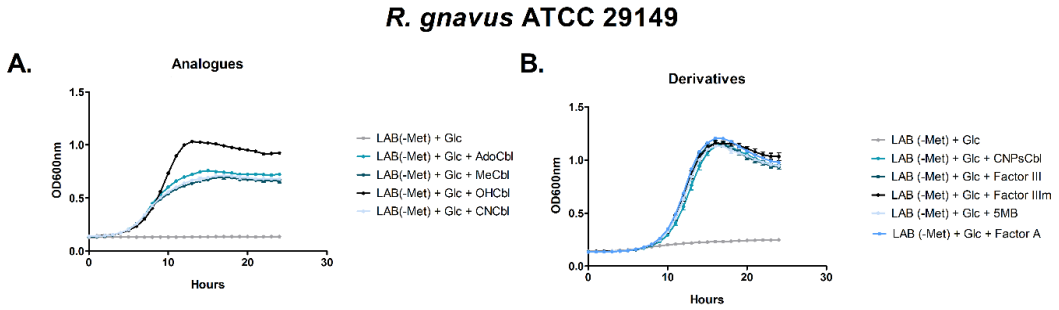

Figure 27 Effect of cobamide supplementation on *R. gnavus* ATCC 29149 anaerobic growth under Met-deficient conditions. Growth curves of *R. gnavus* ATCC 29149 in LAB(-Met) supplemented with A. Cobalamin analogues AdoCbl, MeCbl, OHCbl, CNCbl and B. Cobamide derivatives PsCbl, vitB12 – Factor III, vitB12 – Factor IIIm, vitamin B12 – 5MB and vitB12 – Factor A, with glucose (Glc) as carbon source.

No or limited growth was detected in LAB(-Met) + Glc, indicating that *R. gnavus* is not able to synthesise Met in sufficient amount to support its growth in these conditions. *R. gnavus* ATCC 29149 showed enhanced growth upon supplementation with cobalamin analogues and cobamide derivatives, suggesting that in Met-deficient conditions, *R. gnavus* can utilise these cobamides to support Met synthesis via the cobamide-dependent pathway.

More specifically, *R. gnavus* ATCC 29149 demonstrated preferential growth in the presence of OHCbl compared to all other cobalamin analogues tested. In the presence of AdoCbl, MeCbl and CNCbl, *R. gnavus* growth rates remained similar across these conditions. *R. gnavus* ATCC 29149 demonstrated similar levels of enhanced growth in the presence of all cobamide derivatives tested.

The growth assays were then extended to five *R. gnavus* strains (ATCC 29149, ATCC 35913, E1, CC55_001C, 2_1_58FAA and Finegold) anaerobically grown in monocultures. Supplementation of cobalamin analogues or cobamide derivatives resulted in enhanced growth for all strains tested compared to the control, demonstrating the ability of *R. gnavus* to utilise cobamide in different forms (see Supplementary Figure 6 and 7 for growth results of all strains).

R. gnavus strain ATCC 29149 was then used to examine cobamide utilisation by *R. gnavus* in co-culture with PsCbl-producing *L. reuteri* strain MM4-1A or non-

cobamide producing *L. reuteri* strain L1600-1 (characterised for cobamide production in Chapter 3). Here, *R. gnavus* ATCC 29149 was grown in co-culture with either *L. reuteri* strain MM4-1A or *L. reuteri* strain L1600-1 in LAB(-Met) and in LAB(+Met). *R. gnavus* growth was monitored over 24 h by qPCR using 16S rDNA primers (Chapter 1, section 2.3.3, Table 1). The results (depicted in gene copies per mL of culture) are shown in Figure 28.

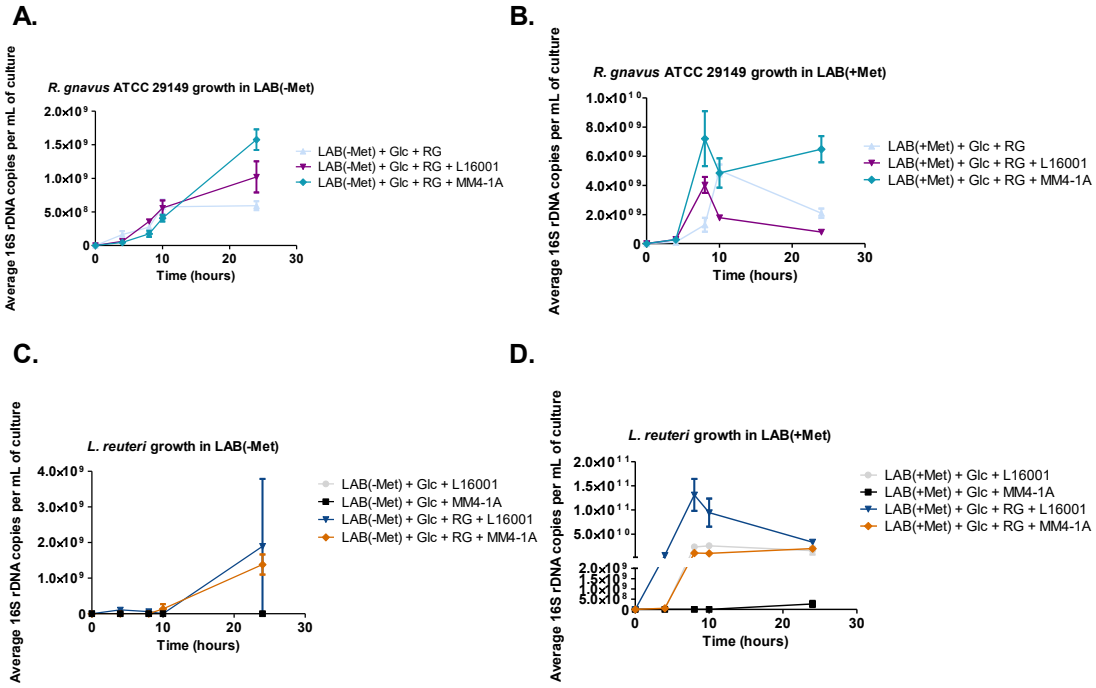

Figure 28 Bacterial quantification of *R. gnavus* ATCC 29149 and *L. reuteri* growth in monoculture and in co-culture by qPCR. Bacterial quantifications are expressed as 16S rDNA copy number/mL of culture for *R. gnavus* ATCC 29149 (A and B) and *L. reuteri* L1600-1 or MM4-1A (C and D) grown in LAB(-Met) or LAB(+Met) media, respectively. Glucose (Glc) is used as carbon source. Data points mark the mean of 3 replicates. The error bars correspond to standard deviations between replicates. Samples were collected at 0, 4, 8, 10 and 24 h. RG corresponds to *R. gnavus*.

The results of the qPCR analysis showed that *R. gnavus* growth in LAB(-Met) was enhanced by the presence of PsCbl-producing *L. reuteri* MM4-1A and to a lesser extent by the non-cobamide producing *L. reuteri* L1600-1 compared to the monoculture (Figure 28A). *L. reuteri* MM4-1A and *L. reuteri* L1600-1 were unable to grow in monoculture in LAB(-Met), however, in co-culture with *R. gnavus*, both strains showed enhanced growth (Figure 28B), indicating that *R. gnavus* is able to support their growth in these conditions, potentially as a result of cross-feeding.

In LAB(+Met), *R. gnavus* growth appeared to be inhibited by *L. reuteri* L1600-1 and increased by *L. reuteri* MM4-1A compared to *R. gnavus* grown in monoculture (Figure 28C). *L. reuteri* MM4-1A showed reduced growth in monoculture in LAB(+Met) while L1600-1 displayed enhanced growth in LAB(+Met), when compared to LAB(-Met). In co-culture with *R. gnavus* in LAB (+Met), both *L. reuteri* L1600-1 and MM4-1A showed enhanced growth compared to when grown under Met-deficient conditions (Figure 28D), similar to what was observed in (LAB-Met), providing strong indication of nutrient cross-feeding for supported *L. reuteri* growth under the conditions tested.

These results suggest that *R. gnavus* ATCC 29149 may benefit from cross-feeding of PsCbl produced by *L. reuteri* MM4-1A and also provide indication of the role of *R. gnavus* ATCC 29149 in supporting *L. reuteri* growth via nutrient exchange.

Overall, *R. gnavus* growth was significantly enhanced in LAB(+Met) across all conditions tested, underscoring *R. gnavus*' preference for acquiring Met from the medium rather than synthesising Met via the cobamide-dependent pathway. More specifically, a 311% increase in *R. gnavus* growth was seen when in co-culture with *L. reuteri* MM4-1A in the presence of Met compared to growth in monoculture.

The results of these co-culture assays demonstrate that PsCbl-producing *L. reuteri* strain is able to support *R. gnavus* growth and suggests cobamide cross-feeding activity between *R. gnavus* ATCC 29194 and *L. reuteri* MM4-1A.

4.2.3 Transcriptomic analyses shed light on *R. gnavus* metabolism of PsCbl and PBG

4.2.3.1 *R. gnavus* ATCC 29149 growth conditions for RNA seq analyses

To gain further insights into the molecular mechanisms underpinning the cobamide utilisation capacity of *R. gnavus* and cross-feeding interactions with *L. reuteri*, RNA seq-based transcriptomic analyses of *R. gnavus* ATCC 29149 in mono- and co-cultures with *L. reuteri* MM4-1A were carried out.

Briefly, *R. gnavus* ATCC 29149 was grown in LAB(-Met) or in LAB(+Met) media in the presence or absence of exogenous CNPsCbl, PBG or PsCbl-producing *L. reuteri* MM4-1A (Table 3). Glucose (Glc) was used as carbon source.

Table 3 Growth conditions used for RNA seq-based transcriptomic analysis of *R. gnavus* ATCC 29149.

Condition	Met	CNPsCbl	PBG	*L. reuteri* MM4-1A
LAB(-Met) medium + Glc	-	-	-	-
LAB(-Met) medium + Glc + CNPsCbl	-	+	-	-
LAB(-Met) medium + Glc + PBG	-	-	+	-
LAB media (-Met) + Glc + *L. reuteri* MM4-1A	-	-	-	+
LAB(+Met) medium + Glc	+	-	-	-
LAB(+Met) medium + Glc + CNPsCbl	+	+	-	-
LAB(+Met) medium + Glc + PBG	+	-	+	-
LAB(+Met) medium + Glc + *L. reuteri* MM4-1A	+	-	-	+

Under Met-deficient conditions, *R. gnavus* growth was significantly increased upon addition of PsCbl-producing *L. reuteri* MM4-1A as measured at 9 and 12 h (Figure 29A) while PBG addition led to a reduction of *R. gnavus* growth compared to growth without, being statistically significant at 12 h (Figure 29A). In Met-deficient conditions, *R. gnavus* growth was unaffected by CNPsCbl (Figure 29A) differing from the results in section 4.2.2 showing enhanced growth in the presence of cobamides in monoculture. *R. gnavus* overall growth was markedly increased by the addition of Met. In this medium, the addition of CNPsCbl resulted in a significant increased *R. gnavus* growth at 8 and 9 h (Figure 29B) while PBG had no effect on *R. gnavus* growth up until 12 h where growth was significantly reduced (Figure 29B). The presence of PsCbl-producing *L. reuteri* MM4-1A had no significant impact on *R. gnavus* growth in Met-supplemented conditions (Figure 29B). Together, these data indicate that cobamide availability has an influence on *R. gnavus* growth both in the form of PsCbl derived from *L. reuteri* MM4-1A when grown in Met deficient and supplemented conditions and as CNPsCbl when grown in Met supplemented conditions only.

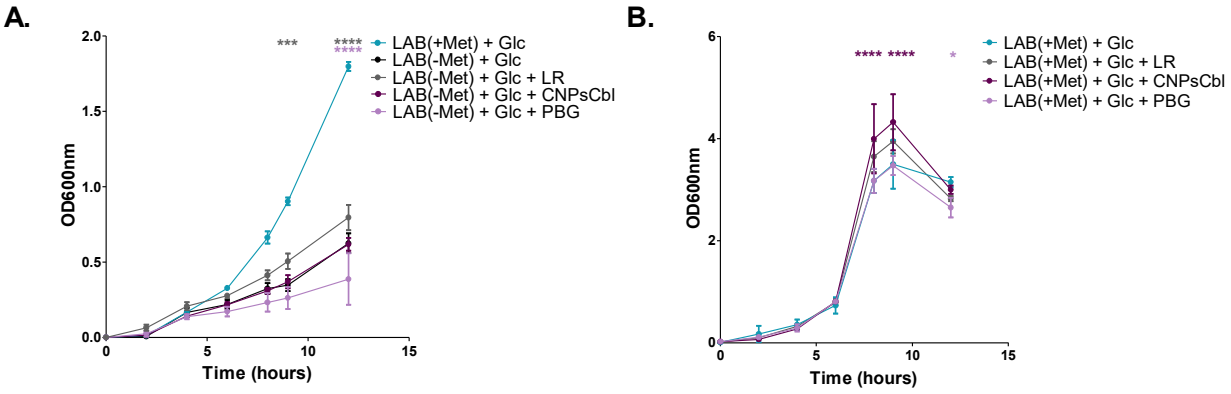

Figure 29 Growth of *R. gnavus* ATCC 29149 in monocultures and co-culture with PsCbl-producing *L. reuteri* MM4-1. *R. gnavus* ATCC 29149 was grown in monoculture in media supplemented with CNPsCbl or PBG and in co-culture with *L. reuteri* MM4-1A. Monoculture and co-cultures were carried out in A. LAB(-Met) media supplemented with CNPsCbl, PBG or inoculated with *L. reuteri* MM4-1A (LR) or B. LAB(+Met) media supplemented with CNPsCbl, PBG or inoculated with *L. reuteri* MM4-1A (LR). Glucose (Glc) was used as carbon source. Growth was monitored by spectrophotometric measurements of optical density (OD) at 600 nm. Data points mark the mean of 4 replicates. The error bars correspond to standard deviations between replicates. Samples were collected at mid exponential (9 h, T9) and late exponential (12 h, T12) growth phase for RNA extraction. LR corresponds to *L. reuteri*. Statistical significance between control (LAB(-Met) + Glc or LAB(+Met) + Glc) and treatment groups (LAB(-Met) + Glc + LR, LAB(-Met) + Glc + CNPsCbl, LAB(-Met) + Glc + PBG or LAB(+Met) + Glc + LR, LAB(+Met) + Glc + CNPsCbl, LAB(+Met) + Glc + PBG) at 0, 2, 4, 6, 8, 9 or 12 h was determined by Two-way ANOVA with Bonferroni multiple comparisons and is indicated by asterisks. A p-value below 0.05 is represented with one star (*), indicating significance. A p-value below 0.01 is denoted with two stars (**), signifying higher significance, a p-value below 0.001 is denoted with three stars (***), indicating highest statistical significance.

RNA was extracted from *R. gnavus* cultures grown in LAB(-Met) and LAB(+Met) media collected at mid exponential (9 h, T9) and late exponential (12 h, T12) growth phase (Figure 29). The extracted RNAs were sequenced using Illumina PE150 technology (Novogene).

4.2.3.2 Overview of the effect of cobamide on *R. gnavus* transcriptome

The RNA seq data from *R. gnavus* ATCC 29149 grown in conditions described in 4.2.3.1 were first analysed by Principal component analyses (PCA) to determine the global changes in gene expression.

Figure 30A shows that the transcriptome data obtained from *R. gnavus* cultures grown in LAB(-Met) supplemented with CNPsCbl, PBG or PsCbl-producing *L. reuteri* MM4-1A or LAB(+Met) control clustered into 3 groups (clusters 1, 2 and 3) according to cobamide availability. Replicates from the same growth conditions

showed similar gene expression levels independent of the time the sample was collected except for one replicate from the *R. gnavus* co-culture with *L. reuteri* sampled at 12 h (T12) (LAB(-Met) + Glc + *L. reuteri* (LR)), which appeared more spatially distinct.

Cluster 1a covers transcriptomics data from *R. gnavus* monocultures grown in LAB(-Met) media for 9 h (T9) and 12 h (T12) in the presence or absence of PBG (Figure 30A).

Cluster 2a covers transcriptomics data from *R. gnavus* monocultures grown in LAB(-Met) media at T9 and T12 in the presence of CNPsCbl or *R. gnavus* co-cultures with PsCbl-producing *L. reuteri* strain MM4-1A (Figure 30A).

R. gnavus monocultures grown in LAB(+Met) control alone at T9 and T12 formed a single spatially distinct cluster (cluster 3a) (Figure 30A).

Together these data suggest that PBG has no influence on *R. gnavus* transcriptome, while CNPsCbl and PsCbl-produced by *L. reuteri* share similar effects on gene expression, suggesting their potential utilisation in line with growth assays (sections 4.2.2). The presence of Met drives a different response, independent of the cobamide-dependent pathway.

Figure 30B shows that the transcriptome data obtained from *R. gnavus* cultures grown in LAB(+Met) supplemented with CNPsCbl, PBG or PsCbl-producing *L. reuteri* MM4-1A clustered into 2 groups (clusters 1b and 2b) according to sample collection time. Replicates from the same growth conditions showed similar gene expression levels.

Cluster 1b covers transcriptomics data of *R. gnavus* grown in LAB(+Met) in monoculture in the presence or absence of CNPsCbl and PBG and in co-culture with *L. reuteri* MM4-1A collected at T9 (Figure 30B).

Cluster 2b covers data from the same conditions as in cluster 1 but with these samples collected at T12 (Figure 30B).

These data suggest that the presence of Met in the medium reduced the need for *R. gnavus* to use the cobamide-dependent pathway for Met synthesis, in line with the results of the growth assays (section 4.2.2).

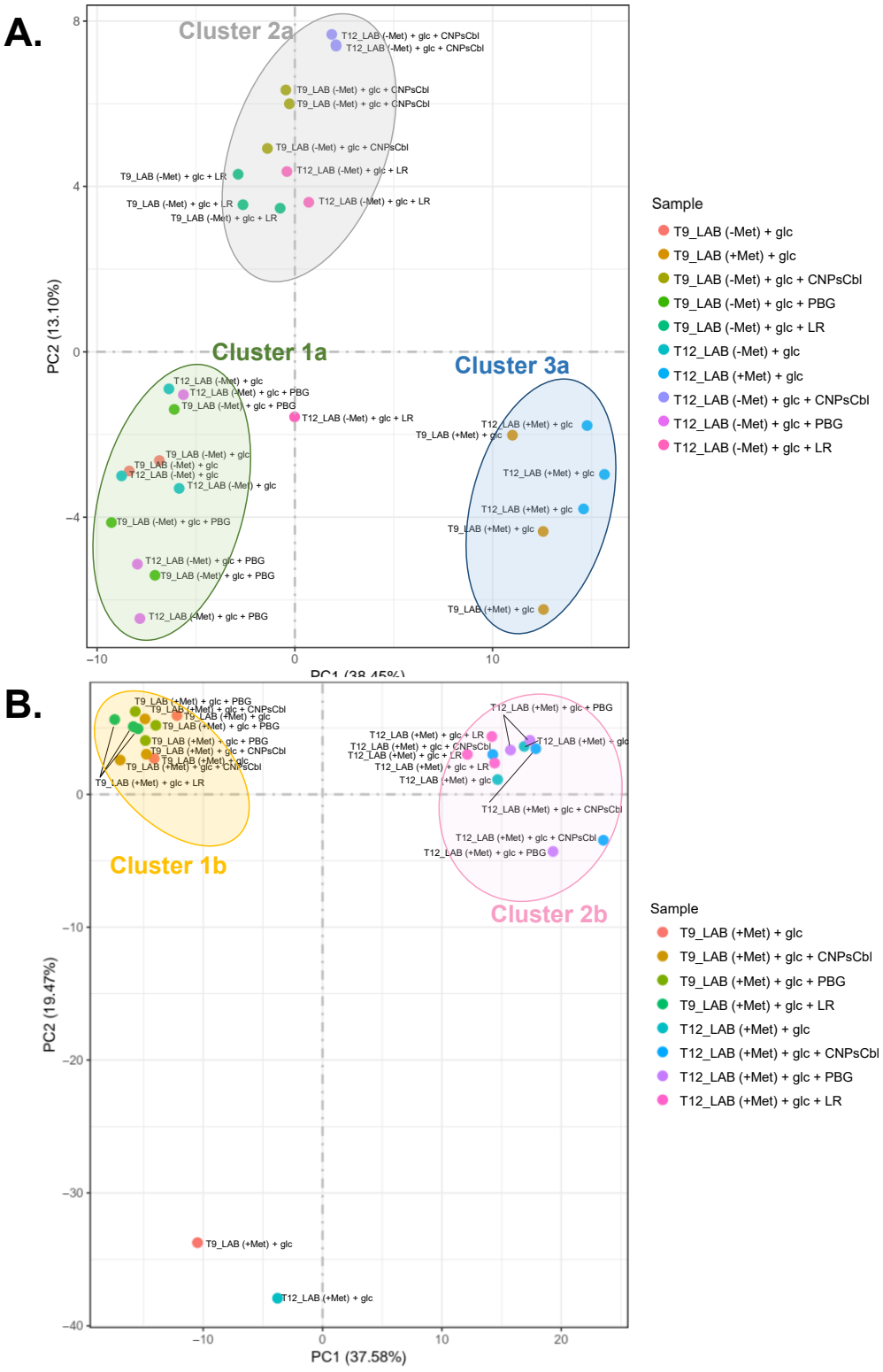

Figure 30 Principal component analysis (PCA) of transcriptomic data of *R. gnavus* ATCC 29149 grown in different media. A. *R. gnavus* gene expression when grown in LAB(-Met) media supplemented with CNPsCbl, PBG or inoculated with *L. reuteri* MM4-1A (LR) or B. *R. gnavus* gene expression when grown in LAB(+Met) media supplemented with CNPsCbl, PBG or inoculated with *L. reuteri* MM4-1A (LR). Glucose (Glc) was used as carbon source. Sample corresponds to different *R. gnavus* growth conditions; T9 denotes gene expression at 9 h bacterial culture (mid exponential phase), whilst T12 denotes gene expression at 12 h bacterial culture (late exponential phase). The growth conditions are color-coded as indicated.

These results are supported by the Pearson's correlation analysis of RNA seq samples (Figure 31A). High similarity was demonstrated between the transcription profiles of *R. gnavus* grown in monoculture in LAB(-Met) media in the presence or absence of PBG. The analysis also showed high similarity between the transcription profiles of *R. gnavus* grown in monoculture in LAB(-Met) supplemented with CNPsCbl compared to the co-culture in LAB(-Met) with PsCbl-producing *L. reuteri* MM4-1A. The transcription profiles of *R. gnavus* grown in LAB(+Met) at both T9 and T12 were most dissimilar to the transcription profiles of *R. gnavus* grown in LAB(-Met) supplemented with CNPsCbl or PBG or in co-culture with *L. reuteri* MM4-1A (Figure 31A).

When examining the correlation between the transcriptional profiles of *R. gnavus* grown in LAB(+Met) supplemented with CNPsCbl or PBG or in co-culture with *L. reuteri* MM4-1A, similarity was greatest between samples collected at the same time (Figure 31B).

A.

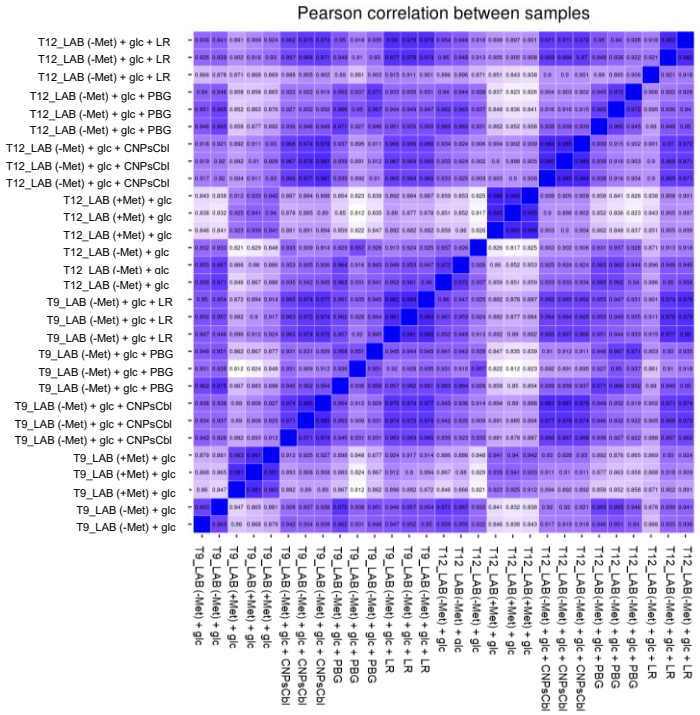

B.

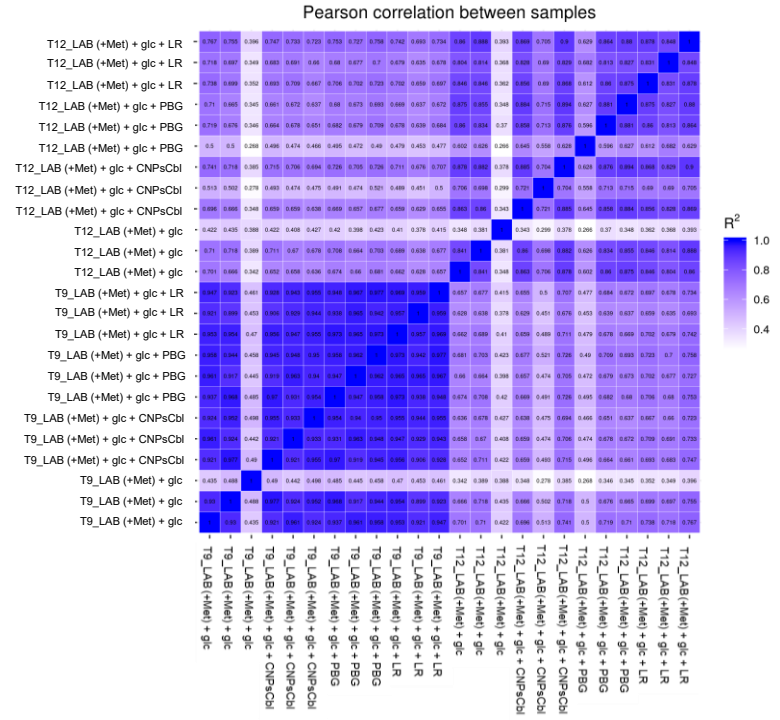

Figure 31 Hierarchical clustering heatmap of Pearson correlation coefficients between *R. gnavus* ATCC 29149 gene expression across different conditions. A. Correlation between RNA seq samples when *R. gnavus* is grown in LAB(-Met) media supplemented with CNPsCbl, PBG or inoculated with *L. reuteri* MM4-1A (LR) or B. Correlation between RNA seq samples when *R. gnavus* is grown in LAB(+Met) media supplemented with CNPsCbl, PBG or inoculated with *L. reuteri* MM4-1A (LR). Darker purple-coloured boxes indicate high similarity between RNA seq data whilst lighter purple shades indicate increased variability between dataset. The growth conditions are depicted on the Table 3. The correlation coefficient is labelled on the heatmap as an R^2 value.

These expression profiles suggest that, under Met-deficient conditions, *R. gnavus* ATCC 29149 can utilise PsCbl from *L. reuteri* or exogenously added CNPsCbl via similar mechanisms while this strain may not be capable of metabolising PBG. However, under Met-supplemented conditions, the largest determinant of overall transcriptional differences was sample collection time with CNPsCbl, PBG, or PsCbl-producing *L. reuteri* MM4-1A having minor effect on *R. gnavus* gene expression profile, underscoring *R. gnavus* preference for acquiring Met from the medium. The next sections will focus on the effect of individual treatments/conditions on *R. gnavus* transcriptome in order to gain insights into the underpinning molecular pathways.

4.2.3.3 Effect of exogenous cobamide (CNPsCbl) supplementation on *R. gnavus* transcriptome

Differential gene expression analysis was carried out using DESeq2 package to determine the influence of cobamide availability in the form of CNPsCbl on the transcriptional profiles of *R. gnavus* ATCC 29149 when grown in LAB(-Met) or LAB(+Met).

4.2.3.3.1 Effect of CNPsCbl supplementation on the transcriptome profile of *R. gnavus* grown in LAB(-Met)

When *R. gnavus* was grown in LAB(-Met), the differential expression analysis showed high dissimilarity between the transcriptome of *R. gnavus* when grown in the presence or absence of CNPsCbl, as illustrated in the volcano plot (Figure 32A and 35B). A total of 351 genes were significantly upregulated in the presence of CNPsCbl at T9 and 424 genes at T12. An upregulation of genes encoding membrane transport proteins (RGna_RS15170, RGna_RS15160, RGna_RS15165, RGna_RS15155, RGna_RS07645, RGna_RS14320, RGna_RS012540), proteins involved in alcohol metabolism (RGna_RS01515 and Novel00029), a leucine-rich repeat protein involved in protein-protein interactions, RGna_RS06295, a YgeY family selenium metabolism-linked hydrolase involved in selenium metabolism, RGna_RS16080 and a knotted carbamoyltransferase involved in cellular metabolism, RGna_RS16075, were amongst the top 10 genes significantly upregulated in the presence of cobamide in Met-deficient conditions across both time points (Figure 32B and 32D).

With reference to 'cobamide specific' genes (covering genes encoding cobamide-dependent, biosynthetic or transport proteins), at T9, there was a specific upregulation of *MetH*, encoding cobamide-dependent methionine synthase, in addition to *MetH2*, encoding cobamide-dependent methionine synthase activation subunit (see Supplementary Table 9 for list of significantly upregulated cobamide specific genes) (Figure 32A and B). *CobU/CobP*, encoding the bifunctional cobinamide kinase/cobinamide phosphate guanyltransferase, involved in cobamide

biosynthesis, was also among these genes. No change in the expression of defined cobamide-transport encoding genes was identified.

At T12, the gene expression of *MetH, MetH2* and *CobU/CobP* was unaffected. Similarly, no defined cobamide transport encoding gene was identified as being differentially induced, however, an uncharacterised ECF transporter S component, RGna_RS03450, was shown to be significantly upregulated by 0.19-fold.

A.

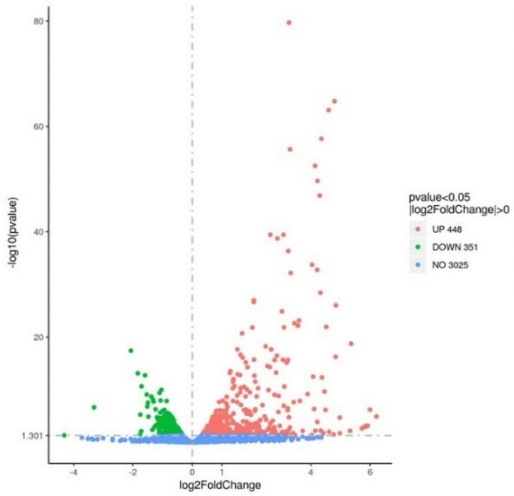

B.

T9 - Top 10 significantly upregulated genes in LAB(-Met) + Glc + CNPsCbl vs LAB(-Met) + Glc		
Gene ID	**Encoding protein**	**P value**
RGna_RS15175	Hypothetical protein	3.92×10^{-18}
RGna_RS15170	Substrate-binding domain-containing protein	7.80×10^{-14}
RGna_RS15160	Sugar ABC transporter atp-binding protein	1.87×10^{-13}
RGna_RS15165	ABC transporter permease	2.25×10^{-11}
RGna_RS06295	Leucine-rich repeat protein	1.08×10^{-10}
RGna_RS01515	Iron-containing alcohol dehydrogenase	3.94×10^{-10}
RGna_RS15155	ABC transporter permease	8.55×10^{-10}
RGna_RS16080	Ygey family selenium metabolism-linked hydrolase	2.09×10^{-09}
RGna_RS16075	Knotted carbamoyltransferase ygew	8.63×10^{-09}
RGna_RS07645	BMP family ABC transporter substrate-binding protein	1.10×10^{-08}

C.

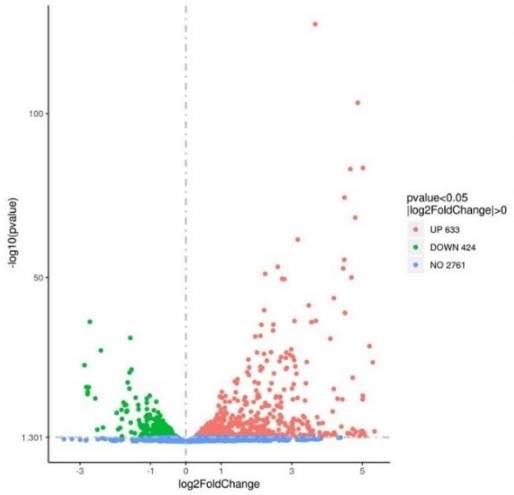

D.

T12 - Top 10 significantly upregulated genes in LAB(-Met) + Glc + CNPsCbl vs LAB(-Met) + Glc		
Gene ID	**Encoding protein**	**P value**
RGna_RS12540	ABC transporter substrate-binding protein	3.17×10^{-37}
RGna_RS06295	Leucine-rich repeat protein	2.59×10^{-32}
RGna_RS14320	ECF transporter S component	1.73×10^{-28}
RGna_RS15155	ABC transporter permease	5.39×10^{-24}
RGna_RS07645	BMP family ABC transporter substrate-binding protein	1.16×10^{-22}
Novel00029	Pf00465:iron-containing alcohol dehydrogenase	9.05×10^{-22}
RGna_RS15430	Hypothetical protein	9.66×10^{-19}
RGna_RS15175	Hypothetical protein	2.63×10^{-17}
Novel00317	unknown	3.06×10^{-17}
RGna_RS01515	Iron-containing alcohol dehydrogenase	7.80×10^{-17}

Figure 32 Effect of CNPsCbl supplementation on *R. gnavus* differentially expressed genes under Met-deficient conditions. Overall distribution of differentially expressed genes in samples collected at T9 (A) and T12 (C) and top 10 most statistically significant upregulated *R. gnavus* genes upon CNPsCbl supplementation in samples collected at T9 (B) and T12 (D). Volcano plots (A and C) depict the log2 fold change and corresponding -log10 p-value of all genes expressed by *R. gnavus* under the tested conditions. Differentially expressed genes (pvalue < 0.05, log2 fold-change| > 0) are shown in colour (Red, up-regulated in LAB(-Met) + Glc and Green, up-regulated in LAB(-Met) + Glc + CNPsCbl). Genes that did not have significant differences in expression are shown in Blue.

When examining the differential expression of the genes encoding cobamide-dependent proteins conserved across the 160 *R. gnavus* strains (section 4.2.1), all genes (*MetH, MetH2, PduCDE, DhaBCE, MtaB*, RGna_03200 and RGna_12670) were shown to be transcribed by *R. gnavus* ATCC 29149, confirming the *in silico* predictions (Figure 33). This analysis also revealed that the genes encoding the large, medium and small propanediol and glycerol dehydratase subunits, *PduC* or *DhaB* (large subunits), *PduD* or *DhaC* (medium subunits) and *PduE* or *DhaE* (small subunits), were transcribed as single propanediol/glycerol dehydratase family subunits i.e *PduC/DhaB* as the large propanediol/glycerol dehydratase subunit, *PduD/DhaC* as the medium propanediol/glycerol dehydratase subunit and *PduE/DhaE* as the small propanediol/glycerol dehydratase subunit.

Upon CNPsCbl supplementation, *MetH, MetH2, PduC/DhaB, PduD/DhaC, PduE/DhaE, MtaB*, RGna_03200 and RGna_12670 were all differentially induced at T9, however only the enhanced expression of *MetH* and the *MetH* subunit, *MetH2,* was significant, showing 0.17- and 0.57-fold increase, confirming the ability of *R. gnavus* to utilise CNPsCbl as a co-factor for cobamide-dependent reactions (Figure 33A). At T12, *MetH*, *PduC/DhaB, PduD/DhaC, PduE/DhaE* and RGna_03200 were upregulated, whilst *MetH2, MtaB*, and RGna_12670 were downregulated upon CNPsCbl supplementation, however changes in these expression levels were not significant (Figure 33B).

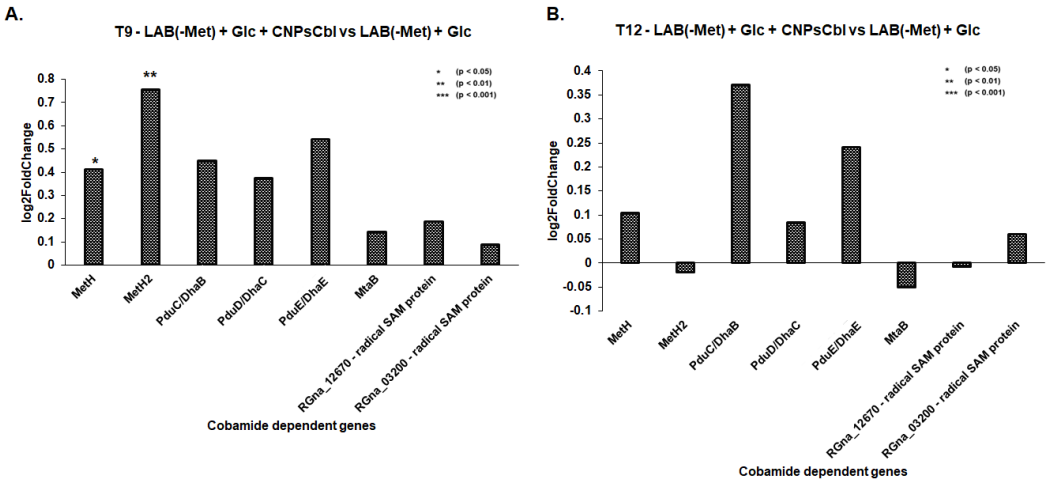

Figure 33 Effect of CNPsCbl supplementation on *R. gnavus* expression of genes encoding cobamide-dependent proteins under Met-deficient conditions. A bar plot showing the mean log2(fold change), y-axis, for putative genes encoding cobamide-dependent proteins, MetH, MetH2, PduC/DhaB, PduD/DhaC, PduE/DhaE, MtaB, RGna_03200 and RGna_12670 from samples collected at T9 A) and T12 B) Statistical significance is indicated by asterisks. A p-value below 0.05 is represented with one star (*), indicating significance. A p-value below 0.01 is denoted with two stars (**), signifying higher significance, a p-value below 0.001 is denoted with three stars (***), indicating highest statistical significance.

4.2.3.3.2 Effect of CNPsCbl supplementation on the transcriptome profile of *R. gnavus* grown in LAB(+Met)

When grown in LAB(+Met), *R. gnavus* demonstrated a significant upregulation of 4 genes at T9 upon supplementation with CNPsCbl, as illustrated in the volcano plot (Figure 34A) including RGna_RS08195 and RGna_RS08250 genes which encode proteins involved in mRNA translation and protein synthesis (Figure 34B). When *R. gnavus* was grown in the presence of CNPsCbl, RGna_RS11210, encoding a protein involved in energy metabolism and electron transport and RGna_RS13515 encoding a riboflavin (vitamin B2) transporter were amongst the genes significantly upregulated by 1.36- and 1.94-fold, respectively (Figure 34B).

At T12, a total of 13 genes were significantly upregulated upon CNPsCbl supplementation, with genes encoding proteins involved in DNA repair (RGna_RS06760), post-translational modification of chaperones and protein turnover (RGna_RS14085), signal transduction mechanisms (RGna_RS14620) and molybdenum cofactor biosynthesis (RGna_RS15475) being amongst the top 10 genes significantly upregulated (Figure 34B and D).

With reference to 'cobamide-specific' genes, no genes encoding proteins involved in cobamide-dependent or biosynthetic reactions or transport were identified amongst the significantly upregulated genes at T9 or T12.

A.

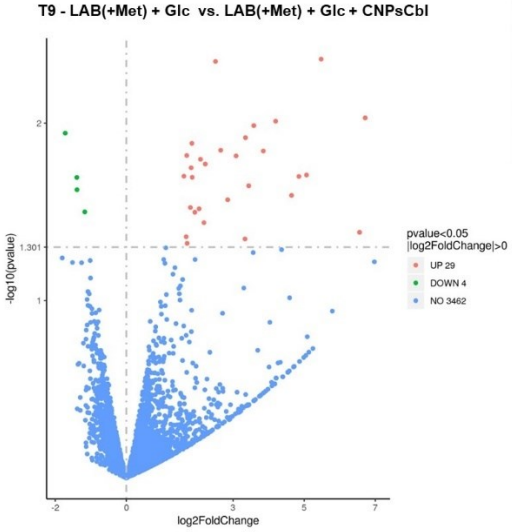

B.

T9 – Significantly upregulated genes in LAB(+Met) + Glc + CNPsCbl vs LAB(+Met) + Glc		
Gene ID	**Gene description**	**P value**
RGna_RS08195	Large ribosomal subunit protein uL30	0.011391
RGna_RS13515	ECF-type riboflavin transporter, S component	0.020244
RGna_RS08250	Large ribosomal subunit protein uL16	0.023732
RGna_RS11210	DUF1858 domain-containing protein	0.031651

C.

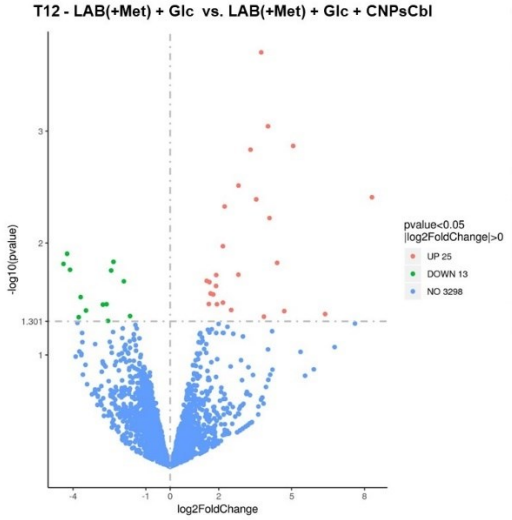

D.

T12 - Top 10 significantly upregulated genes in LAB(+Met) + Glc + CNPsCbl vs LAB(+Met) + Glc		
Gene ID	**Encoding protein**	**P value**
RGna_RS06760	GGDEF domain-containing protein	0.012455
RGna_RS14785	Ribosome-binding GTPase	0.01471
RGna_RS12750	Hypothetical protein	0.01535
RGna_RS14085	FAD-dependent oxidoreductase	0.017324
RGna_RS14620	Histidine kinase	0.017585
RGna_RS02600	Hypothetical protein	0.021973
RGna_RS18310	Hypothetical protein	0.030397
RGna_RS07795	Hypothetical protein	0.035222
RGna_RS15475	MogA/MoaB family molybdenum cofactor biosynthesis protein	0.035478
RGna_RS02515	Hypothetical protein	0.040054

Figure 34 Effect of CNPsCbl supplementation on *R. gnavus* differentially expressed genes under Met-supplemented conditions. Overall distribution of differentially expressed genes in samples collected at T9 (A) and T12 (C) and top 10 most statistically significant upregulated *R. gnavus* genes upon CNPsCbl supplementation compared to without in samples collected at T9 (B) and T12 (D). Volcano plots (A and C) depict the log2 fold change and corresponding -log10 p-value of all genes expressed by *R. gnavus* under the tested conditions. Differentially expressed genes (pvalue < 0.05, log2 fold-change| > 0) are shown in colour (Red, up-regulated in LAB(+Met) + Glc and Green, up-regulated in LAB(+Met) + Glc + CNPsCbl). Genes that did not have significant differences in expression are shown in Blue.

When examining the differential expression of genes encoding cobamide-dependent proteins, CNPsCbl supplementation led to enhanced expression of

MetH, PduC/DhaB, PduD/DhaC, PduE/DhaE, MtaB, and RGna_12670 and reduced expression of *MetH2* and RGna_03200 at T9 however these changes were not statistically significant (Figure 35A). At T12, the expression level of *MetH2, PduD/DhaC, PduE/DhaE, MtaB* and RGna_03200 was induced upon CNPsCbl supplementation, whilst the expression of *MetH* and RGna_12670 was reduced, although these changes in expression levels were not statistically significant (Figure 35B).

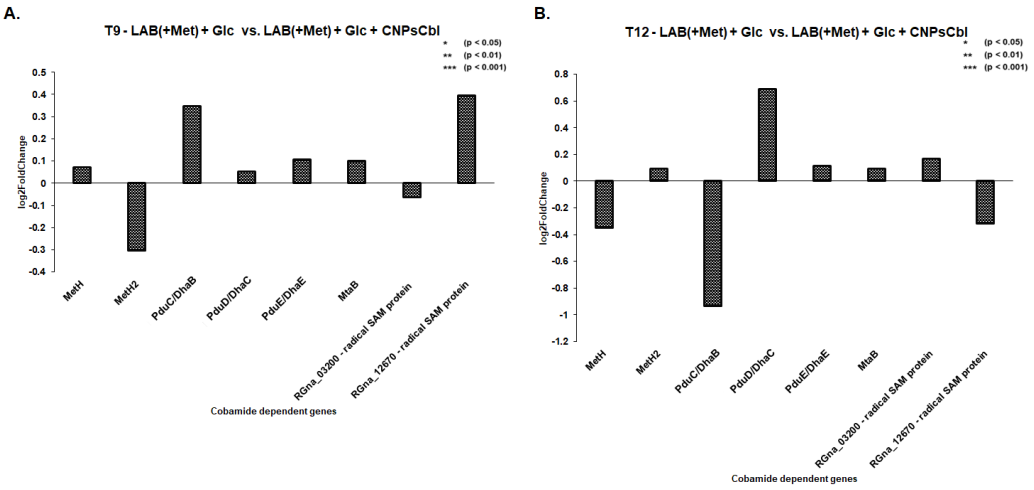

Figure 35 Effect of CNPsCbl supplementation on *R. gnavus* expression of genes encoding cobamide-dependent proteins under Met-supplemented conditions. A bar plot showing the mean log2(fold change), y-axis, for MetH, MetH2, PduC/DhaB, PduD/DhaC, PduE/DhaE, MtaB, RGna_03200 and RGna_12670 for samples collected at T9 (**A**) and T12 (**B**). Statistical significance is indicated by asterisks. A p-value below 0.05 is represented with one star (*), indicating significance, a p-value below 0.01 is denoted with two stars (**), signifying higher significance, a p-value below 0.001 is denoted with three stars (***), indicating highest statistical significance.

Together, these transcriptomic profiles suggest that *R. gnavus* ATCC 29149 can utilise cobamide in the form of CNPsCbl to carry out cobamide-dependent reactions. These results also support the reduced *R. gnavus* requirement for cobamide when Met is available in the medium to perform cobamide dependent reactions.

4.2.3.4 Effect of PsCbl-producing *L. reuteri* strain MM4-1A on *R. gnavus* transcriptome

To investigate the influence of PsCbl-producing *L. reuteri* MM4-1A on *R. gnavus* ATCC 29149*,* the transcriptomes of *R. gnavus* ATCC 29149 grown in monoculture or in co-culture with *L. reuteri* MM4-1A were compared in both LAB(-Met) and LAB(+Met) media. It is important to note that while *L. reuteri* MM4-1A grew in LAB(+Met) over the 12 h period (see supplementary Figure 8A) in co-culture, as determined by qPCR using *L. reuteri* specific primers targeting the 16S rDNA gene, this strain did not grow in LAB(-Met) as demonstrated a-posteriori by *L. reuteri* MM4-1A and *R. gnavus* ATCC 29149 read count estimation (see Supplementary Figure 8B), suggesting that, in this condition, the transcriptional effect is likely to be due to *L. reuteri* cells present in the initial inoculum. For read count estimation, reads generated from RNA seq were mapped to either a *R. gnavus* ATCC 29149 reference genome or a *L. reuteri* MM4-1A reference genome.

4.2.3.4.1 Effect of PsCbl-producing *L. reuteri* strain MM4-1A on the transcriptome of *R. gnavus* grown in LAB(-Met)

The analysis showed differential gene expression between *R. gnavus* grown in monoculture and in co-culture with *L. reuteri* MM4-1A in LAB(-Met) at both time points, with the upregulation of 427 genes at T9 and 207 genes at T12 (Figure 36). The top 10 genes being significantly upregulated across both time points included genes encoding proteins involved in nutrient transport (RGna_RS01285), amino acid transport and metabolism (RGna_RS03970, RGna_RS03960, RGna_RS03965 and RGna_RS04425), branched-chain amino acid synthesis (RGna_RS04420 and Novel00102), signal transduction mechanisms (RGna_RS03390), amino acid biosynthesis (RGna_RS01420 and RGna_RS01415), cell wall biosynthesis (RGna_RS17555, RGna_RS11215 and Novel00244), and RNA/DNA binding (RGna_RS00980) (Figure 36).

With regards to 'cobamide specific' genes, at T9, there was a significant upregulation of 2 genes involved in cobamide biosynthesis, *CobU/CobP* and *CobA* (RGna_RS05510), and 3 genes encoding cobamide-dependent proteins, *MetH,*

MetH2 and *PduC/DhaB*. Although no defined cobamide transport gene was identified to be differentially regulated, 2 uncharacterised ECF transporter S component encoding genes, RGna_RS03450 and RGna_RS14310 were amongst the 427 genes being significantly upregulated by 0.11- and 0.20-fold, respectively (see supplementary Table 11 for significantly upregulated cobamide specific genes) (Figure 36).

RGna_RS03450 was also significantly upregulated at T12 in addition to RGna_RS05590 encoding a cobalt ECF transporter T component CbiQ involved in cobamide biosynthesis (see supplementary Table 12 for significantly upregulated cobamide specific genes). *CobU/CobP* and *CobA, MetH, MetH2* and *PduC/DhaB* and RGna_RS14310 were not significantly upregulated at T12 (Figure 36).

A.

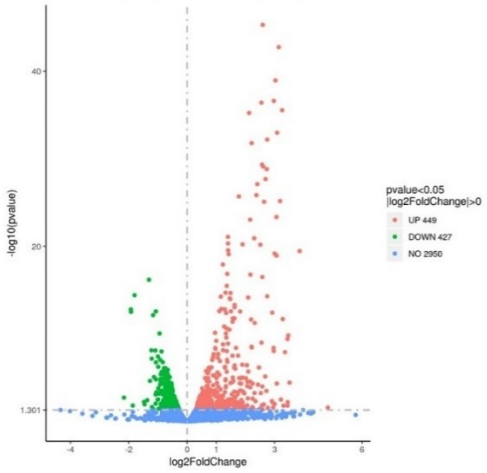

B.

T9 - Top 10 significantly upregulated genes in LAB(-Met) + Glc + LR vs LAB(-Met) + Glc		
Gene ID	**Encoding protein**	**P value**
RGna_RS01285	Sodium-dependent transporter	6.73×10^{-17}
RGna_RS03970	Amino acid ABC transporter substrate-binding protein	3.87×10^{-15}
RGna_RS03960	Amino acid ABC transporter ATP-binding protein	1.63×10^{-13}
RGna_RS04420	Ketol-acid reductoisomerase	2.74×10^{-13}
RGna_RS03965	Amino acid ABC transporter permease	3.00×10^{-13}
RGna_RS03390	Carbon starvation protein A	7.34×10^{-13}
RGna_RS01420	Phosphoglycerate dehydrogenase	9.16×10^{-11}
Novel00102	Acetohydroxy acid isomeroreductase	7.64×10^{-09}
RGna_RS17555	LCP family protein	7.93×10^{-09}
RGna_RS01415	3-phosphoserine/phosphohydroxythreonine transaminase	1.02×10^{-08}

C.

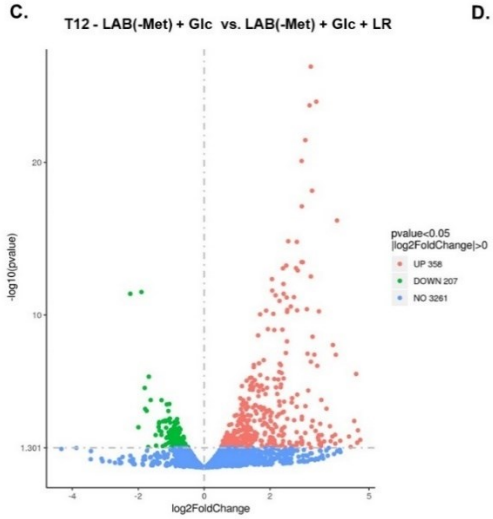

D.

T12 - Top 10 significantly upregulated genes in LAB(-Met) + Glc + LR vs LAB(-Met) + Glc		
Gene ID	**Encoding protein**	**P value**
RGna_RS03965	Amino acid ABC transporter permease	3.14×10^{-12}
RGna_RS03960	Amino acid ABC transporter ATP-binding protein	4.09×10^{-12}
RGna_RS01285	Sodium-dependent transporter	1.10×10^{-06}
RGna_RS00980	Cold shock domain-containing protein	6.05×10^{-06}
RGna_RS11215	Nlpc/P60 family protein-Bacterial SH3 domain	3.74×10^{-05}
Novel00102	Acetohydroxy acid isomeroreductase	3.81×10^{-05}
RGna_RS04425	Acetolactate synthase small subunit	6.71×10^{-05}
RGna_RS04420	Ketol-acid reductoisomerase	7.19×10^{-05}
Novel00244	Nlpc/P60 family-Bacterial SH3 domain	0.000142
RGna_RS03970	Amino acid ABC transporter substrate-binding protein	0.00019

Figure 36 Effect of PsCbl-producing *L. reuteri* MM4-1A on *R. gnavus* differentially expressed genes under Met-deficient conditions. Overall distribution of differentially expressed genes in samples collected at T9 (A) and 12 h (C) and top 10 most statistically significant upregulated *R. gnavus* genes when grown in co-culture with PsCbl producing *L. reuteri* MM4-1A in Met-deficient media in samples collected at 9 h (B) and T12 (D). LR corresponds to *L. reuteri*. Volcano plots (A and C) depict the log2

fold change and corresponding -log10 p-value of all genes expressed by *R. gnavus* under the tested conditions. Differentially expressed genes (pvalue < 0.05, log2 fold-change| > 0) are shown in colour (Red, up-regulated in LAB(-Met) + Glc and Green, up-regulated in LAB(-Met) + Glc + LR). Genes that did not have significant differences in expression are shown in Blue.

With regards to genes encoding cobamide-dependent proteins, we observed a significant induction, at T9, of *MetH, MetH2 and PduC/DhaB* in co-culture compared to monoculture with 0.1-, 0.4- and 0.26-fold increase, respectively. At T9, *PduD/DhaC*, *PduE/DhaE, MtaB*, RGna_03200 and RGna_12670 showed reduced expression in co-culture compared to monoculture, however these changes in expression levels were not significant (Figure 37A). At T12, the expression of *MetH, PduC/DhaB,* and *MtaB* was induced in co-culture compared to monoculture whilst *MetH2, PduD/DhaC, PduE/DhaE,* RGna_03200 and RGna_12670 showed reduced expression in co-culture compared to monoculture, although these changes in expression level were not statistically significant (Figure 37B).

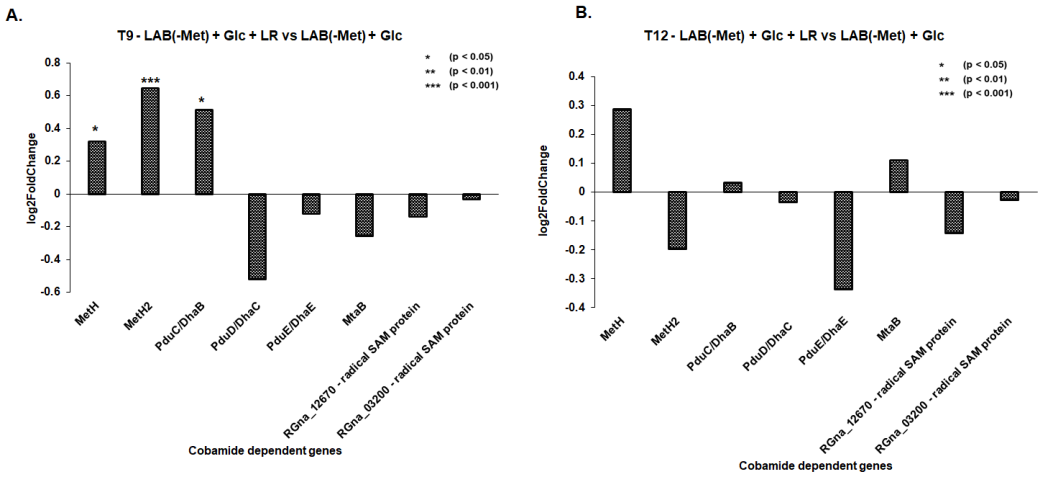

Figure 37 Effect of *L. reuteri* MM4-1A on *R. gnavus* expression of genes encoding cobamide-dependent proteins under Met-deficient conditions. A bar plot showing the mean log2(fold change), y-axis, for putative cobamide-dependent genes MetH, MetH2, PduC/DhaB, PduD/DhaC, PduE/DhaE, MtaB, RGna_03200 and RGna_12670 for samples collected at T9 (A) and T12 (B). Statistical significance is indicated by asterisks. A p-value below 0.05 is represented with one star (*), indicating significance, a p-value below 0.01 is denoted with two stars (**), signifying higher significance, a p-value below 0.001 is denoted with three stars (***), indicating highest statistical significance. LR corresponds to *L. reuteri*.

4.2.3.4.2 Effect of PsCbl-producing *L. reuteri* strain MM4-1A on the transcriptome of *R. gnavus* grown in LAB(+Met)

The differential expression analysis showed upregulation of the expression of 50 genes at T9 and 34 genes at T12 when *R. gnavus* ATCC 29149 was grown in LAB(+Met) in co-culture with *L. reuteri* MM4-1A as compared to *R. gnavus* grown in monoculture (Figure 38).

At T9, there was a significant induction of expression of genes encoding proteins involved in amino sugar and nucleotide sugar metabolism (RGna_RS11950), glycogen biosynthetic process (RGna_RS08875), transcription and protein synthesis (RGna_RS15375), protein and peptide secretion and trafficking (RGna_RS12925) and post-translational modification of chaperones and protein turnover (RGna_RS03675) (Figure 38B).

At T12, there was a significant induction of expression of genes encoding proteins involved in antiviral defence (RGna_RS16680), nucleotide transport and metabolism (RGna_RS07670 and RGna_RS07655) and intracellular trafficking, secretion, and vesicular transport (RGna_RS09230) (Figure 38D).

There was no difference in the expression level of 'cobamide specific' genes, at T9 and T12, when *R. gnavus* was grown in co-culture with *L. reuteri* compared to when *R. gnavus* was grown in monoculture.

A.

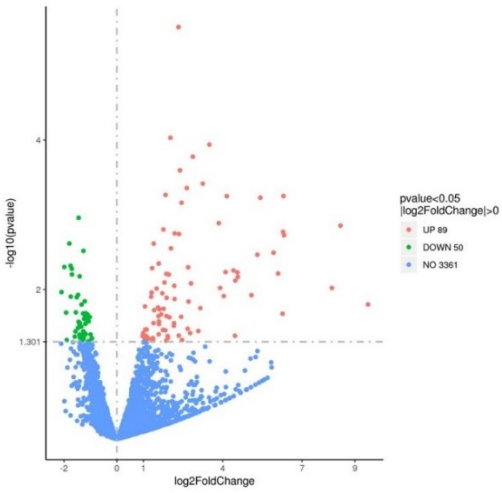

B.

T9 - Top 10 significantly upregulated genes in LAB(+Met) + Glc + LR vs LAB(+Met) + Glc		
Gene ID	**Encoding protein**	**P value**
RGna_RS10930	Hypothetical protein	0.001099
RGna_RS11950	UDP-N-acetylglucosamine 2-epimerase	0.002425
RGna_RS08875	Nucleotidyl transferase	0.003043
RGna_RS15375	Helix-turn-helix transcriptional regulator	0.004806
RGna_RS12925	Signal peptidase S26	0.004998
RGna_RS00540	Hypothetical protein	0.005276
RGna_RS16650	Protein of unknown function (DUF3990)	0.006272
RGna_RS14060	Protein of unknown function (DUF1016)	0.006662
RGna_RS03675	GCN5-related N-acetyltransferases family (GNAT) family N-acetyltransferase	0.010822
RGna_RS16455	Protein of unknown function (DUF6176)	0.011783

C.

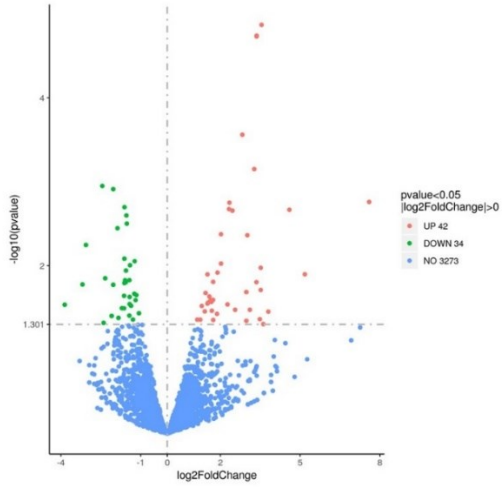

D.

T12 - Top 10 significantly upregulated genes in LAB(+Met) + Glc + LR vs LAB(+Met) + Glc		
Gene ID	**Encoding protein**	**P value**
RGna_RS02600	Hypothetical protein	0.001123
RGna_RS16680	type I-C CRISPR-associated endonuclease	0.001226
RGna_RS07670	ABC-type guanosine uptake protein	0.002009
RGna_RS17720	Hypothetical protein	0.00252
RGna_RS09230	Cna B-type domain-containing protein	0.003152
RGna_RS17750	Hypothetical protein	0.003577
RGna_RS10380	Hypothetical protein	0.005663
RGna_RS15520	Bacterial protein of unknown function (DUF965)	0.008259
RGna_RS09885	Hypothetical protein	0.00883
RGna_RS07655	Pyrimidine nucleoside phosphorylase C-terminal domain	0.009873

Figure 38 Effect of PsCbl-producing *L. reuteri* MM4-1A on *R. gnavus* differentially expressed genes under Met-supplemented conditions. Overall distribution of differentially expressed genes in samples collected at T9 (A) and 12 h (C) and top 10 most statistically significant upregulated *R. gnavus* genes when grown in co-culture with PsCbl producing *L. reuteri* MM4-1A in Met-supplemented media in samples collected at 9 h (B) and T12 (D). LR corresponds to *L. reuteri*. Volcano plots (A and C) depict the log2 fold change and corresponding -log10 p-value of all genes expressed by *R. gnavus* under the tested conditions. Differentially expressed genes (pvalue < 0.05, log2 fold-change| > 0) are shown in colour (Red, up-regulated in LAB(+Met) + Glc and Green, up-regulated in LAB(+Met) + Glc + LR). Genes that did not have significant differences in expression are shown in Blue.

With regards to genes encoding cobamide-dependent proteins, at T9, with the exception of RGna_03200 and RGna_12670, all 'cobamide-dependent' genes were induced when *R. gnavus* was grown in co-culture with *L. reuteri* as compared to growth in monoculture. RGna_03200 and RGna_12670 showed reduced expression levels. However, these changes in expression levels were not statistically significant (Figure 39A). At T12, the expression of *PduD/DhaC, PduE/DhaE, MtaB* and RGna_03200 was enhanced when *R. gnavus* was grown in co-culture with *L.*

reuteri compared to monoculture (Figure 39B). The upregulation of *PduE/DhaE, MtaB* and RGna_03200 was not statistically significant, however the enhanced expression of *PduD/DhaC* was statistically significant with a 2.43-fold increase in co-culture. The expression of *MetH, MetH2, PduC/DhaB* and RGna_12670 was reduced when *R. gnavus* was grown in co-culture with *L. reuteri* compared to monoculture, but this change was not statistically significant (Figure 39B).

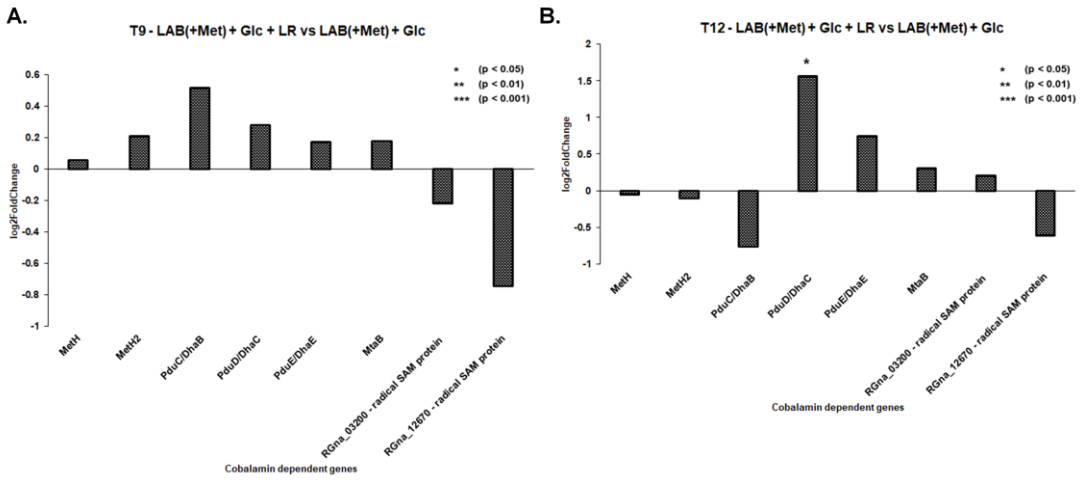

Figure 39 Effect of *L. reuteri* MM4-1A on *R. gnavus* expression of genes encoding cobamide-dependent proteins under Met-supplemented conditions. A bar plot showing the mean log2(fold change), y-axis, for putative cobamide-dependent genes MetH, MetH2, PduC/DhaB, PduD/DhaC, PduE/DhaE, MtaB, RGna_03200 and RGna_12670 for samples collected at T9 (A) and T12 (B). Statistical significance is indicated by asterisks. A p-value below 0.05 is represented with one star (*), indicating significance, a p-value below 0.01 is denoted with two stars (**), signifying higher significance, a p-value below 0.001 is denoted with three stars (***), indicating highest statistical significance.LR corresponds to *L. reuteri*.

The enhanced expression of genes encoding cobamide-dependent proteins when *R. gnavus* ATCC 29149 was grown for up to 12 h in the presence of *L. reuteri* MM4-1A in both LAB(-Met) and LAB(+Met) suggests PsCbl cross-feeding between *L. reuteri* and *R. gnavus* strains. This in line with the growth assays showing enhanced growth when *R. gnavus* is in co-culture with *L. reuteri* compared to when *R. gnavus* was grown in monoculture in both LAB(-Met) and LAB(+Met) during this period (section 4.2.3.1).

4.2.3.5 Effect of PBG supplementation on *R. gnavus* transcription profile

To investigate the potential capacity of *R. gnavus* ATCC 29149 to metabolise PBG, we analysed the effect of PBG supplementation on the transcription of genes involved in cobamide biosynthesis. The differential expression analysis, graphically represented by a volcano plot (Figure 40A and C and Figure 41A and C), revealed changes in *R. gnavus* gene expression upon PBG availability in both LAB(-Met) and LAB(+Met) media.

4.2.3.5.1 Effect of PBG supplementation on the overall transcriptome of *R. gnavus* grown in LAB(-Met) and LAB(+Met)

When *R. gnavus* was grown in LAB(-Met) in the presence of PBG, there was a significant increased expression of genes encoding proteins involved in cell wall biosynthesis (RGna_RS14345 and RGna_RS11215, Novel00244), membrane transport (RGna_RS14590), cellular metabolism (RGna_RS16075), carbohydrate transport and metabolism (RGna_RS04910), cell motility (RGna_RS08650), selenium metabolism (RGna_RS16080), secondary metabolites biosynthesis, transport and catabolism, signal transduction mechanisms (RGna_RS04960), alcohol metabolism (Novel00029 and Novel00184) and ammonia lysis (RGna_RS16085) (Figure 40).

With regards to 'cobamide specific' genes, at T9, there was a significant upregulation of *MetH2* and *PduE/DhaE* but no significant upregulation of 'cobamide specific' genes at T12.

A.

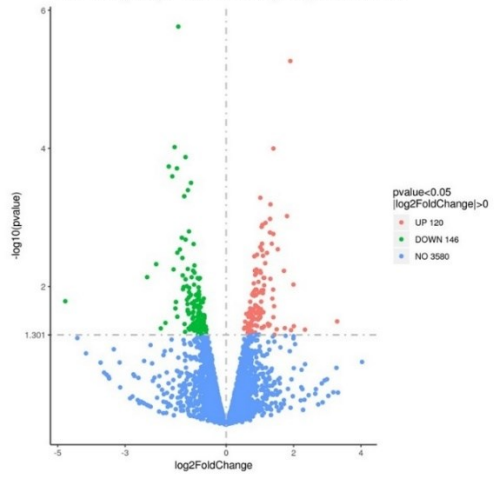

B.

T9 - Top 10 significantly upregulated genes in LAB(-Met) + Glc + PBG vs LAB(-Met) + Glc		
Gene ID	**Encoding protein**	**P value**
RGna_RS14345	Cell wall hydrolase	1.72×10^{-06}
RGna_RS14590	ABC transporter atp-binding protein	9.57×10^{-05}
RGna_RS16075	Knotted carbamoyltransferase ygew	0.000133
Novel00265	Unknown	0.000183
RGna_RS17685	Hypothetical protein	0.000195
RGna_RS04910	1-phosphofructokinase	0.000254
RGna_RS08650	Gldg family protein	0.000315
RGna_RS16080	Ygey family selenium metabolism-linked hydrolase	0.000402
RGna_RS11215	Nlpc/P60 family protein	0.000492
RGna_RS04960	Phasin family protein	0.001591

C.

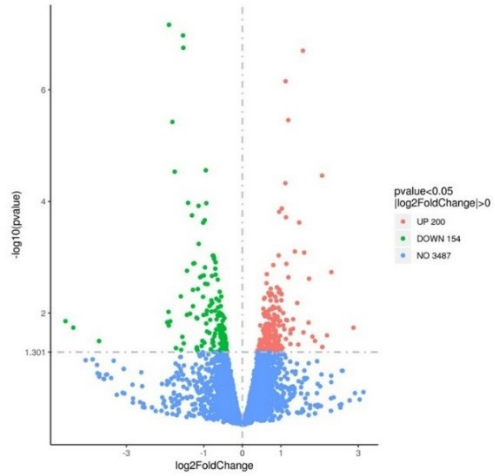

D.

T12 - Top 10 significantly upregulated genes in LAB(-Met) + Glc + PBG vs LAB(-Met) + Glc		
Gene ID	**Encoding protein**	**P value**
Novel00265	Unknown	6.87×10^{-08}
RGna_RS16080	YgeY family selenium metabolism-linked hydrolase	1.07×10^{-07}
RGna_RS16075	Knotted carbamoyltransferase YgeW	1.78×10^{-07}
Novel00264	Unknown	3.77×10^{-05}
Novel00029	PF00465:Iron-containing alcohol dehydrogenase	2.77×10^{-05}
Novel00244	PF00877:NlpC/P60 family|PF08239:Bacterial SH3 domain	2.94×10^{-05}
RGna_RS11215	NlpC/P60 family protein	0.000106
Novel00184	PF00465:Iron-containing alcohol dehydrogenase|PF00171:Aldehyde dehydrogenase family	0.000108
RGna_RS11540	Hypothetical protein	0.00012
RGna_RS16085	Diaminopropionate ammonia-lyase	0.000178

Figure 40 Effect of PBG on *R. gnavus* differentially expressed genes under Met-deficient conditions. Overall distribution of differentially expressed genes in samples collected at T9 (A) and T12 (C) and top 10 most statistically significant upregulated *R. gnavus* genes when grown in the presence and absence of PBG, in Met-deficient media in samples collected at T9 (B) and T12 (D). Volcano plots (A and C) depict the log2 fold change and corresponding -log10 p-value of all genes expressed by *R. gnavus* under the tested conditions. Differentially expressed genes (pvalue < 0.05, log2 fold-change| > 0) are shown in colour (Red, up-regulated in LAB(-Met) + Glc and Green, up-regulated in LAB(-Met) + Glc + PBG). Genes that did not have significant differences in expression are shown in Blue.

When *R. gnavus* was grown in LAB(+Met) in the presence of PBG, there was a significant increased expression of genes encoding proteins involved in transmembrane transport (RGna_RS15990) and transcription (RGna_RS16170 and RGna_RS15375) at T9 (Figure 41B). At T12, there was a significant upregulation of genes encoding proteins involved in cell cycle control, cell division and chromosome partitioning (RGna_RS13665), carbohydrate metabolism (RGna_RS00715), signal transduction mechanisms (RGna_RS14620), cobalt transport (RGna_RS05585), periplasmic solute transport (RGna_RS11430),

carbohydrate transport (RGna_RS15135), sugar uptake (RGna_RS14740), cell wall /membrane/envelope biogenesis (RGna_RS05045) and translation (RGna_RS14785) (Figure 41D).

There was no significant upregulation of 'cobamide specific' genes under these conditions.

A.

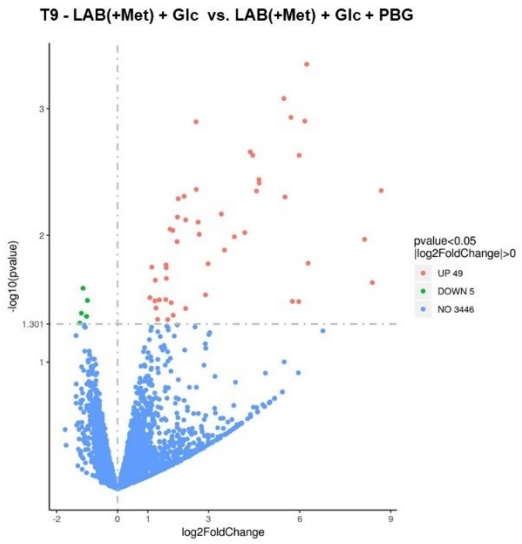

B.

T9 - Significantly upregulated genes in LAB(+Met) + Glc + PBG vs LAB(+Met) + Glc		
Gene ID	**Encoding protein**	**P value**
RGna_RS03280	Hypothetical protein	0.02612
RGna_RS10930	Hypothetical protein	0.032611
RGna_RS15990	Nicotinamide mononucleotide transporter	0.041129
RGna_RS16170	Helix-turn-helix transcriptional regulator	0.04353
RGna_RS15375	Helix-turn-helix transcriptional regulator	0.049139

C.

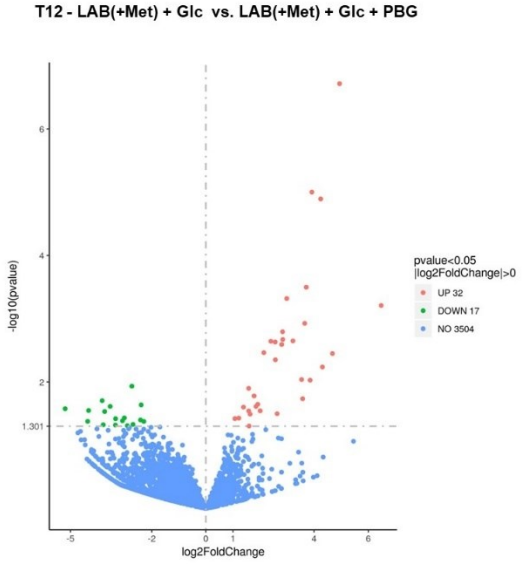

D.

T12 - Top 10 significantly upregulated genes in LAB(+Met) + Glc + PBG vs LAB(+Met) + Glc		
Gene ID	**Encoding protein**	**P value**
RGna_RS13665	ParB-like nuclease domain	0.011655
RGna_RS00715	Glycosyl hydrolases family 28	0.019753
RGna_RS14620	Histidine kinase	0.023038
RGna_RS05585	Cobalt transporter ATP-binding protein	0.024306
RGna_RS11430	Tripartite ATP-independent periplasmic transporter, DctM component	0.026449
RGna_RS06510	Hypothetical protein	0.028222
RGna_RS15135	Phosphotransferase transporter subunit	0.029327
RGna_RS14740	Glycoside-pentoside-hexuronide (GPH):cation symporter	0.036986
RGna_RS05045	Penicillin binding protein transpeptidase	0.038077
RGna_RS14785	50S ribosome-binding GTPase	0.039786

Figure 41 Effect of PBG on *R. gnavus* differentially expressed genes under Met-supplemented conditions. Overall distribution of differentially expressed genes in samples collected at T9 (A) and T12 (C) and top 10 most statistically significant upregulated *R. gnavus* genes when grown in the presence and absence of PBG, in Met-deficient media in samples collected at T9 (B) and T12 (D). Volcano plots (A and C) depict the log2 fold change and corresponding -log10 p-value of all genes expressed by *R. gnavus* under the tested conditions. Differentially expressed genes (pvalue < 0.05, log2 fold-change| > 0) are shown in colour (Red, up-regulated in LAB(+Met) + Glc and Green, up-regulated in LAB(+Met) + Glc + PBG). Genes that did not have significant differences in expression are shown in Blue.

4.2.3.5.2 Effect of PBG supplementation on the transcription of genes involved in the biosynthesis of cobamides of *R. gnavus* grown in LAB(-Met) and LAB(+Met)

Next, we analysed the effect of PBG supplementation on the transcription of genes involved in the biosynthesis of cobamides when *R. gnavus* was grown in LAB(-Met) and LAB(+Met) media.

The data revealed the presence of a cobamide biosynthetic operon in the genome of *R. gnavus* ATCC 29149 using Rockhopper with RNA seq data as input. The operon consists of 27 genes including cobamide biosynthetic genes (*CysG2/SirC, CbiC/CobH, CobU/CobP, CobU, CysGA-hemD/CobA, HemC, CobQ/CbiP, CobD, CbiB, CobC, CobS, CobT, CbiA/CobB, CbiET/CobL, CobJ/CbiH, CobM/CbiF, CobI/CbiL, CbiD, CbiK, CbiO, CbiQ, CbiN* and *CbiM*) and genes encoding proteins involved in peptide uptake (*PBP2_OppA, GsiA, DppC, OppB*) (see Table 4). All cobamide biosynthetic genes within this operon were identified in the *in silico* analysis reported in Chapter 3, section 3.2.1, Figure 9. This transcriptomic analysis also demonstrated the enhanced expression of cobamide biosynthetic genes *GltX, FldA* and *ThiC* by *R. gnavus* ATCC 29149 upon PBG supplementation in Met supplemented conditions (Figure 43B) and cobamide biosynthetic gene *CobW* upon PBG supplementation in Met-deficient conditions (Figure 42B), in line with the *in silico* analysis, although these genes were not identified within the cobamide biosynthetic operon using Rockhopper (Table 4).

Table 4 Cobamide operon in *R. gnavus* ATCC 29149. Operon of 27 genes consisting of cobamide biosynthesis genes and peptide uptake genes identified using Rockhopper with RNA seq data as input.

Gene ID	Gene name
RGna_RS05470	CysG2/SirC
RGna_RS05475	CbiC/CobH
RGna_RS05480	CobU/CobP
RGna_RS05485	CobU
RGna_RS05490	PBP2_OppA
RGna_RS05495	GsiA_1
RGna_RS05500	DppC
RGna_RS05505	OppB_1
RGna_RS05510	CysGA-hemD/CobA
RGna_RS05515	HemC
RGna_RS05520	CobQ/CbiP
RGna_RS05525	CobD
RGna_RS05530	CbiB
RGna_RS05535	CobC
RGna_RS05540	CobS
RGna_RS05545	CobT
RGna_RS05550	CbiA/CobB
RGna_RS05555	CbiET/CobL
RGna_RS05560	CobJ/CbiH
RGna_RS05565	CobM/CbiF
RGna_RS05570	CobI/CbiL
RGna_RS05575	CbiD
RGna_RS05580	CbiK
RGna_RS05585	CbiO
RGna_RS05590	CbiQ
RGna_RS05595	CbiN
RGna_RS05600	CbiM

When *R. gnavus* was grown in LAB(-Met), at T9, the following genes showed enhanced level of expression upon PBG supplementation: *CysG2, CobU/CobP, CobU, CbiB, CobC, CobI, CbiD, CbiO and CobK* (Figure 42A). In contrast, the expression of *CbiC, CysGA-HemD/CobA, HemC, CobQ, CobD, CobS, CobT, CbiA, CbiT, CobJ, CobM, CbiK, CbiQ, CbiN, CbiM, CobA_CobO_BtuR* and *CbiG* was decreased upon PBG supplementation, with *CbiC* showing statistically significant reduced expression by 2.24-fold. At T12, enhanced expression in the presence of PBG was only detected for *CobJ* and *CbiK*, whilst the expression of all other genes was reduced. The expression of *CbiC CysGA-HemD/CobA, HemC, CobD, CobS, CobT, CbiN* and *CbiM* was significantly decreased upon PBG supplementation by 3.15-, 0.44-, 0.8-, 0.71-, 0.58-, 0.47-, 0.49- and 0.67-fold lower (Figure 42B). The reduced expression of such a large number of cobamide biosynthesis genes at both timepoints suggests that under Met-deficient conditions, PBG is unable to be utilised for cobamide production, in line with the growth assays indicating that PBG supplementation does not support *R. gnavus* growth in these conditions.

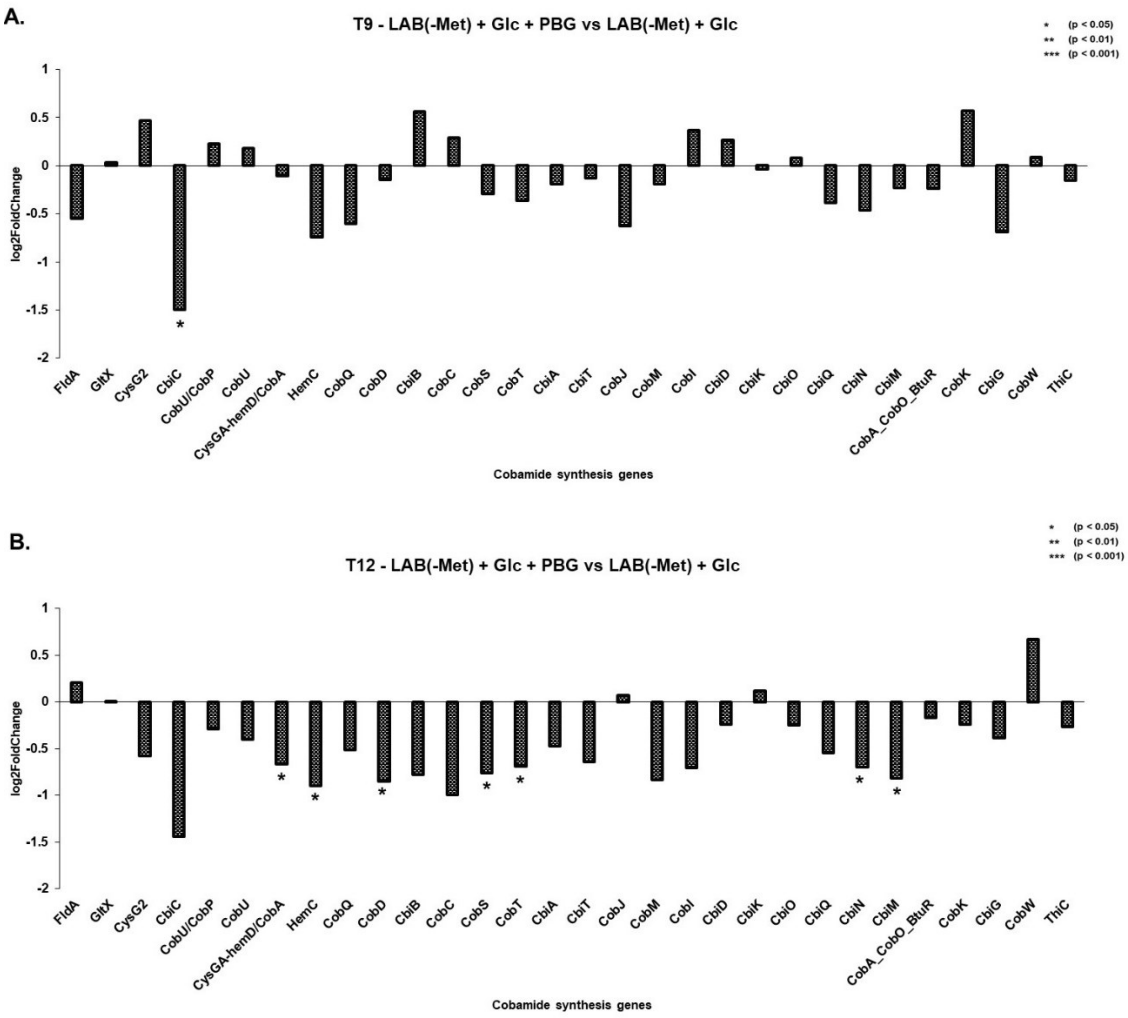

Figure 42 Effect of PBG on *R. gnavus* expression of cobamide-biosynthesis genes under Met-deficient conditions. A bar plot showing the mean log2(fold change), y-axis, for genes involved in cobamide biosynthesis for samples collected at T9 (A) and T12 (B). Statistical significance is indicated by asterisks. A p-value below 0.05 is represented with one star (*), indicating significance. A p-value below 0.01 is denoted with two stars (**), signifying higher significance, a p-value below 0.001 is denoted with three stars (***), indicating highest statistical significance.

Similarly, when *R. gnavus* was grown in LAB(+Met), at T9, the majority of cobamide synthesis genes showed reduced expression level upon PBG supplementation, including *CbiC, CobU, CysGA-hemD/CobA, HemC, CobQ, CobD, CbiB, CbiA, CbiT, CobJ, CobM, CbiD, CbiO, CbiQ, CbiN, CbiM, CobK* and *CbiG.* The following genes showed enhanced levels of expression upon PBG supplementation: *CysG2, CobU/CobP, CobC, CobS, CobT, CobI, CbiK* and *CobA/CobO/BtuR.* However, these were not statistically significant.

In contrast to the transcriptomics data obtained for *R. gnavus* grown in LAB(-Met) at T9 and T12 as well as the data shown for *R. gnavus* gene expression in LAB(+Met) at T9, we found that at T12, most cobamide synthesis genes showed enhanced expression upon PBG supplementation including *CysG2, CbiC, CobU/CobP, CobU, CysGA-HemD/CobA, CobQ, CobD, CbiB, CobS, CbiA, CbiT, CobJ, CobM, CobI, CbiO, CbiM, CobA_CobO_BtuR, CobK* and *CbiG*, however only the increased expression of CbiO upon PBG supplementation was shown to be statistically significant by 12.5-fold. These results suggest PBG metabolism for cobamide production by *R. gnavus* during late exponential phase (T12) but not at mid exponential growth phase (T9) in the presence of Met (Figure 43B).

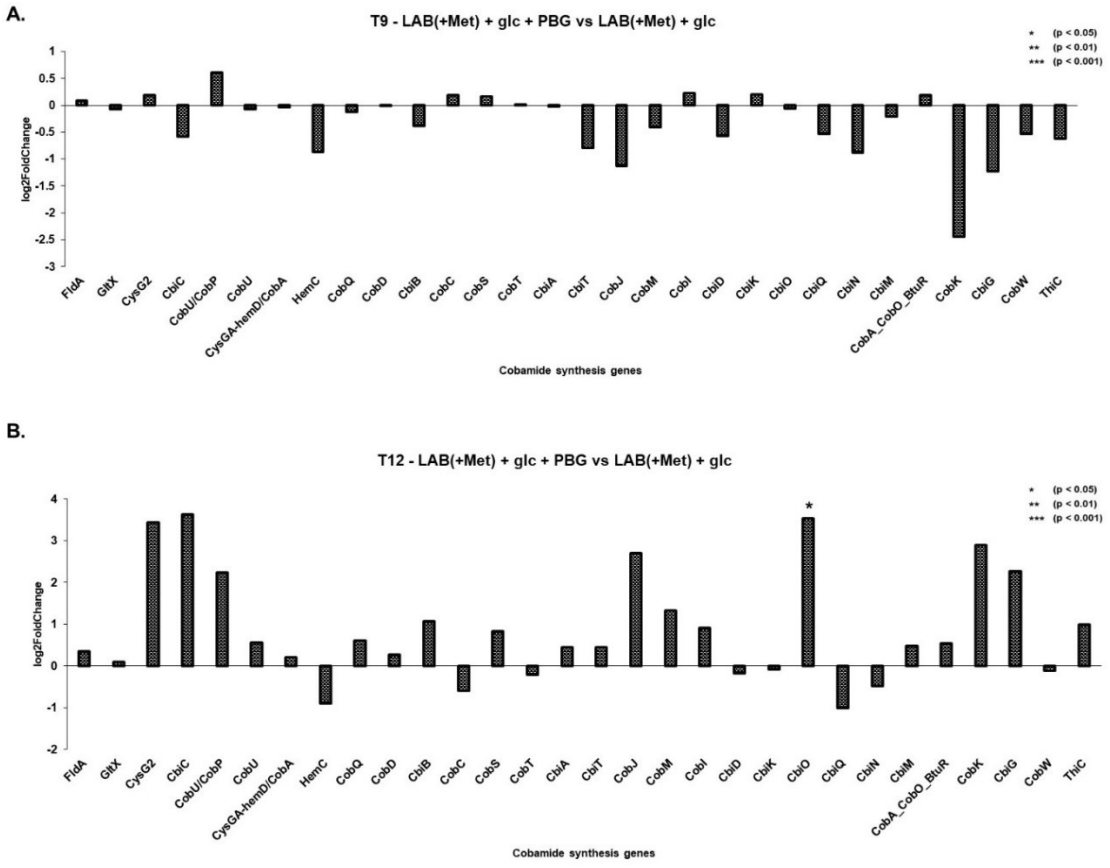

Figure 43 Effect of PBG on *R. gnavus* expression of cobamide-biosynthesis genes under Met-supplemented conditions. A bar plot showing the mean log2(fold change), y-axis, for genes involved in cobamide biosynthesis for samples collected at T9 (A) and T12 (B). Statistical significance is indicated by asterisks. A p-value below 0.05 is represented with one star (*), indicating significance. A p-value below 0.01 is denoted with two stars (**), signifying higher significance, a p-value below 0.001 is denoted with three stars (***), indicating highest statistical significance.

The reduced expression of a large number of genes involved in cobamide synthesis upon PBG supplementation when *R. gnavus* was grown in LAB(-Met) media at T9 and to a greater extent at T12 suggests an inhibitory effect of PBG, reducing the cobamide biosynthesis capacity of *R. gnavus* under the conditions tested. This is in line with growth assays of *R. gnavus* ATCC 29149 monocultures in LAB(-Met) (section 4.2.3.1), which showed reduced bacterial growth upon PBG supplementation (Figure 29) indicating an inhibitory effect of PBG in the conditions tested.

Such reduced expression was also observed when *R. gnavus* was grown in LAB(+Met) supplemented with PBG at T9, whilst at T12 there was a substantial enhancement in the expression of a large number of genes involved in cobamide synthesis, suggesting PBG metabolism by *R. gnavus* at this time point. However, the results of growth assays in LAB(+Met) (section 4.2.3.1 Figure 29), showed that PBG appeared to have no effect on *R. gnavus* growth for up to 9 h, while a slight decrease in growth was observed between 9 and 12 h (section 4.2.3.1 Figure 29). This suggests that, under Met-supplemented conditions, synthesis of cobamide from PBG may be at insufficient levels to support *R. gnavus* growth.

We then compared the differential expression of genes encoding cobamide-dependent proteins and transporters when *R. gnavus* was grown in LAB(-Met) media and LAB(+Met) media.

When *R. gnavus* was grown in LAB(-Met) media supplemented with PBG, at T9, *MetH, MetH2, PduC/DhaB, PduD/DhaC, PduE/DhaE* and *MtaB* showed induced expression in the presence of PBG, with the expression of *MetH* and *PduE/DhaE* being significantly enhanced upon PBG supplementation by 0.67- and 0.56-fold, respectively (Figure 44A). In contrast, the expression of RGna_03200 and RGna_12670 encoding B12-binding radical SAM proteins was reduced upon PBG supplementation although this change in gene expression was not significant (Figure 44A). At T12, the expression of *MetH, PduD/DhaC, PduE/DhaE, MtaB* and RGna_12670 was enhanced upon PBG supplementation whilst the expression of *MetH2, PduC/DhaB* and RGna_03200 was decreased upon PBG supplementation. However, these differences were not statistically significant (Figure 44B).

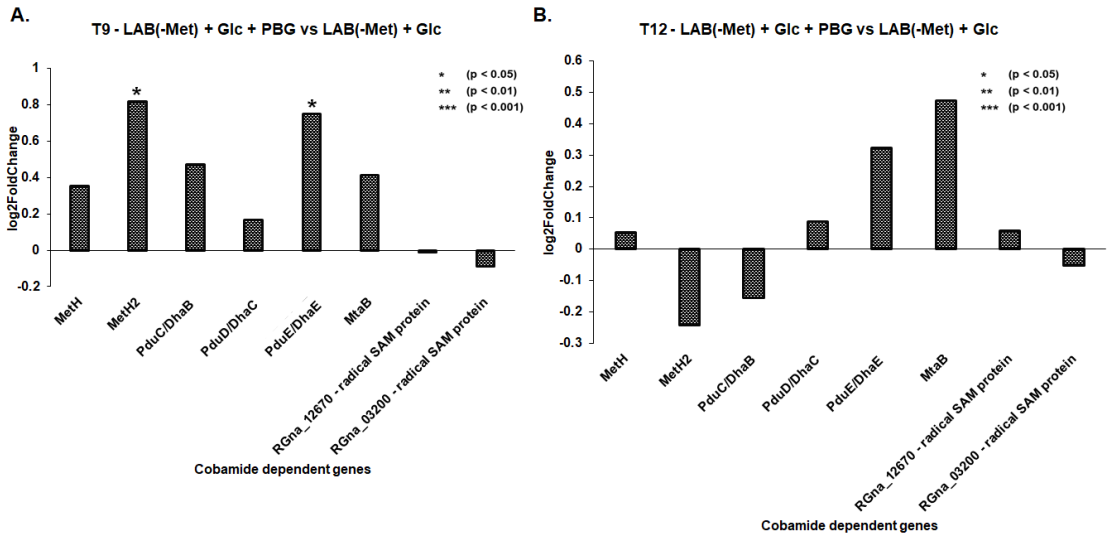

Figure 44 Effect of PBG on the expression of *R. gnavus* genes encoding cobamide-dependent proteins in the absence of Met. A bar plot showing the mean log2(fold change), y-axis, for genes encoding cobamide-dependent proteins, MetH, MetH2, PduC/DhaB, PduD/DhaC, PduE/DhaE, MtaB, RGna_03200 and RGna_12670 for samples collected at T9 (A) and T12 (B). Statistical significance is indicated by asterisks. A p-value below 0.05 is represented with one star (*), indicating significance, p-value below 0.01 is denoted with two stars (**), signifying higher significance, a p-value below 0.001 is denoted with three stars (***), indicating highest level of statistical significance.

When *R. gnavus* was grown in LAB(+Met), at T9, the expression of *PduE/DhaE* and SAM radicals RGna_03200 and RGna_12670 was enhanced upon PBG supplementation, although this was not statistically significant (Figure 45A). *MetH, MetH2, PduC/DhaB, PduD/DhaC* and *MtaB* showed reduced expression in the presence of PBG, although these changes were not significant (Figure 45A). At T12, the expression of *PduD/DhaC, MtaB*, RGna_03200 and RGna_12670 was increased in the presence of PBG but this was not significant (Figure 45B). The expression of MetH, MetH2, *PduC/DhaB* and *PduE/DhaE* was reduced in the presence of PBG with *PduC/DhaB* being statistically significant showing a 1.48-fold reduction (Figure 45B).

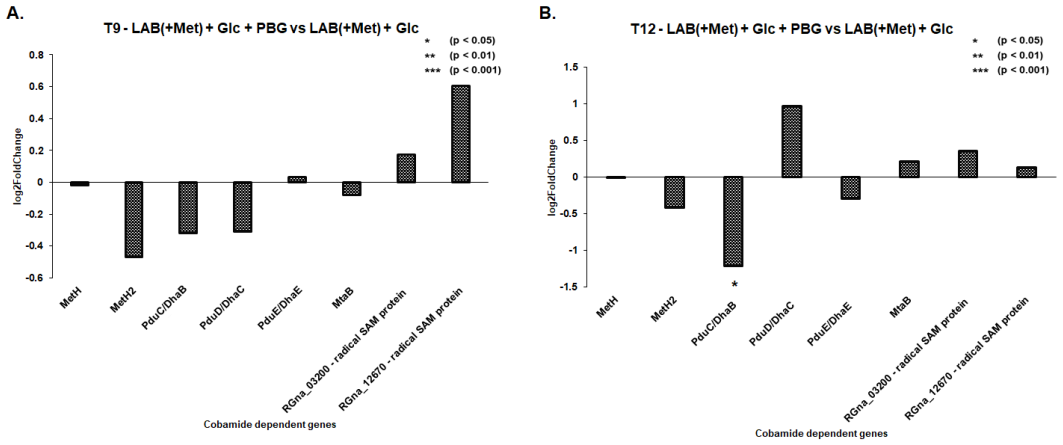

Figure 45 Effect of PBG on the expression of *R. gnavus* genes encoding cobamide-dependent proteins in the presence of Met. A bar plot showing the mean log2(fold change), y-axis, for putative cobamide-dependent genes MetH, MetH2, PduC/DhaB, PduD/DhaC, PduE/DhaE, MtaB, RGna_03200 and RGna_12670 for samples collected at T9 (A) and T12 (B). Statistical significance is indicated by asterisks. A p-value below 0.05 is represented with one star (*), indicating significance. A p-value below 0.01 is denoted with two stars (**), signifying higher significance, a p-value below 0.001 is denoted with three stars (***), indicating highest statistical significance.

Taken together, these transcriptomic results suggest that, under Met-deficient conditions, *R. gnavus* ATCC 29149 does not have the metabolic capacity to convert PBG into cobamide, as suggested by the reduced expression of cobamide biosynthesis genes at both time points. However, PBG supplementation led to the enhanced expression of genes encoding cobamide-dependent proteins in these conditions, which may be due to a regulatory effect of PBG on cobamide-dependent reactions.

Under Met-supplemented conditions, the effect of PBG supplementation on transcription differed between time points. At T9, the reduced expression of a large proportion of both cobamide-biosynthetic genes and genes encoding cobamide-dependent proteins suggests that *R. gnavus* is unable to synthesise a cobamide from PBG while at T12, the increased expression of a large proportion of cobamide biosynthetic genes suggests that PBG could be used to form a cobamide although experimental validation is required to confirm the ability of *R. gnavus* to synthesise cobamide from PBG in these conditions. There was no significantly upregulated genes encoding cobamide-dependent proteins at T12 under Met-supplemented conditions, however there was a significant down regulation of *PduC/DhaB* which may suggest insufficient cobamide production or the production of a cobamide

unable to be utilised by *R. gnavus*, in line with the results of the growth assays (see section 4.2.3.1).

4.3 Discussion

Comparative genomic analyses revealed an uneven distribution in the cobamide dependence and biosynthesis across bacteria, with 86% of bacteria species predicted to encode at least one cobamide-dependent protein family member and only 37% predicted to be *de novo* cobamide synthesisers (Shelton *et al.*, 2018). Here, a comprehensive *in silico* analysis of all publicly available *R. gnavus* genomes predicted that 98% of *R. gnavus* strains have the capacity to utilise cobamide, with the following genes encoding cobamide-dependent proteins being conserved across the genomes of all strains analysed: *MetH* and *MetH* subunit *MetH2* encoding cobamide-dependent methionine synthase; *MtaB* encoding a methanol:coenzyme M methyltransferase; *dhaBCE* encoding the glycerol dehydratase complex; *pduCDE* encoding the propanediol dehydratase complex, and two cobamide-dependent radical SAM proteins encoded by RGna_03200 and RGna_12670, respectively. These results are in line with previous bioinformatic work on *R. gnavus* CC55_001C showing the presence of *MetH*, *dhaBCE* and *pduCDE* within the genome of this strain (Shelton *et al.*, 2018). Shelton *et al.*, (2018) also predicted the absence of genes encoding cobamide-dependent isomerases *GlmS* and *MMUT/MCM*, cobamide-dependent eliminases *EutBC* and *NrdJ*, cobamide-dependent aminomutases *KamDE*, *OraSE,* cobamide-dependent methyltransferases *MtaB, QueG, BchE* and *PceA* (Shelton *et al.*, 2018). However, in our work, *MtaB* was identified in the genomes of 98% *R. gnavus* strains analysed and this was confirmed by transcriptomic analyses showing the increased expression of *MetH, MetH2, PduCDE, DhaBCE, MtaB, RGna_03200* and *RGna_12670* in *R. gnavus* ATCC 29149 upon CNPsCbl supplementation.

In vitro growth assays confirmed the cobamide utilisation capacity of the six *R. gnavus* strains tested i.e. ATCC 29149, ATCC 35913, E1, CC55_001C, 0_1_58FAA and Finegold that all demonstrated enhanced growth upon supplementation with cobalamin analogues AdoCbl, MeCbl, OHCbl, CNCbl and cobamide derivatives PsCbl, vitB12 – Factor III, vitB12 – Factor IIIm, vitamin B12 – 5MB and vitB12 – Factor A.

Using *R. gnavus* ATCC 29149 as a model strain for *R. gnavus*, its ability to cross-feed on cobamide provided by PsCbl-producing *L. reuteri* MM4-1A strain was investigated *in vitro*. *R. gnavus* ATCC 29149 demonstrated enhanced growth in co-culture with *L. reuteri* MM4-1A as compared to monocultures in cobamide-free synthetic media, in the presence or absence of Met. Enhanced *R. gnavus* growth in co-culture with non-cobamide producing *L. reuteri* L16001 strain was only observed when grown in Met-deficient conditions and at a lower level than in the presence of the PsCbl-producing *L. reuteri* MM4-1A strain. These results support the capacity of *R. gnavus* to cross-feed on PsCbl provided by *L. reuteri*.

Transcriptomic analyses were conducted to determine the pathways and genes affected by cobamide supplementation when *R. gnavus* was grown on in Met-deficient or Met-supplemented media. Limiting Met availability allowed the investigation of *R. gnavus* cobamide-dependent pathways essential for Met synthesis. We examined how *R. gnavus* responded to exogenous cobamide provided as CNPsCbl or through cross-feeding with PsCbl-producing *L. reuteri* MM4-1A when environmental Met is scarce.

PCA analysis revealed similar gene expression changes between *R. gnavus* monocultures grown in the presence of CNPsCbl or *R. gnavus* co-cultures with PsCbl-producing *L. reuteri* MM4-1A strain under Met-deficient conditions. These datasets were spatially distinct from *R. gnavus* monocultures grown in Met-deficient media alone. These data further support *R. gnavus* capacity to utilise cobamide and suggest that *R. gnavus* uses similar metabolic pathways in response to CNPsCbl and PsCbl availability. *MetH* and *MetH2* encoding cobamide-dependent methionine synthase and the corresponding activation subunit as well as a cobamide biosynthetic gene *CobU/CobP*, were amongst the most significantly upregulated genes when *R. gnavus* was grown in the presence of either CNPsCbl or PsCbl-producing *L. reuteri* MM4-1A compared to when *R. gnavus* was grown in monoculture under Met-deficient conditions at T9, further supporting the cobamide cross-feeding between *R. gnavus* and *L. reuteri* under the conditions tested.

The ECF-type ABC transport system is a putative vitamin uptake system in Gram-negative prokaryotes (Rodionov *et al.*, 2009) with each ECF transporter harbouring a substrate-specific binding protein, more commonly known as the S component. The S component CbrT, has been shown to be specific for cobamide in

Lactobacillus delbrueckii (Rodionov *et al.*, 2009). No defined cobamide uptake system has been characterised in *R. gnavus* to date and no genes encoding putative cobamide uptake were identified across *R. gnavus* strains by *in silico* analysis in this work. However, in the presence of exogenous CNPsCbl and PsCbl-producing *L. reuteri* MM4-1A, under Met-deficient conditions, *R. gnavus* demonstrated the significant upregulation of an uncharacterised gene, RGna_RS03450, encoding a putative membrane-embedded ECF transporter S component which may be involved in the uptake of cobamide, however this would need to be experimentally validated. The significant upregulation of this vitamin uptake encoding gene in the presence of PsCbl-producing *L. reuteri* MM4-1A provides further support of cobamide cross-feeding between *R. gnavus* and *L. reuteri* under the conditions tested. An additional uncharacterised ECF transporter S component encoding gene, RGna_RS14310, was significantly upregulated in the presence of PsCbl-producing *L. reuteri* MM4-1A but not in the presence of exogenous CNPsCbl, under Met-deficient conditions. This gene product may also be involved in the transport of specific cobamides into the cell, however further work is required to test this hypothesis.

All genes encoding cobamide-dependent proteins, *MetH, MetH2, PduCDE, DhaBCE, MtaB, RGna_03200* and *RGna_12670*, showed upregulation in the presence of exogenous CNPsCbl under Met-deficient conditions during mid-late exponential growth phase. This is also indicative of the ability of *R. gnavus* to utilise CNPsCbl for the metabolism of propanediol and/or glycerol via the propanediol/glycerol family dehydratases encoded by *PduCDE* and *DhaBCE* in addition to utilising CNPsCbl for methylation reactions via methanol-corrinoid protein co-methyltransferase encoded by MtaB and cobamide-dependent radical s-adenosyl-l-methionine (SAM) enzymes encoded by RGna_03200 and RGna_12670. A downregulation of *MetH2, MtaB* and *RGna_03200* was observed at T12 which is likely due to a reduction in the level of cobamide available in the growth media, although this would need to be experimentally determined.

Similarly, under Met-deficient conditions the presence of PsCbl-producing *L. reuteri* MM4-1A led to a significant upregulation of *MetH, MetH2, PduC/DhaB* genes at T9 and *MtaB* gene at T12, strongly supportive of PsCbl utilisation by *R. gnavus.*

Reduced significant upregulation of cobamide specific genes (encoding proteins involved in cobamide-dependent reactions or the biosynthesis or transport of cobamide) was observed when *R. gnavus* was grown in Met-supplemented conditions in the presence of exogenous CNPsCbl or PsCbl-producing *L. reuteri* MM4-1A, demonstrating that addition of Met alleviates the need for cobamide synthesis under these conditions.

Taken together, the results of this work demonstrated *R. gnavus* capacity to cross-feed on cobamide provided exogenous or produced *in situ* by *L. reuteri* MM4-1A for use in cobamide-dependent reactions.

However, whether *R. gnavus* is able to synthesise cobamide from precursors has not been demonstrated. Here, *in silico* analysis identified a partial cobamide biosynthesis pathway across the 152 *R. gnavus* strains analysed, in line with the prediction of *R. gnavus CC55*_001C being a 'tetrapyrrole precursor salvager' (Shelton *et al.*, 2018), potentially allowing for cobamide synthesis from cobamide precursor PBG. *R. gnavus* CC55_001C was amongst the 152 strains harbouring the partial cobamide biosynthesis pathway. In addition, we showed that the strains encoding the partial cobamide biosynthesis pathway also possessed genes *ThiC,* homologous to *BzaA/B/F* and *BluB* encoding proteins involved in the anaerobic biosynthesis of the lower ligand of cobamide compounds (Hazra *et al.*, 2015), *FldA*, encoding proteins involved in the conversion of cobamide to its coenzymic form (Warren *et al.*, 2002), *CbiET* a fusion gene encoding a protein involved in cobyrinic acid a,c-diamide formation (Raux *et al.*, 1998), *CobW* encoding a protein involved in cobalt transportation (Raux *et al.*, 1996) and *CysGA-hemD* a fusion gene involved in the biosynthetic pathway from glutamyl-tRNA to uroporphyrinogen III (Koyama' *et al.*, 1999). However, we were unable to identify *HemA, HemL,* and *HemB*, which are critical for the synthesis of the cobamide precursor uroporphyrinogen III (Warren *et al.*, 2002). Additionally, *CobG, CobF*, and *CobT*, which play roles in the aerobic cobamide biosynthetic pathway (Roth *et al.*, 1993), were absent. The genes *CbiT* and *CbiE*, essential for the anaerobic biosynthetic pathway (Moore and Warren, 2012), were also not detected. Moreover, we did not find *PduX*, responsible for the formation of the aminopropanol linker, or *CbiZ*, which is involved in corrinoid remodeling (Gray and Escalante-Semerena, 2009). Additionally, *CblS*, a gene implicated in the salvage of alpha-ribazole during the later stages of the

biosynthetic pathway (Gray and Escalante-Semerena, 2010), and *BluB*, essential for the synthesis of the lower ligand 5,6-dimethylbenzimidazole (DMB) (Taga *et al.*, 2007), were not identified. However, we did identify *GltX*, the first gene in the biosynthetic route to adenosylcobalamin from the five-carbon precursor, 5-aminolaevulinic acid (ALA) (Scott and Roessner, 2002), in the genome of all *R. gnavus* strains analysed. These results confirm the inability of *R. gnavus* to synthesis cobamide *de novo* but suggests the ability to synthesis cobamide from a cobamide precursor.

Transcriptomic analyses of *R. gnavus* ATCC 29149 when grown in the presence of PBG revealed the presence of a cobamide operon of 27 genes, made up of cobamide biosynthetic genes and genes involved in peptide uptake (*PBP2_OppA, GsiA, DppC, OppB*). This validates the findings of the *in silico* analysis in this work, which predicted the presence of these genes across 93% of *R. gnavus* strains, including *R. gnavus* ATCC 29149. Although not included in the cobamide operon, transcriptomic analyses also demonstrated the transcription of cobamide biosynthetic genes *GltX, FldA, CobW* and *ThiC* by *R. gnavus.* These genes were also predicted present across *R. gnavus* strains, including *R. gnavus* ATCC 29149, in the comparative genomic analysis in this work.

The genomic analyses suggested that *R. gnavus* strains may be able to synthesise cobamide from the cobamide precursor PBG. However, we found that *in vitro* under Met-deficient conditions, *R. gnavus* ATCC 29149 growth was reduced in the presence of PBG and transcriptomic analysis showed downregulation of most cobamide synthetic genes. However, under Met-supplemented conditions, a significant increase in the expression of these biosynthetic genes was observed at late exponential growth phase although this was not reflected in the growth assays, and the ability of *R. gnavus* to convert PBG to a cobamide remains to be determined experimentally.

The requirement of supplemented Met by *R. gnavus* to metabolise PBG, is likely due to the role of Met in the synthesis of S-adenosylmethionine (SAM), a crucial methyl donor necessary for the methylation reactions that take place during cobamide biosynthesis. In the cobamide biosynthesis pathway, the first reaction requiring Met is the methylation of uroporphyrinogen III, an early intermediate in the pathway. This methylation leads to the formation of precorrin-2, a cobamide

precursor (Martens *et al.*, 2002). The protein encoded by *CobA* catalyses this reaction in *P. denitrificans,* whilst a fusion gene *CysGA* encodes the protein that catalyses this reaction in *S.* Typhimurium and *E. coli* (Warren *et al.*, 1990; Raux *et al.*, 1998). In *R. gnavus* ATCC 29149, *in silico* analyses and transcriptomic data revealed the presence of the fusion gene *CysGA-hemD/CobA* within the genome, suggesting a similar functional role in catalysing the initial methylation steps of cobamide biosynthesis as observed in *S.* Typhimurium and *E. coli*. In the anaerobic cobamide biosynthesis pathway, 8 methylation reactions are required for the formation of cobyrinic acid, a precursor compound formed in the later stages of the cobamide biosynthesis pathway (Warren and Escalante-Semerena, 2008). Thus, the dependency of *R. gnavus* on supplemented Met to metabolise PBG can be attributed to the necessity of Met for critical methylation reactions.

Chapter 5

The effect of cobamide supplementation and PsCbl-producing *L. reuteri* MM4-1A on *R. gnavus* growth in the context of a complex microbial community

5.1 Introduction

Cobamides have been proposed to be modulators of mammalian gut ecosystems due to their involvement in several microbial metabolic pathways, the restriction of their production to a subset of prokaryotes, and their diverse structures which are differentially accessible to microbes (Degnan, Taga and Goodman, 2014).

Genomic analysis revealed that 83% of sequenced human gut microbial species (260 out of 313) encoded cobamide-dependent genes, while fewer than 25% had the genetic capacity to synthesise cobamides (Degnan et al. (2014). Subsequently, a comparative genomics study of 11,000 bacterial species found that 37% of these bacteria could synthesise cobamides, with 86% of the species possessing at least one cobamide-dependent enzyme (Shelton *et al.*, 2018). These findings provide genomic evidence for the widespread sharing of cobamides in microbial communities such as the human gut microbiota.

Cobalamin and 7 cobamide analogues account for the largest proportion of total cobamides present in human faeces (Allen and Stabler, 2008). This human *in vivo* study also showed that gut microbes can convert cyanocobalamin (CNCbl) from the diet into other cobamide analogues, including cobinamide and four analogues that contain 2-methyladenine, p-cresol, adenine, and 2-(methylthio)adenine in their lower ligand (Allen and Stabler, 2008). This conversion of cobamides into different forms is advantageous in the human gut microbiome, as corrinoid-dependent enzymes exhibit native specificity for their preferred cofactors. In *Bacteroides thetaiotaomicron,* a dominant member of the human gut microbiota, cobamide specific transporters were shown to exhibit distinct cobamide preferences *in vitro* and to contribute differentially to microbial fitness in gnotobiotic mice (Degnan *et al.*, 2014).

Cobamides can influence microbial interactions not only by facilitating cobamide-dependent metabolism but also by altering metabolic networks through cobamide-dependent reactions and cross-feeding. This concept has been illustrated in *Eubacterium hallii*, where pseudocobalamin (PsCbl) produced by this gut bacterium has been shown to enhance propionate production by *Akkermansia muciniphila*, a beneficial microbe of the human gut microbiota (Belzer *et al.*, 2017). Another *in vitro* study demonstrated the impact of cobamide availability on short chain fatty acid

(SCFA) production, showing that low-dose of CNCbl-enriched spinach enhanced the production of butyrate and acetate (Zheng et al., 2021). Similarly, it was shown, in mice, that dietary CNCbl restriction led to a reduction in SCFAs in faecal samples (Ge, Zadeh and Mohamadzadeh, 2022).

We previously showed that *R. gnavus* could benefit from cobamide analogues and from PsCbl released by *L. reuteri* MM4-1A in co-cultures. Here, we used an *in vitro* batch model seeded with faecal microbiota from a healthy donor to investigate the impact of cobamide supplementation and PsCbl-producing *L. reuteri* MM4-1A on *R. gnavus* expansion within a complex microbial community and on the overall gut microbial structure and function.

5.2 Results

5.2.1 The impact of cobamide supplementation on *R. gnavus* and gut microbial community composition

The effect of cobamide supplementation on *R. gnavus* growth within a complex microbial community was investigated using a human faecal obtained from a healthy donor positive for the presence of *R. gnavus* as determined by qPCR using *R. gnavus* 16S specific primers (see Supplementary Figure 9). This donor was also screened for the presence of *L. reuteri* using *L. reuteri* 16S specific primers. *L. reuteri* was not detectable by qPCR (see Supplementary Figure 9).

Batch fermentation media were supplemented with the cobamide precursor porphobilinogen (PBG), or a low dose (5 ng/mL) or high dose (2500 ng/mL) of cyanopseudocobalamin (CNPsCbl) or inoculated with either pseudocobalamin (PsCbl)-producing *L. reuteri* strain MM4-1A or with the non-cobamide-producing *L. reuteri* strain L16001 as a control. A batch culture media-only condition was also included as a control. All batch cultures were then inoculated with thawed faecal suspension and the batch cultures carried out anaerobically for 24 h.

R. gnavus and *L. reuteri* growth was monitored by qPCR over a 24 h period. In the untreated control batch culture, *R. gnavus* exhibited a 2.75-fold growth increase between 0 and 4 h, but *R. gnavus* was no longer detectable at 8 and 24 h (Figure 46A). *L. reuteri* MM4-1A and L16001 both demonstrated sustained and improved growth between 0 and 24 h with a 297.86- and 119.12-fold increase, respectively,

with *L. reuteri* MM4-1A showing more enhanced growth compared to *L. reuteri* L16001 (Figure 46B). In the presence of *L. reuteri* MM4-1A or L16001, *R. gnavus* showed a 1.49- and a 2.70-fold decrease in growth, respectively, as compared to the untreated control. However, *R. gnavus* growth was detected for up to 24 h in the presence of *L. reuteri* L16001, and up to 8 h in the presence of *L. reuteri* MM4-1A; *R. gnavus* growth was only sustained for up to 4 h in the presence of low dose CNPsCbl whilst in the presence of high dose CNPsCbl or PBG*R. gnavus* growth was sustained for up to 8 h. Supplementation with high dose of CNPsCbl led to the highest growth effect on *R. gnavus* in the faecal sample with *R. gnavus* exhibiting a 1.98-fold growth increase at 4 h compared the untreated control (Figure 46).

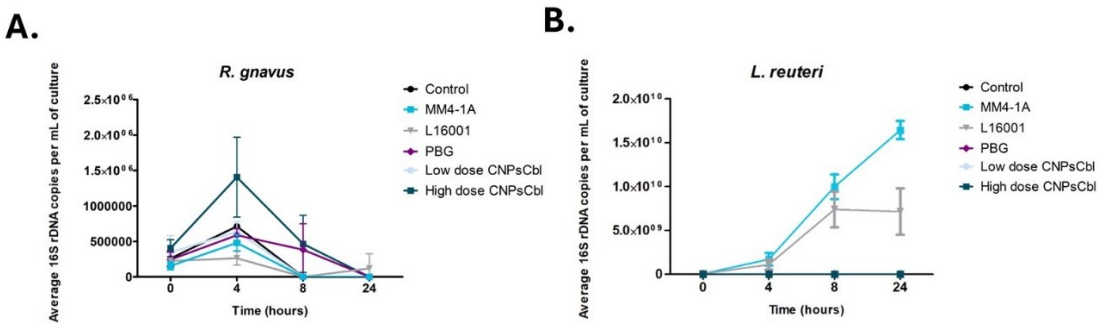

Figure 46 Analysis of *R. gnavus* and *L. reuteri* growth in a colonic fermentation batch model. Bacterial quantification is expressed as 16S rDNA copy number/mL of culture for *R. gnavus* and *L. reuteri* in anaerobic batch cultures. Data points mark the mean of 3 replicates. The error bars correspond to standard deviations between replicates. Samples were collected at 0, 4, 8 and 24 h.

In order to determine the effect of the treatments on the composition of the gut microbiota, DNA was extracted from samples collected at 0, 4 and 8 h and analysed by shotgun metagenomic sequencing.

The microbial composition of the initial donor faecal sample used to inoculate batch cultures was analysed using the DIAMOND software and the MicroNR database. *Bacillota* (formerly *Firmicutes*) was found to be present at a relative abundance of 67%. The second most abundant phylum was *Bacteroidata (*formerly *Bacteroidetes)* at 17%, followed by *Actinomycetota (*formerly *Actinobacteria)* at 5% and *Pseudomonadota* (formerly *Proteobacteria*) at 1% (Figure 47A).

At the genus level, the top 10 most abundant taxa included *Roseburia,* being the most dominant genus, with a relative abundance of 13%, followed by

Streptococcus, Bacteroides, Eubacterium, Holdemanella, Escherichia, Enterobacter, Citrobacter, Enterococcus and *Limosilactobacillus* (Figure 47B).

The most abundant species were *Streptococcus thermophilus* at 4% relative abundance, followed by *Roseburia faecis, Phocaeicola vulgatus, Roseburia intestinalis, Eubacterium ventriosum, Escherichia coli, Enterococcus faecalis, Citrobacter farmer, Enterobacter hormaechei* and *L. reuteri*. This result showed that *L. reuteri* was present in the donor sample although not detected by qPCR in the initial screening, which may be due to differences in the sensitivity of the methods. *R. gnavus* presence in the donor sample, determined by qPCR in the initial screening, was confirmed by shotgun metagenomic sequencing where taxonomic annotation revealed *R. gnavus* as one of the top 35 most dominant species in the faecal sample (Supplementary Table 14).

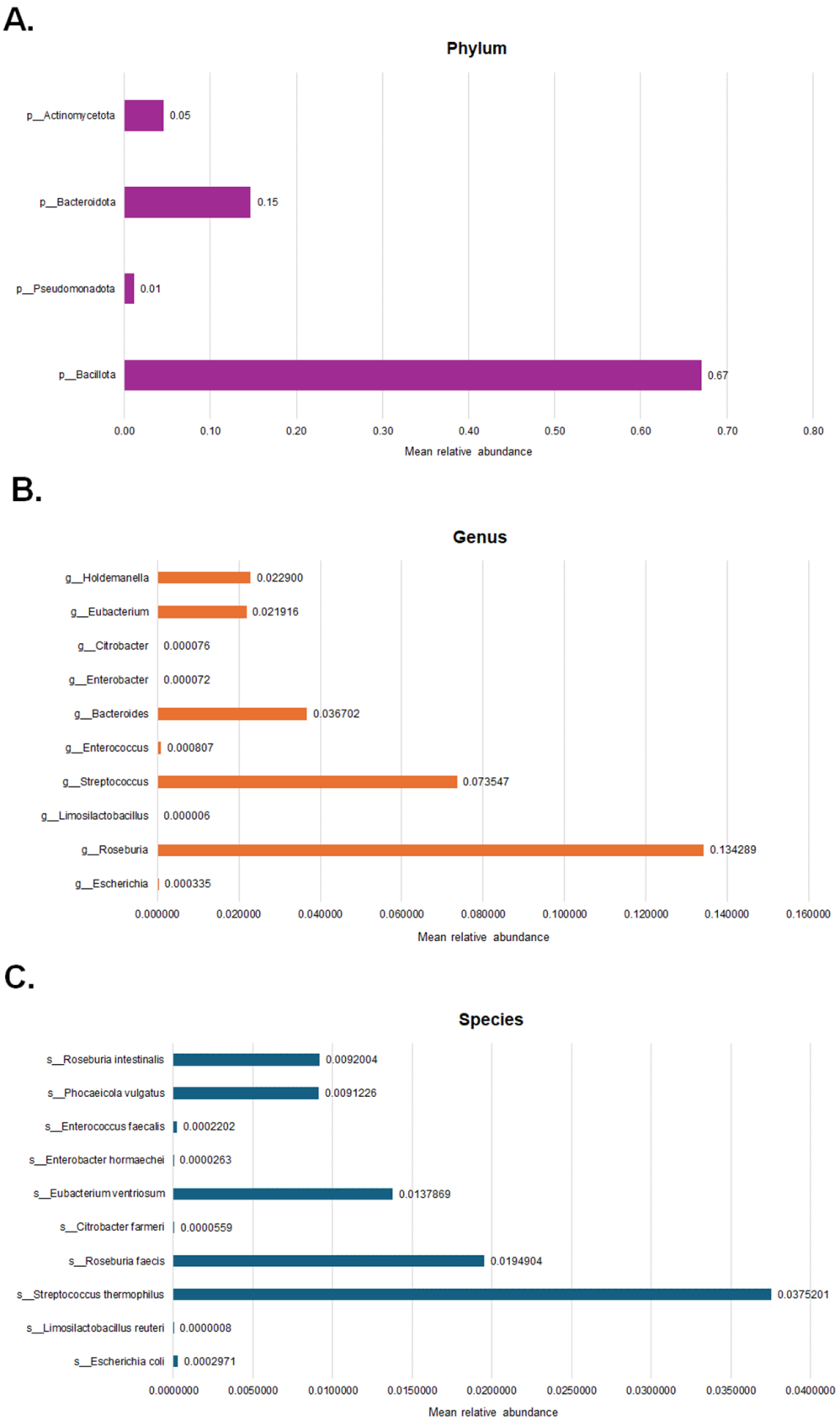

Figure 47 Microbial composition of the initial donor faecal microbiota. The mean relative abundance of the top 4 taxa is displayed at the phylum level (A) and the relative abundance of the top 10 taxa is displayed at the genus (B) and species (C) level. Mean relative abundance calculated from triplicate faecal samples.

When investigating the impact of cobamide availability on the overall faecal microbiota composition, no significant differences were observed across groups (control, PBG, low dose CNPsCbl, high dose CNPsCbl, L16001 and MM4-1A), as confirmed by beta diversity analysis using Bray–Curtis distance matrices (Figure 48A) and Analysis of similarities (ANOSIM) statistical tests (Figure 48B-F).

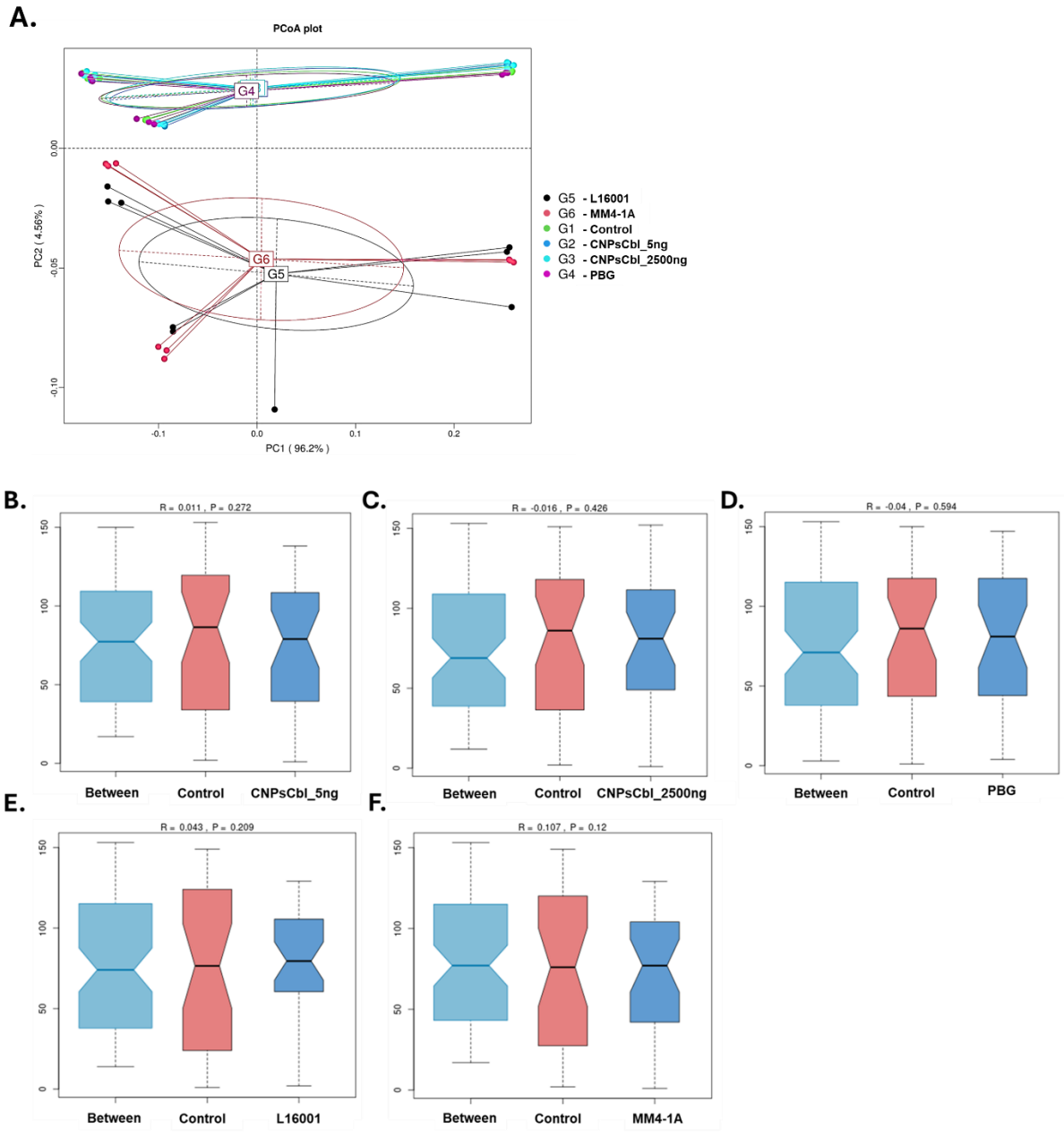

Figure 48 Effect of cobamide supplementation on beta diversity and Analysis of similarities (ANOSIM) of faecal microbiota composition from batch cultures. (A) Principal Coordinates Analysis (PCoA) plot of beta diversity based on Bray Curtis distances for microbial communities in faecal batch cultures across all conditions (Control, PBG, low dose CNPsCbl, high dose CNPsCbl, L16001 and MM4-1A). (B-F) ANOSIM analysis with R-values ranging from -1 to 1. R-values close to 0 indicate no significant differences between inter-group and intra-group variations. An R-value close to 1 indicates that the differences between groups are greater than the differences within groups. P-values provide the

statistical significance of the observed R-value. A P-value below 0.05 indicates that the observed separation between groups is statistically significant.

In addition, *L. reuteri* inoculation, PBG, high dose CNPsCbl or low dose CNPsCbl supplementation did not significantly impact alpha diversity when compared to the control, as demonstrated by observed species and shannon index measurements (Figure 49 A-C).

A.

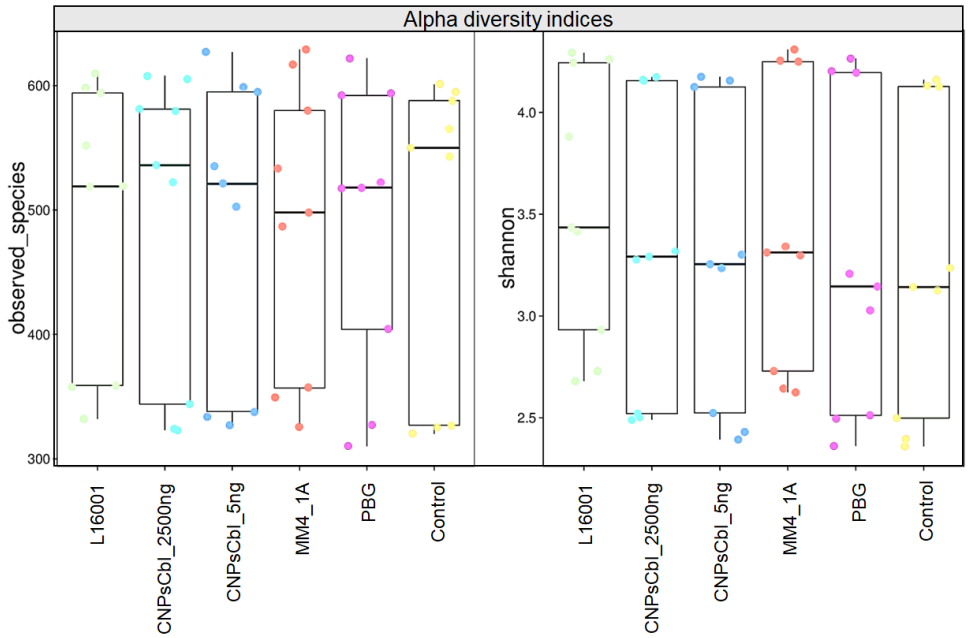

B.

Observed species	Difference	P value
Control vs low dose CNPsCbl	-0.61111	0.9377
Control vs high dose CNPsCbl	-0.66667	0.932
Control vs PBG	1.277778	0.8702
Control vs L16001	-2	0.7981
Control vs MM4-1A	0	1

C.

Shannon index	Difference	P value
Control vs low dose CNPsCbl	-4.55556	0.5465
Control vs high dose CNPsCbl	-2.55556	0.7348
Control vs PBG	-3.22222	0.6694
Control vs L16001	-11.8889	0.1196
Control vs MM4-1A	-10.1111	0.184

Figure 49 Effect of cobamide supplementation on alpha diversity of faecal microbiota composition from batch cultures at genus level. (A) The box plot depicts alpha diversity of microbial communities from batch cultures inoculated with *L. reuteri* L16001 or MM4-1A or supplemented with PBG, high dose CNPsCbl or low dose CNPsCbl compared to the control (untreated) batch culture. (B) Observed species index and (C) Shannon index. The tables (B) and (C) display results of Wilcoxon statistical analysis which determine the significance in alpha diversity between treated batch cultures (*L. reuteri* L16001, high dose CNPsCbl, MM4-1A and PBG) and the control.

More specifically, when investigating taxonomic changes over time, at 4 h, *Pseudomonadota* was the most dominant phyla and *Bacillota* the second most dominant across all conditions (Figure 50A) in contrast to the initial dominance of *Bacillota* prior to culturing. The largest proportion of *Bacillota* was identified in cultures inoculated with *L. reuteri* L16001 or MM4-1A, with this phylum showing an average relative abundance of 32% under these conditions, as compared to an average relative abundance of 17% in the control, low dose of CNPsCbl, high dose of CNPsCbl or PBG conditions. At 8 h, *Pseudomonadota* remained the most dominant phyla, followed by *Bacillota.* The relative abundance of *Bacillota* decreased in cultures inoculated with *L. reuteri* L16001 or MM4-1A, with an average relative abundance of 32% at 8 h compared to 15% at 4 h (Figure 50B).

At the genus level, the most abundant taxa at 4 h and 8 h across all conditions tested included *Escherichia, Roseburia, Limosilactobacillus, Streptococcus, Enterococcus, Bacteroides, Enterobacter, Citrobacter, Eubacterium* and *Holdemanella,* with these taxa also the most abundant in the initial faecal microbial composition, indicating stability in microbial composition over time (Figure 50C and 50B).

Similarly, the top 10 most abundant species observed in the initial faecal microbial composition remained the top 10 most abundant species at 4 h and 8 h (Figure 50C).

Escherichia was the most dominant taxa observed across all conditions at both 8 h and 4 h, with *Escherichia coli* being the most dominant species at both time points (Figure 50C). Although *E. coli* was the most dominant species, its relative abundance at 4 h was lowest in cultures inoculated with *L. reuteri* strains L16001 and MM4-1A, suggesting an inhibitory/competitive effect of *L. reuteri* on *E. coli* expansion (Figure 50C). At 8 h, the relative abundance of *L. reuteri* decreased and the relative abundance of *E. coli* increased, again indicative of a potential inhibitory effect of *L. reuteri* on *E. coli* expansion (Figure 50C).

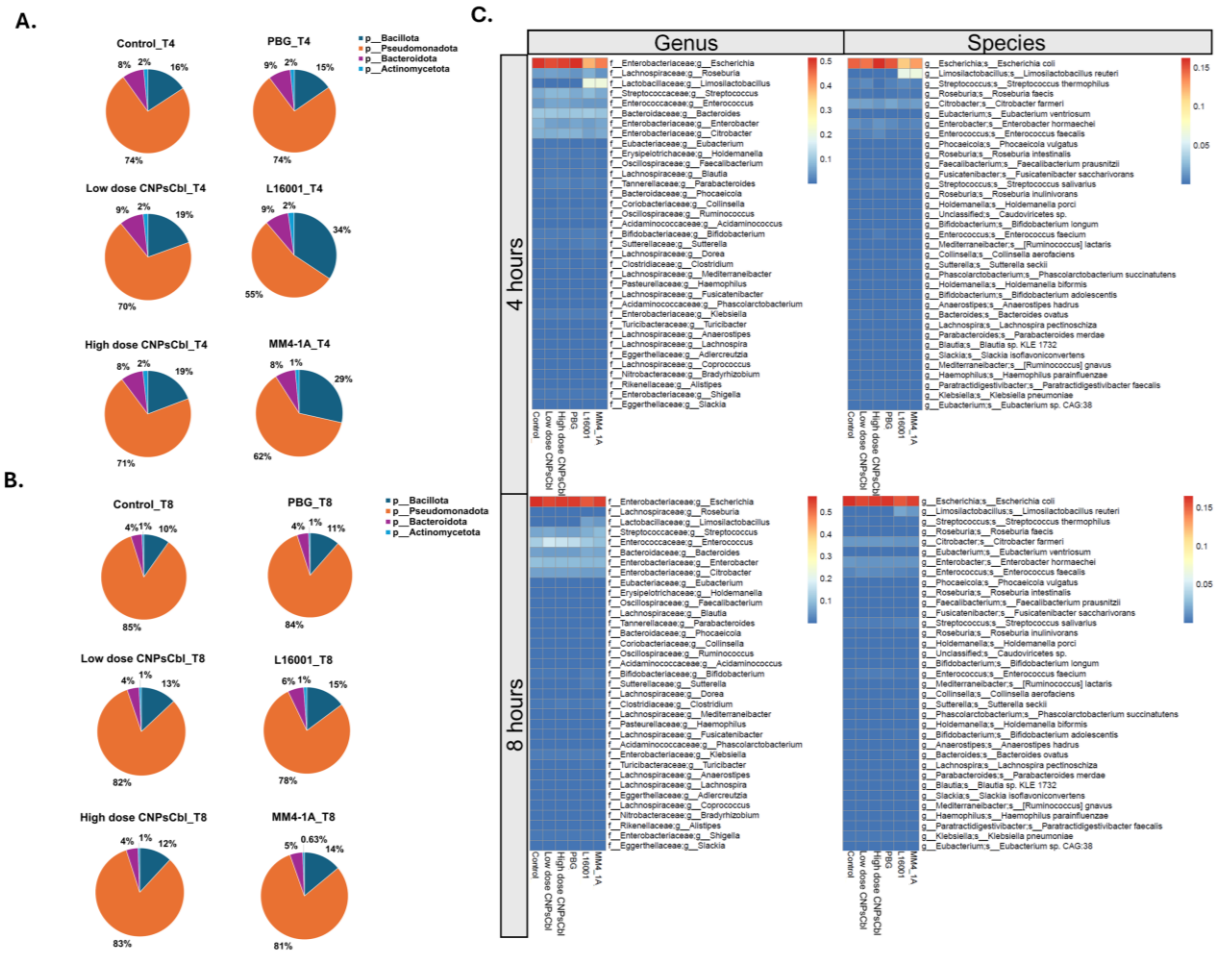

Figure 50 Effect of cobamide supplementation on the composition of faecal microbiota from batch cultures at 4 and 8 h. Relative abundance of the top 4 taxa displayed at phylum level across all conditions (Control, PBG, low dose CNPsCbl, high dose CNPsCbl, L16001 and MM4-1A) with relative abundance of phyla displayed as a percentage (A and B) and relative abundance of the dominant 35 genera and species across all conditions displayed in a heatmap of Z-score transformed relative abundance (C).

The metagenomeSeq tool was then used to determine significantly differentially abundant taxa between groups at genus and species level.

At the genus level only *Limosilactobacillus, Mycobacterium, Neobittarella* and *Winogradskyella* were detected as being significantly differentially abundant across groups (Figure 51).

Limosilactobacillus was significantly increased in batch cultures inoculated with *L. reuteri* L16001, compared to the untreated control (log fold change of 9.80) or to the low dose CNPsCbl group (log fold change of 9.73) (Figure 51).

In batch cultures inoculated with *L. reuteri* MM4-1A, there was a significant increase in the abundance of *L. reuteri* compared to the control group (log fold change of 9.78), or to the low dose CNPsCbl group (log fold change of 9.71) or to the high dose CNPsCbl group (log fold change of 10.12) (Figure 51).

The addition of *L. reuteri* MM4-1A in batch cultures resulted in a significant reduction in *Mycobacterium* (log fold change of -1.54) and *Winogradskyella* (log fold change of -1.74) abundance compared to the control group (Figure 51).

The addition of *L. reuteri* L16001 in batch cultures resulted in a significant reduction (log fold change of -1.32) in *Neobittarella* abundance compared to the control group (Figure 51).

In summary, when evaluating the changes in relative abundance of bacterial genera in response to cobamide availability, it was observed that *Lactobacillus, Mycobacterium* and *Winogradskyella* showed significant differential abundance upon inoculation of PsCbl-producing *L. reuteri* MM4-1A compared to the control group. However, these genera were not identified as differentially abundant in the low and high dose CNPsCbl groups or the PBG group, which could indicate this response may not be driven by increased cobamide availability in the form of PsCbl. Instead, the presence of *L. reuteri* MM4-1A itself may play a critical role in modulating these specific bacterial populations through other metabolic interactions.

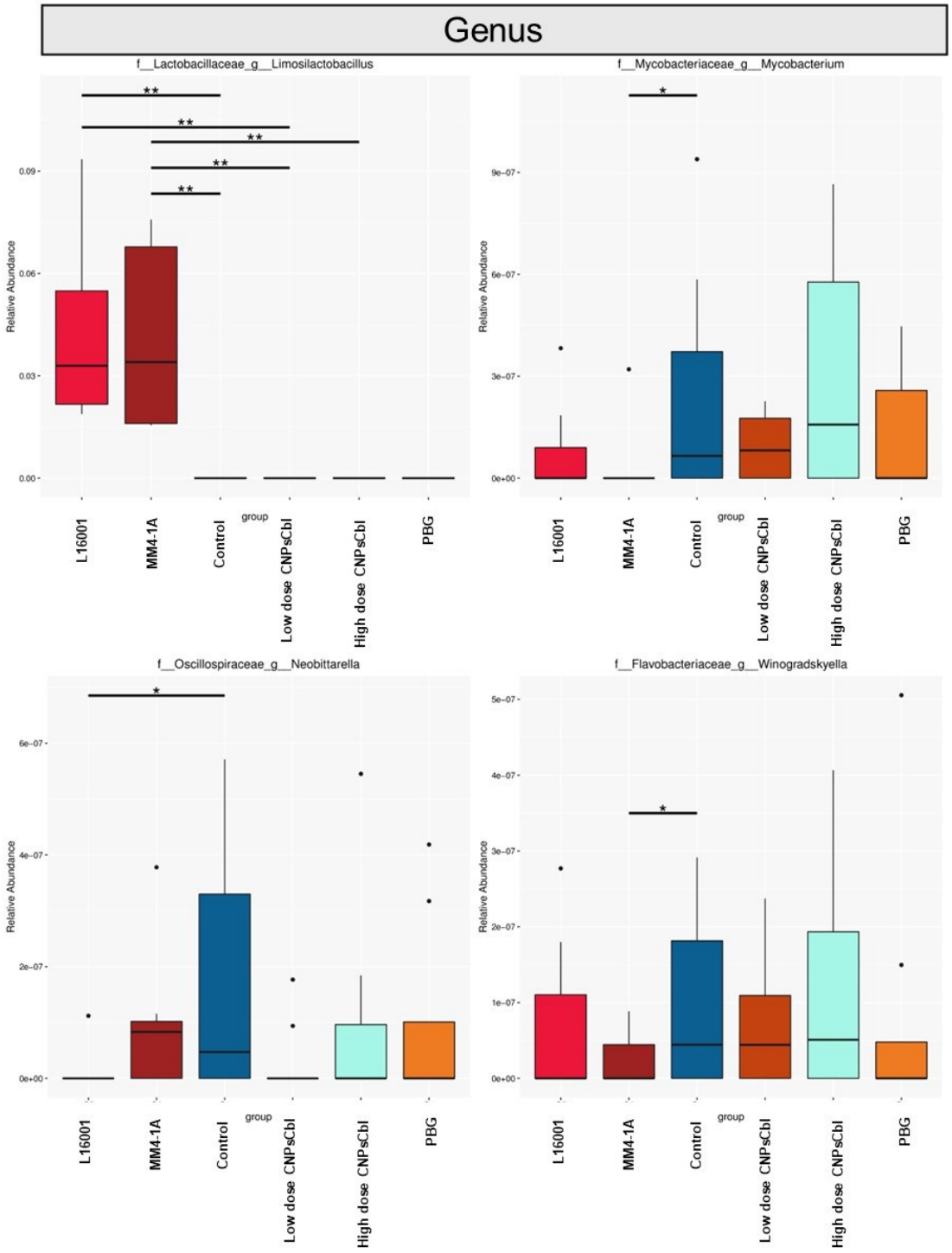

Figure 51 Effect of cobamide treatment on relative abundance in human gut microbiota at genus level. The X-axis indicates the group of samples; the Y-axis indicates the relative abundance of corresponding species. "*" means the variation between the two groups is significant (q <0.05); "**" means the variation between the two groups is extremely significant (q <0.01).

At the species level, *L. reuteri, Limosilactobacillus fermentum, Lactobacillus sp.* M31, *Limosilactobacillus pontis, Actinomyces* sp. HMSC062G12 were determined as being significantly differentially abundant across groups (Figure 52).

In batch cultures inoculated with *L. reuteri* L16001, there was a significant increase in the abundance of *L. reuteri* compared to both the control group (log fold change of 11.03) and low dose CNPsCbl group (log fold change of 10.75) (Figure 52).

Similarly, in batch cultures inoculated with *L. reuteri* MM4-1A, there was a significant increase in the abundance of *L. reuteri* compared to the control group (log fold change of 11.08), low dose CNPsCbl group (log fold change of 10.80) or high dose CNPsCbl group (log fold change of 11.22) (Figure 52).

Limosilactobacillus fermentum was significantly increased in batch cultures inoculated with *L. reuteri* L16001 compared to batch cultures supplemented with low dose CNPsCbl group (log fold change of 3.77) (Figure 52).

Lactobacillus sp. M31 was significantly increased in batch cultures inoculated with *L. reuteri* L16001 compared to batch cultures inoculated with *L. reuteri* MM4-1A (log fold change of 7.79) or supplemented with low dose CNPsCbl (log fold change of 7.84) and the control group (log fold change of 7.77) (Figure 52).

Limosilactobacillus pontis was significantly increased in batch cultures inoculated with *L. reuteri* L16001 compared to the control group (log fold change of 7.16) and in the low dose CNPsCbl group (log fold change of 7.23) (Figure 52).

In addition, *Limosilactobacillus pontis* was significantly increased in batch cultures inoculated with *L. reuteri* MM4-1A compared to the control group (log fold change of 7.19) and both the low dose CNPsCbl group (log fold change of 7.26) and high dose CNPsCbl group (log fold change of 7.28) (Figure 52).

Actinomyces sp. HMSC062G12 was significantly increased in batch cultures supplemented with low dose CNPsCbl by a log fold of 1.14 compared to batch cultures inoculated with *L. reuteri* MM4-1A (Figure 52).

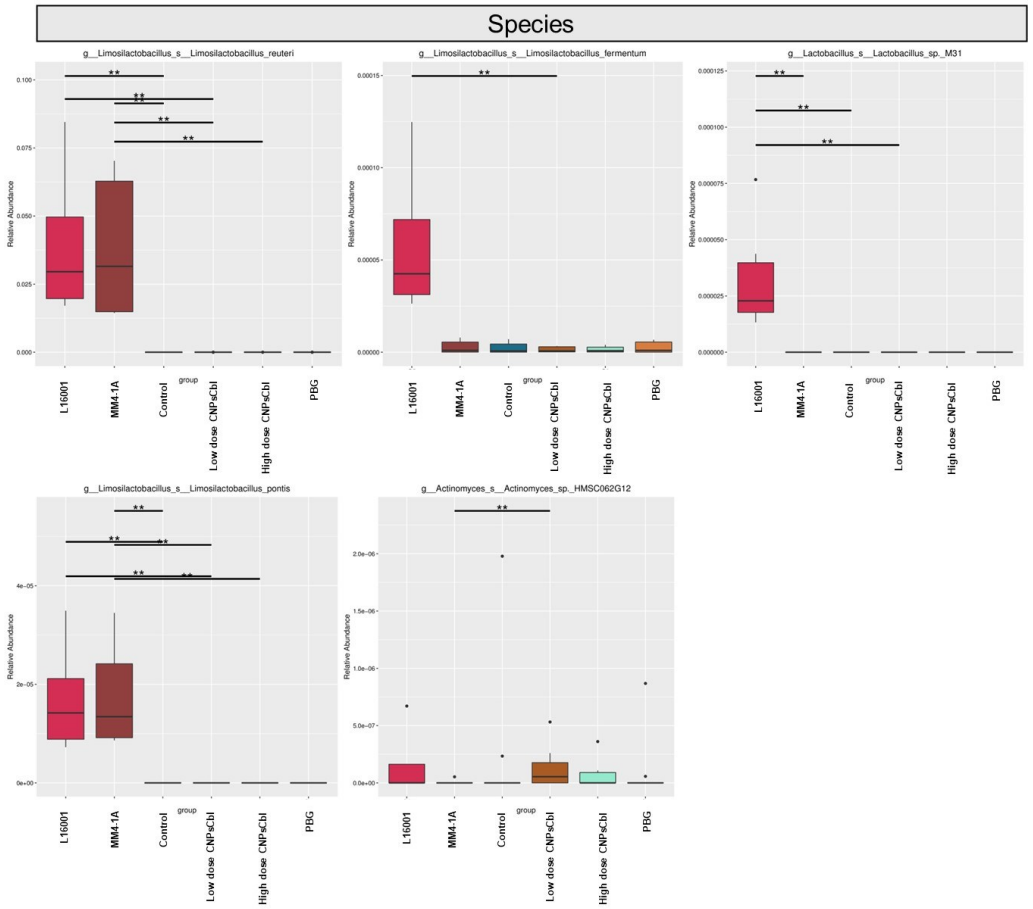

Figure 52 Effect of cobamide treatment on relative abundance in human gut microbiota at species level. The X-axis indicates the group of samples; the Y-axis indicates the relative abundance of corresponding species. "*" means the variation between the two groups is significant (q <0.05); "**" means the variation between the two groups is extremely significant (q <0.01).

In summary, when evaluating the changes in relative abundance of bacterial species in response to cobamide availability, there was no significant differential changes in species in response to CNPsCbl supplementation at various doses. There were however significant differential enhancements in the abundance of *L. reuteri* and *L. pontis* in response to the inoculation of PsCbl producing *L. reuteri* MM4-1 in batch cultures (Figure 52). However, these significant differential enhancements in abundance were also observed in response to inoculation of non-PsCbl producing *L. reuteri* L16001 in batch cultures, indicating that these changes may be driven by *L. reuteri* inoculation as opposed to being in response to increased cobamide availability.

5.2.2 The impact of cobamide supplementation on metabolite production by the human gut microbiota

To monitor the effect of cobamide supplementation on SCFA production by the human gut microbiota, the supernatant of batch cultures collected at 0, 4 and 8 h were analysed by UPLC-MS/MS.

Analysis of the metabolite profile of the initial faecal microbiota from the donor showed acetate as being the dominant SCFA followed by lactate, butyrate, propionate and isobutyrate with concentrations at 0.049 to 0.017, 0.009, 0.005, 0.0004 mg/mL, respectively (Figure 53A and B).

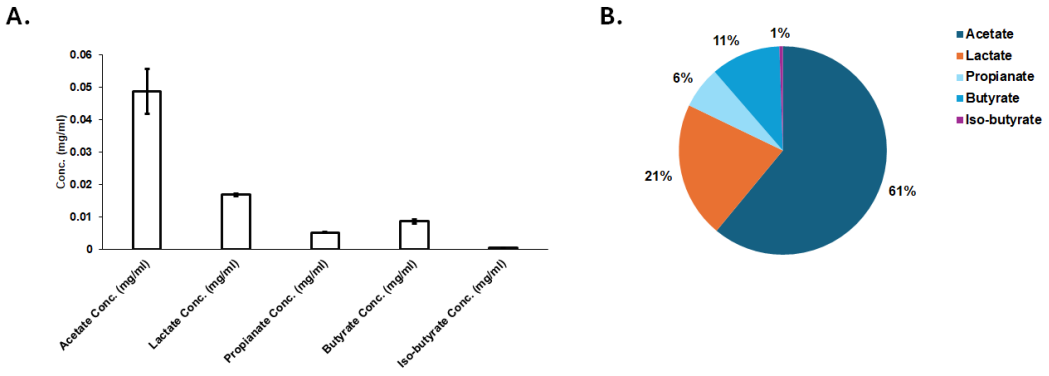

Figure 53 SCFA profile of the initial donor faecal microbiota. Batch cultures inoculated with *L. reuteri* L16001 or MM4-1A or supplemented with PBG, high dose CNPsCbl, low dose CNPsCbl or untreated (control group) (A) Bar plot demonstrates the concentration of SCFAs, acetate, lactate, propionate, butyrate and isobutyrate. The values represent averages of 3 replicates and error bars correspond to the standard deviations. (B) Pie chart representing the proportions of acetate, lactate, propionate, butyrate and isobutyrate as percentages.

At 4 h, acetate remained the most abundant SCFA in the control as well as in the cultures supplemented with PBG and high dose of CNPsCbl. In cultures inoculated with *L. reuteri* MM4-1A and those supplemented with a low dose of CNPsCbl, the proportions of acetate and lactate were comparable, although acetate remained the most abundant SCFA compared to lactate. Lactate was the most abundant SCFA produced in *L. reuteri* L16001 inoculated cultures with a statistically significant fold increase of 6.14 compared to the control. The concentration of total SCFA in *L. reuteri* L16001 inoculated cultures was also significantly enhanced by 3.21-fold compared to the control (Figure 54).

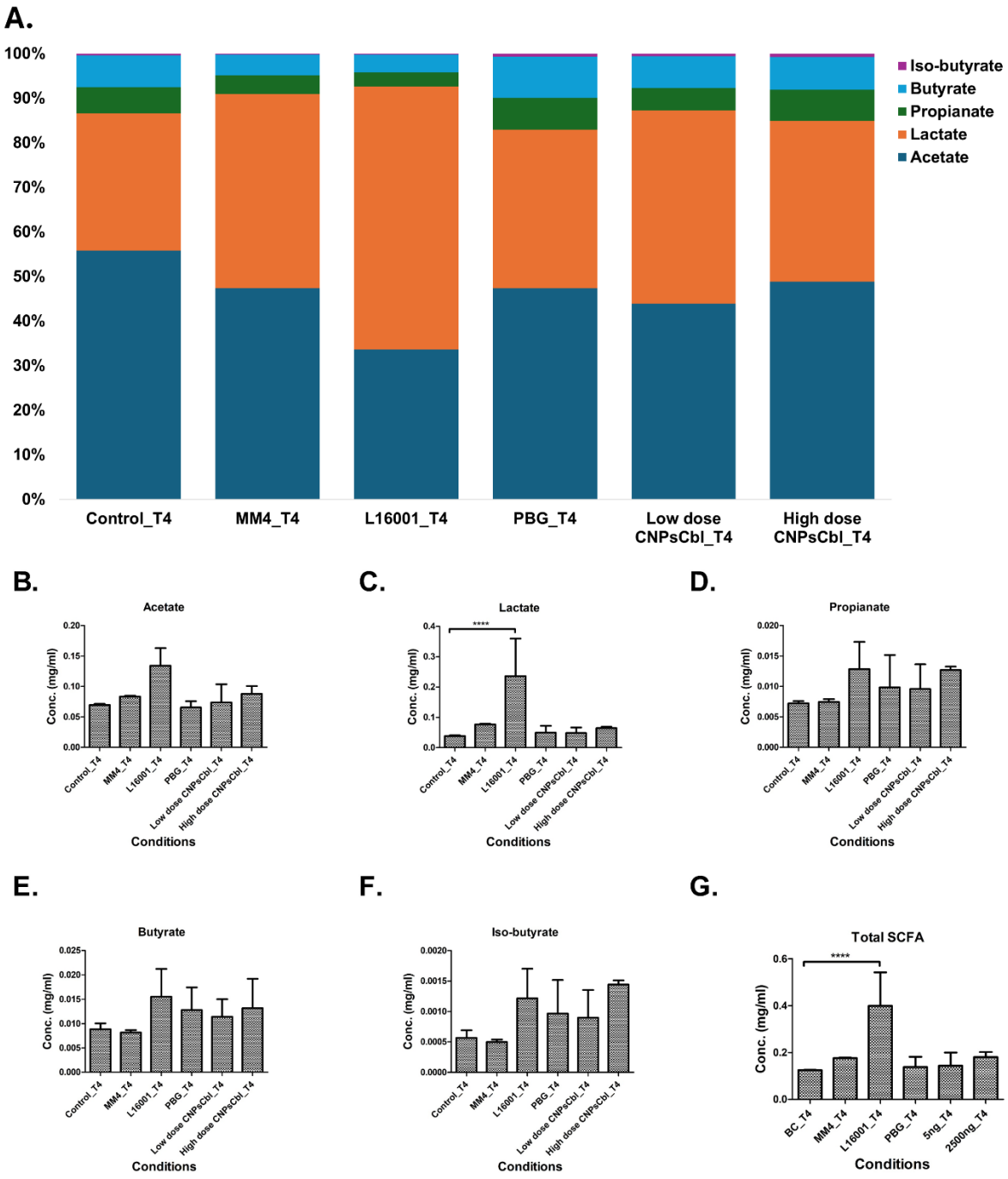

Figure 54 Effect of cobamide supplementation SCFA concentrations in batch cultures at 4 h. Batch cultures inoculated with *L. reuteri* L16001 or MM4-1A or supplemented with PBG, high dose CNPsCbl, low dose CNPsCbl or untreated (control group) (A) Stacked column chart of SCFA proportions in batch cultures displayed as percentages. Concentration of acetate (B), lactate (C), propionate (D), butyrate (E), isobutyrate (F) and total SCFA (G) displayed as bar plots. Concentrations are displayed in mg/mL and represent the average of 3 replicates. Error bars correspond to the standard deviations. Significance was determined by Two-way ANOVA with Bonferroni multiple correction. $p < 0.05$ denoted with "*", $p < 0.01$ denoted with "**", $p < 0.001$ denoted with "***" and $p < 0.0001$ denoted with "****".

At 8 h, lactate was found to be the most abundant SCFA across all groups, with the largest proportion detected in cultures supplemented with high dose of CNPsCbl. Lactate concentrations were significantly increased in batch cultures inoculated with *L. reuteri* L16001 or MM4-1A or supplemented with PBG, high dose CNPsCbl and low dose CNPsCbl compared to the control, with a fold increase of 1.65, 1.49, 1.73, 2.39 and 1.68, respectively. The abundance of lactate was also significantly higher in batch cultures inoculated in high dose CNPsCbl compared to low dose CNPsCbl, with a 1.41-fold increase. Acetate was the second most abundant SCFA across all groups. *L. reuteri* L16001 inoculated cultures displayed the highest levels of acetate with an increased abundance of 2.68-fold being statistically significant compared to the control. Total SCFA production was significantly enhanced across all groups compared to the control group, which is likely driven by high lactate levels (Figure 55).

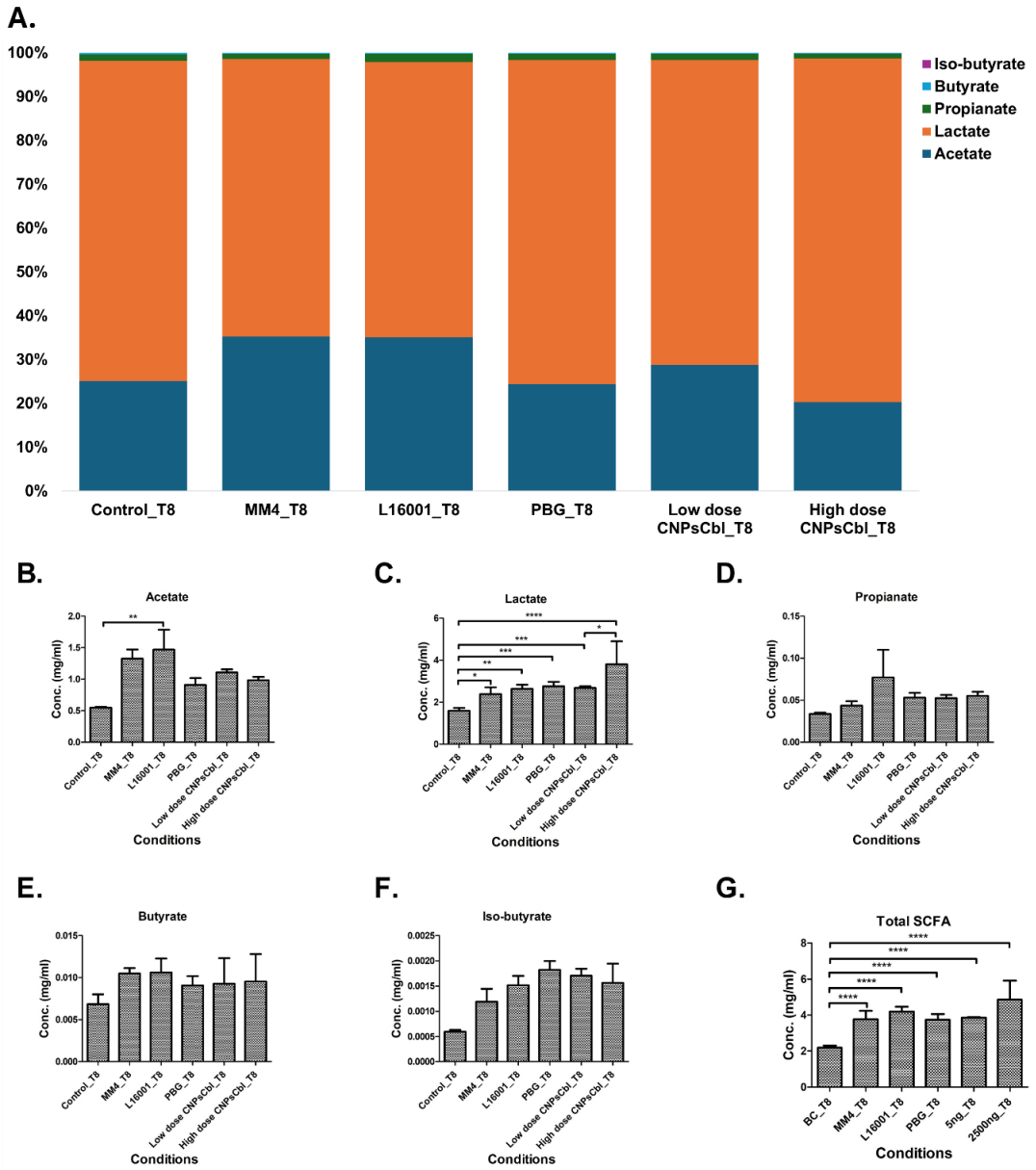

Figure 55 Effect of cobamide supplementation on SCFA concentrations in batch cultures at 8 h. Batch cultures inoculated with *L. reuteri* L16001 or MM4-1A or supplemented with PBG, high dose CNPsCbl, low dose CNPsCbl or untreated (control group) (A) Stacked column chart of SCFA proportions across batch cultures, displayed as percentages. Concentration of acetate (B), lactate (C), propionate (D), butyrate (E), isobutyrate (F) and total SCFA (G) displayed as bar plots. Concentrations are displayed in mg/mL and represent the average of 3 replicates. Error bars correspond to the standard deviations. Significance was determined by Two-way ANOVA with Bonferroni multiple correction. $p < 0.05$ denoted with "*", $p < 0.01$ denoted with "**", $p < 0.001$ denoted with "***" and $p < 0.0001$ denoted with "****".

Together, these data indicate that cobamide availability in the form of CNPsCbl enhances lactate levels in a microbial community at high doses whilst this is less pronounced at lower doses. Despite the observation that cobamides do not significantly alter the overall composition of the microbiota, the elevated lactate

levels in response to high doses of CNPsCbl imply that CNPsCbl may enhance lactate yield by promoting a higher conversion rate of substrates into lactate although this would need to be validated experimentally.

5.3 Discussion

Cobamides in the gut environment can either come from unabsorbed dietary sources or from microbial biosynthesis (Watanabe and Bito, 2018). The exclusivity of cobamide production by a subset of bacteria and archaea, in contrast to other vitamins (Roth, Lawrence and Bobik, 1996), led to the suggestion that cobamides may be modulators of the gut microbial ecology, shaping its structure and function (Degnan, Taga and Goodman, 2014).

In chapter 4 sections 4.2.1 and 4.2.2, we showed using *in silico* and *in vitro* approaches that *R. gnavus* was a cobamide auxotroph but with a partial synthetic pathway from the PBG precursor. We showed that *R. gnavus* could benefit from CNPsCbl supplementation and from PsCbl produced by *L. reuteri* MM4-1A in co-culture. Here, we investigated the role of cobamide supplementation on the growth of *R. gnavus* within a complex microbial community. Additionally, we examined the effect of cobamide availability on the overall composition of the gut microbiota. These investigations were carried out *in vitro* using an anaerobic batch culture model inoculated with a human faecal sample from a healthy donor. The donor sample was positive for *R. gnavus* as determined by qPCR and confirmed by shotgun metagenomic sequencing where it was measured at a relative abundance of 0.2%. This is in line with previous reports of *R. gnavus* presence across ~90% of healthy individuals where it has been measured at a relative abundance of approximately 0.1% in adult faecal samples (Qin *et al.*, 2010; Kraal *et al.*, 2014). More recently *R. gnavus* was identified in 65% (39/60) of intestinal metagenomes from healthy subjects from Spain, China, Ethiopia, Sweden and USA at a mean relative abundance of 0.3% (Candeliere *et al.*, 2022). *L. reuteri* was not initially determined present due to being undetectable by qPCR, however shotgun metagenomics confirmed the presence of *L. reuteri* making up 0.00008% of the microbial population in line with previous reports documenting *L. reuteri* at low abundance in the human gut (Walter, 2008b; Ghosh, Arnoux and O'Toole, 2020).

The batch fermentation model used in this work primarily represents the microbiota of the distal colon and rectum with reduced representation of the small intestine and the upper colon (Mukhopadhya *et al.*, 2022).

At the phylum level, the faecal microbiota composition of the donor consisted of 67% *Bacillota*, 17% *Bacteroidata,* 5% *Actinomycetota* and 1% *Pseudomonadota*. This result was consistent with the gut microbiota composition of a human adult being dominated by *Bacillota, Bacteroidata, Actinomycetota,* and *Pseudomonadota,* with *Bacillota* and *Bacteroidata* comprising 90% of the gut microbiota (Arumugam *et al.*, 2011). At the genus level, *Roseburia* was shown to be the most abundant taxa with species of this genera being predominant in the *Bacillota* phylum (Madhogaria, Bhowmik and Kundu, 2022). *Roseburia* spp. are considered beneficial due to their SCFA-producing capacity and their anti-inflammatory properties (Patterson *et al.*, 2017; Tamanai-Shacoori *et al.*, 2017; Luo *et al.*, 2019; Nie *et al.*, 2021). *Streptococcus* was the second most abundant genus, also a dominant member of the *Bacillota* phylum (Madhogaria, Bhowmik and Kundu, 2022), along with *Limosilactobacillus* and *Eubacterium*, both within the top 10 most dominant genera. *Bacteroides* and *Escherichia* were consistently among the top 10 most dominant genera observed. These genera are predominant members of the *Bacteroidota* and *Pseudomonadota* phyla, respectively (Madhogaria, Bhowmik and Kundu, 2022).

At the genus level, *Escherichia, Roseburia, Limosilactobacillus, Streptococcus, Enterococcus, Bacteroides, Enterobacter, Citrobacter, Eubacterium* and *Holdemanella* were amongst the most dominant genera in supplemented cultures and in the control. *Escherichia* spp. including *E. coli* have been predicted as cobamide precursor salvagers in addition to *Roseburia intestinalis* strain L1-82 (Shelton *et al.*, 2018). *Roseburia faecis* M27, *Citrobacter farmer* GTC 1319 have both been predicted as likely cobamide producers, whilst *Streptococcus* spp. and *Eubacterium ventriosum* ATCC 27560 were predicted as likely non cobamide producers. Most *Enterobacter* and *Enterococcus* spp. have been predicted as likely non-producers, including *Enterobacter hormaechei* CCBH10892 and *Enterococcus faecalis* B4638 (Shelton *et al.*, 2018).

At 4 h, *Escherichia* became the most abundant genus at the expense of *Roseburia*, and *E. coli* was the most abundant species at the expense of *Streptococcus*

thermophilus in all treated cultures and in the control. *E. coli* strains can be commensal, providing resistance against pathogens, or pathogenic, causing disease (Salyers, 1994). Although some studies indicate a high abundance of *E. coli* in human faeces (Martinson *et al.*, 2019), others suggest it is relatively low within the gut microbiota (W. Zhang *et al.*, 2019). Recently, whole-genome shotgun metagenomic sequencing revealed that *E. coli* typically exists at low abundance (average abundance 1.21%) in the human gut but can undergo short-term blooms, with temporary spikes in abundance reaching up to 50.91% (Han *et al.*, 2024). These blooms can result in "latent infections" of non-pathogenic strains in healthy individuals, while also posing a potential risk for the introduction of pathogenic strains (Han *et al.*, 2024).

Altogether, these data reflect the typical composition of a "healthy" adult gut environment, comprising a mix of cobamide users and producers. This provides a robust foundation for investigating the effects of cobamide availability on complex microbial communities.

Upon investigation of the effect of cobamide availability on *R. gnavus* in the form of CNPsCbl it was observed that *R. gnavus* growth was most enhanced in the presence of high dose of CNPsCbl, compared to all other conditions tested. This growth was sustained for up to 8 h, whilst in the control or in the presence of low dose of CNPsCbl or *L. reuteri* MM4-1A, *R. gnavus* growth was only sustained for up to 4 h with no enhancement of growth. These results demonstrate that high dose of CNPsCbl enhances and supports *R. gnavus* growth in the context of a microbial community. The cobamide precursor PBG was also able to sustain *R. gnavus* for up to 8 h, which would suggest the ability of *R. gnavus* to salvage the precursor for cobamide production within a microbial community. This is in line with our *in silico* analysis showing the presence of a partial cobamide biosynthetic pathway across 94% (152/161) of *R. gnavus* strains, allowing for the potential synthesis of a cobamide from PBG, although we could not demonstrate this in mono-cultures (Chapter 4, section 4.2.1).

Overall, cobamide availability did not affect the overall faecal microbiota composition, as shown by measures of alpha or beta diversity compared to the control. However, specific changes were observed at the species level. In batch cultures, the inoculation of PsCbl-producing *L. reuteri* MM4-1A significantly

enhanced the abundance of *L. reuteri* and *L. pontis.* Interestingly, this response was also observed with the inoculation of non-PsCbl-producing *L. reuteri* L16001. This observation is likely due to the inoculated *Limosilactobacillus* species modifying the culture environment in ways that are favourable to the colonisation of *Limosilactobacillus* species. These modifications could include alterations in pH, production of growth-promoting metabolites, or competitive interactions that suppress other microbial groups, thereby creating a more conducive environment for the proliferation of *L. reuteri* and *L. pontis*. Overall, these results indicate that cobamide supplementation had no effect on changes in microbiota composition.

Our results are in line with previous *in vitro* and *in vivo* studies investigating the effect of cobamide availability on gut microbiota composition. Sharma *et al.* (2019) reported no significant impact adenosylcobalamin at normal (2500 ng/mL) or high (75000 ng/mL) concentrations on the abundance of auxotrophic species in both humanised gnotobiotic mice and *in vitro* anaerobic human faecal cultures. Similarly, Kelly *et al.* (2019) reported no major changes in the faecal microbiome of mice supplemented with 3.94 µg/mL of CNCbl, a dose equivalent to a 5 mg supplement administered to adult humans.

Lurz *et al.* (2020) also observed no distinct alterations in the murine gut microbiota when healthy mice were provided a low dose (50 mg/kg) or high dose (200 mg/kg) of CNCbl, compared to healthy mice on a CNCbl-deficient diet. However, within this same study, mouse models with dextran sodium sulphate (DSS)-induced colitis exhibited significant changes in gut microbial composition upon CNCbl supplementation or when on a CNCbl-deficient diet whilst upon receiving adequate levels of CNCbl from the diet, no microbial alternations were observed (Lurz *et al.*, 2020). These findings indicate a selective effect of cobamides on the intestinal microbial community dependent on disease status.

More recently, Kundra *et al.* (2022) reported that high (2500 mg/mL) and normal (5 mg/mL) CNCbl doses did not affect total bacterial growth, community richness, diversity, or total metabolite production in an anaerobic batch culture model seeded with faecal samples from healthy donors, compared to a low vitB12 control. Kundra *et al.*, (2022) concluded that in homeostatic conditions, the human adult gut microbiota produces sufficient levels of cobamides and, as a result, exogenous cobamide supplementation has limited impact on the composition and function of

gut microbial communities from healthy individuals. This is to put in the context of comparative genomic analyses which predicted that approximately 57% of *Actinomycetota*, 45% of *Pseudomonadota*, and 30% of *Bacillota* could be *de novo* cobamide producers with the presence of a complete cobamide biosynthetic pathway. In contrast only 0.6% of *Bacteroidata* were predicted to be *de novo* cobamide producers. *Bacteroidata* were predicted to have the highest proportion of species capable of salvaging cobamide precursors through a partial cobamide biosynthesis pathway, additionally a large proportion of precursor salvagers belonged to the *Bacillota* phylum (Shelton *et al.*, 2018).

It is important to note that the findings of prior studies investigating the effects of cobamides on the human gut microbiota have been highly varied. A recent systematic review, which included 22 studies on the effects of cobamides on the gut microbiome (comprising 3 in vitro studies, 8 animal studies, and 11 human observational studies), highlighted significant heterogeneity in current findings. Some studies reported significant shifts in both alpha and beta diversity, as well as taxonomic alterations in response to cobamide availability. *In vitro,* Zheng *et al.*, (2021) found that low-dose CNCbl-enriched spinach (0.78 µg/g) increased alpha diversity, while high-dose CNCbl-enriched spinach (0.94 µg/g) significantly decreased it, with no changes observed in the control group. PCA plots showed distinct clustering of both low and high-dose groups away from the control, indicating shifts in microbial community composition due to CNCbl supplementation. Additionally, the relative abundance of Bacteroidetes increased more in the low-dose group compared to the high-dose group. In mouse models, Zhu *et al.*, (2019) demonstrated that CNCbl and MeCbl supplementation reduced alpha diversity compared to untreated controls, though statistical significance was not reported. Additionally at the phylum level, CNCbl supplementation increased the relative abundances of Bacteroidetes and Proteobacteria and decreased Firmicutes compared to MeCbl supplementation. In humans, Carrothers *et al.*, (2015) demonstrated in a cohort of lactating women, that alpha diversity was significantly higher with vitamin B12 intake of 3.0–6.3 µg/day compared to lower and higher intake ranges, suggesting a dose effect. Similarly, Gurwara *et al.*, (2019) showed that men aged 50-75 years with higher dietary vitamin B12 intake showed increased alpha diversity based on the Shannon index.

Guetterman et al. (2022) highlighted that this lack of consistency across current findings may be attributed to several factors. Methodological differences, such as variations in study design, sample sizes, and analytical techniques. Additionally, the forms and doses of cobamides used in these studies vary widely. Different cobamide analogues, such as methylcobalamin and cyanocobalamin, have been shown to elicit distinct biological effects on the gut microbiota (Kundra *et al.*, 2024).

In relation to the findings of this work and previous studies reporting similar findings, the observed stability in gut microbiota composition upon cobamide supplementation under the conditions tested indicates a non-linear relationship between cobamide availability and microbial growth i.e. beyond a certain threshold, additional cobamide supplementation does not significantly impact microbial composition. However further investigation into the potential differential effects of other cobamide analogues on microbial composition is required.

Metabolically, acetate, propionate and butyrate are the major SCFAs in the human gut accounting for over 95% of all SCFAs in the gut. In a healthy adult gut acetate, propionate and butyrate are found in a ratio of approximately 3:1:1 (Cummings *et al.*, 1987). Lactate and isobutyrate concentrations in the healthy adult are typically low, relative to the proportion of acetate, propionate and butyrate, with lactate sometimes undetectable in faecal samples (Cummings *et al.*, 1987; Duncan *et al.*, 2007; Rios-Covian *et al.*, 2020). Lactate does not usually accumulate in the healthy human gut, with elevated levels of lactate often linked to dysbiosis (Duncan *et al.*, 2007), rapid fermentation by lactate-producing bacteria (Louis *et al.*, 2022) or reduced abundance of lactate-utilising bacteria (Wang *et al.*, 2020). In this work, the SCFA profile of the donor showed that acetate was the most abundant SCFA, followed by lactate, butyrate, propionate, and with isobutyrate being the least abundant. Prior to culturing, *Streptococcus thermophilus* was the most dominant species in the donor faecal sample. *S. thermophilus* is a lactic acid bacterium commonly used in the production of fermented dairy products such as yogurt and cheese (Ren, Liu and Zhang, 2015; Linares *et al.*, 2016; Dan *et al.*, 2018). During fermentation, *S. thermophilus* metabolises lactose primarily into lactate through the process of lactic acid fermentation (Han *et al.*, 2022). *E. faecalis*, *E. hormaechei*, and *E. coli* also among the dominant taxa, are known lactate producers (Liu *et al.*, 2011; Subramanian, Talluri and Christopher, 2015; Kumar, Agyeman-Duah and Ujor,

2023). *R. intestinalis* also observed as a dominant species has been shown to be unable to utilise lactate (Duncan, Louis and Flint, 2004). The presence of dominant lactate producers such as *S. thermophilus*, *E. faecalis*, *E. hormaechei*, and E. coli aligns with the higher lactate levels detected in the SCFA profile.

Cobamide supplementation did not significantly affect individual or total SCFA production compared to the control at 4 h. However, at 8 h, lactate production significantly increased in the presence of PsCbl-producing *L. reuteri* MM4-1A, PBG, and at both low and high doses of CNPsCbl with high CNPsCbl dose resulting in most enhanced lactate production. Microbial composition analyses revealed that cobamide availability did not alter the overall composition of the microbiota. This suggests that CNPsCbl may enhance lactate production by promoting a more efficient conversion of substrates into lactate. In line with the findings of this work, Kundra *et al.* (2024) reported a significant increase in lactate production by *Bacteroides thetaiotaomicron in vitro* when cultured in anaerobic gut basal medium in response to both high (200 µg/L) and low (10 µg/L) doses of CNCbl supplementation as well as in response to pseudocobalamin (PsCbl) derived from *Blautia hydrogenotrophica*, *Blautia producta* and *Marvinbryantia formatexigens* at concentrations of 44.2, 75.1, and 65.3 ng/mL respectively. In contrast, supplementation with adenosylcobalamin (AdoCbl) and hydroxycobalamin (OHCbl) at both high (200 µg/L) and low (10 µg/L) doses resulted in considerably lower lactate production (Kundra *et al.*, 2024). This demonstrates that different cobamide analogues can differentially impact lactate production by gut commensals. The findings suggest that while CNCbl and PsCbl promotelactate production under specific conditions, AdoCbl and OHCbl do not have the same effect, indicating a unique metabolic response to different forms of cobamides among members of the gut microbiota. However, further investigation in the differential effects of varying cobamide forms is necessary to establish these relationships before definitive conclusions can be made.

Total SCFA levels were significantly higher in all treated conditions compared to the control at 4 and 8 h, likely driven by lactate accumulation, which was the most abundant SCFA at 8 h. This sustained elevation of lactate is likely due to the sustained dominance of lactate-producing bacteria and non-lactate utilising bacteria observed over the 8 h incubation period. In a batch culture model, lactate

accumulation could also be a result of a low pH in the culture medium (Wang *et al.*, 2020). The initial pH of the batch culture medium was 6.5, but pH was not controlled during incubation. Therefore, a likely decrease in pH over time could also have contributed to the observed lactate accumulation (Wang *et al.*, 2020). Future work should focus on controlling and monitoring pH levels during incubation to better understand its impact on SCFA production and microbial dynamics.

Altogether, this study demonstrated that, at high doses, CNPsCbl is able to improve *R. gnavus* expansion within the context of a microbial community, in line with *in vitro* monocultures. Moreover, this study corroborates previous research that demonstrated that, in the context of a healthy human adult gut microbiome, cobamide supplementation exerts limited effects on overall microbial structure and function. However further work is required to determine the potential differential effects of different cobamide analogues on members of the human gut microbiota.

Chapter 6

Conclusions and Future perspectives

6.1. Overview

R. gnavus is an early coloniser of the human gut, persisting throughout adulthood where it is present in approximately 90% of individuals (Henke *et al.*, 2019). Its prevalence in the gut is facilitated by diverse strategies, including bacteriocin production and carbohydrate metabolism, enabling it to thrive in the competitive and dynamic environment of the human gut where it influences host metabolic processes as reviewed by Crost *et al.*, (2023). In early life, *R. gnavus* plays a prominent role by metabolising human milk oligosaccharides (HMOs) and mucin glycans, supporting gut colonisation and maturation, and is associated with normative weight gain and gut development in infants (Subramanian *et al.*, 2014; Mennella *et al.*, 2022). In adulthood, it contributes to gut health by producing SCFAs like acetate, crucial for gut homeostasis (Roblin *et al.*, 2021). Despite its role in a healthy gut microbiota, *R. gnavus* shows disproportionate representation in disorders such as IBD (Hall *et al.*, 2017; Henke *et al.*, 2019; Wu *et al.*, 2024), metabolic diseases (Blanton *et al.*, 2016; Azzouz *et al.*, 2019; Y. Zhang *et al.*, 2019; Mineharu *et al.*, 2022; Yan *et al.*, 2022), and neurological disorders (Wan *et al.*, 2020; Nishiwaki, Ito, *et al.*, 2022; Nishiwaki, Ueyama, *et al.*, 2022), with strain-specific differences contributing to its varied roles in health and disease. This underscores the importance of targeting and modulating *R. gnavus* to promote gut health and prevent disease. *In vitro* transcription studies suggested that *R. gnavus* can utilise cobamide when in co-culture with *R. bromii* L2-63 (Crost *et al.*, 2018). Cobamides are shared resources in the gut microbiota, and have been suggested to act as modulators due to their roles in microbial metabolic pathways, limited production among prokaryotes, and structurally diverse forms accessible to different microbes (Degnan, Taga and Goodman, 2014). Genomic analyses revealed that a significant proportion of human gut microbial species encode cobamide-dependent genes, with less than 40% of them having the genetic machinery to synthesise cobamides *de novo*, suggesting widespread sharing of cobamides within the gut (Degnan *et al.*, 2014; Shelton *et al.*, 2018). *Lactobacillus reuteri* is an example of a cobamide-synthesising organism, as first shown in *L. reuteri* CRL1098 (Taranto *et al.*, 2003), a strain isolated from sourdough, producing pseudocobalamin (PsCbl) (Santos *et al.*, 2007), a vitamin B12-like compound. This cobamide capacity has since been demonstrated in *L. reuteri* DSM 20016 (Sriramulu *et al.*, 2008) and

JCM1112 (Santos, Wegkamp, *et al.*, 2008) strains, both isolated from the human gut.

In this work, we aimed to gain mechanistic insights into the cobamide trophic interactions between *L. reuteri* and *R. gnavus* strains. To address this aim, we used a combination of *in silico* and *in vitro* approaches focused on cobamide production and metabolism by *L. reuteri* and *R. gnavus* strains. Following *in silico* identification of cobamide-producing *L. reuteri* strains and cobamide-utilising and partial cobamide-synthesising *R. gnavus* strains, we performed targeted growth assays, metabolomics and transcriptomics analyses to determine the pathways involved in *R. gnavus* ATCC 29149 capacity to utilise, cyanopseudocobalamin (CNPsCbl), the cobamide precursor porphobilinogen (PBG) or PsCbl produced by *L. reuteri* MM4-1A. Finally, an *in vitro* batch fermentation model of the human gut microbiota was used to investigate the impact of cobamide supplementation and PsCbl-producing *L. reuteri* MM4-1A on *R. gnavus* fitness within a complex microbial community and on the overall gut microbial structure and function. The key findings of this thesis and future directions are outlined in the next sections.

6.2 *R. gnavus* strains utilise exogenously provided CNPsCbl and *L. reuteri* derived PsCbl for enhanced growth

The *in silico* analysis of all publicly available *R. gnavus* genomes outlined in Chapter 4, predicted that 98% (159 out of 162 strains) of *R. gnavus* strains possess the capacity to utilise cobamides (Chapter 4, section 4.2.1.1). This prediction was based on the conservation of genes encoding cobalamin-dependent proteins across the genomes of all strains analysed, including *MetH* (encoding cobamide-dependent methionine synthase), *MetH2* (encoding a cobamide-dependent methionine synthase subunit), *MtaB* (encoding a methanol M methyltransferase), *dhaBCE* (encoding the glycerol dehydratase complex), *pduCDE* (encoding the propanediol dehydratase complex), and two cobalamin-dependent radical SAM proteins encoded by *RGna_03200* and *RGna_12670* (Chapter 4, section 4.2.1.1). Growth assays in methionine deficient media confirmed that *R. gnavus* strains ATCC 29149, ATCC 35913, E1, CC55_001C, 2_1_58FAA, and Finegold could utilise cobamide analogues (adenosylcobalamin (AdoCbl), methylcobalamin (MeCbl),

hydroxycobalamin (OHCbl) and cyanocobalamin (CNCbl)) and cobamide derivatives (PsCbl, vitB12-Factor III, vitB12-Factor IIIm, vitamin B12-5MB, and vitB12-Factor A) supporting the bioinformatic predictions (Chapter 4, section 4.2.2 and Supplementary Figures 2 and 3).

In the presence of CNPsCbl, *R. gnavus* exhibited upregulation of genes involved in cobamide-dependent pathways, indicating efficient utilisation of CNPsCbl for its metabolic processes. This was observed under both methionine-deficient and methionine-supplemented conditions. However, the degree of upregulation of cobamide-dependent genes was notably lower upon methionine supplementation. This suggests that when methionine is present in sufficient amounts, the requirement for cobamides to perform cobamide-dependent reactions diminishes. This reduced reliance on cobamides in the presence of methionine highlights the adaptability of *R. gnavus* in optimising its metabolic functions based on nutrient availability in its environment (Chapter 4, section 4.2.3.3).

The results of the comparative genomic analysis, presented in Chapter 3 revealed that approximately 50% (191 out of 381) of *L. reuteri* strains, including CRL1098, JCM 1112, and DSM 20016, previously reported for cobamide synthesis (Santos *et al.*, 2007; Morita *et al.*, 2008; Sriramulu *et al.*, 2008), exhibited the genetic capacity for *de novo* cobamide synthesis with the presence of *cbiABCDETFGHJ, cobA/hemD, cbiKLMNQOP, CysG, hemACBL, cobUSC hemD, cobT, cobI, cobL, cobM, cobJ, cobB, cobD, GltX and FldA* (Chapter 3, section 3.2.1). Through use of UPLC-MS/MS and cobamide bioassays, it was confirmed that PsCbl is synthesised intracellularly in *L. reuteri* strains DSM 20016, MM4-1A, 20-2, and ATCC 53608, with extracellularly PsCbl production only detected in *L. reuteri* MM4-1A (Chapter 3, section 3.2.2).

In vitro co-culture assays showed that *R. gnavus* ATCC 29149 growth was enhanced in the presence of PsCbl-producing *L. reuteri* MM4-1A compared to growth in monoculture, indicative of cross-feeding (Chapter 4, section 4.2.3.4).

The results from transcriptomic analyses supported PsCbl cross-feeding between *R. gnavus* and *L. reuteri* with the upregulation of genes encoding cobamide-dependent proteins in *R. gnavus* when grown in co-culture with *L. reuteri* MM4-1A (Chapter 4, section 4.2.3.3 and 4.2.3.4). Cobamide utilisation was also

demonstrated in the context of a microbial community with *R. gnavus* growth enhanced and sustained for up to 8 h upon high dose CNPsCbl supplementation in human faecal batch cultures, while in control, low-dose CNPsCbl, or PsCbl-producing *L. reuteri* MM4-1A conditions, *R. gnavus* growth was only sustained for up to 4 h (Chapter 5, section 5.2.1).

The cobamide uptake system of *R. gnavus* is currently not known, however our transcriptomic analyses of *R. gnavus* ATCC 29149 in mono and co-cultures with *L. reuteri* MM4-1A highlighted significant changes in the *R. gnavus* transcriptome upon cobamide availability including the upregulation of an energy coupling factor (ECF) transporter S component, RGna_RS14310, upon CNPsCbl supplementation (Chapter 4, section 4.2.3.3) and in the presence of PsCbl-producing *L. reuteri* MM4-1A (Chapter 4, section 4.2.3.4). The ECF transporter S component, RGna_RS14310, was identified as being uncharacterised in terms of substrate specificity, however this family of transmembrane proteins has been shown to be involved in the uptake of vitamins in Gram-negative prokaryotes (Rodionov *et al.*, 2009). More specifically, in the Gram negative *Lactobacillus delbrueckii*, the S component CbrT has been identified as being cobamide-specific (Rodionov *et al.*, 2009). Further characterisation of the ligand specificity of this transporter to cobamides will help elucidate the molecular pathways by which *R. gnavus* takes up cobamides from its environment.

In addition, fluorescently labelled cobamide analogues could be used to further study the mechanisms underpinning the uptake, transport, and localisation of cobamides within *R. gnavus* cells. The use of fluorescent cobamide analogues and precursors for monitoring their uptake and distribution in bacteria has previously been demonstrated in *E. coli* and *Mycobacterium tuberculosis* (Lawrence et al., 2018). This approach could significantly enhance our understanding of *R. gnavus* cobamide trafficking and metabolism at a cellular level.

The results of this work provide strong indications of cobamide cross-feeding between *L. reuteri* and *R. gnavus* however further work is required to directly monitor *L. reuteri*-derived PsCbl uptake by *R. gnavus.* An approach for investigating this would involve the use of fluorescently labelled cyanocobalamin (Cy5-CNCbl) in a competition assay. This approach would allow fluorescence intensity to be monitored over time in *R. gnavus* monocultures supplemented with Cy5-CNCbl

which could then be compared to the fluorescence intensity in *R. gnavus* co-cultures with PsCbl-producing *L. reuteri* MM4-1A, also supplemented with Cy5-CNCbl. When the native PsCbl from *L. reuteri* MM4-1A is taken up by *R. gnavus*, the fluorescence intensity in *R. gnavus* cells in co-culture should become reduced compared to that in monoculture, providing strong evidence of PsCbl cross-feeding. However, *Lactobacillus* species are able to uptake cobamides through use of a cobamide-specific ECF-type ABC transporter (ECF-CbrT) (Santos *et al.*, 2018). The ability of *L. reuteri* MM4-1A to also uptake Cy5-CNCbl would interfere with the ability to accurately assess PsCbl uptake by *R. gnavus*, thus preventing a clear demonstration of PsCbl cross-feeding using this method. Taking this into consideration future work would require the development of an ECF-CbrT *L. reuteri* MM4-1A mutant preventing the uptake of Cy5-CNCbl by *L. reuteri* MM4-1A and allowing for a more accurate assessment of PsCbl uptake by *R. gnavus* in co-cultures.

6.3 *R. gnavus* strains possess a partial cobamide biosynthetic pathway allowing metabolism of cobamide precursor PBG under methionine-supplemented conditions and in faecal batch cultures

R. gnavus CC55_001C has previously been identified as a tetrapyrrole precursor salvager (Shelton *et al.*, 2018). Our comparative genomic analyses of publicly available genome-sequenced *R. gnavus* strains revealed a partial cobamide biosynthesis pathway across 94% (152 out of 162 strains) of *R. gnavus* strains analysed, potentially allowing for cobamide synthesis from cobamide precursor porphobilinogen (PBG) (Chapter 4, section 4.2.1.2). This was supported by the absence of genes encoding proteins required for the *de novo* synthesis of PBG, specifically *HemA, HemL,* and *HemB* while genes encoding proteins for the subsequent conversion of PBG to a complete cobamide compound were present, starting from *HemC* (see Chapter 1 Figure 10 for the cobamide biosynthesis pathway). *HemC* encodes PBG deaminase, which catalyses the conversion of PBG into hydroxymethylbilane (Warren *et al.*, 2002). Hydroxymethylbilane is further converted into uroporphyrinogen III, the first macrocyclic intermediate in cobamide biosynthesis (Warren *et al.*, 2002).

Here, we observed that under methionine-supplemented conditions and in the presence of PBG, *R. gnavus* demonstrated indications of PBG metabolism during

late exponential growth phase (Chapter 4, section 4.2.3.5). This was evidenced by the upregulation of cobamide biosynthetic genes during the late exponential growth phase. It is likely that this metabolism of PBG observed exclusively in the presence of Met is due to the requirement of Met in the biosynthesis of cobamides, with approximately 8 methylation reactions occurring during the *de novo* synthesis of cobamides (Warren and Escalante-Semerena, 2008). However, overall, PBG inhibited the expression of cobamide biosynthesis genes under methionine-deficient conditions, suggesting a limited capacity for *R. gnavus* to synthesise cobamides from PBG alone without additional metabolic support (Chapter 4, section 4.2.3.5).

Furthermore, in faecal batch cultures, the supplementation of PBG resulted in enhanced and prolonged growth of *R. gnavus*, suggesting active PBG metabolism (Chapter 5, section 5.2.1). This is likely due to the availability of a diverse range of cobamide lower ligands in the faecal environment which *R. gnavus* can use for synthesis of a wide variety of cobamide analogues for supported growth. This potential adaptability of *R. gnavus* in utilising available precursors in its environment would contribute to its persistence and proliferation in the gut microbiota. *R. gnavus*

The development of a *HemC R. gnavus* mutant could be used to confirm PBG salvaging for cobamide production by *R. gnavus*. *HemC* encodes PBG deaminase involved in the synthesis of uroporphyrinogen III (an intermediate in the synthesis of cobamides) from PBG (see Chapter 1 Figure 10 for cobamide biosynthesis pathway). It is expected that a *HemC R. gnavus* mutant would be unable to fulfil downstream cobamide biosynthesis from PBG. The inability of a *HemC R. gnavus* mutant to enhance and sustain *R. gnavus* growth *in vitro* as observed with native *R. gnavus* strains in the presence of PBG and Met would confirm *R. gnavus* as a tetrapyrrole precursor salvager, specifically, able to salvage PBG for cobamide production.

The development of fluorescently labelled cobamide precursors described above would facilitate the study of cobamide salvaging mechanisms in *R. gnavus* inform on potential strategies for modulating the growth of *R. gnavus* within the gut microbiota.

6.4 Cobamide supplementation does not significantly impact gut microbiota composition but alters SCFA profiles

Here, cobamide supplementation, at high-dose of CNPsCbl, low-dose of CNPsCbl, through PsCbl-producing *L. reuteri* MM4-1A, or in the presence of the cobamide precursor PBG did not significantly alter the overall composition of the gut microbiota (Chapter 5, section 5.2.1). Measures of alpha and beta diversity showed no significant differences between treated and control groups, additionally there were no significant taxonomic changes over time indicating stability in microbial composition in response to cobamide supplementation (Chapter 5, section 5.2.1). These findings were in line with *in vitro* fermentation systems and animal models showing that cobamide supplementation has no effect on overall microbial composition (Kelly *et al.*, 2019; Sharma *et al.*, 2019; Lurz *et al.*, 2020; Kundra *et al.*, 2022). Additionally, observational studies conducted in humans have also shown no significant changes in alpha diversity or beta diversity in response to cobamide availability (Boran *et al.*, 2020; Herman *et al.*, 2020).

However, to date, the findings from *in vitro* studies, animal studies, and observational human studies investigating the effects of cobamides on the human gut microbiota remain heterogeneous (Guetterman *et al.*, 2022). Some studies have reported significant shifts in both alpha and beta diversity as well as taxonomic alterations in response to cobamide supplementation (Carrothers *et al.*, 2015; Xu *et al.*, 2018; Gurwara *et al.*, 2019; Park, Kang and Sol Kim, 2019; Zhu *et al.*, 2019; Zheng *et al.*, 2021).
These variations in cobamide response may also be due to varying effects elicited by different cobamide forms or to differences in methodological approaches, as recently reviewed by Guetterman *et al.*, (2022). This review also highlighted that there is currently a lack of observational studies and no randomised controlled trials conducted to investigate the effects of cobamides on the human gut microbiome, limiting our current understanding (Guetterman *et al.*, 2022).

To address some of these discrepancies, future work should involve testing a range of cobamide analogues in human faecal batch cultures to better understand the specific impacts of each form on the gut microbiome. This approach will help clarify

the role of cobamides in modulating gut microbial communities and their potential therapeutic applications.

Here, we showed that high dose of CNPsCbl resulted in significantly elevated lactate levels compared to the lower concentrations observed with a lower dose (Chapter 5, section 5.2.2). Since cobamide availability had no significant effect on the gut microbiome composition, these results suggest that CNPsCbl may enhance lactate production by facilitating a more efficient conversion of substrates into lactate by specific bacteria rather than a change in bacteria abundance. A recent study showed that when cultured in anaerobic gut basal medium with high or low doses of CNCbl or with microbially derived PsCbl, *Bacteroides thetaiotaomicron* demonstrates significantly increased production of lactate (Kundra *et al.*, 2024). Conversely, supplementation with high and low doses of AdoCbl and OHCbl resulted in substantially lower lactate production (Kundra *et al.*, 2024), indicative of a unique metabolic response elicited by CNCbl and PsCbl. Future work would require metabolic profiling and transcriptomic analyses to identify the specific pathways and regulatory mechanisms involved upon supplementation of cobamide analogues in human faecal batch cultures.

6.5 Concluding remarks and limitations

In summary, we showed that the ability of *R. gnavus* to utilise cobamides, particularly through cross-feeding with PsCbl-producing *L. reuteri*, underscores the importance of microbial interdependencies for nutrient acquisition and metabolic function. Despite the observed stability in microbial community composition, the enhanced growth of *R. gnavus* in response to cobamide availability highlights the potential for targeted dietary interventions to modulate specific microbial populations for improved gut health and disease prevention. Future research should explore these interactions *in vivo* to better understand their implications in health and disease. Indeed, while *in vitro* approaches provide valuable mechanistic insights into the molecular pathways underpinning cobamide synthesis and utilisation by gut bacteria, they come with physiological limitations when used alone to draw conclusions on factors influencing the human gut microbiota (Isenring *et al.*, 2023). Investigating microbial interactions *in vivo* such as in humanised animal

models provides controlled and physiologically representative conditions mimicking the complexity of the human gut (Kostic, Howitt and Garrett, 2013; Hugenholtz and de Vos, 2018; Park and Im, 2020). Through use of *in vivo* approaches, we can validate the *in vitro* findings and ensure they are applicable in living organisms. Using these approaches, it will also be interesting to determine the effects of PBG, cobamides and *L. reuteri* supplementation on *R. gnavus* in models of disease to validate the therapeutic potential of PBG, cobamide and *L. reuteri* supplementation in preventing or alleviating disease, whilst informing the development of future targeted interventions. The combined use of *in vitro* and *in vivo* models to study the effect of cobamides on human gut microbiota provides a foundation for future clinical trials in humans.

References

Abdel-Rahman, L. I. H. and Morgan, X. C. (2023) 'Searching for a Consensus Among Inflammatory Bowel Disease Studies: A Systematic Meta-Analysis', *Inflammatory Bowel Diseases*. Oxford Academic, 29(1), pp. 125–139. doi: 10.1093/IBD/IZAC194.

Abdugheni, R. *et al.* (2023) 'Comparative genomics reveals extensive intra-species genetic divergence of the prevalent gut commensal Ruminococcus gnavus', *Microbial Genomics*. Microbiology Society, 9(7), p. 1071. doi: 10.1099/MGEN.0.001071.

Aggarwal, N. *et al.* (2023) 'Microbiome and Human Health: Current Understanding, Engineering, and Enabling Technologies'. doi: 10.1021/acs.chemrev.2c00431.

Ahrodia, T. *et al.* (2022) 'Structure, functions, and diversity of the healthy human microbiome', *Progress in Molecular Biology and Translational Science*. Academic Press, 191(1), pp. 53–82. doi: 10.1016/BS.PMBTS.2022.07.003.

Al-Amrah, H. *et al.* (2023) 'Composition of the gut microbiota in patients with inflammatory bowel disease in Saudi Arabia: A pilot study', *Saudi Journal of Gastroenterology : Official Journal of the Saudi Gastroenterology Association*. Wolters Kluwer -- Medknow Publications, 29(2), p. 102. doi: 10.4103/SJG.SJG_368_22.

Albenberg, L. *et al.* (2014) 'Correlation between intraluminal oxygen gradient and radial partitioning of intestinal microbiota', *Gastroenterology*. W.B. Saunders, 147(5), pp. 1055-1063.e8. doi: 10.1053/J.GASTRO.2014.07.020.

Albert, T. K. *et al.* (2010) 'Human intestinal TFF3 forms disulfide-linked heteromers with the mucus-associated FCGBP protein and is released by hydrogen sulfide', *Journal of proteome research*. J Proteome Res, 9(6), pp. 3108–3117. doi: 10.1021/PR100020C.

Allen, R. H. and Stabler, S. P. (2008) 'Identification and quantitation of cobalamin and cobalamin analogues in human feces', *American Journal of Clinical Nutrition*. American Society for Nutrition, 87(5), pp. 1324–1335. doi: 10.1093/ajcn/87.5.1324.

Altschul, S. F. *et al.* (1990) 'Basic local alignment search tool', *Journal of Molecular Biology*, 215(3), pp. 403–410. doi: 10.1016/S0022-2836(05)80360-2.

Ambort, D. *et al.* (2012) 'Perspectives on mucus properties and formation--lessons from the biochemical world', *Cold Spring Harbor perspectives in medicine*. Cold Spring Harb Perspect Med, 2(11). doi: 10.1101/CSHPERSPECT.A014159.

De Angelis, M. *et al.* (2014) 'Lactobacillus rossiae, a vitamin B12 producer, represents a metabolically versatile species within the genus lactobacillus', *PLoS ONE*. Public Library of Science, 9(9). doi: 10.1371/journal.pone.0107232.

Ankar, A. and Bhimji, S. S. (2021) 'Vitamin B12 Deficiency', *StatPearls*. StatPearls Publishing. Available at: https://www.ncbi.nlm.nih.gov/books/NBK441923/ (Accessed: 21 April 2022).

Are, A. *et al.* (2008) 'Enterococcus faecalis from newborn babies regulate endogenous PPARγ activity and IL-10 levels in colonic epithelial cells', *Proceedings of the National Academy of Sciences of the United States of America*. National Academy of Sciences, 105(6), pp. 1943–1948. doi: 10.1073/PNAS.0711734105/ASSET/FF4AA237-4776-42D2-9AFC-9EB27C95A77D/ASSETS/GRAPHIC/ZPQ0050892960004.JPEG.

Arike, L., Holmén-Larsson, J. and Hansson, G. C. (2017) 'Intestinal Muc2 mucin O-glycosylation is affected by microbiota and regulated by differential expression of glycosyltranferases', *Glycobiology*. Glycobiology, 27(4), pp. 318–328. doi: 10.1093/GLYCOB/CWW134.

Aroda, V. R. *et al.* (2016) 'Long-term Metformin Use and Vitamin B12 Deficiency in the Diabetes Prevention Program Outcomes Study', *The Journal of clinical endocrinology and metabolism*. J Clin Endocrinol Metab, 101(4), pp. 1754–1761. doi: 10.1210/JC.2015-3754.

Arumugam, M. *et al.* (2011) 'Enterotypes of the human gut microbiome', *Nature*. Nature Publishing Group, 473(7346), pp. 174–180. doi: 10.1038/nature09944.

Asnicar, F. *et al.* (2021) 'Microbiome connections with host metabolism and habitual diet from 1,098 deeply phenotyped individuals', *Nature Medicine*. Nature Research, 27(2), pp. 321–332. doi: 10.1038/S41591-020-01183-8.

Asseri, A. H. *et al.* (2023) 'The gut dysbiosis-cancer axis: illuminating novel insights and implications for clinical practice', *Frontiers in Pharmacology*. Frontiers Media SA, 14, p. 1208044. doi: 10.3389/FPHAR.2023.1208044/BIBTEX.

Avissar, Y. J., Ormerod, J. G. and Beale, S. I. (1989) 'Distribution of δ-aminolevulinic acid biosynthetic pathways among phototrophic bacterial groups', *Archives of Microbiology*. Springer-Verlag, 151(6), pp. 513–519. doi: 10.1007/BF00454867.

Azzouz, D. *et al.* (2019) 'Lupus nephritis is linked to disease-activity associated expansions and immunity to a gut commensal', *Annals of the Rheumatic Diseases*. BMJ Publishing Group, 78(7), pp. 947–956. doi: 10.1136/annrheumdis-2018-214856.

Baker, K. *et al.* (2018) 'BLASTmap: A Shiny-Based Application to Visualize BLAST Results as Interactive Heat Maps and a Tool to Design Gene-Specific Baits for Bespoke Target Enrichment Sequencing', *Methods in Molecular Biology*. Humana Press, New York, NY, 1848, pp. 199–206. doi: 10.1007/978-1-4939-8724-5_14.

Balabanova, L. *et al.* (2021) 'Microbial and Genetic Resources for Cobalamin (Vitamin B12) Biosynthesis: From Ecosystems to Industrial Biotechnology', *International Journal of Molecular Sciences 2021, Vol. 22, Page 4522*. Multidisciplinary Digital Publishing Institute, 22(9), p. 4522. doi: 10.3390/IJMS22094522.

Balty, C. *et al.* (2019) 'Ruminococcin C, an anti-clostridial sactipeptide produced by a prominent member of the human microbiota Ruminococcus gnavus', *The Journal of biological chemistry*. J Biol Chem, 294(40), pp. 14512–14525. doi: 10.1074/JBC.RA119.009416.

Banerjee, R. and Ragsdale, S. W. (2003) 'The Many Faces of Vitamin B12: Catalysis by Cobalamin-Dependent Enzymes1', *http://dx.doi.org/10.1146/annurev.biochem.72.121801.161828*. Annual Reviews 4139 El Camino Way, P.O. Box 10139, Palo Alto, CA 94303-0139, USA , 72, pp. 209–247. doi: 10.1146/ANNUREV.BIOCHEM.72.121801.161828.

Bansil, R. and Turner, B. S. (2006) 'Mucin structure, aggregation, physiological functions and biomedical applications', *Current Opinion in Colloid and Interface Science*, 11(2–3), pp. 164–170. doi: 10.1016/J.COCIS.2005.11.001.

Bartolomaeus, H. *et al.* (2019) 'Short-Chain Fatty Acid Propionate Protects From Hypertensive Cardiovascular Damage', *Circulation*. Lippincott Williams &

WilkinsHagerstown, MD, 139(11), pp. 1407–1421. doi: 10.1161/CIRCULATIONAHA.118.036652.

Basavanna, G. and Prapulla, S. G. (2013) 'Evaluation of functional aspects of Lactobacillus fermentum CFR 2195 isolated from breast fed healthy infants' fecal matter', *Journal of Food Science and Technology*. Springer, 50(2), pp. 360–366. doi: 10.1007/S13197-011-0345-9.

Battat, R. *et al.* (2014) 'Vitamin B12 deficiency in inflammatory bowel disease: prevalence, risk factors, evaluation, and management', *Inflammatory bowel diseases*. Inflamm Bowel Dis, 20(6), pp. 1120–1128. doi: 10.1097/MIB.0000000000000024.

Beam, A., Clinger, E. and Hao, L. (2021) 'Effect of Diet and Dietary Components on the Composition of the Gut Microbiota', *Nutrients*. Multidisciplinary Digital Publishing Institute (MDPI), 13(8). doi: 10.3390/NU13082795.

Bell, A. *et al.* (2019) 'Elucidation of a sialic acid metabolism pathway in mucus-foraging Ruminococcus gnavus unravels mechanisms of bacterial adaptation to the gut', *Nature microbiology*. Nat Microbiol, 4(12), pp. 2393–2404. doi: 10.1038/S41564-019-0590-7.

Bell, A. and Juge, N. (2021) 'Mucosal glycan degradation of the host by the gut microbiota', *Glycobiology*. Glycobiology, 31(6), pp. 691–696. doi: 10.1093/GLYCOB/CWAA097.

Belzer, C. *et al.* (2017) 'Microbial metabolic networks at the mucus layer lead to diet-independent butyrate and vitamin B12 production by intestinal symbionts', *mBio*. American Society for Microbiology, 8(5). doi: 10.1128/MBIO.00770-17/SUPPL_FILE/MBO004173482ST2.PDF.

Belzer, C. and De Vos, W. M. (2012) 'Microbes inside--from diversity to function: the case of Akkermansia', *The ISME journal*. ISME J, 6(8), pp. 1449–1458. doi: 10.1038/ISMEJ.2012.6.

Bennett, B. J. *et al.* (2013) 'Trimethylamine-N-oxide, a metabolite associated with atherosclerosis, exhibits complex genetic and dietary regulation', *Cell metabolism*. Cell Metab, 17(1), pp. 49–60. doi: 10.1016/J.CMET.2012.12.011.

Bennion, R. S. *et al.* (1990) 'The bacteriology of gangrenous and perforated appendicitis--revisited.', *Annals of Surgery*. Lippincott, Williams, and Wilkins, 211(2), p. 165. doi: 10.1097/00000658-199002000-00008.

Bergstrom, K. S. B. and Xia, L. (2013) 'Mucin-type O-glycans and their roles in intestinal homeostasis', *Glycobiology*, 23(9), pp. 1026–1037. doi: 10.1093/glycob/cwt045.

Bergstrom, K. and Xia, L. (2022) 'The barrier and beyond: Roles of intestinal mucus and mucin-type O-glycosylation in resistance and tolerance defense strategies guiding host-microbe symbiosis'. doi: 10.1080/19490976.2022.2052699.

Berkhout, M. D., Plugge, C. M. and Belzer, C. (2022) 'How microbial glycosyl hydrolase activity in the gut mucosa initiates microbial cross-feeding', *Glycobiology*. Glycobiology, 32(3), pp. 182–200. doi: 10.1093/GLYCOB/CWAB105.

Berry, S. E. *et al.* (2020) 'Human postprandial responses to food and potential for precision nutrition', *Nature Medicine*. Nature Research, 26(6), pp. 964–973. doi: 10.1038/S41591-020-0934-0.

Berry, S., Spector, T. and Wolf, J. (2023) *Whitepaper: The PREDICT program*. Available at: https://zoe.com/whitepapers/the-predict-program (Accessed: 21 June 2024).

Bertani, G. (1951) 'STUDIES ON LYSOGENESIS I.', *Journal of Bacteriology*, 62(3).

Bicknell, B. *et al.* (2023) 'Neurodegenerative and Neurodevelopmental Diseases and the Gut-Brain Axis: The Potential of Therapeutic Targeting of the Microbiome', *International Journal of Molecular Sciences 2023, Vol. 24, Page 9577*. Multidisciplinary Digital Publishing Institute, 24(11), p. 9577. doi: 10.3390/IJMS24119577.

Bito, T. *et al.* (2020) 'Biological Activity of Pseudovitamin B12 on Cobalamin-Dependent Methylmalonyl-CoA Mutase and Methionine Synthase in Mammalian Cultured COS-7 Cells', *Molecules 2020, Vol. 25, Page 3268*. Multidisciplinary Digital Publishing Institute, 25(14), p. 3268. doi: 10.3390/MOLECULES25143268.

Bjørke-Monsen, A. L. *et al.* (2008) 'Common Metabolic Profile in Infants Indicating Impaired Cobalamin Status Responds to Cobalamin Supplementation', *Pediatrics*. American Academy of Pediatrics, 122(1), pp. 83–91. doi: 10.1542/PEDS.2007-2716.

Blanton, L. V *et al.* (2016) 'Gut bacteria that rescue growth impairments transmitted by immature microbiota from undernourished children', *Science*, 351(6275), pp. 1–18. doi: 10.1126/science.aad3311.Gut.

Bloom, S. M. *et al.* (2011) 'Commensal Bacteroides species induce colitis in host-genotype-specific fashion in a mouse model of inflammatory bowel disease', *Cell Host and Microbe*, 9(5), pp. 390–403. doi: 10.1016/j.chom.2011.04.009.

Bobik, T. A. *et al.* (1999) 'The propanediol utilization (pdu) operon of Salmonella enterica serovar Typhimurium LT2 includes genes necessary for formation of polyhedral organelles involved in coenzyme B12-dependent 1,2-propanediol degradation', *Journal of Bacteriology*. American Society for Microbiology, 181(19), pp. 5967–5975. doi: 10.1128/jb.181.19.5967-5975.1999.

Boran, P. *et al.* (2020) 'The impact of vitamin B12 deficiency on infant gut microbiota', *European Journal of Pediatrics*. Springer, 179(3), pp. 385–393. doi: 10.1007/S00431-019-03517-2/FIGURES/7.

Bousbaine, D. *et al.* (2022) 'A conserved Bacteroidetes antigen induces anti-inflammatory intestinal T lymphocytes', *Science (New York, N.Y.)*. Science, 377(6606), pp. 660–666. doi: 10.1126/SCIENCE.ABG5645.

Brandt, L. J., Bernstein, L. H. and Wagle, A. (1977) 'Production of vitamin B12 analogues in patients with small-bowel bacterial overgrowth', *Annals of Internal Medicine*, 87(5), pp. 546–551. doi: 10.7326/0003-4819-87-5-546.

Bridwell-Rabb, J., Grell, T. A. J. and Drennan, C. L. (2018) 'A Rich Man, Poor Man Story of S -Adenosylmethionine and Cobalamin Revisited', *Annual Review of Biochemistry*. Annual Reviews Inc., 87(Volume 87, 2018), pp. 555–584. doi: 10.1146/ANNUREV-BIOCHEM-062917-012500/CITE/REFWORKS.

Brown, J. R. M. *et al.* (2018) 'Changes in microbiota composition, bile and fatty acid metabolism, in successful faecal microbiota transplantation for Clostridioides difficile infection', *BMC Gastroenterology*. BioMed Central Ltd., 18(1), pp. 1–15. doi: 10.1186/S12876-018-0860-5/FIGURES/6.

Bruellman, R. and Llorente, C. (2021) 'A Perspective Of Intestinal Immune-Microbiome Interactions In Alcohol-Associated Liver Disease', *International Journal of Biological*

Sciences. Ivyspring International Publisher, 17(1), p. 307. doi: 10.7150/IJBS.53589.

Bullman, S. *et al.* (2017) 'Analysis of Fusobacterium persistence and antibiotic response in colorectal cancer', *Science*. American Association for the Advancement of Science, 358(6369), pp. 1443–1448. doi: 10.1126/SCIENCE.AAL5240.

Bult, C. J. *et al.* (1996) 'Complete genome sequence of the Methanogenic archaeon, Methanococcus jannaschii', *Science*. American Association for the Advancement of Science, 273(5278), pp. 1058–1073. doi: 10.1126/SCIENCE.273.5278.1058.

Caballero-Flores, G., Pickard, J. M. and Núñez, G. (2023) 'Microbiota-mediated colonization resistance: mechanisms and regulation', *Nature Reviews Microbiology*. Nature Research, 21(6), pp. 347–360. doi: 10.1038/s41579-022-00833-7.

Candeliere, F. *et al.* (2022) 'β-Glucuronidase Pattern Predicted From Gut Metagenomes Indicates Potentially Diversified Pharmacomicrobiomics', *Frontiers in Microbiology*, 13(March), pp. 1–12. doi: 10.3389/fmicb.2022.826994.

Capela, D. *et al.* (2001) 'Analysis of the chromosome sequence of the legume symbiont Sinorhizobium meliloti strain 1021', *Proceedings of the National Academy of Sciences of the United States of America*, 98(17), pp. 9877–9882. doi: 10.1073/PNAS.161294398.

Carrothers, J. M. *et al.* (2015) 'Fecal microbial community structure is stable over time and related to variation in macronutrient and micronutrient intakes in lactating women1-3', *Journal of Nutrition*. American Society for Nutrition, 145(10), pp. 2379–2388. doi: 10.3945/jn.115.211110.

Cauthen, S. E., Foster, M. A. and Woods, D. D. (1966) 'Methionine synthesis by extracts of Salmonella typhimurium', *Biochemical Journal*. Portland Press, 98(2), pp. 630–635. doi: 10.1042/BJ0980630.

Cervera-Tison, M. *et al.* (2012) 'Functional analysis of family GH36 α-galactosidases from Ruminococcus gnavus E1: Insights into the metabolism of a plant oligosaccharide by a human gut symbiont', *Applied and Environmental Microbiology*. American Society for Microbiology, 78(21), pp. 7720–7732. doi: 10.1128/AEM.01350-12/SUPPL_FILE/ZAM999103803SO8.PDF.

Chang, Y. C. *et al.* (2017) 'TLR2 and interleukin-10 are involved in Bacteroides fragilis-mediated prevention of DSS-induced colitis in gnotobiotic mice', *PLoS ONE*. Public Library of Science, 12(7). doi: 10.1371/JOURNAL.PONE.0180025.

Chen, J., Pitmon, E. and Wang, K. (2017) 'Microbiome, inflammation and colorectal cancer', *Seminars in Immunology*. Academic Press, 32, pp. 43–53. doi: 10.1016/j.smim.2017.09.006.

Chen, S. *et al.* (2018) 'fastp: an ultra-fast all-in-one FASTQ preprocessor', *Bioinformatics (Oxford, England)*. Bioinformatics, 34(17), pp. i884–i890. doi: 10.1093/BIOINFORMATICS/BTY560.

Chen, S. *et al.* (2019) 'Trimethylamine N-Oxide Binds and Activates PERK to Promote Metabolic Dysfunction', *Cell metabolism*. Cell Metab, 30(6), pp. 1141-1151.e5. doi: 10.1016/J.CMET.2019.08.021.

Cheng, C. C. *et al.* (2020) 'Ecological importance of cross-feeding of the intermediate metabolite 1,2-propanediol between bacterial gut symbionts', *Applied and Environmental Microbiology*. American Society for Microbiology, 86(11). doi:

10.1128/AEM.00190-20.

Cheng, H. and Leblond, C. P. (1974) 'Origin, differentiation and renewal of the four main epithelial cell types in the mouse small intestine I. Columnar cell', *American Journal of Anatomy*, 141(4), pp. 461–479. doi: 10.1002/AJA.1001410403.

Cheng, J. and Zhou, J. (2024) 'Unraveling the gut health puzzle: exploring the mechanisms of butyrate and the potential of High-Amylose Maize Starch Butyrate (HAMSB) in alleviating colorectal disturbances', *Frontiers in Nutrition*. Frontiers, 11, p. 1285169. doi: 10.3389/FNUT.2024.1285169.

Cheng, Y., Ling, Z. and Li, L. (2020) 'The Intestinal Microbiota and Colorectal Cancer', *Frontiers in Immunology*. Frontiers Media S.A., 11, p. 615056. doi: 10.3389/FIMMU.2020.615056/BIBTEX.

Chiumento, S. *et al.* (2019) 'Ruminococcin C, a promising antibiotic produced by a human gut symbiont', *Science advances*. Sci Adv, 5(9). doi: 10.1126/SCIADV.AAW9969.

Chrysant, S. G. and Chrysant, G. S. (2018) 'The current status of homocysteine as a risk factor for cardiovascular disease: a mini review', *Expert Review of Cardiovascular Therapy*. Taylor & Francis, 16(8), pp. 559–565. doi: 10.1080/14779072.2018.1497974.

Clairembault, T. *et al.* (2015) 'Structural alterations of the intestinal epithelial barrier in Parkinson's disease', *Acta neuropathologica communications*, 3, p. 12. doi: 10.1186/S40478-015-0196-0.

Clooney, A. G. *et al.* (2021) 'Ranking microbiome variance in inflammatory bowel disease: a large longitudinal intercontinental study', *Gut*. Gut, 70(3), pp. 499–510. doi: 10.1136/GUTJNL-2020-321106.

Colella, M. *et al.* (2023) 'Microbiota revolution: How gut microbes regulate our lives', *World Journal of Gastroenterology*. Baishideng Publishing Group Inc, 29(28), p. 4368. doi: 10.3748/WJG.V29.I28.4368.

Costa, F. G. *et al.* (2020) 'New Insights Into the Biosynthesis of Cobamides and Their Use', in *Comprehensive Natural Products III*. Elsevier, pp. 364–394. doi: 10.1016/b978-0-12-409547-2.14737-7.

Costea, P. I. *et al.* (2017) 'Enterotypes in the landscape of gut microbial community composition', *Nature Microbiology 2017 3:1*. Nature Publishing Group, 3(1), pp. 8–16. doi: 10.1038/s41564-017-0072-8.

Craciun, S. and Balskus, E. P. (2012) 'Microbial conversion of choline to trimethylamine requires a glycyl radical enzyme', *Proceedings of the National Academy of Sciences of the United States of America*. Proc Natl Acad Sci U S A, 109(52), pp. 21307–21312. doi: 10.1073/PNAS.1215689109.

Crofts, T. S. *et al.* (2013) 'Cobamide Structure Depends on Both Lower Ligand Availability and CobT Substrate Specificity', *Chemistry & Biology*. Cell Press, 20(10), pp. 1265–1274. doi: 10.1016/J.CHEMBIOL.2013.08.006.

Crost, E. H. *et al.* (2013) 'Utilisation of Mucin Glycans by the Human Gut Symbiont Ruminococcus gnavus Is Strain-Dependent', *PLoS ONE*, 8(10), p. e76341. doi: 10.1371/journal.pone.0076341.

Crost, E. H. *et al.* (2016) 'The mucin-degradation strategy of Ruminococcus gnavus:

The importance of intramolecular trans-sialidases', *Gut Microbes*. Taylor and Francis Inc., 7(4), pp. 302–312. doi: 10.1080/19490976.2016.1186334.

Crost, E. H. *et al.* (2018) 'Mechanistic Insights Into the Cross-Feeding of Ruminococcus gnavus and Ruminococcus bromii on Host and Dietary Carbohydrates', *Frontiers in Microbiology*. Frontiers Media S.A., 9(NOV), p. 2558. doi: 10.3389/fmicb.2018.02558.

Crost, E. H. *et al.* (2023) 'Ruminococcus gnavus: friend or foe for human health', *FEMS Microbiology Reviews*, 47(2), pp. 1–23. doi: 10.1093/femsre/fuad014.

Crouzet, J. *et al.* (1990) 'Nucleotide sequence of a Pseudomonas denitrificans 5.4-kilobase DNA fragment containing five cob genes and identification of structural genes encoding S-adenosyl-L-methionine: uroporphyrinogen III methyltransferase and cobyrinic acid a,c-diamide synthase', *Journal of bacteriology*. J Bacteriol, 172(10), pp. 5968–5979. doi: 10.1128/JB.172.10.5968-5979.1990.

Crouzet, J. *et al.* (1991) 'Nucleotide sequence and genetic analysis of a 13.1-kilobase-pair Pseudomonas denitrificans DNA fragment containing five cob genes and identification of structural genes encoding Cob(I)alamin adenosyltransferase, cobyric acid synthase, and bifunctional cobinamide kinase-cobinamide phosphate guanylyltransferase.', *Journal of Bacteriology*. American Society for Microbiology (ASM), 173(19), p. 6074. doi: 10.1128/JB.173.19.6074-6087.1991.

Crudele, L. *et al.* (2023) 'Gut microbiota in the pathogenesis and therapeutic approaches of diabetes', *eBioMedicine*. Elsevier B.V., 97. doi: 10.1016/j.ebiom.2023.104821.

Cryan, J. F. *et al.* (2019) 'The Microbiota-Gut-Brain Axis', *Physiological reviews*. Physiol Rev, 99(4), pp. 1877–2013. doi: 10.1152/PHYSREV.00018.2018.

Cummings, J. H. *et al.* (1987) 'Short chain fatty acids in human large intestine, portal, hepatic and venous blood', *Gut*. Gut, 28(10), pp. 1221–1227. doi: 10.1136/GUT.28.10.1221.

D'Amelio, P. (2019) 'Connections Between Gut Microbiota and Bone Health', *Microbiome and Metabolome in Diagnosis, Therapy, and other Strategic Applications*. Academic Press, pp. 341–348. doi: 10.1016/B978-0-12-815249-2.00035-X.

Dabard, J. *et al.* (2001) 'Ruminococcin A, a New Lantibiotic Produced by a Ruminococcus gnavus Strain Isolated from Human Feces', *Applied and Environmental Microbiology*, 67(9), pp. 4111–4118. doi: 10.1128/AEM.67.9.4111-4118.2001.

Dai, Z. *et al.* (2019) 'The role of microbiota in the development of colorectal cancer', *International Journal of Cancer*. Wiley-Liss Inc., 145(8), pp. 2032–2041. doi: 10.1002/ijc.32017.

Dan, T. *et al.* (2018) 'Characteristics of Milk Fermented by Streptococcus thermophilus MGA45-4 and the Profiles of Associated Volatile Compounds during Fermentation and Storage', *Molecules : A Journal of Synthetic Chemistry and Natural Product Chemistry*. Multidisciplinary Digital Publishing Institute (MDPI), 23(4). doi: 10.3390/MOLECULES23040878.

Daniel, R., Bobik, T. A. and Gottschalk, G. (1998) 'Biochemistry of coenzyme B_{12}-dependent glycerol and diol dehydratases and organization of the encoding genes', *FEMS Microbiology Reviews*. Oxford University Press (OUP), 22(5), pp. 553–566. doi:

10.1111/j.1574-6976.1998.tb00387.x.

Davies, C. *et al.* (2021) 'Altering the gut microbiome to potentially modulate behavioral manifestations in autism spectrum disorders: A systematic review', *Neuroscience and Biobehavioral Reviews*. Elsevier Ltd, 128, pp. 549–557. doi: 10.1016/J.NEUBIOREV.2021.07.001.

Day-Walsh, P. *et al.* (2021) 'The use of an in-vitro batch fermentation (human colon) model for investigating mechanisms of TMA production from choline, l-carnitine and related precursors by the human gut microbiota', *European Journal of Nutrition*. Springer, 60(7), p. 3987. doi: 10.1007/S00394-021-02572-6.

Degnan, P. H. *et al.* (2014) 'Human gut microbes use multiple transporters to distinguish vitamin B_{12} analogs and compete in the gut', *Cell host & microbe*. Cell Host Microbe, 15(1), pp. 47–57. doi: 10.1016/J.CHOM.2013.12.007.

Degnan, P. H., Taga, M. E. and Goodman, A. L. (2014) 'Vitamin B12 as a modulator of gut microbial ecology', *Cell Metabolism*. Cell Press, pp. 769–778. doi: 10.1016/j.cmet.2014.10.002.

Delanghe, L. *et al.* (2021) 'The role of lactobacilli in inhibiting skin pathogens', *Biochemical Society Transactions*. Portland Press Ltd. doi: 10.1042/bst20200329.

Deng, Q. *et al.* (2020) 'Streptococcus bovis contributes to the development of colorectal cancer via recruiting CD11b+TLR-4+Cells', *Medical Science Monitor*. International Scientific Information, Inc., 26. doi: 10.12659/MSM.921886.

Derrien, M. *et al.* (2004) 'Akkermansia muciniphila gen. nov., sp. nov., a human intestinal mucin-degrading bacterium', *International journal of systematic and evolutionary microbiology*. Int J Syst Evol Microbiol, 54(Pt 5), pp. 1469–1476. doi: 10.1099/IJS.0.02873-0.

Dethlefsen, L. *et al.* (2008) 'The pervasive effects of an antibiotic on the human gut microbiota, as revealed by deep 16s rRNA sequencing', *PLoS Biology*, 6(11), pp. 2383–2400. doi: 10.1371/journal.pbio.0060280.

DeVeaux, L. C. and Kadner, R. J. (1985) 'Transport of vitamin B12 in Escherichia coli: cloning of the btuCD region.', *Journal of Bacteriology*, 162(3).

Dhonukshe-Rutten, R. A. M. *et al.* (2009) 'Dietary intake and status of folate and vitamin B12 and their association with homocysteine and cardiovascular disease in European populations', *European journal of clinical nutrition*. Eur J Clin Nutr, 63(1), pp. 18–30. doi: 10.1038/SJ.EJCN.1602897.

Dion, H. W., Calkins, D. G. and Pfiffner, J. J. (1952) 'Hydrolysis products of pseudovitamin B12', *Journal of the American Chemical Society*, 74(4), p. 1108. doi: 10.1021/ja01124a535.

Dodd, D. *et al.* (2017) 'A gut bacterial pathway metabolizes aromatic amino acids into nine circulating metabolites', *Nature 2017 551:7682*. Nature Publishing Group, 551(7682), pp. 648–652. doi: 10.1038/nature24661.

Dominguez-Bello, M. G. *et al.* (2016) 'Partial restoration of the microbiota of cesarean-born infants via vaginal microbial transfer', *Nature medicine*. Nat Med, 22(3), pp. 250–253. doi: 10.1038/NM.4039.

Donaldson, G. P., Melanie Lee, S. and Mazmanian, S. K. (2015) 'Gut biogeography of

the bacterial microbiota', *Nature Publishing Group*. doi: 10.1038/nrmicro3552.

Donoso, F. *et al.* (2022) 'Inflammation, Lifestyle Factors, and the Microbiome-Gut-Brain Axis: Relevance to Depression and Antidepressant Action', *Clinical Pharmacology & Therapeutics*. John Wiley & Sons, Ltd. doi: 10.1002/CPT.2581.

Duar, R. M. *et al.* (2017) 'Experimental evaluation of host adaptation of Lactobacillus reuteri to different vertebrate species', *Applied and Environmental Microbiology*. American Society for Microbiology, 83(12). doi: 10.1128/AEM.00132-17.

Duar, R. M., Kyle, D. and Casaburi, G. (2020) 'Colonization Resistance in the Infant Gut: The Role of B. infantis in Reducing pH and Preventing Pathogen Growth', *High-Throughput*. Multidisciplinary Digital Publishing Institute (MDPI), 9(2). doi: 10.3390/HT9020007.

Duncan, S. H. *et al.* (2007) 'Reduced dietary intake of carbohydrates by obese subjects results in decreased concentrations of butyrate and butyrate-producing bacteria in feces', *Applied and Environmental Microbiology*. American Society for Microbiology, 73(4), pp. 1073–1078. doi: 10.1128/AEM.02340-06/ASSET/A522D5CD-485A-468C-BAAD-234367688E08/ASSETS/GRAPHIC/ZAM0040775080003.JPEG.

Duncan, S. H., Louis, P. and Flint, H. J. (2004) 'Lactate-utilizing bacteria, isolated from human feces, that produce butyrate as a major fermentation product', *Applied and environmental microbiology*. Appl Environ Microbiol, 70(10), pp. 5810–5817. doi: 10.1128/AEM.70.10.5810-5817.2004.

Durazzi, F. *et al.* (2021) 'Comparison between 16S rRNA and shotgun sequencing data for the taxonomic characterization of the gut microbiota', *Scientific Reports*. Nature Research, 11(1). doi: 10.1038/S41598-021-82726-Y.

Elangovan, R. and Baruteau, J. (2022) 'Inherited and acquired vitamin B12 deficiencies: Which administration route to choose for supplementation?', *Frontiers in Pharmacology*. Frontiers Media S.A., 13, p. 972468. doi: 10.3389/FPHAR.2022.972468/BIBTEX.

Elliott, D., Kufera, J. A. and Myers, R. A. M. (2000) 'The microbiology of necrotizing soft tissue infections', *American Journal of Surgery*, 179(5), pp. 361–366. doi: 10.1016/S0002-9610(00)00360-3.

Escalante-Semerena, J. C., Suh, S. J. and Roth, J. R. (1990) 'cobA Function is required for both de novo cobalamin biosynthesis and assimilation of exogenous corrinoids in Salmonella typhimurium', *Journal of Bacteriology*, 172(1), pp. 273–280. doi: 10.1128/JB.172.1.273-280.1990.

Escherich, T. (1886) *Die darmbakterien des säuglings und ihre beziehungen zur physiologie der Verdauung*. Available at: https://books.google.com/books?hl=en&lr=&id=LCsLAQAAIAAJ&oi=fnd&pg=PA92&ots=RqWw8lz7a1&sig=JDiufYsEzP_LYrUZqZLMuWdYd1Y (Accessed: 9 April 2022).

Evans, P. R. and Mancia, F. (2007) 'Insights on the Reaction Mechanism of Methyl-malonyl-CoA mutase from the Crystal Structure', *Vitamin B12 and B12-Proteins*. Wiley, pp. 217–226. doi: 10.1002/9783527612192.CH13.

Falentin, H. *et al.* (2010) 'The Complete Genome of Propionibacterium freudenreichii CIRM-BIA1T, a Hardy Actinobacterium with Food and Probiotic Applications', *PLOS ONE*. Public Library of Science, 5(7), p. e11748. doi:

10.1371/JOURNAL.PONE.0011748.

Fang, H., Kang, J. and Zhang, D. (2017) 'Microbial production of vitamin B12: A review and future perspectives', *Microbial Cell Factories*. BioMed Central Ltd., 16(1), p. 15. doi: 10.1186/s12934-017-0631-y.

Fedosov, S. N., Nexo, E. and Heegaard, C. W. (2024) 'Kinetics of Cellular Cobalamin Uptake and Conversion: Comparison of Aquo/Hydroxocobalamin to Cyanocobalamin', *Nutrients*. Multidisciplinary Digital Publishing Institute (MDPI), 16(3), p. 378. doi: 10.3390/NU16030378/S1.

Feng, R. J. *et al.* (2021) '[Dysbiosis of Gut Microbiota in Patients with Post-Stroke Cognitive Impairment]', *Sichuan da xue xue bao. Yi xue ban = Journal of Sichuan University. Medical science edition*. Sichuan Da Xue Xue Bao Yi Xue Ban, 52(6), pp. 966–974. doi: 10.12182/20211160507.

Ferlazzo, G. *et al.* (2011) 'Role of natural killer and dendritic cell crosstalk in immunomodulation by commensal bacteria probiotics', *Journal of Biomedicine and Biotechnology*, 2011. doi: 10.1155/2011/473097.

Fink, L. N. *et al.* (2007) 'Distinct gut-derived lactic acid bacteria elicit divergent dendritic cell-mediated NK cell responses', *International Immunology*, 19(12), pp. 1319–1327. doi: 10.1093/INTIMM/DXM103.

Van Der Flier, L. G. and Clevers, H. (2009) 'Stem cells, self-renewal, and differentiation in the intestinal epithelium', *Annual review of physiology*. Annu Rev Physiol, 71, pp. 241–260. doi: 10.1146/ANNUREV.PHYSIOL.010908.163145.

Forgie, A. J. *et al.* (2023) 'Over supplementation with vitamin B12 alters microbe-host interactions in the gut leading to accelerated Citrobacter rodentium colonization and pathogenesis in mice', *Microbiome*. BioMed Central Ltd, 11(1). doi: 10.1186/s40168-023-01461-w.

Forsyth, C. B. *et al.* (2011) 'Increased intestinal permeability correlates with sigmoid mucosa alpha-synuclein staining and endotoxin exposure markers in early Parkinson's disease', *PLoS ONE*, 6(12). doi: 10.1371/journal.pone.0028032.

Frese, S. A. *et al.* (2011) 'The Evolution of Host Specialization in the Vertebrate Gut Symbiont Lactobacillus reuteri', *PLoS Genetics*. Edited by D. S. Guttman. Public Library of Science, 7(2), p. e1001314. doi: 10.1371/journal.pgen.1001314.

Friedman, E. S. *et al.* (2018) 'Microbes vs. chemistry in the origin of the anaerobic gut lumen', *Proceedings of the National Academy of Sciences of the United States of America*. National Academy of Sciences, 115(16), pp. 4170–4175. doi: 10.1073/PNAS.1718635115.

Frioux, C. *et al.* (2023) 'Enterosignatures define common bacterial guilds in the human gut microbiome', *Cell Host and Microbe*. Cell Press, 31(7), pp. 1111-1125.e6. doi: 10.1016/j.chom.2023.05.024.

Fuentes, S. *et al.* (2017) 'Microbial shifts and signatures of long-term remission in ulcerative colitis after faecal microbiota transplantation', *The ISME Journal*. Oxford Academic, 11(8), pp. 1877–1889. doi: 10.1038/ISMEJ.2017.44.

Gabriel, I. *et al.* (2018) 'The influence of maternal vaginal flora on the intestinal colonization in newborns and 3-month-old infants', *Journal of Maternal-Fetal and Neonatal Medicine*. Taylor and Francis Ltd, 31(11), pp. 1448–1453. doi:

10.1080/14767058.2017.1319352.

Gart, E. *et al.* (2021) 'Butyrate Protects against Diet-Induced NASH and Liver Fibrosis and Suppresses Specific Non-Canonical TGF-β Signaling Pathways in Human Hepatic Stellate Cells', *Biomedicines*. MDPI, 9(12). doi: 10.3390/BIOMEDICINES9121954.

Gassler, N. (2017) 'Paneth cells in intestinal physiology and pathophysiology', *World Journal of Gastrointestinal Pathophysiology*. Baishideng Publishing Group Inc, 8(4), p. 150. doi: 10.4291/WJGP.V8.I4.150.

Ge, Y., Zadeh, M. and Mohamadzadeh, M. (2022) 'Vitamin B12 coordinates ileal epithelial cell and microbiota functions to resist Salmonella infection in mice', *Journal of Experimental Medicine*. Rockefeller University Press, 219(7). doi: 10.1084/JEM.20220057/213271.

Ghosh, T. S., Arnoux, J. and O'Toole, P. W. (2020) 'Metagenomic analysis reveals distinct patterns of gut lactobacillus prevalence, abundance, and geographical variation in health and disease', *Gut Microbes*. Taylor & Francis, 12(1), pp. 1–19. doi: 10.1080/19490976.2020.1822729.

Giambò, F. *et al.* (2022) 'Role-Playing Between Environmental Pollutants and Human Gut Microbiota: A Complex Bidirectional Interaction', *Frontiers in Medicine*. Frontiers Media SA, 9, p. 215. doi: 10.3389/FMED.2022.810397/BIBTEX.

Giri, S. S. *et al.* (2018) 'Use of a Potential Probiotic, Lactobacillus casei L4, in the Preparation of Fermented Coconut Water Beverage', *Frontiers in Microbiology*. Frontiers Media SA, 9(AUG). doi: 10.3389/FMICB.2018.01976.

Giuseppe Rizzello, C. *et al.* (2020) 'A Phylogenetic View on the Role of Glycerol for Growth Enhancement and Reuterin Formation in Limosilactobacillus reuteri', *Front. Microbiol*, 11, p. 601422. doi: 10.3389/fmicb.2020.601422.

González-Morelo, K. J., Vega-Sagardía, M. and Garrido, D. (2020) 'Molecular Insights Into O-Linked Glycan Utilization by Gut Microbes', *Frontiers in Microbiology*. Frontiers Media S.A., 11. doi: 10.3389/FMICB.2020.591568/TEXT.

Gonzalez, J. C. *et al.* (1992) 'Comparison of Cobalamin-independent and Cobalamin-Dependent Methionine Synthases from Escherichia coli : Two Solutions to the Same Chemical Problem', *Biochemistry*. American Chemical Society, 31(26), pp. 6045–6056. doi: 10.1021/BI00141A013/ASSET/BI00141A013.FP.PNG_V03.

Goodman, A. L. *et al.* (2009) 'Identifying genetic determinants needed to establish a human gut symbiont in its habitat', *Cell host & microbe*. Cell Host Microbe, 6(3), pp. 279–289. doi: 10.1016/J.CHOM.2009.08.003.

Gough, S. P., Petersen, B. O. and Duus, J. Ø. (2000) 'Anaerobic chlorophyll isocyclic ring formation in Rhodobacter capsulatus requires a cobalamin cofactor', *PNAS June*, 6(12), pp. 6908–6913. Available at: www.tigr.org. (Accessed: 11 April 2024).

'Government Dietary Recommendations Government recommendations for energy and nutrients for males and females aged 1-18 years and 19+ years' (2016). Available at: www.gov.uk/phe (Accessed: 17 January 2024).

Grabinger, T. *et al.* (2019) 'Alleviation of intestinal inflammation by oral supplementation with 2-fucosyllactose in mice', *Frontiers in Microbiology*, 10(JUN), pp. 1–14. doi: 10.3389/fmicb.2019.01385.

Gray, M. J. and Escalante-Semerena, J. C. (2009) ‘The cobinamide amidohydrolase (cobyric acid-forming) CbiZ enzyme: A critical activity of the cobamide remodeling system of Rhodobacter sphaeroides’, *Molecular microbiology*. NIH Public Access, 74(5), p. 1198. doi: 10.1111/J.1365-2958.2009.06928.X.

Gray, M. J. and Escalante-Semerena, J. C. (2010) ‘A new pathway for the synthesis of a-ribazole-phosphate in Listeria innocuam mi_7294 1429..1438’. doi: 10.1111/j.1365-2958.2010.07294.x.

Gray, M. J., Tavares, N. K. and Escalante-Semerena, J. C. (2008) ‘The genome of Rhodobacter sphaeroides strain 2.4.1 encodes functional cobinamide salvaging systems of archaeal and bacterial origins’, *Molecular microbiology*. Mol Microbiol, 70(4), pp. 824–836. doi: 10.1111/J.1365-2958.2008.06437.X.

Greibe, E. *et al.* (2013) ‘Metformin increases liver accumulation of vitamin B12 - an experimental study in rats’, *Biochimie*. Biochimie, 95(5), pp. 1062–1065. doi: 10.1016/J.BIOCHI.2013.02.002.

Grondin, J. A. *et al.* (2020) ‘Mucins in Intestinal Mucosal Defense and Inflammation: Learning From Clinical and Experimental Studies’, *Frontiers in Immunology*. Frontiers Media S.A., 11, p. 559710. doi: 10.3389/FIMMU.2020.02054/BIBTEX.

Grundke-Iqbal, I. *et al.* (1986) ‘Abnormal phosphorylation of the microtubule-associated protein tau (tau) in Alzheimer cytoskeletal pathology’, *Proceedings of the National Academy of Sciences of the United States of America*. Proc Natl Acad Sci U S A, 83(13), pp. 4913–4917. doi: 10.1073/PNAS.83.13.4913.

Guetterman, H. M. *et al.* (2022) ‘Vitamin B-12 and the Gastrointestinal Microbiome: A Systematic Review’, *Advances in Nutrition*. Oxford Academic, 13(2), pp. 530–558. doi: 10.1093/ADVANCES/NMAB123.

Gulrandhe, P. *et al.* (2023) ‘Neuropsychiatric and Neurological Diseases in Relation to the Microbiota-Gut-Brain Axis: From Research to Clinical Care’, *Cureus*. Cureus Inc., 15(9). doi: 10.7759/CUREUS.44819.

Gurwara, S. *et al.* (2019) ‘Dietary Nutrients Involved in One-Carbon Metabolism and Colonic Mucosa-Associated Gut Microbiome in Individuals with an Endoscopically Normal Colon’, *Nutrients*. Multidisciplinary Digital Publishing Institute (MDPI), 11(3), p. 613. doi: 10.3390/NU11030613.

Guzior, D. V. and Quinn, R. A. (2021) ‘Review: microbial transformations of human bile acids’, *Microbiome*. BioMed Central Ltd, 9(1), pp. 1–13. doi: 10.1186/S40168-021-01101-1/FIGURES/5.

Haileselassie, Y. *et al.* (2016) ‘Lactobacillus reuteri and Staphylococcus aureus differentially influence the generation of monocyte-derived dendritic cells and subsequent autologous T cell responses’, *Immunity, Inflammation and Disease*. John Wiley & Sons, Ltd, 4(3), pp. 315–326. doi: 10.1002/IID3.115.

Hajjar, R., Richard, C. S. and Santos, M. M. (2021) ‘The role of butyrate in surgical and oncological outcomes in colorectal cancer’, *American Journal of Physiology - Gastrointestinal and Liver Physiology*. American Physiological Society, 320(4), pp. G601–G608. doi: 10.1152/AJPGI.00316.2020/ASSET/IMAGES/LARGE/AJPGI.00316.2020_F001.JPEG.

Halczuk, K. *et al.* (2023) ‘Vitamin B12—Multifaceted In Vivo Functions and In Vitro

Applications', *Nutrients*. Multidisciplinary Digital Publishing Institute (MDPI), 15(12). doi: 10.3390/NU15122734.

Hall, A. B. *et al.* (2017) 'A novel Ruminococcus gnavus clade enriched in inflammatory bowel disease patients', *Genome Medicine*. BioMed Central Ltd., 9(1), p. 103. doi: 10.1186/s13073-017-0490-5.

Han, M. *et al.* (2022) 'Milk fermentation by monocultures or co-cultures of Streptococcus thermophilus strains', *Frontiers in Bioengineering and Biotechnology*. Frontiers Media SA, 10. doi: 10.3389/FBIOE.2022.1097013.

Han, N. *et al.* (2024) 'Rapid turnover and short-term blooms of Escherichia coli in the human gut', *Journal of Bacteriology*. American Society for Microbiology, 206(1). doi: 10.1128/JB.00239-23/SUPPL_FILE/JB.00239-23-S0003.DOCX.

Hansson, G. C. (2012) 'Role of mucus layers in gut infection and inflammation', *Current Opinion in Microbiology*, 15(1), pp. 57–62. doi: 10.1016/j.mib.2011.11.002.

Hazra, A. B. *et al.* (2015) 'Anaerobic biosynthesis of the lower ligand of vitamin B12', *Proceedings of the National Academy of Sciences of the United States of America*. National Academy of Sciences, 112(34), pp. 10792–10797. doi: 10.1073/PNAS.1509132112/SUPPL_FILE/PNAS.1509132112.SAPP.PDF.

Heller, K. and Kadner, R. J. (1985) 'Nucleotide sequence of the gene for the vitamin B12 receptor protein in the outer membrane of Escherichia coli.', *Journal of Bacteriology*. American Society for Microbiology (ASM), 161(3), p. 904. doi: 10.1128/JB.161.3.904-908.1985.

Helliwell, K. E. *et al.* (2016) 'Cyanobacteria and Eukaryotic Algae Use Different Chemical Variants of Vitamin B12', *Current Biology*. Cell Press, 26(8), pp. 999–1008. doi: 10.1016/J.CUB.2016.02.041.

Henke, M. T. *et al.* (2019) 'Ruminococcus gnavus, a member of the human gut microbiome associated with Crohn's disease, produces an inflammatory polysaccharide', *Proceedings of the National Academy of Sciences of the United States of America*. National Academy of Sciences, 116(26), pp. 12672–12677. doi: 10.1073/PNAS.1904099116/SUPPL_FILE/PNAS.1904099116.SD03.XLSX.

Henrick, B. M. *et al.* (2021) 'Bifidobacteria-mediated immune system imprinting early in life', *Cell*. Elsevier B.V., 184(15), pp. 3884-3898.e11. doi: 10.1016/j.cell.2021.05.030.

Herman, D. R. *et al.* (2020) 'Dietary Habits of 2- to 9-Year-Old American Children Are Associated with Gut Microbiome Composition', *Journal of the Academy of Nutrition and Dietetics*. Elsevier, 120(4), pp. 517–534. doi: 10.1016/J.JAND.2019.07.024.

Hickman, F. W. *et al.* (1982) 'Identification of Proteus penneri sp nov., Formerly known as Proteus vulgaris indole negative or as Proteus vulgaris biogroup 1', *Journal of Clinical Microbiology*, 15(6), pp. 1097–1102. doi: 10.1128/JCM.15.6.1097-1102.1982.

Hinton, C. F. *et al.* (2010) 'Maternal and Neonatal Vitamin B12 Deficiency Detected through Expanded Newborn Screening—United States, 2003–2007', *The Journal of Pediatrics*. Mosby, 157(1), pp. 162–163. doi: 10.1016/J.JPEDS.2010.03.006.

Hodgkin, D. C. *et al.* (1956) 'Structure of Vitamin B12', *Nature 1956 178:4524*. Nature Publishing Group, 178(4524), pp. 64–66. doi: 10.1038/178064a0.

Hofmann, A. F. (1999) 'Bile acids: The good, the bad, and the ugly', *News in*

Physiological Sciences. American Physiological Society, 14(1), pp. 24–29. doi: 10.1152/PHYSIOLOGYONLINE.1999.14.1.24.

Holden, M. T. G. *et al.* (2009) 'The genome of Burkholderia cenocepacia J2315, an epidemic pathogen of cystic fibrosis patients', *Journal of Bacteriology*. American Society for Microbiology, 91(1), pp. 261–277. doi: 10.1128/JB.01230-08/SUPPL_FILE/TABLE_S2_J2315_RODS.ZIP.

Homuth, G. *et al.* (1999) 'Transcriptional control of Bacillus subtilis hemN and hemZ', *Journal of Bacteriology*. American Society for Microbiology, 181(19), pp. 5922–5929. doi: 10.1128/JB.181.19.5922-5929.1999/ASSET/71A19DAC-9213-4778-B661-58F5E8960DCC/ASSETS/GRAPHIC/JB1990636003.JPEG.

Horrocks, V. *et al.* (2023) 'Role of the gut microbiota in nutrient competition and protection against intestinal pathogen colonization', *Microbiology*. Microbiology Society, 169(8), p. 1377. doi: 10.1099/MIC.0.001377.

Hoskins, L. C. *et al.* (1985) 'Mucin degradation in human colon ecosystems. Isolation and properties of fecal strains that degrade ABH blood group antigens and oligosaccharides from mucin glycoproteins', *The Journal of clinical investigation*. J Clin Invest, 75(3), pp. 944–953. doi: 10.1172/JCI111795.

Hossain, K. S., Amarasena, S. and Mayengbam, S. (2022) 'B Vitamins and Their Roles in Gut Health', *Microorganisms 2022, Vol. 10, Page 1168*. Multidisciplinary Digital Publishing Institute, 10(6), p. 1168. doi: 10.3390/MICROORGANISMS10061168.

Hou, K. *et al.* (2022) 'Microbiota in health and diseases', *Signal Transduction and Targeted Therapy 2022 7:1*. Nature Publishing Group, 7(1), pp. 1–28. doi: 10.1038/s41392-022-00974-4.

Howden, C. W. (2000) 'Vitamin B12 levels during prolonged treatment with proton pump inhibitors', *Journal of clinical gastroenterology*. J Clin Gastroenterol, 30(1), pp. 29–33. doi: 10.1097/00004836-200001000-00006.

Hubbard, T. D. *et al.* (2015) 'Adaptation of the human aryl hydrocarbon receptor to sense microbiota-derived indoles', *Scientific Reports*. Nature Publishing Group, 5. doi: 10.1038/SREP12689.

Hugenholtz, F. and de Vos, W. M. (2018) 'Mouse models for human intestinal microbiota research: a critical evaluation', *Cellular and Molecular Life Sciences: CMLS*. Springer, 75(1), p. 149. doi: 10.1007/S00018-017-2693-8.

Hugon, P. *et al.* (2015) 'A comprehensive repertoire of prokaryotic species identified in human beings', *The Lancet Infectious Diseases*. Elsevier, 15(10), pp. 1211–1219. doi: 10.1016/S1473-3099(15)00293-5.

Isenring, J. *et al.* (2023) 'In vitro human gut microbiota fermentation models: opportunities, challenges, and pitfalls', *Microbiome Research Reports*. OAE Publishing Inc, 2(1). doi: 10.20517/MRR.2022.15.

Issac, T. *et al.* (2015) 'Vitamin B12 deficiency: An important reversible co-morbidity in neuropsychiatric manifestations', *Indian Journal of Psychological Medicine*. Medknow Publications, 37(1), pp. 26–29. doi: 10.4103/0253-7176.150809.

Jacobsen, C. N. *et al.* (1999) *Screening of Probiotic Activities of Forty-Seven Strains of Lactobacillus spp. by In Vitro Techniques and Evaluation of the Colonization Ability of Five Selected Strains in Humans*, *APPLIED AND ENVIRONMENTAL MICROBIOLOGY*.

Available at: http://aem.asm.org/ (Accessed: 17 April 2021).

Janati, A. I. *et al.* (2020) 'Detection of Fusobaterium nucleatum in feces and colorectal mucosa as a risk factor for colorectal cancer: a systematic review and meta-analysis', *Systematic Reviews*. BioMed Central Ltd, 9(1), pp. 1–15. doi: 10.1186/S13643-020-01526-Z/FIGURES/4.

Jandhyala, S. M. *et al.* (2015) 'role of the normal gut microbiota', *World J Gastroenterol*, 21(29), pp. 8787–8803. doi: 10.3748/wjg.v21.i29.8787.

Jardon, K. M. *et al.* (2022) 'Dietary macronutrients and the gut microbiome: a precision nutrition approach to improve cardiometabolic health Human Biology, School of Nutrition and Translational Research in Metabolism', *Gut*, 0, pp. 1–13. doi: 10.1136/gutjnl-2020-323715.

Jensen, K. P. (2005) 'Electronic structure of Cob(I)alamin: the story of an unusual nucleophile', *The journal of physical chemistry. B*. J Phys Chem B, 109(20), pp. 10505–10512. doi: 10.1021/JP050802M.

Jess, A. T. *et al.* (2023) 'Short-Chain Fatty Acid Levels after Fecal Microbiota Transplantation in a Pediatric Cohort with Recurrent Clostridioides difficile Infection', *Metabolites*. Multidisciplinary Digital Publishing Institute (MDPI), 13(10), p. 1039. doi: 10.3390/METABO13101039/S1.

Johansson, M. E. V. *et al.* (2008) 'The inner of the two Muc2 mucin-dependent mucus layers in colon is devoid of bacteria', *Proceedings of the National Academy of Sciences of the United States of America*. Proc Natl Acad Sci U S A, 105(39), pp. 15064–15069. doi: 10.1073/PNAS.0803124105.

Johansson, M. E. V., Holmén Larsson, J. M. and Hansson, G. C. (2011) 'The two mucus layers of colon are organized by the MUC2 mucin, whereas the outer layer is a legislator of host-microbial interactions', *Proceedings of the National Academy of Sciences of the United States of America*. National Academy of Sciences, 108(SUPPL. 1), pp. 4659–4665. doi: 10.1073/PNAS.1006451107.

Johansson, M. E. V., Thomsson, K. A. and Hansson, G. C. (2009) 'Proteomic analyses of the two mucus layers of the colon barrier reveal that their main component, the Muc2 mucin, is strongly bound to the Fcgbp protein', *Journal of proteome research*. J Proteome Res, 8(7), pp. 3549–3557. doi: 10.1021/PR9002504.

Jones, R. C. *et al.* (2022) 'The Tabula Sapiens: A multiple-organ, single-cell transcriptomic atlas of humans', *Science*. American Association for the Advancement of Science, 376(6594). doi: 10.1126/SCIENCE.ABL4896/SUPPL_FILE/SCIENCE.ABL4896_MDAR_REPRODUCIBILITY_CHECKLIST.PDF.

Joossens, M. *et al.* (2011) 'Dysbiosis of the faecal microbiota in patients with Crohn's disease and their unaffected relatives', *Gut*. BMJ Publishing Group, 60(5), pp. 631–637. doi: 10.1136/GUT.2010.223263.

Juge, N. (2022) 'Relationship between mucosa-associated gut microbiota and human diseases', *Biochemical Society transactions*. Biochem Soc Trans, 50(5), pp. 1225–1236. doi: 10.1042/BST20201201.

Kadner, R. J. and McElhaney, G. (1978) 'Outer membrane-dependent transport systems in Escherichia coli: turnover of TonB function.', *Journal of Bacteriology*,

134(3).

Kaval, K. G. and Garsin, D. A. (2018) ‘Ethanolamine utilization in bacteria’, *mBio*. American Society for Microbiology, 9(1). doi: 10.1128/MBIO.00066-18.

Keck, B. and Renz, P. (2000) ‘Salmonella typhimurium forms adenylcobamide and 2-methyladenylcobamide, but no detectable cobalamin during strictly anaerobic growth’, *Archives of microbiology*. Arch Microbiol, 173(1), pp. 76–77. doi: 10.1007/S002030050011.

Keller, S. *et al.* (2018) ‘Selective utilization of benzimidazolylnorcobamides as cofactors by the tetrachloroethene reductive dehalogenase of Sulfurospirillum multivorans’, *Journal of Bacteriology*. American Society for Microbiology, 200(8). doi: 10.1128/JB.00584-17/SUPPL_FILE/ZJB999094688S1.PDF.

Kelly, C. J. *et al.* (2019) ‘Oral vitamin B12 supplement is delivered to the distal gut, altering the corrinoid profile and selectively depleting Bacteroides in C57BL/6 mice’, *Gut Microbes*. Taylor & Francis, 10(6), pp. 654–662. doi: 10.1080/19490976.2019.1597667.

Kerimi, A. *et al.* (2020) ‘The gut microbiome drives inter-and intra-individual differences in metabolism of bioactive small molecules’. doi: 10.1038/s41598-020-76558-5.

Kesika, P. *et al.* (2021) ‘Role of gut-brain axis, gut microbial composition, and probiotic intervention in Alzheimer’s disease’, *Life Sciences*. Pergamon, 264, p. 118627. doi: 10.1016/J.LFS.2020.118627.

Kim, E. R. and Rhee, P. L. (2012) ‘How to interpret a functional or motility test - colon transit study’, *Journal of neurogastroenterology and motility*. J Neurogastroenterol Motil, 18(1), pp. 94–99. doi: 10.5056/JNM.2012.18.1.94.

Kirmiz, N. *et al.* (2020) ‘Comparative Genomics Guides Elucidation of Vitamin B12 Biosynthesis in Novel Human-Associated Akkermansia Strains’, *Applied and environmental microbiology*. Appl Environ Microbiol, 86(3). doi: 10.1128/AEM.02117-19.

Klann, E. M. *et al.* (2021) ‘The Gut–Brain Axis and Its Relation to Parkinson’s Disease: A Review’, *Frontiers in Aging Neuroscience*. Frontiers Media SA, 13. doi: 10.3389/FNAGI.2021.782082.

Kleine Bardenhorst, S. *et al.* (2023) ‘Gut microbiota dysbiosis in Parkinson disease: A systematic review and pooled analysis’, *European journal of neurology*. Eur J Neurol, 30(11), pp. 3581–3594. doi: 10.1111/ENE.15671.

Kobayashi, N. *et al.* (2019) ‘The Roles of Peyer’s Patches and Microfold Cells in the Gut Immune System: Relevance to Autoimmune Diseases’, *Frontiers in Immunology*. Frontiers Media SA, 10, p. 2345. doi: 10.3389/FIMMU.2019.02345.

Koeth, R. A. *et al.* (2014) ‘γ-butyrobetaine is a proatherogenic intermediate in gut microbial metabolism of L-carnitine to TMAO’, *Cell Metabolism*. Cell Press, 20(5), pp. 799–812. doi: 10.1016/j.cmet.2014.10.006.

Koren, O. *et al.* (2013) ‘A Guide to Enterotypes across the Human Body: Meta-Analysis of Microbial Community Structures in Human Microbiome Datasets’, *PLoS Computational Biology*. Public Library of Science, 9(1). doi: 10.1371/journal.pcbi.1002863.

Kostic, A. D. *et al.* (2013) 'Fusobacterium nucleatum potentiates intestinal tumorigenesis and modulates the tumor immune microenvironment', *Cell host & microbe*. NIH Public Access, 14(2), p. 207. doi: 10.1016/J.CHOM.2013.07.007.

Kostic, A. D., Howitt, M. R. and Garrett, W. S. (2013) 'Exploring host-microbiota interactions in animal models and humans', *Genes & development*. Genes Dev, 27(7), pp. 701–718. doi: 10.1101/GAD.212522.112.

Kotarski, S. F. and Savage, D. C. (1979) 'Models for study of the specificity by which indigenous lactobacilli adhere to murine gastric epithelia', *Infection and Immunity*, 26(3), pp. 966–975. doi: 10.1128/IAI.26.3.966-975.1979.

Kovatcheva-Datchary, P. *et al.* (2015) 'Dietary Fiber-Induced Improvement in Glucose Metabolism Is Associated with Increased Abundance of Prevotella', *Cell Metabolism*. Cell Press, 22(6), pp. 971–982. doi: 10.1016/j.cmet.2015.10.001.

Koyama', M. *et al.* (1999) 'A Clostridium perfringens hem Gene Cluster Contains a cysGB Homologue That Is Involved in Cobalamin Biosynthesis', *Microbiot. Immunol*, 43(10), pp. 947–957.

Kraal, L. *et al.* (2014) 'The Prevalence of Species and Strains in the Human Microbiome: A Resource for Experimental Efforts', *PLOS ONE*. Public Library of Science, 9(5), p. e97279. doi: 10.1371/JOURNAL.PONE.0097279.

Kumar, N., Bucher, D. and Kozlowski, P. M. (2019) 'Mechanistic Implications of Reductive Co-C Bond Cleavage in B12-Dependent Methylmalonyl CoA Mutase', *Journal of Physical Chemistry B*. American Chemical Society, 123(10), pp. 2210–2216. doi: 10.1021/ACS.JPCB.8B10820/ASSET/IMAGES/LARGE/JP-2018-10820X_0003.JPEG.

Kumar, S., Agyeman-Duah, E. and Ujor, V. C. (2023) 'Whole-Genome Sequence and Fermentation Characteristics of Enterobacter hormaechei UW0SKVC1: A Promising Candidate for Detoxification of Lignocellulosic Biomass Hydrolysates and Production of Value-Added Chemicals', *Bioengineering*. Multidisciplinary Digital Publishing Institute (MDPI), 10(9), p. 1090. doi: 10.3390/BIOENGINEERING10091090.

Kundra, P. *et al.* (2022) 'Healthy adult gut microbiota sustains its own vitamin B12 requirement in an in vitro batch fermentation model', *Frontiers in Nutrition*. Frontiers Media S.A., 9, p. 1070155. doi: 10.3389/FNUT.2022.1070155/BIBTEX.

Kundra, P. *et al.* (2024) 'Vitamin B12 analogues from gut microbes and diet differentially impact commensal propionate producers of the human gut', *Frontiers in Nutrition*. Frontiers, 11, p. 1360199. doi: 10.3389/FNUT.2024.1360199.

Kurpad, A. V. *et al.* (2023) 'Bioavailability and daily requirement of vitamin B12 in adult humans: an observational study of its colonic absorption and daily excretion as measured by [13C]-cyanocobalamin kinetics', *The American Journal of Clinical Nutrition*. Elsevier, 118(6), pp. 1214–1223. doi: 10.1016/J.AJCNUT.2023.08.020.

Kwon, Y. *et al.* (2014) 'Anemia, iron and vitamin B12 deficiencies after sleeve gastrectomy compared to Roux-en-Y gastric bypass: a meta-analysis', *Surgery for obesity and related diseases : official journal of the American Society for Bariatric Surgery*. Surg Obes Relat Dis, 10(4), pp. 589–597. doi: 10.1016/J.SOARD.2013.12.005.

Langmead, B. and Salzberg, S. L. (2012) 'Fast gapped-read alignment with Bowtie 2', *Nature Methods*. NIH Public Access, 9(4), pp. 357–359. doi: 10.1038/nmeth.1923.

Larsson, J. M. H. *et al.* (2009) 'A complex, but uniform O-glycosylation of the human

MUC2 mucin from colonic biopsies analyzed by nanoLC/MSn', *Glycobiology*. Oxford University Press, 19(7), pp. 756–766. doi: 10.1093/glycob/cwp048.

Larsson, J. M. H. *et al.* (2013) 'Studies of mucus in mouse stomach, small intestine, and colon. III. Gastrointestinal Muc5ac and Muc2 mucin O-glycan patterns reveal a regiospecific distribution', *American Journal of Physiology - Gastrointestinal and Liver Physiology*, 305(5). doi: 10.1152/AJPGI.00048.2013.

Lasaviciute, G. *et al.* (2022) 'Gut commensal Limosilactobacillus reuteri induces atypical memory-like phenotype in human dendritic cells in vitro', *Gut Microbes*. Taylor and Francis Ltd., 14(1). doi: 10.1080/19490976.2022.2045046/SUPPL_FILE/KGMI_A_2045046_SM0954.DOCX.

Lawrence, A. D. *et al.* (2008) 'Identification, characterization, and structure/function analysis of a corrin reductase involved in adenosylcobalamin biosynthesis', *The Journal of biological chemistry*. J Biol Chem, 283(16), pp. 10813–10821. doi: 10.1074/JBC.M710431200.

Lawrence, J. G. (2003) 'Gene Organization: Selection, Selfishness, and Serendipity', *Annual Review of Microbiology*. Annual Reviews 4139 El Camino Way, P.O. Box 10139, Palo Alto, CA 94303-0139, USA , 57(1), pp. 419–440. doi: 10.1146/annurev.micro.57.030502.090816.

Lee, J. H. and Lee, J. (2010) 'Indole as an intercellular signal in microbial communities', *FEMS Microbiology Reviews*. Blackwell Publishing Ltd, 34(4), pp. 426–444. doi: 10.1111/J.1574-6976.2009.00204.X.

Lee, Y. Y., Erdogan, A. and Rao, S. S. C. (2014) 'How to Assess Regional and Whole Gut Transit Time With Wireless Motility Capsule', *Journal of Neurogastroenterology and Motility*. Korean Society of Neurogastroenterology and Motility, 20(2), pp. 265–270. doi: 10.5056/JNM.2014.20.2.265.

Leite, G. *et al.* (2021) 'In brief Age and the aging process significantly alter the small bowel microbiome', *Cell Reports*, 36. doi: 10.1016/j.celrep.2021.109765.

Lester Smith, E. (1948) 'Purification of Anti-pernicious Anæmia Factors from Liver', *Nature 1948 161:4095*. Nature Publishing Group, 161(4095), pp. 638–639. doi: 10.1038/161638a0.

Li, F. *et al.* (2023) 'A phylogenomic analysis of Limosilactobacillus reuteri reveals ancient and stable evolutionary relationships with rodents and birds and zoonotic transmission to humans', *BMC Biology*. BioMed Central Ltd, 21(1), pp. 1–17. doi: 10.1186/S12915-023-01541-1/FIGURES/7.

Li, J. *et al.* (2014) 'An integrated catalog of reference genes in the human gut microbiome', *Nature Biotechnology*. Nature Publishing Group, 32(8), pp. 834–841. doi: 10.1038/nbt.2942.

Li, N. *et al.* (2021) 'Fecal Microbiota Transplantation Relieves Gastrointestinal and Autism Symptoms by Improving the Gut Microbiota in an Open-Label Study', *Frontiers in Cellular and Infection Microbiology*. Frontiers Media S.A., 11, p. 759435. doi: 10.3389/FCIMB.2021.759435/BIBTEX.

Li, P. *et al.* (2017) 'Novel vitamin B12-producing Enterococcus spp. and preliminary in vitro evaluation of probiotic potentials', *Applied Microbiology and Biotechnology*. Springer Verlag, 101(15), pp. 6155–6164. doi: 10.1007/S00253-017-8373-7/TABLES/4.

Li, Q. *et al.* (2020) 'Implication of the gut microbiome composition of type 2 diabetic patients from northern China', *Scientific Reports*. Nature Research, 10(1). doi: 10.1038/S41598-020-62224-3.

Li, S. *et al.* (2022) 'Tumorigenic bacteria in colorectal cancer: mechanisms and treatments', *Cancer Biology and Medicine*. Cancer Biology and Medicine, 19(2), pp. 147–162. doi: 10.20892/J.ISSN.2095-3941.2020.0651.

Li, Z. *et al.* (2023) 'Gut bacterial profiles in Parkinson's disease: A systematic review', *CNS Neuroscience & Therapeutics*. Wiley-Blackwell, 29(1), p. 140. doi: 10.1111/CNS.13990.

Lichtenstern, C. R. and Lamichhane-Khadka, R. (2023) 'A tale of two bacteria – Bacteroides fragilis, Escherichia coli, and colorectal cancer', *Frontiers in Bacteriology*. Frontiers, 2, p. 1229077. doi: 10.3389/FBRIO.2023.1229077.

Lin, X. B. *et al.* (2018) 'The evolution of ecological facilitation within mixed-species biofilms in the mouse gastrointestinal tract', *The ISME Journal*. Nature Publishing Group, 12(11), p. 2770. doi: 10.1038/S41396-018-0211-0.

Linares, D. M. *et al.* (2016) 'Streptococcus thermophilus APC151 strain is suitable for the manufacture of naturally gaba-enriched bioactive yogurt', *Frontiers in Microbiology*. Frontiers Research Foundation, 7(NOV). doi: 10.3389/FMICB.2016.01876.

Lindner, J. G. E. M., Plantema, F. H. F. and Hoogkamp-Korstanje, J. A. A. (1978) 'Quantitative studies of the vaginal flora of healthy women and of obstetric and gynaecological patients', *Journal of medical microbiology*. J Med Microbiol, 11(3), pp. 233–241. doi: 10.1099/00222615-11-3-233.

Litvak, Y. *et al.* (2017) 'Dysbiotic Proteobacteria expansion: a microbial signature of epithelial dysfunction', *Current Opinion in Microbiology*. Elsevier Ltd, 39, pp. 1–6. doi: 10.1016/j.mib.2017.07.003.

Liu, H. *et al.* (2011) 'Production of lactate in Escherichia coli by redox regulation genetically and physiologically', *Applied Biochemistry and Biotechnology*. Springer, 164(2), pp. 162–169. doi: 10.1007/S12010-010-9123-9/FIGURES/2.

Liu, L. *et al.* (2022) 'Bacteroides vulgatus attenuates experimental mice colitis through modulating gut microbiota and immune responses', *Frontiers in Immunology*. Frontiers Media S.A., 13. doi: 10.3389/FIMMU.2022.1036196/FULL.

Liu, M. *et al.* (2022) 'Microbial Tryptophan Metabolism Tunes Host Immunity, Metabolism, and Extraintestinal Disorders', *Metabolites 2022, Vol. 12, Page 834*. Multidisciplinary Digital Publishing Institute, 12(9), p. 834. doi: 10.3390/METABO12090834.

Loh, G. and Blaut, M. (2012) 'Role of commensal gut bacteria in inflammatory bowel diseases', *Gut Microbes*. Taylor & Francis, 3(6), p. 544. doi: 10.4161/GMIC.22156.

Lopera-Maya, E. A. *et al.* (no date) 'Effect of host genetics on the gut microbiome in 7,738 participants of the Dutch Microbiome Project'. doi: 10.1038/s41588-021-00992-y.

Lopez-Siles, M. *et al.* (2018) 'Alterations in the Abundance and Co-occurrence of Akkermansia muciniphila and Faecalibacterium prausnitzii in the Colonic Mucosa of Inflammatory Bowel Disease Subjects', *Frontiers in Cellular and Infection*

Microbiology. Frontiers Media S.A., 8(SEP), p. 281. doi: 10.3389/FCIMB.2018.00281/FULL.

Louis, P. *et al.* (2022) 'Microbial lactate utilisation and the stability of the gut microbiome', *Gut Microbiome*. Cambridge University Press, 3, p. e3. doi: 10.1017/GMB.2022.3.

Love, M. I., Huber, W. and Anders, S. (2014) 'Moderated estimation of fold change and dispersion for RNA-seq data with DESeq2', *Genome Biology*. BioMed Central Ltd., 15(12), pp. 1–21. doi: 10.1186/S13059-014-0550-8/FIGURES/9.

Lubomski, M. *et al.* (2022) 'The Gut Microbiome in Parkinson's Disease: A Longitudinal Study of the Impacts on Disease Progression and the Use of Device-Assisted Therapies', *Frontiers in Aging Neuroscience*. Frontiers Media S.A., 14. doi: 10.3389/FNAGI.2022.875261.

Lundrigan, M. D. *et al.* (1987) 'Separate regulatory systems for the repression of metE and btuB by vitamin B12 in Escherichia coli', *Molecular & general genetics : MGG*. Mol Gen Genet, 206(3), pp. 401–407. doi: 10.1007/BF00428878.

Luo, W. *et al.* (2019) 'Roseburia intestinalis supernatant ameliorates colitis induced in mice by regulating the immune response', *Molecular Medicine Reports*. Spandidos Publications, 20(2), p. 1007. doi: 10.3892/MMR.2019.10327.

Lurz, E. *et al.* (2020) 'Vitamin B12 Deficiency Alters the Gut Microbiota in a Murine Model of Colitis', *Frontiers in Nutrition*. Frontiers Media S.A., 7, p. 541042. doi: 10.3389/FNUT.2020.00083/BIBTEX.

Macchione, I. G. *et al.* (2019) 'Akkermansia muciniphila: Key player in metabolic and gastrointestinal disorders', *European Review for Medical and Pharmacological Sciences*. Verduci Editore s.r.l, 23(18), pp. 8075–8083. doi: 10.26355/EURREV_201909_19024.

Madhogaria, B., Bhowmik, P. and Kundu, A. (2022) 'Correlation between human gut microbiome and diseases', *Infectious Medicine*. Elsevier B.V., 1(3), pp. 180–191. doi: 10.1016/J.IMJ.2022.08.004.

Magnúsdóttir, S. *et al.* (2015) 'Systematic genome assessment of B-vitamin biosynthesis suggests cooperation among gut microbes', *Frontiers in Genetics*. Frontiers Media S.A., 6(MAR), p. 129714. doi: 10.3389/FGENE.2015.00148/ABSTRACT.

Majumder, S. *et al.* (2013) 'Vitamin B12 deficiency in patients undergoing bariatric surgery: preventive strategies and key recommendations', *Surgery for obesity and related diseases : official journal of the American Society for Bariatric Surgery*. Surg Obes Relat Dis, 9(6), pp. 1013–1019. doi: 10.1016/J.SOARD.2013.04.017.

Mallott, E. K. *et al.* (2023) 'Human microbiome variation associated with race and ethnicity emerges as early as 3 months of age', *PLoS Biology*. Public Library of Science, 21(8 August). doi: 10.1371/JOURNAL.PBIO.3002230.

Manoppo, J. *et al.* (2019) 'The role of Lactobacillus reuteri DSM 17938 for the absorption of iron preparations in children with iron deficiency anemia', *Korean Journal of Pediatrics*. Korean Pediatric Society, 62(5), p. 173. doi: 10.3345/KJP.2018.07024.

Marcobal, A. *et al.* (2011) 'Bacteroides in the infant gut consume milk oligosaccharides via mucus-utilization pathways', *Cell host & microbe*. Cell Host Microbe, 10(5), pp. 507–514. doi: 10.1016/J.CHOM.2011.10.007.

Martens, J. H. *et al.* (2002) 'Microbial production of vitamin B12', *Applied Microbiology and Biotechnology*. Springer, pp. 275–285. doi: 10.1007/s00253-001-0902-7.

Martin-Gallausiaux, C. *et al.* (2024) 'Fusobacterium nucleatum promotes inflammatory and anti-apoptotic responses in colorectal cancer cells via ADP-heptose release and ALPK1/TIFA axis activation', *Gut microbes*. Gut Microbes, 16(1). doi: 10.1080/19490976.2023.2295384.

Martin, H. L. *et al.* (1999) 'Vaginal lactobacilli, microbial flora, and risk of human immunodeficiency virus type 1 and sexually transmitted disease acquisition', *Journal of Infectious Diseases*. J Infect Dis, 180(6), pp. 1863–1868. doi: 10.1086/315127.

Martín, R. *et al.* (2023) 'Faecalibacterium: a bacterial genus with promising human health applications', *FEMS Microbiology Reviews*. Oxford University Press, 47(4), pp. 1–18. doi: 10.1093/FEMSRE/FUAD039.

Martínez-Martínez, Misael *et al.* (2024) 'Influence of feeding practices in the composition and functionality of infant gut microbiota and its relationship with health', *PloS one*. Edited by R. Singh. PLoS One, 19(1), p. e0294494. doi: 10.1371/JOURNAL.PONE.0294494.

Martinson, J. N. V. *et al.* (2019) 'Rethinking gut microbiome residency and the Enterobacteriaceae in healthy human adults', *The ISME journal*. ISME J, 13(9), pp. 2306–2318. doi: 10.1038/S41396-019-0435-7.

Mascarenhas, R. *et al.* (2022) 'Human B12-dependent enzymes: Methionine synthase and Methylmalonyl-CoA mutase', *Methods in enzymology*. NIH Public Access, 668, p. 309. doi: 10.1016/BS.MIE.2021.12.012.

Masters, C. L. *et al.* (1985) 'Amyloid plaque core protein in Alzheimer disease and Down syndrome.', *Proceedings of the National Academy of Sciences*. Proceedings of the National Academy of Sciences, 82(12), pp. 4245–4249. doi: 10.1073/PNAS.82.12.4245.

Mazmanian, S. K., Round, J. L. and Kasper, D. L. (2008) 'A microbial symbiosis factor prevents intestinal inflammatory disease', *Nature*. Nature Publishing Group, 453(7195), pp. 620–625. doi: 10.1038/NATURE07008.

McCallum, G. and Tropini, C. (2023) 'The gut microbiota and its biogeography', *Nature Reviews Microbiology*. Nature Research. doi: 10.1038/S41579-023-00969-0.

McClure, R. *et al.* (2013) 'Computational analysis of bacterial RNA-Seq data', *Nucleic Acids Research*. Oxford University Press, 41(14), p. e140. doi: 10.1093/NAR/GKT444.

McLean, N. W. and Rosenstein, I. J. (2000) 'Characterisation and selection of a Lactobacillus species to re-colonise the vagina of women with recurrent bacterial vaginosis', *Journal of Medical Microbiology*. Lippincott Williams and Wilkins, 49(6), pp. 543–552. doi: 10.1099/0022-1317-49-6-543.

Mendoza, J. *et al.* (2023) 'Structure of full-length cobalamin-dependent methionine synthase and cofactor loading captured in crystallo', *Nature Communications 2023 14:1*. Nature Publishing Group, 14(1), pp. 1–12. doi: 10.1038/s41467-023-42037-4.

Mennella, J. A. *et al.* (2022) 'The Macronutrient Composition of Infant Formula Produces Differences in Gut Microbiota Maturation That Associates with Weight Gain Velocity and Weight Status', *Nutrients*, 14(6). doi: 10.3390/nu14061241.

Meroth, C. B. *et al.* (2003) 'Monitoring the bacterial population dynamics in sourdough fermentation processes by using PCR-denaturing gradient gel electrophoresis', *Applied and Environmental Microbiology*. Appl Environ Microbiol, 69(1), pp. 475–482. doi: 10.1128/AEM.69.1.475-482.2003.

Merrick, B. *et al.* (2023) 'Modulation of the Gut Microbiota to Control Antimicrobial Resistance (AMR)—A Narrative Review with a Focus on Faecal Microbiota Transplantation (FMT)', *Infectious Disease Reports*. Multidisciplinary Digital Publishing Institute (MDPI), 15(3), pp. 238–254. doi: 10.3390/IDR15030025.

Meyer, M. (2019) 'Processing of collagen based biomaterials and the resulting materials properties', *BioMedical Engineering OnLine 2019 18:1*. BioMed Central, 18(1), pp. 1–74. doi: 10.1186/S12938-019-0647-0.

Milani, C. *et al.* (2017) 'The First Microbial Colonizers of the Human Gut: Composition, Activities, and Health Implications of the Infant Gut Microbiota', *Microbiology and Molecular Biology Reviews*. American Society for Microbiology, 81(4). doi: 10.1128/mmbr.00036-17.

Mineharu, Y. *et al.* (2022) 'Increased abundance of Ruminococcus gnavus in gut microbiota is associated with moyamoya disease and non-moyamoya intracranial large artery disease', *Scientific Reports 2022 12:1*. Nature Publishing Group, 12(1), pp. 1–15. doi: 10.1038/s41598-022-24496-9.

Minot, G. R. and Murphy, W. P. (1926) 'Treatment of pernicious anemia by a special diet', *Journal of the American Medical Association*, 87(7), pp. 470–476. doi: 10.1001/JAMA.1926.02680070016005.

Mitrea, L. *et al.* (2022) 'Guts Imbalance Imbalances the Brain: A Review of Gut Microbiota Association With Neurological and Psychiatric Disorders', *Frontiers in Medicine*. Frontiers Media S.A., 9, p. 813204. doi: 10.3389/FMED.2022.813204/FULL.

Mohammad, F. K. *et al.* (2022) 'A Computational Framework for Studying Gut-Brain Axis in Autism Spectrum Disorder', *Frontiers in Physiology*. Frontiers Media S.A., 13, p. 760753. doi: 10.3389/FPHYS.2022.760753/BIBTEX.

Mok, K. C. *et al.* (2020) 'Identification of a Novel Cobamide Remodeling Enzyme in the Beneficial Human Gut Bacterium Akkermansia muciniphila', *mBio*. American Society for Microbiology (ASM), 11(6), pp. 1–18. doi: 10.1128/MBIO.02507-20.

Mok, K. C. and Taga, M. E. (2013) 'Growth inhibition of Sporomusa ovata by incorporation of benzimidazole bases into cobamides', *Journal of bacteriology*. J Bacteriol, 195(9), pp. 1902–1911. doi: 10.1128/JB.01282-12.

Monsen, A. L. B. *et al.* (2001) 'Determinants of Cobalamin Status in Newborns', *Pediatrics*. American Academy of Pediatrics, 108(3), pp. 624–630. doi: 10.1542/PEDS.108.3.624.

Monte, M. J. *et al.* (2009) 'Bile acids: Chemistry, physiology, and pathophysiology', *World Journal of Gastroenterology*. Baishideng Publishing Group Co, 15(7), pp. 804–816. doi: 10.3748/WJG.15.804.

Moore, S. J. *et al.* (2013) 'Elucidation of the anaerobic pathway for the corrin component of cobalamin (vitamin B12)', *Proceedings of the National Academy of Sciences of the United States of America*. National Academy of Sciences, 110(37), pp. 14906–14911. doi: 10.1073/PNAS.1308098110/SUPPL_FILE/PNAS.201308098SI.PDF.

Moore, S. J. and Warren, M. J. (2012) 'The anaerobic biosynthesis of vitamin B12', in *Biochemical Society Transactions*, pp. 581–586. doi: 10.1042/BST20120066.

Moore, W. E. C. and Holdeman, L. V. (1974a) 'Human Fecal Flora: The Normal Flora of 20 Japanese-Hawaiians', *Applied Microbiology*. American Society for Microbiology, 27(5), pp. 961–979. doi: 10.1128/AM.27.5.961-979.1974.

Moore, W. E. C. and Holdeman, L. V. (1974b) 'Human Fecal Flora: The Normal Flora of 20 Japanese-Hawaiians', *Applied Microbiology*. American Society for Microbiology, 27(5), pp. 961–979. doi: 10.1128/AM.27.5.961-979.1974.

Moore, W. E. C., Johnson, J. L. and Holdeman, L. V. (1976) 'Emendation of Bacteroidaceae and Butyrivibrio and descriptions of Desulfomonas gen. nov. and ten new species in the genera Desulfomonas, Butyrivibrio, Eubacterium, Clostridium, and Ruminococcus', *International Journal of Systematic Bacteriology*. Microbiology Society, 26(2), pp. 238–252. doi: 10.1099/00207713-26-2-238.

Morgan, X. C. *et al.* (2012) 'Dysfunction of the intestinal microbiome in inflammatory bowel disease and treatment', *Genome biology*. Genome Biol, 13(9). doi: 10.1186/GB-2012-13-9-R79.

Morimoto, T. *et al.* (2016) 'Significant Association of the RNF213 p.R4810K Polymorphism with Quasi-Moyamoya Disease', *Journal of stroke and cerebrovascular diseases : the official journal of National Stroke Association*. J Stroke Cerebrovasc Dis, 25(11), pp. 2632–2636. doi: 10.1016/J.JSTROKECEREBROVASDIS.2016.07.004.

Morita, H. *et al.* (2008) 'Comparative Genome Analysis of Lactobacillus reuteri and Lactobacillus fermentum Reveal a Genomic Island for Reuterin and Cobalamin Production', *DNA Research*. Oxford Academic, 15(3), pp. 151–161. doi: 10.1093/dnares/dsn009.

Morton, J. T. *et al.* (2023) 'Multi-level analysis of the gut–brain axis shows autism spectrum disorder-associated molecular and microbial profiles', *Nature Neuroscience 2023 26:7*. Nature Publishing Group, 26(7), pp. 1208–1217. doi: 10.1038/s41593-023-01361-0.

Mu, Q., Tavella, V. J. and Luo, X. M. (2018) 'Role of Lactobacillus reuteri in human health and diseases', *Frontiers in Microbiology*. Frontiers Media S.A., p. 757. doi: 10.3389/fmicb.2018.00757.

Mukhopadhya, I. *et al.* (2022) 'Comparison of microbial signatures between paired faecal and rectal biopsy samples from healthy volunteers using next-generation sequencing and culturomics', *Microbiome*. BMC, 10(1). doi: 10.1186/S40168-022-01354-4.

Mullish, B. H. *et al.* (2019) 'Microbial bile salt hydrolases mediate the efficacy of faecal microbiota transplant in the treatment of recurrent Clostridioides difficile infection', *Gut*. BMJ Publishing Group, 68(10), pp. 1791–1800. doi: 10.1136/GUTJNL-2018-317842.

Mullish, B. H., McDonald, J. A. K. and Marchesi, J. R. (2022) 'Intestinal microbiota transplantation: do not forget the metabolites', *The Lancet Gastroenterology & Hepatology*. Elsevier, 7(7), p. 594. doi: 10.1016/S2468-1253(22)00101-7.

Nakano, E. *et al.* (2011) 'Riboflavin depletion impairs cell proliferation in adult human duodenum: Identification of potential effectors', *Digestive Diseases and Sciences*,

56(4), pp. 1007–1019. doi: 10.1007/S10620-010-1374-3.

Ndeh, D. and Gilbert, H. J. (2018) 'Biochemistry of complex glycan depolymerisation by the human gut microbiota', *FEMS Microbiology Reviews*. Oxford University Press, pp. 146–164. doi: 10.1093/femsre/fuy002.

Neil, E. and Marsh, G. (1999) 'Coenzyme B12 (cobalamin)-dependent enzymes', *Essays in biochemistry*. Essays Biochem, 34, pp. 139–154. doi: 10.1042/BSE0340139.

Neurath, M. F. (2020) 'Host–microbiota interactions in inflammatory bowel disease', *Nature Reviews Gastroenterology and Hepatology*. Nature Research, 17(2), pp. 76–77. doi: 10.1038/S41575-019-0248-1.

Nie, K. *et al.* (2021) 'Roseburia intestinalis: A Beneficial Gut Organism From the Discoveries in Genus and Species', *Frontiers in Cellular and Infection Microbiology*. Frontiers Media S.A., 11. doi: 10.3389/FCIMB.2021.757718/FULL.

NIH Office of Dietary Supplements. Dietary Supplement Label Database (DSLD). (2022) (no date). Available at: https://dsld.od.nih.gov/search/cyanocobalamin/bWFya2V0X3N0YXR1cz1vbl9tYXJrZXQvZW50cnlfZGF0ZT0yMDExLDIwMjIvc29ydD1uZXdlc3Qvdmlldz0xL3BhZ2Vfc2l6ZT0xMDAv.

Nishiwaki, H., Ueyama, J., *et al.* (2022) 'Gut microbiota in dementia with Lewy bodies', *npj Parkinson's Disease 2022 8:1*. Nature Publishing Group, 8(1), pp. 1–10. doi: 10.1038/s41531-022-00428-2.

Nishiwaki, H., Ito, M., *et al.* (2022) 'Short chain fatty acids-producing and mucin-degrading intestinal bacteria predict the progression of early Parkinson's disease', *npj Parkinson's Disease 2022 8:1*. Nature Publishing Group, 8(1), pp. 1–12. doi: 10.1038/s41531-022-00328-5.

Nomura, K. *et al.* (2021) 'Bacteroidetes species are correlated with disease activity in ulcerative colitis', *Journal of Clinical Medicine*. MDPI, 10(8), p. 1749. doi: 10.3390/JCM10081749/S1.

Notarbartolo, V. *et al.* (2023) 'The First 1000 Days of Life: How Changes in the Microbiota Can Influence Food Allergy Onset in Children', *Nutrients 2023, Vol. 15, Page 4014*. Multidisciplinary Digital Publishing Institute, 15(18), p. 4014. doi: 10.3390/NU15184014.

O'Hara, A. M. and Shanahan, F. (2006) 'The gut flora as a forgotten organ', *EMBO Reports*, 7(7), pp. 688–693. doi: 10.1038/SJ.EMBOR.7400731.

Ochoa-Repáraz, J. *et al.* (2009) 'Role of gut commensal microflora in the development of experimental autoimmune encephalomyelitis', *Journal of immunology (Baltimore, Md. : 1950)*. J Immunol, 183(10), pp. 6041–6050. doi: 10.4049/JIMMUNOL.0900747.

Odamaki, T. *et al.* (2016) 'Age-related changes in gut microbiota composition from newborn to centenarian: a cross-sectional study', *BMC microbiology*. BMC Microbiol, 16(1). doi: 10.1186/S12866-016-0708-5.

Oh, P. L. *et al.* (2010) 'Diversification of the gut symbiont lactobacillus reuteri as a result of host-driven evolution', *ISME Journal*. Nature Publishing Group, 4(3), pp. 377–387. doi: 10.1038/ismej.2009.123.

Olaisen, M. *et al.* (2021) 'Bacterial Mucosa-associated Microbiome in Inflamed and

Proximal Noninflamed Ileum of Patients With Crohn's Disease', *Inflammatory bowel diseases*. Inflamm Bowel Dis, 27(1), pp. 12–24. doi: 10.1093/IBD/IZAA107.

Otte, M. M. and Escalante-Semerena, J. C. (2009) 'Biochemical characterization of the GTP:Adenosylcobinamide-phosphate guanylyltransferase (CobY) enzyme of the hyperthermophilic archaeon Methanocaldococcus jannaschii', *Biochemistry*, 48(25), pp. 5882–5889. doi: 10.1021/BI8023114.

Oviedo-Boyso, J., Bravo-Patiño, A. and Baizabal-Aguirre, V. M. (2014) 'Collaborative Action of Toll-Like and Nod-Like Receptors as Modulators of the Inflammatory Response to Pathogenic Bacteria', *Mediators of Inflammation*. Wiley, 2014. doi: 10.1155/2014/432785.

Owen, C. D. *et al.* (2017) 'Unravelling the specificity and mechanism of sialic acid recognition by the gut symbiont Ruminococcus gnavus', *Nature communications*. Nat Commun, 8(1). doi: 10.1038/S41467-017-02109-8.

Palmieri, O. *et al.* (2023) 'Mucosal Microbiota from Colorectal Cancer, Adenoma and Normal Epithelium Reveals the Imprint of Fusobacterium nucleatum in Cancerogenesis', *Microorganisms*. MDPI, 11(5), p. 1147. doi: 10.3390/MICROORGANISMS11051147/S1.

Panda, S. *et al.* (2014) 'Short-term effect of antibiotics on human gut microbiota', *PLoS ONE*. Public Library of Science, 9(4). doi: 10.1371/journal.pone.0095476.

Park, J. C. and Im, S. H. (2020) 'Of men in mice: the development and application of a humanized gnotobiotic mouse model for microbiome therapeutics', *Experimental & Molecular Medicine 2020 52:9*. Nature Publishing Group, 52(9), pp. 1383–1396. doi: 10.1038/s12276-020-0473-2.

Park, S., Kang, S. and Sol Kim, D. (2019) 'Folate and vitamin B-12 deficiencies additively impaire memory function and disturb the gut microbiota in amyloid-β infused rats', *https://doi.org/10.1024/0300-9831/a000624*. Hogrefe AG , 92(3–4), pp. 169–181. doi: 10.1024/0300-9831/A000624.

Parmanand, B. A. *et al.* (2019) 'A decrease in iron availability to human gut microbiome reduces the growth of potentially pathogenic gut bacteria; an in vitro colonic fermentation study', *The Journal of Nutritional Biochemistry*. Elsevier, 67, p. 20. doi: 10.1016/J.JNUTBIO.2019.01.010.

Patterson, A. M. *et al.* (2017) 'Human gut symbiont Roseburia hominis promotes and regulates innate immunity', *Frontiers in Immunology*. Frontiers Media S.A., 8(SEP), p. 281394. doi: 10.3389/FIMMU.2017.01166/BIBTEX.

Paulson, J. N. *et al.* (2013) 'Differential abundance analysis for microbial marker-gene surveys', *Nature Methods 2013 10:12*. Nature Publishing Group, 10(12), pp. 1200–1202. doi: 10.1038/nmeth.2658.

Peng, K. *et al.* (2023) 'Butyrate and obesity: Current research status and future prospect', *Frontiers in Endocrinology*. Frontiers Media S.A., 14, p. 1098881. doi: 10.3389/FENDO.2023.1098881/BIBTEX.

Pérez, A. A., Rodionov, D. A. and Bryant, D. A. (2016) 'Identification and Regulation of Genes for Cobalamin Transport in the Cyanobacterium Synechococcus sp. Strain PCC 7002', *Journal of Bacteriology*. American Society for Microbiology (ASM), 198(19), p. 2753. doi: 10.1128/JB.00476-16.

Peterson, J. *et al.* (2009) 'The NIH Human Microbiome Project', *Genome Research*. Cold Spring Harbor Laboratory Press, 19(12), pp. 2317–2323. doi: 10.1101/gr.096651.109.

Pfeiffer, F. *et al.* (2008) 'Evolution in the laboratory: The genome of Halobacterium salinarum strain R1 compared to that of strain NRC-1', *Genomics*, 91(4), pp. 335–346. doi: 10.1016/j.ygeno.2008.01.001.

Pollich, M. and Klug, G. (1995) 'Identification and sequence analysis of genes involved in late steps of cobalamin (vitamin B12) synthesis in Rhodobacter capsulatus', *Journal of Bacteriology*. American Society for Microbiology, 177(15), pp. 4481–4487. doi: 10.1128/JB.177.15.4481-4487.1995.

Price, C. E. *et al.* (2024) 'Intestinal Bacteroides modulates inflammation, systemic cytokines, and microbial ecology via propionate in a mouse model of cystic fibrosis', *mBio*. American Society for Microbiology, 15(2). doi: 10.1128/MBIO.03144-23.

Pritchard, S. E. *et al.* (2014) 'Fasting and postprandial volumes of the undisturbed colon: normal values and changes in diarrhea-predominant irritable bowel syndrome measured using serial MRI', *Neurogastroenterology and motility*. Neurogastroenterol Motil, 26(1), pp. 124–130. doi: 10.1111/NMO.12243.

Qin, J. *et al.* (2010) 'A human gut microbial gene catalogue established by metagenomic sequencing', *Nature*. Nature Publishing Group, 464(7285), pp. 59–65. doi: 10.1038/nature08821.

Qin, Y. *et al.* (2022) 'Combined effects of host genetics and diet on human gut microbiota and incident disease in a single population cohort', *Nature Genetics 2022 54:2*. Nature Publishing Group, 54(2), pp. 134–142. doi: 10.1038/s41588-021-00991-z.

Rahman, S. *et al.* (2023) 'Gut microbial metabolites and its impact on human health'. doi: 10.20524/aog.2023.0809.

Ramakrishna, C. *et al.* (2019) 'Bacteroides fragilis polysaccharide A induces IL-10 secreting B and T cells that prevent viral encephalitis', *Nature Communications*. Nature Publishing Group, 10(1). doi: 10.1038/S41467-019-09884-6.

Ramare, F. *et al.* (1993) 'Trypsin-dependent production of an antibacterial substance by a human Peptostreptococcus strain in gnotobiotic rats and in vitro.', *Applied and Environmental Microbiology*, 59(9).

Rao Jala, V. *et al.* (2020) 'Current Sampling Methods for Gut Microbiota: A Call for More Precise Devices', *Frontiers in Cellular and Infection Microbiology | www.frontiersin.org*, 1, p. 151. doi: 10.3389/fcimb.2020.00151.

Rasmussen, S. A., Fernhoff, P. M. and Scanlon, K. S. (2001) 'Vitamin B12 deficiency in children and adolescents', *The Journal of Pediatrics*. Mosby, 138(1), pp. 10–17. doi: 10.1067/MPD.2001.112160.

Rattanaprasert, M. *et al.* (2014) 'Quantitative evaluation of synbiotic strategies to improve persistence and metabolic activity of Lactobacillus reuteri DSM 17938 in the human gastrointestinal tract', *Journal of Functional Foods*. Elsevier Ltd, 10, pp. 85–94. doi: 10.1016/j.jff.2014.05.017.

Raux, E. *et al.* (1996) 'Salmonella typhimurium cobalamin (vitamin B12) biosynthetic genes: Functional studies in S. typhimurium and Escherichia coli', *Journal of Bacteriology*. American Society for Microbiology, 178(3), pp. 753–767. doi:

10.1128/jb.178.3.753-767.1996.

Raux, E. *et al.* (1998) 'Cobalamin (vitamin B12) biosynthesis: functional characterization of the Bacillus megaterium cbi genes required to convert uroporphyrinogen III into cobyrinic acid a,c-diamide.', *Biochemical Journal*. Portland Press Ltd, 335(Pt 1), p. 167. doi: 10.1042/BJ3350167.

RAUX, E. *et al.* (1999) 'The role of Saccharomyces cerevisiae Met1p and Met8p in sirohaem and cobalamin biosynthesis', *Biochemical Journal*. Portland Press Ltd., 338(3), pp. 701–708. doi: 10.1042/bj3380701.

Reed, K. K. and Wickham, R. (2009) 'Review of the Gastrointestinal Tract: From Macro to Micro', *Seminars in Oncology Nursing*. W.B. Saunders, 25(1), pp. 3–14. doi: 10.1016/J.SONCN.2008.10.002.

Rempel, S. *et al.* (2018) 'Cysteine-mediated decyanation of vitamin B12 by the predicted membrane transporter BtuM', *Nature communications*. Nat Commun, 9(1). doi: 10.1038/S41467-018-05441-9.

Ren, J. *et al.* (2023) 'Gut microbiome-mediated mechanisms in aging-related diseases: are probiotics ready for prime time?', *Frontiers in Pharmacology*. Frontiers Media S.A., 14. doi: 10.3389/FPHAR.2023.1178596.

Ren, Y., Liu, W. and Zhang, H. (2015) 'Identification of coccoidal bacteria in traditional fermented milk products from Mongolia, and the fermentation properties of the predominant species, Streptococcus thermophilus', *Korean Journal for Food Science of Animal Resources*. Korean Society for Food Science of Animal Resources, 35(5), pp. 683–691. doi: 10.5851/KOSFA.2015.35.5.683.

Reyman, M. *et al.* (2022) 'Effects of early-life antibiotics on the developing infant gut microbiome and resistome: a randomized trial', *Nature Communications 2022 13:1*. Nature Publishing Group, 13(1), pp. 1–12. doi: 10.1038/s41467-022-28525-z.

Rickes, E. L. *et al.* (1948) 'Crystalline vitamin B12', *Science*. American Association for the Advancement of Science , 107(2781), pp. 396–397. doi: 10.1126/SCIENCE.107.2781.396/ASSET/95A1FD25-CB89-4E25-96C1-773498DD4D6A/ASSETS/SCIENCE.107.2781.396.FP.PNG.

Rios-Covian, D. *et al.* (2020) 'An Overview on Fecal Branched Short-Chain Fatty Acids Along Human Life and as Related With Body Mass Index: Associated Dietary and Anthropometric Factors', *Frontiers in Microbiology*. Frontiers Media S.A., 11. doi: 10.3389/FMICB.2020.00973/FULL.

Rizzatti, G. *et al.* (2017) 'Proteobacteria: A Common Factor in Human Diseases', *BioMed Research International*. Wiley, 2017. doi: 10.1155/2017/9351507.

Robbe, C. *et al.* (2003) 'Evidence of regio-specific glycosylation in human intestinal mucins: presence of an acidic gradient along the intestinal tract', *The Journal of biological chemistry*. J Biol Chem, 278(47), pp. 46337–46348. doi: 10.1074/JBC.M302529200.

Robbe, C. *et al.* (2004) 'Structural diversity and specific distribution of O-glycans in normal human mucins along the intestinal tract', *Biochemical Journal*, 384(2), pp. 307–316. doi: 10.1042/BJ20040605.

Roblin, C. *et al.* (2020) 'The unusual structure of Ruminococcin C1 antimicrobial peptide confers clinical properties', *Proceedings of the National Academy of Sciences*

of the United States of America. Proc Natl Acad Sci U S A, 117(32), pp. 19168–19177. doi: 10.1073/PNAS.2004045117.

Roblin, C. *et al.* (2021) 'The Multifunctional Sactipeptide Ruminococcin C1 Displays Potent Antibacterial Activity In Vivo as Well as Other Beneficial Properties for Human Health', *International journal of molecular sciences*. Int J Mol Sci, 22(6). doi: 10.3390/IJMS22063253.

Robscheit-Robbins, F. S. and Whipple, G. H. (1925) 'BLOOD REGENERATION IN SEVERE ANEMIA', *https://doi.org/10.1152/ajplegacy.1925.72.3.408*. American Physiological Society, 72(3), pp. 408–418. doi: 10.1152/AJPLEGACY.1925.72.3.408.

Rodionov, D. A. *et al.* (2003) 'Comparative Genomics of the Vitamin B12 Metabolism and Regulation in Prokaryotes', *Journal of Biological Chemistry*, 278(42), pp. 41148–41159. doi: 10.1074/jbc.M305837200.

Rodionov, D. A. *et al.* (2009) 'A novel class of modular transporters for vitamins in prokaryotes', *Journal of bacteriology*. J Bacteriol, 191(1), pp. 42–51. doi: 10.1128/JB.01208-08.

Rodríguez-Piñeiro, A. M. *et al.* (2013) 'Studies of mucus in mouse stomach, small intestine, and colon. II. Gastrointestinal mucus proteome reveals Muc2 and Muc5ac accompanied by a set of core proteins', *American journal of physiology. Gastrointestinal and liver physiology*. Am J Physiol Gastrointest Liver Physiol, 305(5). doi: 10.1152/AJPGI.00047.2013.

Rodríguez, J. M. *et al.* (2015) 'The composition of the gut microbiota throughout life, with an emphasis on early life', *Microbial ecology in health and disease*. Microb Ecol Health Dis, 26(0). doi: 10.3402/MEHD.V26.26050.

Romano, S. *et al.* (2021) 'Meta-analysis of the Parkinson's disease gut microbiome suggests alterations linked to intestinal inflammation', *npj Parkinson's Disease 2021 7:1*. Nature Publishing Group, 7(1), pp. 1–13. doi: 10.1038/s41531-021-00156-z.

Roncal, C. *et al.* (2019) 'Trimethylamine-N-Oxide (TMAO) Predicts Cardiovascular Mortality in Peripheral Artery Disease', *Scientific Reports*. Nature Publishing Group, 9(1). doi: 10.1038/S41598-019-52082-Z.

Roth, J. R. *et al.* (1993) *Characterization of the Cobalamin (Vitamin B12) Biosynthetic Genes of Salmonella typhimurium Downloaded from*, *JOURNAL OF BACTERIOLOGY*. Available at: http://jb.asm.org/ (Accessed: 15 April 2021).

Roth, J. R., Lawrence, J. G. and Bobik, T. A. (1996) 'Cobalamin (coenzyme B12): Synthesis and biological significance', *Annual Review of Microbiology*. Annu Rev Microbiol, 50, pp. 137–181. doi: 10.1146/annurev.micro.50.1.137.

Sagheddu, V. *et al.* (2016) 'Infant Early Gut Colonization by Lachnospiraceae: High Frequency of Ruminococcus gnavus', *Frontiers in pediatrics*. Front Pediatr, 4(JUN). doi: 10.3389/FPED.2016.00057.

Sagheddu, V. *et al.* (2020) 'The Biotherapeutic Potential of Lactobacillus reuteri Characterized Using a Target-Specific Selection Process', *Frontiers in Microbiology*. Frontiers Media S.A., 11, p. 532. doi: 10.3389/FMICB.2020.00532/BIBTEX.

Salyers, A. . (1994) 'Bacterial pathogenesis. A molecular approach', p. pp.190-204.

Salzman, N. H. (2011) 'Microbiota-immune system interaction: An uneasy alliance',

Current Opinion in Microbiology, 14(1), pp. 99–105. doi: 10.1016/J.MIB.2010.09.018.

Santos, F. *et al.* (2007) 'Pseudovitamin B12 is the corrinoid produced by Lactobacillus reuteri CRL1098 under anaerobic conditions', *FEBS Letters*. FEBS Lett, 581(25), pp. 4865–4870. doi: 10.1016/j.febslet.2007.09.012.

Santos, F., Wegkamp, A., *et al.* (2008) 'High-level folate production in fermented foods by the B12 producer Lactobacillus reuteri JCM1112', *Applied and Environmental Microbiology*. Appl Environ Microbiol, 74(10), pp. 3291–3294. doi: 10.1128/AEM.02719-07.

Santos, F., Vera, J. L., *et al.* (2008) 'The complete coenzyme B12 biosynthesis gene cluster of Lactobacillus reuteri CRL1098', *Microbiology*. Microbiology Society, 154(1), pp. 81–93. doi: 10.1099/mic.0.2007/011569-0.

Santos, J. A. *et al.* (2018) 'Functional and structural characterization of an ECF-type ABC transporter for vitamin B12'. doi: 10.7554/eLife.35828.001.

Dos Santos, S. J. *et al.* (2023) 'Maternal vaginal microbiome composition does not affect development of the infant gut microbiome in early life', *Frontiers in Cellular and Infection Microbiology*. Frontiers Media S.A., 13. doi: 10.3389/FCIMB.2023.1144254.

Sarafoglou, K. *et al.* (2011) 'Expanded Newborn Screening for Detection of Vitamin B12 Deficiency', *JAMA*. American Medical Association, 305(12), pp. 1198–1200. doi: 10.1001/JAMA.2011.310.

Schroeder, B. O. (2019) 'Fight them or feed them: How the intestinal mucus layer manages the gut microbiota', *Gastroenterol. Rep. (Oxf.)*. Oxford University Press, 7(1), pp. 3–12. doi: 10.1093/gastro/goy052.

Scott, A. I. and Roessner, C. A. (2002) 'Biosynthesis of cobalamin (vitamin B(12))', *Biochemical Society transactions*. Biochem Soc Trans, 30(4), pp. 613–620. doi: 10.1042/BST0300613.

Seekatz, A. M. *et al.* (2018) 'Restoration of short chain fatty acid and bile acid metabolism following fecal microbiota transplantation in patients with recurrent Clostridium difficile infection', *Anaerobe*. Academic Press, 53, pp. 64–73. doi: 10.1016/J.ANAEROBE.2018.04.001.

Seekatz, A. M. *et al.* (2019) 'Spatial and Temporal Analysis of the Stomach and Small-Intestinal Microbiota in Fasted Healthy Humans', *mSphere*. American Society for Microbiology, 4(2). doi: 10.1128/MSPHERE.00126-19.

Seetharam, B. and Alpers, D. H. (1982) 'Absorption and transport of cobalamin (vitamin B12).', *Annual review of nutrition*. Annu Rev Nutr, pp. 343–369. doi: 10.1146/annurev.nu.02.070182.002015.

Segata, N. *et al.* (2011) 'Metagenomic biomarker discovery and explanation', *Genome Biology*. BMC, 12(6), p. R60. doi: 10.1186/GB-2011-12-6-R60.

Selma-Royo, M. *et al.* (2020) 'Perinatal environment shapes microbiota colonization and infant growth: impact on host response and intestinal function', *Microbiome*. BioMed Central Ltd, 8(1), pp. 1–19. doi: 10.1186/S40168-020-00940-8/TABLES/1.

Sender, R., Fuchs, S. and Milo, R. (2016) 'Revised Estimates for the Number of Human and Bacteria Cells in the Body', *PLOS Biology*. Deutscher Apotheker Verlag, 14(8), p. e1002533. doi: 10.1371/journal.pbio.1002533.

SG, S. and JM, G. (2019) ‘Chemical and Clinical Aspects of Metal-Containing Antidotes for Poisoning by Cyanide’, *Metal ions in life sciences*. Met Ions Life Sci, 19, pp. 359–392. doi: 10.1515/9783110527872-020.

Shah, T. *et al.* (2017) ‘Combination of vitamin B12 active forms improved fetal growth in Wistar rats through up-regulation of placental miR-16 and miR-21 levels’, *Life sciences*. Life Sci, 191, pp. 97–103. doi: 10.1016/J.LFS.2017.10.017.

Sharma, V. *et al.* (2019) ‘B-Vitamin sharing promotes stability of gut microbial communities’, *Frontiers in Microbiology*. Frontiers Media S.A., 10(JUL), p. 447172. doi: 10.3389/FMICB.2019.01485/BIBTEX.

Shaw, S. *et al.* (2022) ‘Gut Mucosal Microbiome Signatures of Colorectal Cancer Differ According to BMI Status’, *Frontiers in Medicine*. Frontiers Media S.A., 8, p. 800566. doi: 10.3389/FMED.2021.800566/BIBTEX.

Shelton, A. N. *et al.* (2018) ‘Uneven distribution of cobamide biosynthesis and dependence in bacteria predicted by comparative genomics’, *The ISME Journal*, 13, pp. 789–804. doi: 10.1038/s41396-018-0304-9.

Shepherd, G. and Velez, L. I. (2008) ‘Role of hydroxocobalamin in acute cyanide poisoning’, *Annals of Pharmacotherapy*, 42(5), pp. 661–669. doi: 10.1345/aph.1K559.

Shin, N. R., Whon, T. W. and Bae, J. W. (2015) ‘Proteobacteria: Microbial signature of dysbiosis in gut microbiota’, *Trends in Biotechnology*. Elsevier Ltd, 33(9), pp. 496–503. doi: 10.1016/j.tibtech.2015.06.011.

Shu-Wei Su, M. *et al.* (2012) ‘Intestinal Origin of Sourdough Lactobacillus reuteri Isolates as Revealed by Phylogenetic, Genetic, and Physiological Analysis’. doi: 10.1128/AEM.01678-12.

Sivashanmugam, A. *et al.* (2009) ‘Practical protocols for production of very high yields of recombinant proteins using Escherichia coli’, *Protein Science : A Publication of the Protein Society*. Wiley, 18(5), p. 936. doi: 10.1002/PRO.102.

Skrzypczak-Wiercioch, A. and Sałat, K. (2022) ‘Lipopolysaccharide-Induced Model of Neuroinflammation: Mechanisms of Action, Research Application and Future Directions for Its Use’, *Molecules*. Multidisciplinary Digital Publishing Institute (MDPI), 27(17). doi: 10.3390/MOLECULES27175481.

Smajdor, J. *et al.* (2023) ‘The impact of gut bacteria producing long chain homologs of vitamin K2 on colorectal carcinogenesis’, *Cancer Cell International*. BioMed Central Ltd, 23(1), pp. 1–14. doi: 10.1186/S12935-023-03114-2/FIGURES/3.

Smith, T. (1897) ‘A MODIFICATION OF THE METHOD FOR DETERMINING THE PRODUCTION OF INDOL BY BACTERIA’, *Journal of Experimental Medicine*. The Rockefeller University Press, 2(5), pp. 543–547. doi: 10.1084/JEM.2.5.543.

Sokolovskaya, O. M. *et al.* (2019) ‘Cofactor Selectivity in Methylmalonyl Coenzyme A Mutase, a Model Cobamide-Dependent Enzyme’, *mBio*. American Society for Microbiology (ASM), 10(5). doi: 10.1128/MBIO.01303-19.

Sokolovskaya, O. M., Shelton, A. N. and Taga, M. E. (2020) ‘Sharing vitamins: Cobamides unveil microbial interactions’, *Science*. American Association for the Advancement of Science, 369(6499), pp. 48-+. doi: 10.1126/SCIENCE.ABA0165.

Song, C. *et al.* (2023) ‘Intestinal mucus components and secretion mechanisms: what

we do and do not know', *Experimental & Molecular Medicine*. Korean Society for Biochemistry and Molecular Biology, 55(4), p. 681. doi: 10.1038/S12276-023-00960-Y.

Soto, A. *et al.* (2014) 'Lactobacilli and bifidobacteria in human breast milk: Influence of antibiotherapy and other host and clinical factors', *Journal of Pediatric Gastroenterology and Nutrition*. Lippincott Williams and Wilkins, 59(1), pp. 78–88. doi: 10.1097/MPG.0000000000000347.

Sriramulu, D. D. *et al.* (2008) 'Lactobacillus reuteri DSM 20016 produces cobalamin-dependent diol dehydratase in metabolosomes and metabolizes 1,2-propanediol by disproportionation', *Journal of Bacteriology*. American Society for Microbiology Journals, 190(13), pp. 4559–4567. doi: 10.1128/JB.01535-07.

Stamford, N. P. J. *et al.* (1997) 'Biosynthesis of vitamin B12: The multi-enzyme synthesis of precorrin-4 and factor IV', *Chemistry and Biology*. Elsevier Ltd, 4(6), pp. 445–451. doi: 10.1016/S1074-5521(97)90196-4.

Steinert, R. E. *et al.* (2016) 'The prebiotic concept and human health: A changing landscape with riboflavin as a novel prebiotic candidate', *European Journal of Clinical Nutrition*. Nature Publishing Group, 70(12), pp. 1348–1353. doi: 10.1038/EJCN.2016.119.

Stojanov, S., Berlec, A. and Štrukelj, B. (2020) 'The Influence of Probiotics on the Firmicutes/Bacteroidetes Ratio in the Treatment of Obesity and Inflammatory Bowel disease', *Microorganisms 2020, Vol. 8, Page 1715*. Multidisciplinary Digital Publishing Institute, 8(11), p. 1715. doi: 10.3390/MICROORGANISMS8111715.

STUPPERICH, E. and NEXØ, E. (1991) 'Effect of the cobalt-N coordination on the cobamide recognition by the human vitamin B12 binding proteins intrinsic factor, transcobalamin and haptocorrin', *European journal of biochemistry*. Eur J Biochem, 199(2), pp. 299–303. doi: 10.1111/J.1432-1033.1991.TB16124.X.

Suárez-Martínez, C. *et al.* (2023) 'Infant gut microbiota colonization: influence of prenatal and postnatal factors, focusing on diet', *Frontiers in Microbiology*. Frontiers Media SA, 14, p. 1236254. doi: 10.3389/FMICB.2023.1236254/BIBTEX.

Subramanian, M. R., Talluri, S. and Christopher, L. P. (2015) 'Production of lactic acid using a new homofermentative Enterococcus faecalis isolate', *Microbial Biotechnology*. Wiley, 8(2), p. 221. doi: 10.1111/1751-7915.12133.

Subramanian, S. *et al.* (2014) 'Persistent gut microbiota immaturity in malnourished Bangladeshi children'. doi: 10.1038/nature13421.

Sun, Q. *et al.* (2021) 'Sodium Butyrate Alleviates Intestinal Inflammation in Mice with Necrotizing Enterocolitis', *Mediators of Inflammation*. Hindawi Limited, 2021. doi: 10.1155/2021/6259381.

Surana, N. K. and Kasper, D. L. (2017) 'Moving beyond microbiome-wide associations to causal microbe identification', *Nature*, 552(7684), pp. 244–247. doi: 10.1038/nature25019.

Taga, M. E. *et al.* (2007) 'BluB cannibalizes flavin to form the lower ligand of vitamin B12', *Nature*. NIH Public Access, 446(7134), p. 449. doi: 10.1038/NATURE05611.

Tailford, L. E. *et al.* (2015) 'Mucin glycan foraging in the human gut microbiome', *Frontiers in Genetics*. Frontiers Research Foundation, 5(FEB). doi: 10.3389/fgene.2015.00081.

Takahashi-Iñiguez, T. *et al.* (2012) 'Role of vitamin B12 on methylmalonyl-CoA mutase activity', *Journal of Zhejiang University. Science. B*. Zhejiang University Press, 13(6), p. 423. doi: 10.1631/JZUS.B1100329.

Talarico, T. L. *et al.* (1988) 'Production and isolation of reuterin, a growth inhibitor produced by Lactobacillus reuteri', *Antimicrobial Agents and Chemotherapy*. American Society for Microbiology Journals, 32(12), pp. 1854–1858. doi: 10.1128/AAC.32.12.1854.

Talarico, T. L. *et al.* (1990) *Utilization of Glycerol as a Hydrogen Acceptor by Lactobacillus reuteri: Purification of 1,3-Propanediol:NAD+ Oxidoreductaset Downloaded from*, *APPLIED AND ENVIRONMENTAL MICROBIOLOGY*. Available at: http://aem.asm.org/ (Accessed: 29 April 2021).

Tamanai-Shacoori, Z. *et al.* (2017) 'Roseburia spp.: A marker of health?', *Future Microbiology*. Future Medicine Ltd., 12(2), pp. 157–170. doi: 10.2217/FMB-2016-0130.

Taniya, M. A. *et al.* (2022) 'Role of Gut Microbiome in Autism Spectrum Disorder and Its Therapeutic Regulation', *Frontiers in Cellular and Infection Microbiology*. Frontiers Media SA, 12. doi: 10.3389/FCIMB.2022.915701.

Taranto, M. P. *et al.* (2003) 'Lactobacillus reuteri CRL1098 produces cobalamin', *Journal of Bacteriology*. American Society for Microbiology Journals, 185(18), pp. 5643–5647. doi: 10.1128/JB.185.18.5643-5647.2003.

Theriot, C. M., Bowman, A. A. and Young, V. B. (2016) 'Antibiotic-Induced Alterations of the Gut Microbiota Alter Secondary Bile Acid Production and Allow for Clostridium difficile Spore Germination and Outgrowth in the Large Intestine', *mSphere*. American Society for Microbiology, 1(1). doi: 10.1128/MSPHERE.00045-15/SUPPL_FILE/SPH001160046SF6.EPS.

Thomas, A. (1849) 'Anemia-disease of supra renal capsule', *London Med Gazette*, pp. 517–18.

Thompson, C. A., DeLaForest, A. and Battle, M. A. (2018) 'Patterning the gastrointestinal epithelium to confer regional-specific functions', *Developmental biology*. NIH Public Access, 435(2), p. 97. doi: 10.1016/J.YDBIO.2018.01.006.

Thompson, J. P. and Marrs, T. C. (2012) 'Hydroxocobalamin in cyanide poisoning', *Clinical toxicology (Philadelphia, Pa.)*. Clin Toxicol (Phila), 50(10), pp. 875–885. doi: 10.3109/15563650.2012.742197.

Thomson, P., Medina, D. A. and Garrido, D. (2018) 'Human milk oligosaccharides and infant gut bifidobacteria: Molecular strategies for their utilization', *Food microbiology*. Food Microbiol, 75, pp. 37–46. doi: 10.1016/J.FM.2017.09.001.

Thomsson, K. A. *et al.* (2012) 'Detailed O-glycomics of the Muc2 mucin from colon of wild-type, core 1- and core 3-transferase-deficient mice highlights differences compared with human MUC2', *Glycobiology*, 22(8), pp. 1128–1139. doi: 10.1093/glycob/cws083.

Tramontano, M. *et al.* (2018) 'Nutritional preferences of human gut bacteria reveal their metabolic idiosyncrasies', *Nature Microbiology*. Nature Publishing Group, 3(4), pp. 514–522. doi: 10.1038/s41564-018-0123-9.

Trapnell, C. *et al.* (2010) 'Transcript assembly and quantification by RNA-Seq reveals unannotated transcripts and isoform switching during cell differentiation', *Nature*

Biotechnology, 28. doi: 10.1038/nbt.1621.

Ursell, L. K. *et al.* (2012) 'Defining the Human Microbiome', *Nutrition reviews*. NIH Public Access, 70(Suppl 1), p. S38. doi: 10.1111/J.1753-4887.2012.00493.X.

Vitamin B12 - Health Professional Fact Sheet (2022). Available at: https://ods.od.nih.gov/factsheets/VitaminB12-HealthProfessional/ (Accessed: 18 May 2024).

Vrieze, A. *et al.* (2014) 'Impact of oral vancomycin on gut microbiota, bile acid metabolism, and insulin sensitivity', *Journal of Hepatology*. Elsevier, 60(4), pp. 824–831. doi: 10.1016/j.jhep.2013.11.034.

Wallrabenstein, I. *et al.* (2013) 'Human Trace Amine-Associated Receptor TAAR5 Can Be Activated by Trimethylamine', *PLoS ONE*. PLOS, 8(2). doi: 10.1371/JOURNAL.PONE.0054950.

Walter, J. *et al.* (2003) 'Identification of Lactobacillus reuteri genes specifically induced in the mouse gastrointestinal tract', *Applied and Environmental Microbiology*. American Society for Microbiology (ASM), 69(4), pp. 2044–2051. doi: 10.1128/AEM.69.4.2044-2051.2003.

Walter, J. (2008a) 'Ecological role of lactobacilli in the gastrointestinal tract: Implications for fundamental and biomedical research', *Applied and Environmental Microbiology*. American Society for Microbiology, pp. 4985–4996. doi: 10.1128/AEM.00753-08.

Walter, J. (2008b) 'Ecological Role of Lactobacilli in the Gastrointestinal Tract: Implications for Fundamental and Biomedical Research', *Applied and Environmental Microbiology*. American Society for Microbiology (ASM), 74(16), p. 4985. doi: 10.1128/AEM.00753-08.

Walter, J., Britton, R. A. and Roos, S. (2011) 'Host-microbial symbiosis in the vertebrate gastrointestinal tract and the Lactobacillus reuteri paradigm', *Proceedings of the National Academy of Sciences of the United States of America*. National Academy of Sciences, 108(SUPPL. 1), pp. 4645–4652. doi: 10.1073/pnas.1000099107.

Walton, K. D. *et al.* (2016) 'Villification in the mouse: Bmp signals control intestinal villus patterning', *Development (Cambridge)*. Company of Biologists Ltd, 143(3), pp. 427–436. doi: 10.1242/DEV.130112/-/DC1.

Wan, L. *et al.* (2020) 'Case-Control Study of the Effects of Gut Microbiota Composition on Neurotransmitter Metabolic Pathways in Children With Attention Deficit Hyperactivity Disorder', *Frontiers in Neuroscience*, 14(February), pp. 1–9. doi: 10.3389/fnins.2020.00127.

Wang, H. *et al.* (2023) 'Modulating the Human Gut Microbiota through Hypocaloric Balanced Diets: An Effective Approach for Managing Obesity', *Nutrients*. Multidisciplinary Digital Publishing Institute (MDPI), 15(14), p. 3101. doi: 10.3390/NU15143101/S1.

Wang, L. *et al.* (2017) 'Sodium butyrate suppresses angiotensin II-induced hypertension by inhibition of renal (pro)renin receptor and intrarenal renin-Angiotensin system', *Journal of Hypertension*. Lippincott Williams and Wilkins, 35(9), pp. 1899–1908. doi: 10.1097/HJH.0000000000001378.

Wang, Q. *et al.* (2022) 'Effect of oral administration of Limosilactobacillus reuteri on

intestinal barrier function and mucosal immunity of suckling piglets'. doi: 10.1080/1828051X.2022.2048977.

Wang, S. *et al.* (2014) 'Enterococcus faecalis from healthy infants modulates inflammation through MAPK signaling pathways', *PLoS ONE*. Public Library of Science, 9(5). doi: 10.1371/JOURNAL.PONE.0097523.

Wang, S. *et al.* (2021) 'Fusobacterium nucleatum Acts as a Pro-carcinogenic Bacterium in Colorectal Cancer: From Association to Causality', *Frontiers in Cell and Developmental Biology*. Frontiers Media SA, 9. doi: 10.3389/FCELL.2021.710165.

Wang, S. P. *et al.* (2020) 'Pivotal Roles for pH, Lactate, and Lactate-Utilizing Bacteria in the Stability of a Human Colonic Microbial Ecosystem', *mSystems*. American Society for Microbiology (ASM), 5(5). doi: 10.1128/MSYSTEMS.00645-20.

Warren, M. J. *et al.* (1990) 'The Escherichia coli cysG gene encodes S-adenosylmethionine-dependent uroporphyrinogen III methylase', *Biochemical Journal*. Biochem J, 265(3), pp. 725–729. doi: 10.1042/bj2650725.

Warren, M. J. *et al.* (2002) 'The biosynthesis of adenosylcobalamin (vitamin B12)', *Natural Product Reports*. The Royal Society of Chemistry, 19(4), pp. 390–412. doi: 10.1039/B108967F.

Warren, M. J. and Escalante-Semerena, J. C. (2008) 'Biosynthesis and Use of Cobalamin (B12)', *EcoSal Plus*. American Society for Microbiology, 3(1), p. 1. doi: 10.1128/ecosalplus.3.6.3.8.

Watanabe, F. and Bito, T. (2018) 'Vitamin B12 sources and microbial interaction', *Experimental Biology and Medicine*. SAGE Publications Inc., 243(2), pp. 148–158. doi: 10.1177/1535370217746612.

Wegmann, U. *et al.* (2015) 'The pan-genome of Lactobacillus reuteri strains originating from the pig gastrointestinal tract', *BMC Genomics*. BioMed Central Ltd., 16(1), p. 1023. doi: 10.1186/s12864-015-2216-7.

Wheeler, S. (2008) 'Assessment and interpretation of micronutrient status during pregnancy: Symposium on "Translation of research in nutrition II: the bed"', *Proceedings of the Nutrition Society*. Cambridge University Press, 67(4), pp. 437–450. doi: 10.1017/S0029665108008732.

Wilhelm, S. M., Rjater, R. G. and Kale-Pradhan, P. B. (2013) 'Perils and pitfalls of long-term effects of proton pump inhibitors', *Expert review of clinical pharmacology*. Expert Rev Clin Pharmacol, 6(4), pp. 443–451. doi: 10.1586/17512433.2013.811206.

Williams, L. *et al.* (2007) 'The Multiple Amidation Reactions Catalyzed by Cobyric Acid Synthetase from Salmonella typhimurium Are Sequential and Dissociative', *J. AM. CHEM. SOC*, 129, pp. 294–295. doi: 10.1021/ja067962b.

Witkowska-Zimny, M. and Kaminska-El-Hassan, E. (2017) 'Cells of human breast milk', *Cellular and Molecular Biology Letters*. Springer International Publishing, 22(1), pp. 1–11. doi: 10.1186/S11658-017-0042-4/TABLES/2.

Wlodarska, M. *et al.* (2017) 'Indoleacrylic Acid Produced by Commensal Peptostreptococcus Species Suppresses Inflammation', *Cell host & microbe*. Cell Host Microbe, 22(1), pp. 25-37.e6. doi: 10.1016/J.CHOM.2017.06.007.

Wolffenbuttel, B. H. R. *et al.* (2023) 'Therapeutics: Vitamin B12', *The BMJ*. BMJ

Publishing Group, 383. doi: 10.1136/BMJ-2022-071725.

Wong, O. W. H. *et al.* (2022) 'Disentangling the relationship of gut microbiota, functional gastrointestinal disorders and autism: a case–control study on prepubertal Chinese boys', *Scientific Reports 2022 12:1*. Nature Publishing Group, 12(1), pp. 1–13. doi: 10.1038/s41598-022-14785-8.

Woodson, J. D. and Escalante-Semerena, J. C. (2004) 'CbiZ, an amidohydrolase enzyme required for salvaging the coenzyme B12 precursor cobinamide in archaea', *Proceedings of the National Academy of Sciences of the United States of America*. National Academy of Sciences, 101(10), p. 3591. doi: 10.1073/PNAS.0305939101.

Wu, H., Rebello, O., *et al.* (2021) 'Fucosidases from the human gut symbiont Ruminococcus gnavus', *Cellular and molecular life sciences : CMLS*. Cell Mol Life Sci, 78(2), pp. 675–693. doi: 10.1007/S00018-020-03514-X.

Wu, H., Crost, E. H., *et al.* (2021) 'The human gut symbiont Ruminococcus gnavus shows specificity to blood group A antigen during mucin glycan foraging: Implication for niche colonisation in the gastrointestinal tract', *PLoS biology*. PLoS Biol, 19(12). doi: 10.1371/JOURNAL.PBIO.3001498.

Wu, X. *et al.* (2024) 'The impact of gut microbiome enterotypes on ulcerative colitis: identifying key bacterial species and revealing species co-occurrence networks using machine learning', *Gut Microbes*. Taylor and Francis Ltd., 16(1). doi: 10.1080/19490976.2023.2292254.

Xiao, L. and Zhao, F. (2023) 'Microbial transmission, colonisation and succession: from pregnancy to infancy', *Gut*. BMJ Publishing Group, 72(4), p. 772. doi: 10.1136/GUTJNL-2022-328970.

Xu, F. *et al.* (2020) 'The interplay between host genetics and the gut microbiome reveals common and distinct microbiome features for complex human diseases', *Microbiome*. BioMed Central Ltd, 8(1), pp. 1–14. doi: 10.1186/S40168-020-00923-9/FIGURES/5.

Xu, J. and Gordon, J. I. (2003) 'Honor thy symbionts', *Proceedings of the National Academy of Sciences of the United States of America*. Proc Natl Acad Sci U S A, 100(18), pp. 10452–10459. doi: 10.1073/PNAS.1734063100.

Xu, Y. *et al.* (2018) 'Cobalamin (Vitamin B12) induced a shift in microbial composition and metabolic activity in an in vitrocolon simulation', *Frontiers in Microbiology*. Frontiers Media S.A., 9(NOV). doi: 10.3389/fmicb.2018.02780.

Yamaguchi, M. and Yamamoto, K. (2023) 'Mucin glycans and their degradation by gut microbiota', *Glycoconjugate Journal 2023 40:4*. Springer, 40(4), pp. 493–512. doi: 10.1007/S10719-023-10124-9.

Yan, H. *et al.* (2022) 'Gut Microbiome Alterations in Patients With Visceral Obesity Based on Quantitative Computed Tomography', *Frontiers in Cellular and Infection Microbiology*. Frontiers Media S.A., 11, p. 823262. doi: 10.3389/FCIMB.2021.823262/BIBTEX.

Yang, W. and Cong, Y. (2021) 'Gut microbiota-derived metabolites in the regulation of host immune responses and immune-related inflammatory diseases', *Cellular & Molecular Immunology 2021 18:4*. Nature Publishing Group, 18(4), pp. 866–877. doi: 10.1038/s41423-021-00661-4.

Yates, C. A. *et al.* (2003) 'Absence of luminal riboflavin disturbs early postnatal development of the gastrointestinal tract', *Digestive Diseases and Sciences*. Springer, 48(6), pp. 1159–1164. doi: 10.1023/A:1023785200638/METRICS.

Ye, X. *et al.* (2017) 'Fusobacterium Nucleatum Subspecies Animalis Influences Proinflammatory Cytokine Expression and Monocyte Activation in Human Colorectal Tumors', *Cancer prevention research (Philadelphia, Pa.)*. Cancer Prev Res (Phila), 10(7), pp. 398–409. doi: 10.1158/1940-6207.CAPR-16-0178.

Zappa, S., Li, K. and Bauer, C. E. (2010) 'The tetrapyrrole biosynthetic pathway and its regulation in Rhodobacter capsulatus.', *Advances in experimental medicine and biology*. Springer, New York, NY, pp. 229–250. doi: 10.1007/978-1-4419-1528-3_13.

Zeisel, S. H. and Warrier, M. (2017) 'Trimethylamine N-Oxide, the Microbiome, and Heart and Kidney Disease', *Annual Review of Nutrition*. Annual Reviews Inc., 37, pp. 157–181. doi: 10.1146/ANNUREV-NUTR-071816-064732.

Zelante, T. *et al.* (2013) 'Tryptophan catabolites from microbiota engage aryl hydrocarbon receptor and balance mucosal reactivity via interleukin-22', *Immunity*. Immunity, 39(2), pp. 372–385. doi: 10.1016/J.IMMUNI.2013.08.003.

Zhai, L. *et al.* (2023) 'Gut microbiota-derived tryptamine and phenethylamine impair insulin sensitivity in metabolic syndrome and irritable bowel syndrome', *Nature Communications*. Nature Publishing Group, 14(1), p. 4986. doi: 10.1038/S41467-023-40552-Y.

Zhang, L. *et al.* (2023) 'Enterococcus faecalis promotes the progression of colorectal cancer via its metabolite: biliverdin', *Journal of Translational Medicine*. BioMed Central Ltd, 21(1), pp. 1–14. doi: 10.1186/S12967-023-03929-7/FIGURES/5.

Zhang, W. *et al.* (2019) 'Gut microbiota community characteristics and disease-related microorganism pattern in a population of healthy Chinese people', *Scientific reports*. Sci Rep, 9(1). doi: 10.1038/S41598-018-36318-Y.

Zhang, W. *et al.* (2023) 'Role of neuroinflammation in neurodegeneration development', *Signal Transduction and Targeted Therapy 2023 8:1*. Nature Publishing Group, 8(1), pp. 1–32. doi: 10.1038/s41392-023-01486-5.

Zhang, X. *et al.* (2020) 'The Composition and Concordance of Lactobacillus Populations of Infant Gut and the Corresponding Breast-Milk and Maternal Gut', *Frontiers in Microbiology*. Frontiers Media S.A., 11, p. 2985. doi: 10.3389/fmicb.2020.597911.

Zhang, X., Tang, B. and Guo, J. (2023) 'Parkinson's disease and gut microbiota: from clinical to mechanistic and therapeutic studies', *Translational Neurodegeneration 2023 12:1*. BioMed Central, 12(1), pp. 1–30. doi: 10.1186/S40035-023-00392-8.

Zhang, Y. *et al.* (2019) 'Changes of intestinal bacterial microbiota in coronary heart disease complicated with nonalcoholic fatty liver disease', *BMC Genomics*. BioMed Central Ltd., 20(1), pp. 1–12. doi: 10.1186/S12864-019-6251-7/FIGURES/5.

Zhang, Z. *et al.* (2020) 'A Phylogenetic View on the Role of Glycerol for Growth Enhancement and Reuterin Formation in Limosilactobacillus reuteri', *Frontiers in Microbiology*. Frontiers Media S.A., 11, p. 601422. doi: 10.3389/fmicb.2020.601422.

Zheng, J. *et al.* (2015) 'Comparative genomics Lactobacillus reuteri from sourdough reveals adaptation of an intestinal symbiont to food fermentations', *Scientific Reports*.

Nature Publishing Group, 5(1), pp. 1–11. doi: 10.1038/srep18234.

Zheng, J. *et al.* (2020) 'A taxonomic note on the genus Lactobacillus: Description of 23 novel genera, emended description of the genus Lactobacillus beijerinck 1901, and union of Lactobacillaceae and Leuconostocaceae', *International Journal of Systematic and Evolutionary Microbiology*. Microbiology Society, 70(4), pp. 2782–2858. doi: 10.1099/ijsem.0.004107.

Zheng, Y. *et al.* (2021) 'Vitamin B12 enriched in spinach and its effects on gut microbiota', *Journal of Agricultural and Food Chemistry*. American Chemical Society, 69(7), pp. 2204–2212. doi: 10.1021/ACS.JAFC.0C07597/ASSET/IMAGES/LARGE/JF0C07597_0007.JPEG.

Zheng, Y. and He, J.-Q. (2022) 'Pathogenic Mechanisms of Trimethylamine N-Oxide-induced Atherosclerosis and Cardiomyopathy', *Current vascular pharmacology*. NIH Public Access, 20(1), p. 29. doi: 10.2174/1570161119666210812152802.

Zhou, K. (2017) 'Strategies to promote abundance of Akkermansia muciniphila, an emerging probiotics in the gut, evidence from dietary intervention studies', *Journal of Functional Foods*. Elsevier Ltd, 33, pp. 194–201. doi: 10.1016/j.jff.2017.03.045.

Zhou, Q. *et al.* (2022) 'Lactobacillus reuteri improves function of the intestinal barrier in rats with acute liver failure through Nrf-2/HO-1 pathway', *Nutrition*. Elsevier, 99–100, p. 111673. doi: 10.1016/J.NUT.2022.111673.

Zhou, X., Cui, Y. and Han, J. (2018) 'Methylmalonic acidemia: Current status and research priorities', *Intractable & Rare Diseases Research*. International Research and Cooperation Association for Bio & Socio-Sciences Advancement, 7(2), pp. 73–78. doi: 10.5582/IRDR.2018.01026.

Zhou, Y. and Zhi, F. (2016) 'Lower Level of Bacteroides in the Gut Microbiota Is Associated with Inflammatory Bowel Disease: A Meta-Analysis', *BioMed Research International*. Hindawi Limited, 2016. doi: 10.1155/2016/5828959.

Zhu, M. *et al.* (2022) 'Gut Microbiota: A Novel Therapeutic Target for Parkinson's Disease', *Frontiers in Immunology*. Frontiers Media S.A., 13, p. 937555. doi: 10.3389/FIMMU.2022.937555/BIBTEX.

Zhu, X. *et al.* (2019) 'Impact of Cyanocobalamin and Methylcobalamin on Inflammatory Bowel Disease and the Intestinal Microbiota Composition', *Journal of Agricultural and Food Chemistry*. American Chemical Society, 67(3), pp. 916–926. doi: 10.1021/acs.jafc.8b05730.

Zhu, Y. *et al.* (2014) 'Carnitine metabolism to trimethylamine by an unusual Rieske-type oxygenase from human microbiota', *Proceedings of the National Academy of Sciences of the United States of America*. National Academy of Sciences, 111(11), pp. 4268–4273. doi: 10.1073/PNAS.1316569111.

Appendices:

Appendix 1. Supplementary Figures

Supplementary Figure 1 HIS-BtuG2-pet14b plasmid. In this plasmid, the BtuG2-encoding gene lacks the N-terminal lipobox-lipoprotein export signal peptide and is fused to a N-terminal HIS-tag encoding region. The expression of BtuG2 is controlled by the T7 promoter and lac operon. Figure was created with SnapGene.

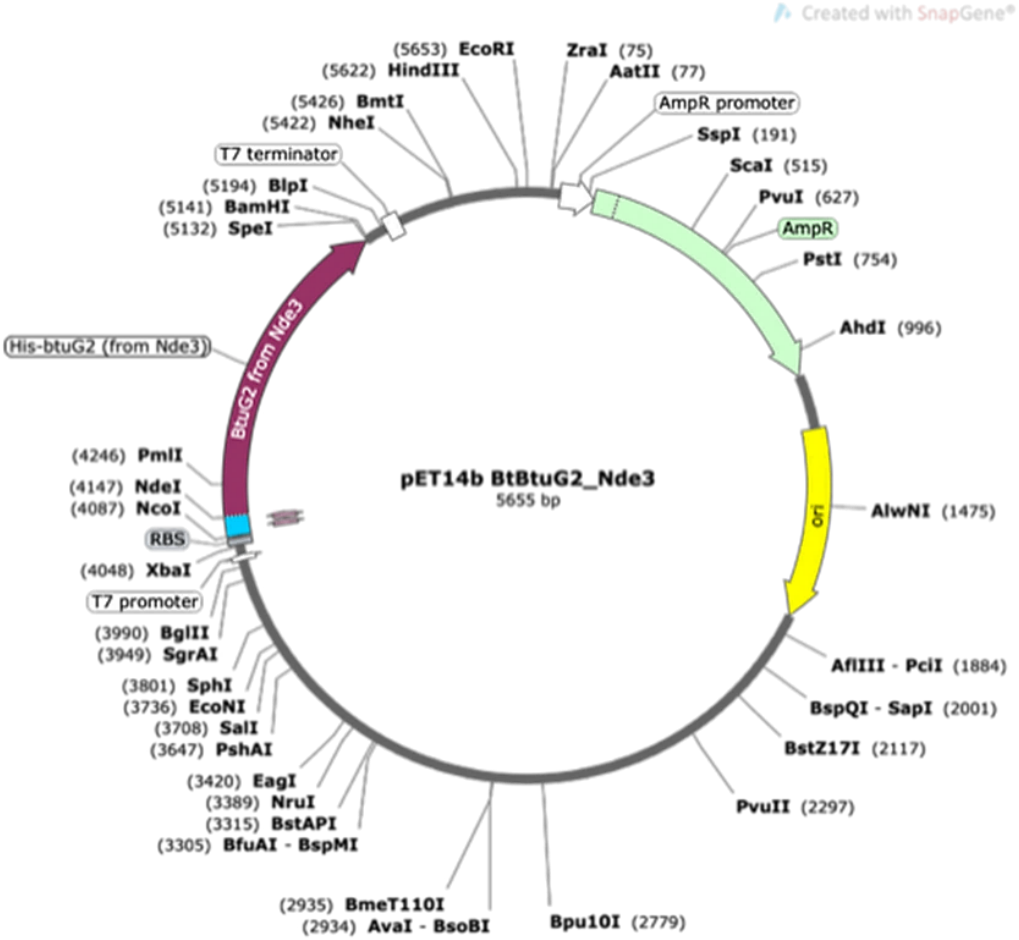

Supplementary Figure 2 Comparative genome analysis of cobamide biosynthetic genes across *L. reuteri* strains. Heat map demonstrates the presence or absence of cobalamin biosynthesis genes (y axis) in *L. reuteri* strains (x axis) based on percentage identity. Predicted gene presence is represented by a red colour (percentage identity > 60%) and predicted gene absence is represented by a blue colour. (percentage identity < 60% 60%). Strains underlined in red and marked with a red Asterix have been tested in vitro for cobamide production in this work.

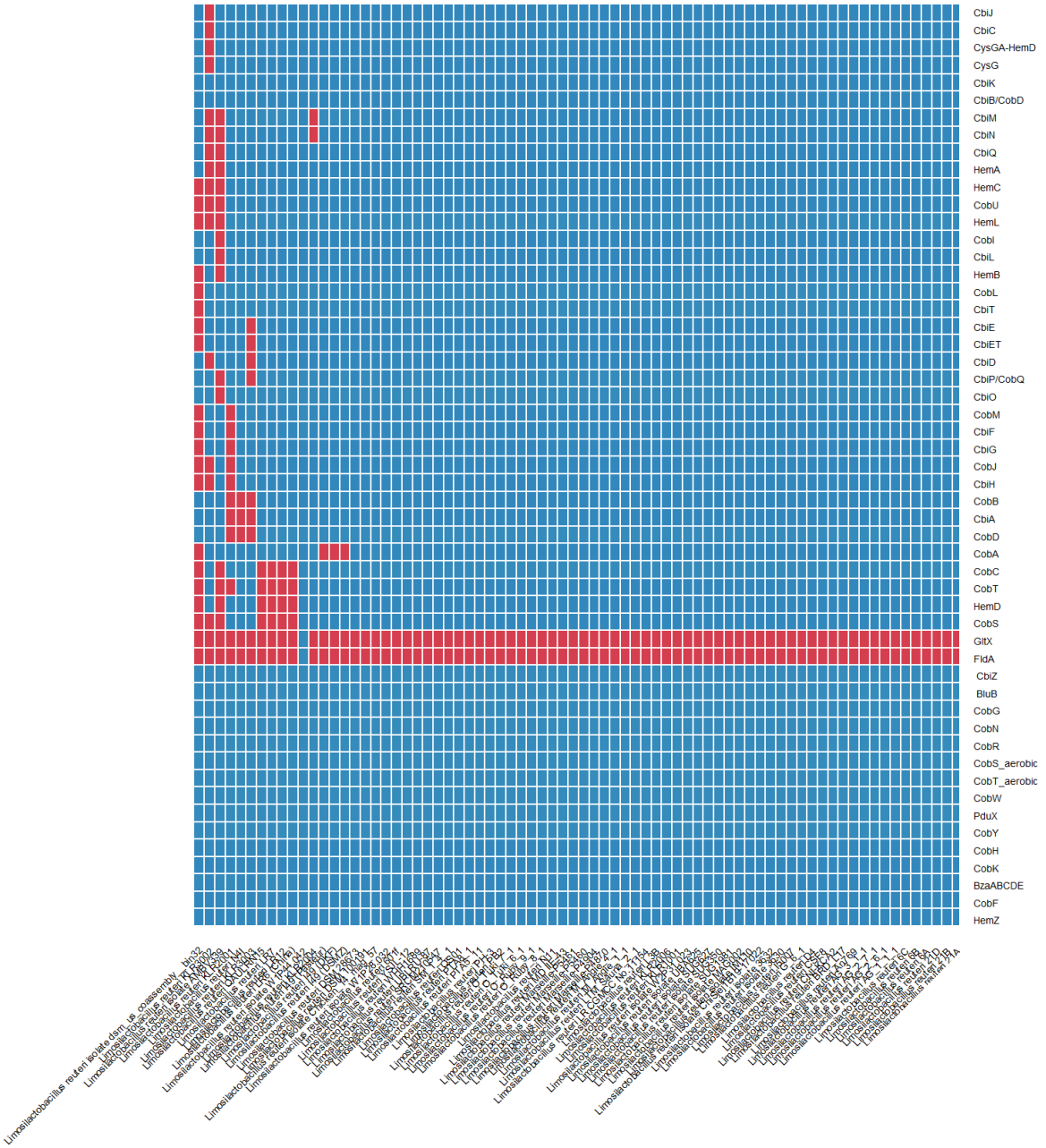

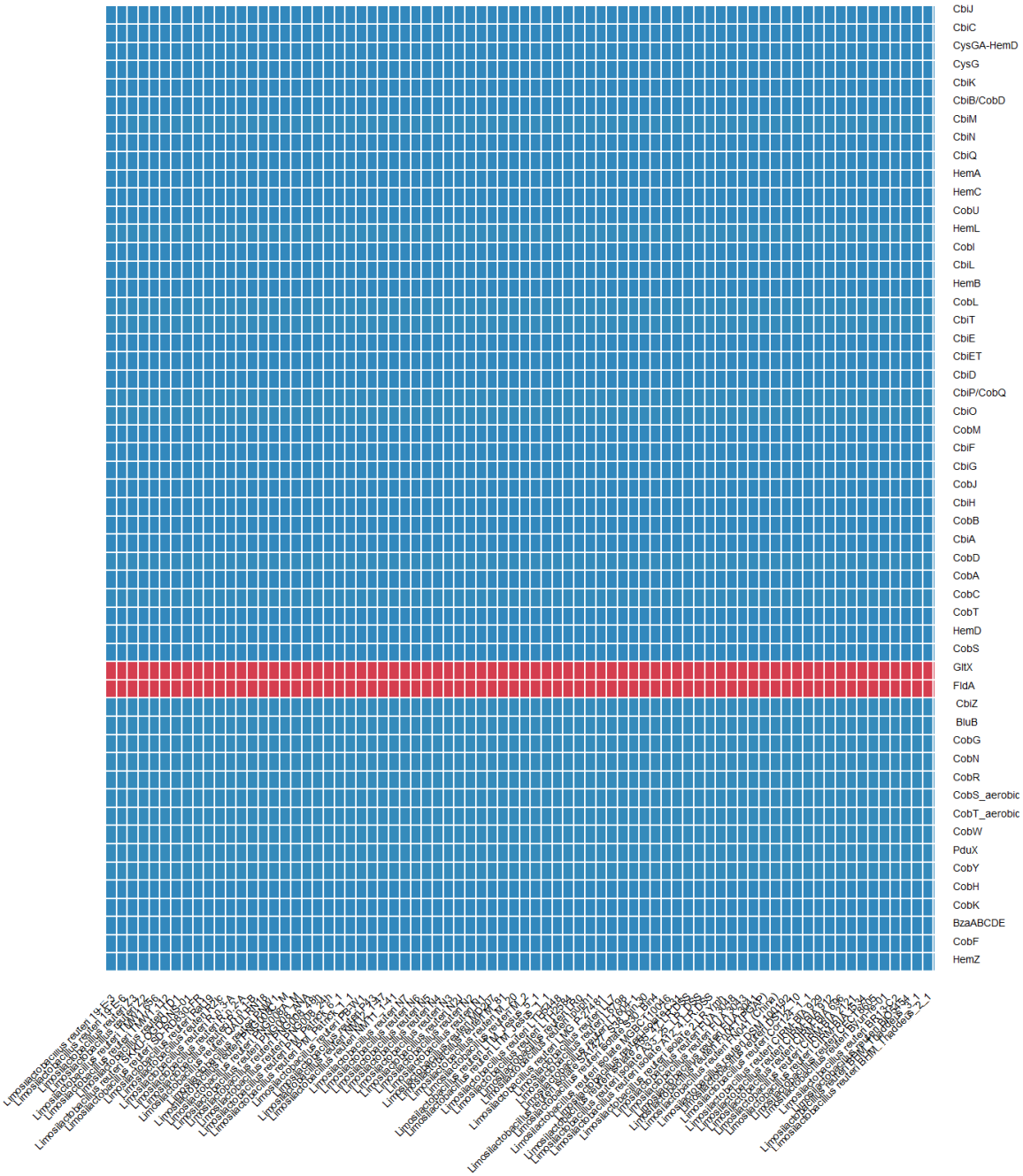
CbiJ
CbiC
CysGA-HemD
CysG
CbiK
CbiB/CobD
CbiM
CbiN
CbiQ
HemA
HemC
CobU
HemL
CobI
CbiL
HemB
CobL
CbiT
CbiE
CbiET
CbiD
CbiP/CobQ
CbiO
CobM
CbiF
CbiG
CobJ
CbiH
CobB
CbiA
CobD
CobA
CobC
CobT
HemD
CobS
GltX
FldA
CbiZ
BluB
CobG
CobN
CobR
CobS_aerobic
CobT_aerobic
CobW
PduX
CobY
CobH
CobK
BzaABCDE
CobF
HemZ

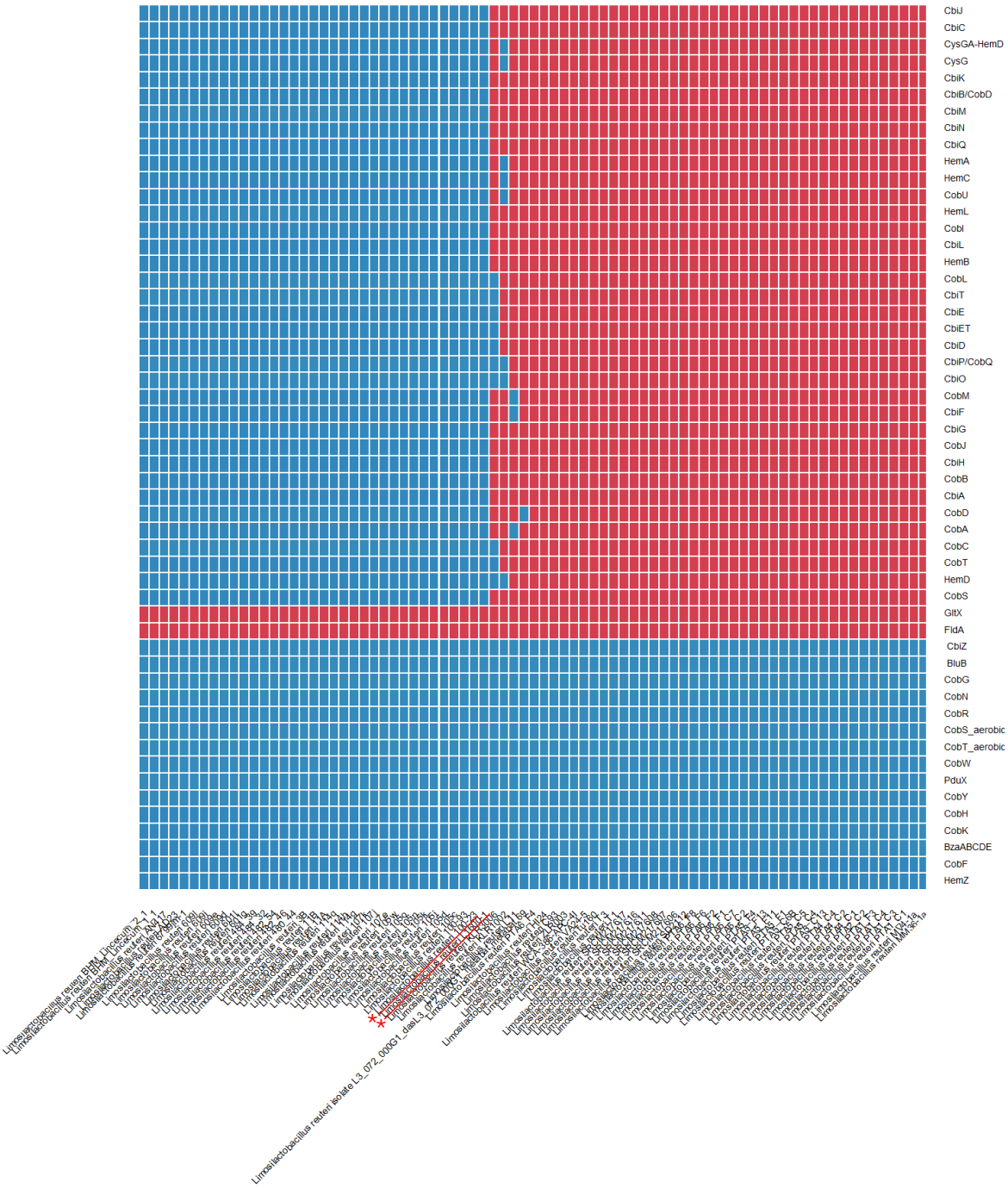
CbiJ
CbiC
CysGA-HemD
CysG
CbiK
CbiB/CobD
CbiM
CbiN
CbiQ
HemA
HemC
CobU
HemL
CobI
CbiL
HemB
CobL
CbiT
CbiE
CbiET
CbiD
CbiP/CobQ
CbiO
CobM
CbiF
CbiG
CobJ
CbiH
CobB
CbiA
CobD
CobA
CobC
CobT
HemD
CobS
GltX
FldA
CbiZ
BluB
CobG
CobN
CobR
CobS_aerobic
CobT_aerobic
CobW
PduX
CobY
CobH
CobK
BzaABCDE
CobF
HemZ

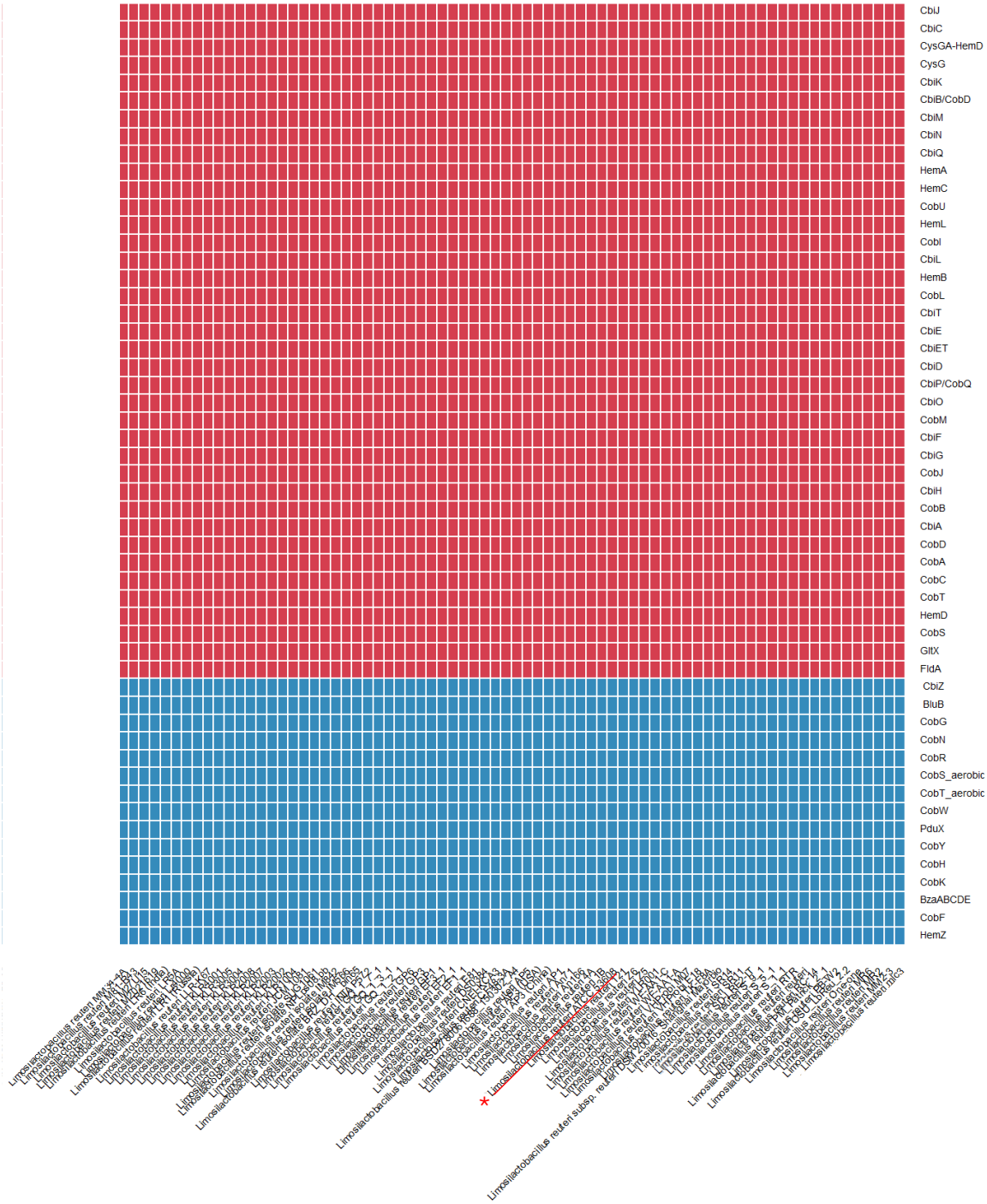
CbiJ
CbiC
CysGA-HemD
CysG
CbiK
CbiB/CobD
CbiM
CbiN
CbiQ
HemA
HemC
CobU
HemL
CobI
CbiL
HemB
CobL
CbiT
CbiE
CbiET
CbiD
CbiP/CobQ
CbiO
CobM
CbiF
CbiG
CobJ
CbiH
CobB
CbiA
CobD
CobA
CobC
CobT
HemD
CobS
GltX
FldA
CbiZ
BluB
CobG
CobN
CobR
CobS_aerobic
CobT_aerobic
CobW
PduX
CobY
CobH
CobK
BzaABCDE
CobF
HemZ

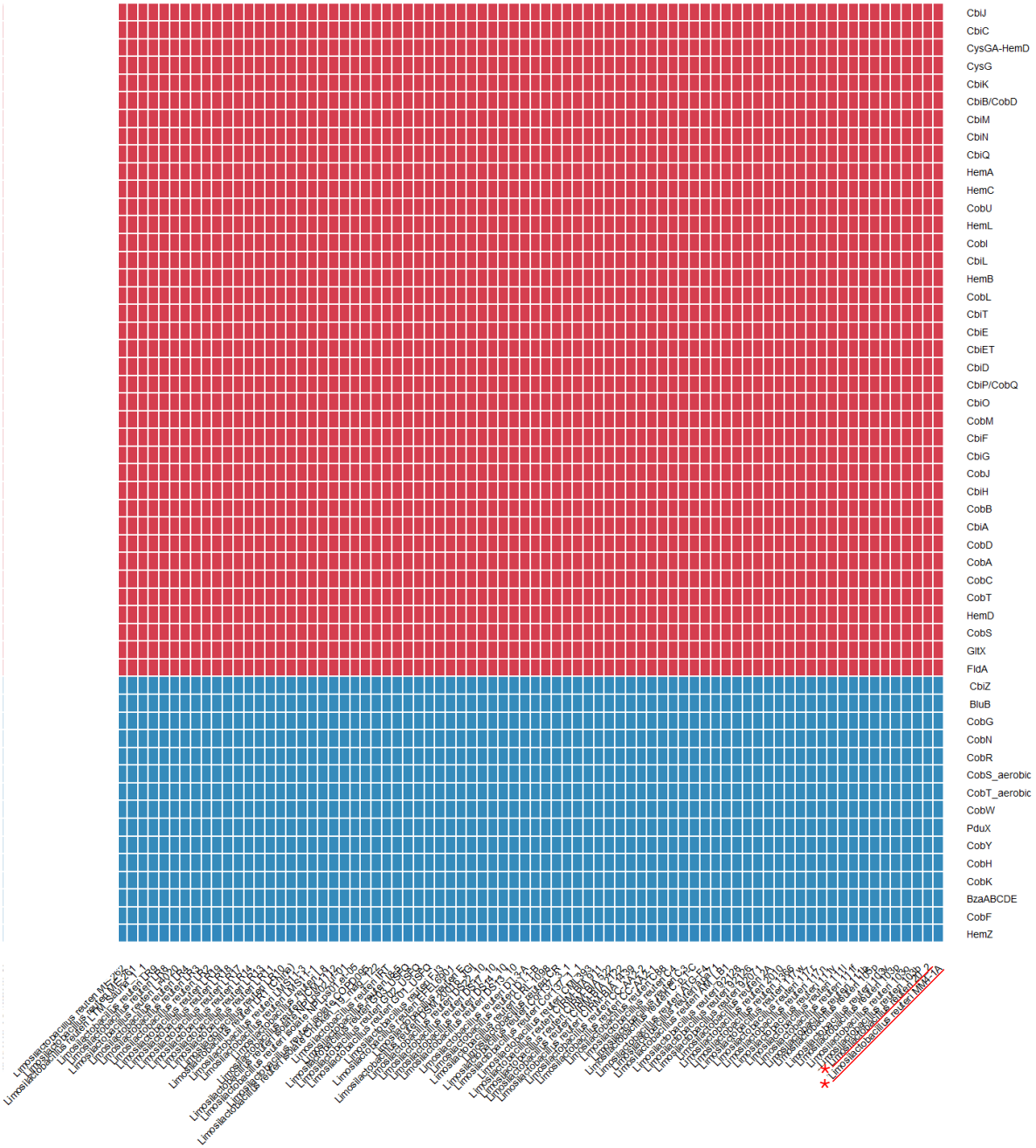
CbiJ
CbiC
CysGA-HemD
CysG
CbiK
CbiB/CobD
CbiM
CbiN
CbiQ
HemA
HemC
CobU
HemL
CobI
CbiL
HemB
CobL
CbiT
CbiE
CbiET
CbiD
CbiP/CobQ
CbiO
CobM
CbiF
CbiG
CobJ
CbiH
CobB
CbiA
CobD
CobA
CobC
CobT
HemD
CobS
GltX
FldA
CbiZ
BluB
CobG
CobN
CobR
CobS_aerobic
CobT_aerobic
CobW
PduX
CobY
CobH
CobK
BzaABCDE
CobF
HemZ

Supplementary Figure 3 Comparative genome analysis of cobamide dependent and transporter genes across *R. gnavus* strains. Visual representation of comparative genomics analysis by BLAST in the form of a heat map. Heat map demonstrates the presence or absence of cobamide dependent and transporter genes (y axis) in *R. gnavus* strains (x axis) based on percentage identity. Predicted gene presence is represented by the red colour (percentage identity > 80%) and predicted gene absence is represented by the blue colour indicating a percentage identity less than 80%. Strains underlined in red and marked with a red Asterix have been tested in vitro for cobamide utilisation in this work.

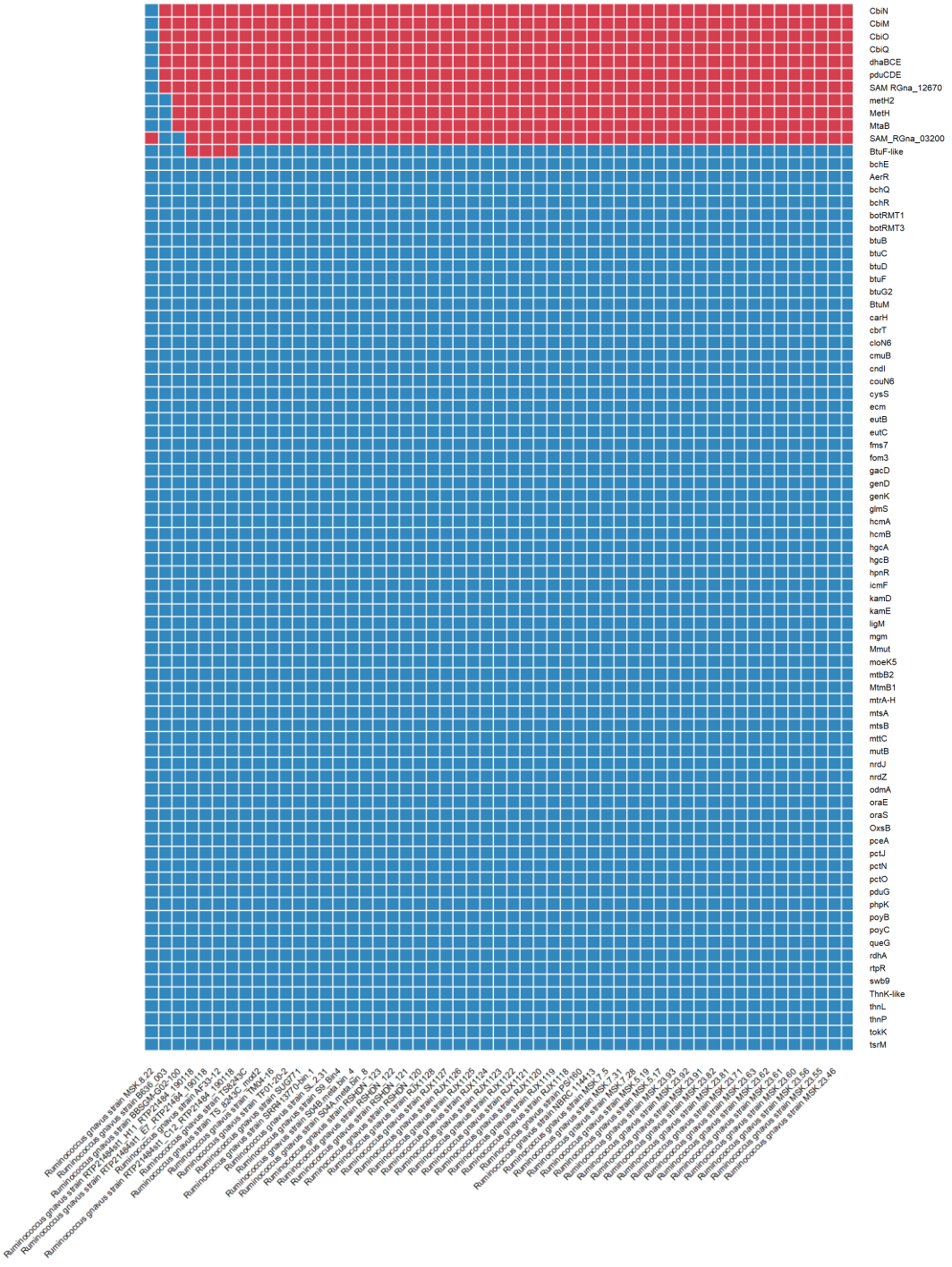

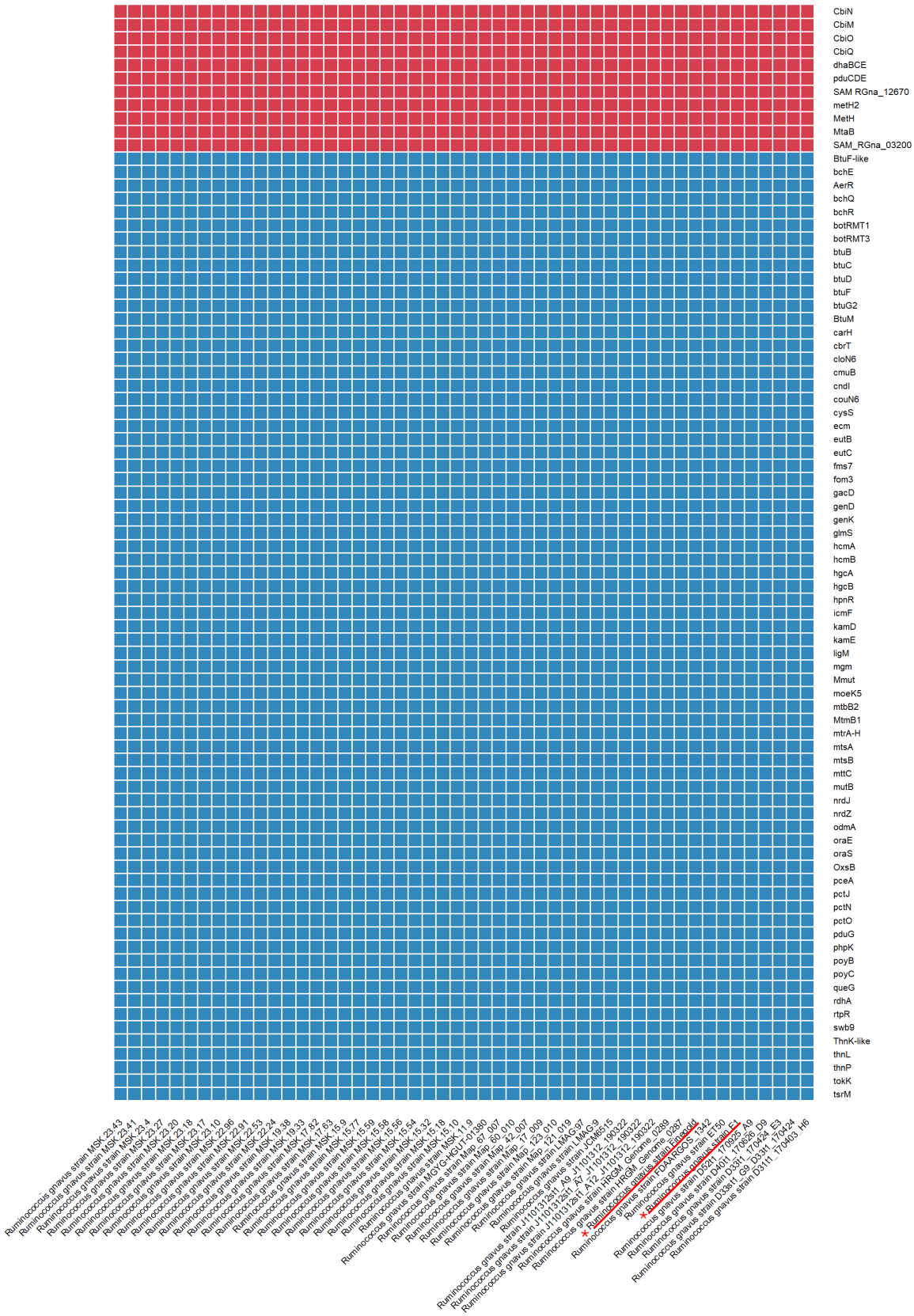
CbiN
CbiM
CbiO
CbiQ
dhaBCE
pduCDE
SAM RGna_12670
metH2
MetH
MtaB
SAM_RGna_03200
BtuF-like
bchE
AerR
bchQ
bchR
botRMT1
botRMT3
btuB
btuC
btuD
btuF
btuG2
BtuM
carH
cbrT
cloN6
cmuB
cndI
couN6
cysS
ecm
eutB
eutC
fms7
fom3
gacD
genD
genK
glmS
hcmA
hcmB
hgcA
hgcB
hpnR
icmF
kamD
kamE
ligM
mgm
Mmut
moeK5
mtbB2
MtmB1
mtrA-H
mtsA
mtsB
mttC
mutB
nrdJ
nrdZ
odmA
oraE
oraS
OxsB
pceA
pctJ
pctN
pctO
pduG
phpK
poyB
poyC
queG
rdhA
rtpR
swb9
ThnK-like
thnL
thnP
tokK
tsrM
Ruminococcus gnavus strain MSK.23.43
Ruminococcus gnavus strain MSK.23.41
Ruminococcus gnavus strain MSK.23.4
Ruminococcus gnavus strain MSK.23.27
Ruminococcus gnavus strain MSK.23.20
Ruminococcus gnavus strain MSK.23.18
Ruminococcus gnavus strain MSK.23.17
Ruminococcus gnavus strain MSK.23.10
Ruminococcus gnavus strain MSK.22.96
Ruminococcus gnavus strain MSK.22.91
Ruminococcus gnavus strain MSK.22.53
Ruminococcus gnavus strain MSK.22.44
Ruminococcus gnavus strain MSK.19.38
Ruminococcus gnavus strain MSK.19.33
Ruminococcus gnavus strain MSK.17.82
Ruminococcus gnavus strain MSK.17.63
Ruminococcus gnavus strain MSK.15.9
Ruminococcus gnavus strain MSK.15.77
Ruminococcus gnavus strain MSK.15.58
Ruminococcus gnavus strain MSK.15.58
Ruminococcus gnavus strain MSK.15.56
Ruminococcus gnavus strain MSK.15.54
Ruminococcus gnavus strain MSK.15.32
Ruminococcus gnavus strain MSK.15.18
Ruminococcus gnavus strain MSK.15.10
Ruminococcus gnavus strain MSK.11.9
Ruminococcus gnavus strain MGYGHGUT-01360
Ruminococcus gnavus strain Map_67_007
Ruminococcus gnavus strain Map_60_010
Ruminococcus gnavus strain Map_42_007
Ruminococcus gnavus strain Map_17_009
Ruminococcus gnavus strain Map_123_010
Ruminococcus gnavus strain Map_121_019
Ruminococcus gnavus strain MAG:97
Ruminococcus gnavus strain JCM6515
Ruminococcus gnavus strain J1101312_198322
Ruminococcus gnavus strain J1101312sH_A6_J1101312_198322
Ruminococcus gnavus strain J1101312sH_A2_J1101312_198322
Ruminococcus gnavus strain HRGM Genome_0289
Ruminococcus gnavus strain FDAARGOS_1342
Ruminococcus gnavus strain ET50
Ruminococcus gnavus strain D42I1_170825_A9
Ruminococcus gnavus strain D40I1_170825_D9
Ruminococcus gnavus strain D32I1_170424_E3
Ruminococcus gnavus strain D33I1_170424_H6

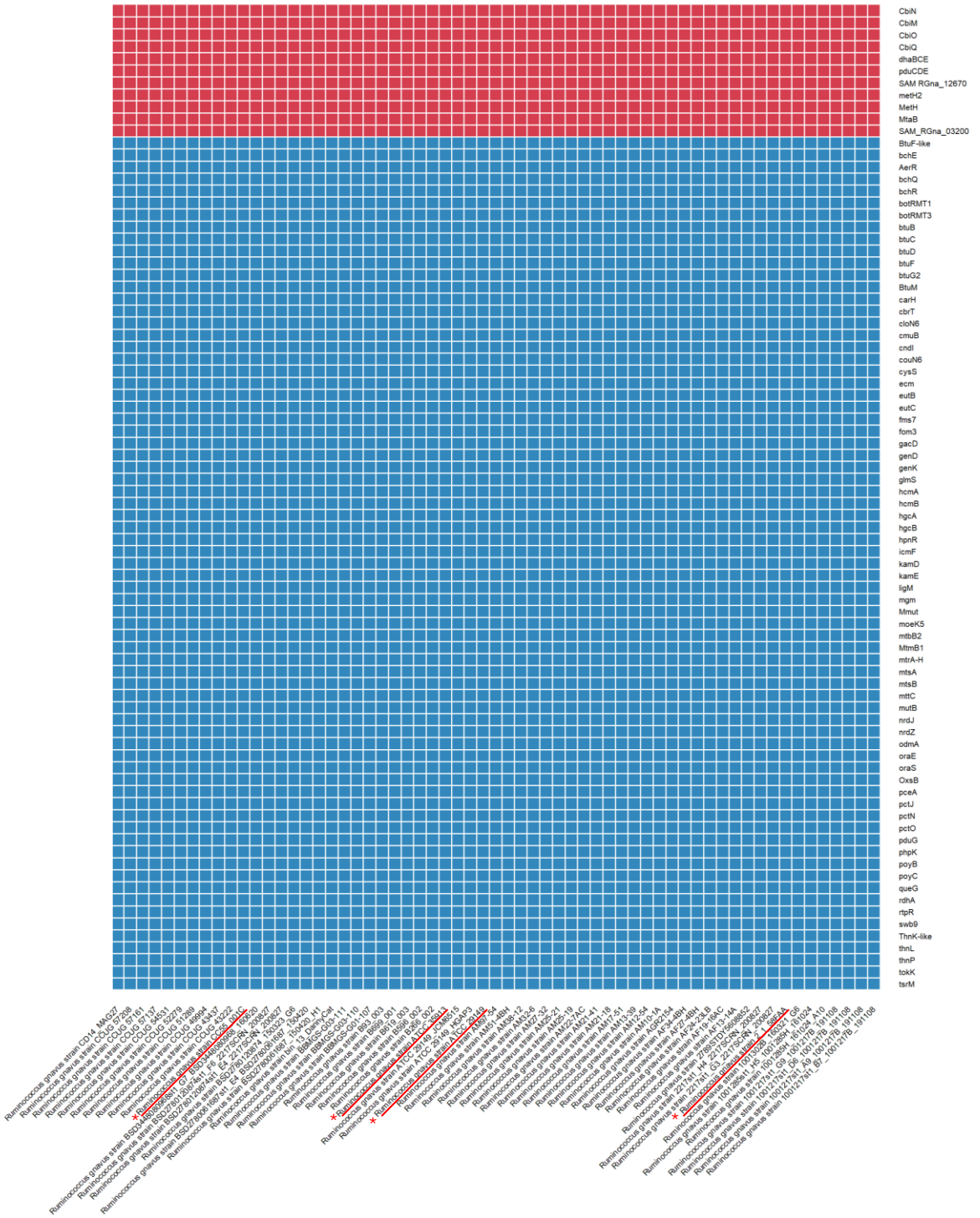
CbiN
CbiM
CbiO
CbiQ
dhaBCE
pduCDE
SAM RGna_12670
metH2
MetH
MtaB
SAM_RGna_03200
BtuF-like
bchE
AerR
bchQ
bchR
botRMT1
botRMT3
btuB
btuC
btuD
btuF
btuG2
BtuM
carH
cbrT
cloN6
cmuB
cndI
couN6
cysS
ecm
eutB
eutC
fms7
fom3
gacD
genD
genK
glmS
hcmA
hcmB
hgcA
hgcB
hpnR
icmF
kamD
kamE
ligM
mgm
Mmut
moeK5
mtbB2
MtmB1
mtrA-H
mtsA
mtsB
mttC
mutB
nrdJ
nrdZ
odmA
oraE
oraS
OxsB
pceA
pctJ
pctN
pctO
pduG
phpK
poyB
poyC
queG
rdhA
rfpR
swb9
ThnK-like
thnL
thnP
tokK
tsrM

Supplementary Figure 4 Comparative genome analysis of cobamide biosynthesis genes across *R. gnavus* strains. Visual representation of comparative genomics analysis by BLAST in the form of a heat map. Heat map demonstrates the presence or absence of cobamide-dependent and transporter genes (y axis) in *R. gnavus* strains (x axis) based on percentage identity. Predicted gene presence is represented by the red colour (percentage identity > 80%) and predicted gene absence is represented by the blue colour indicating a percentage identity less than 80%.

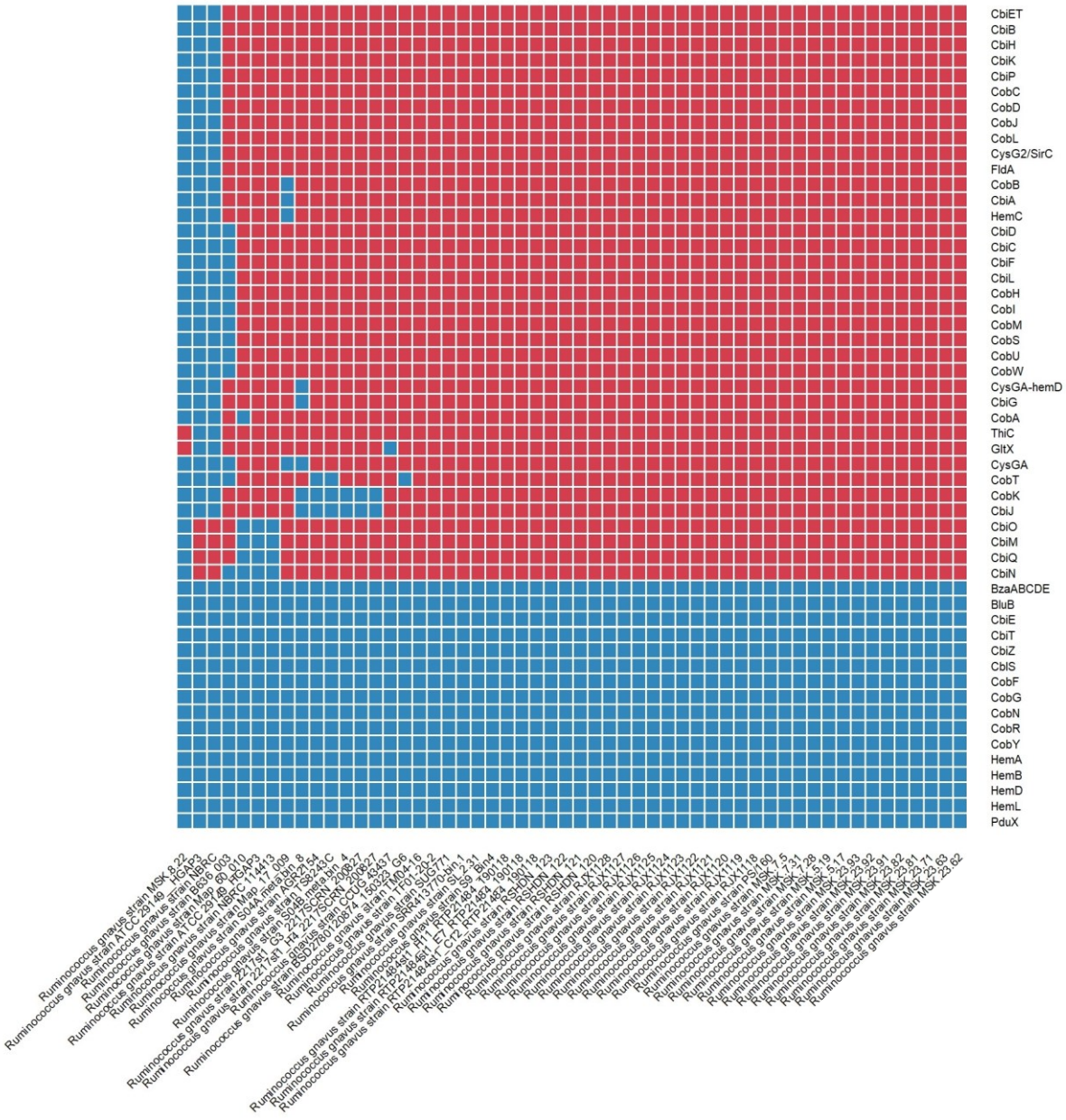

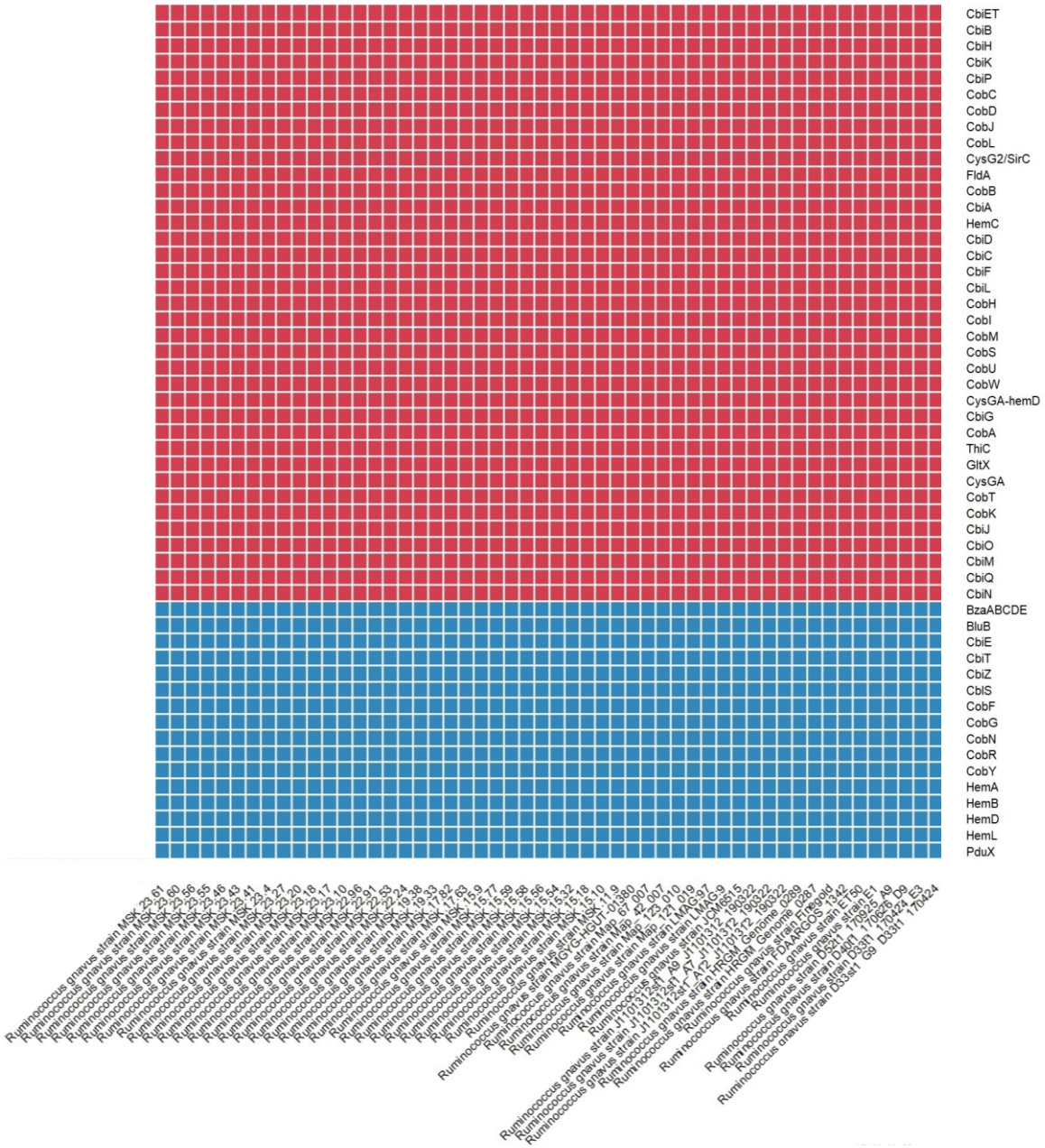
CbiET
CbiB
CbiH
CbiK
CbiP
CobC
CobD
CobJ
CobL
CysG2/SirC
FldA
CobB
CbiA
HemC
CbiD
CbiC
CbiF
CbiL
CobH
CobI
CobM
CobS
CobU
CobW
CysGA-hemD
CbiG
CobA
ThiC
GltX
CysGA
CobT
CobK
CbiJ
CbiO
CbiM
CbiQ
CbiN
BzaABCDE
BluB
CbiE
CbiT
CbiZ
CblS
CobF
CobG
CobN
CobR
CobY
HemA
HemB
HemD
HemL
PduX
Ruminococcus gnavus strain MSK.23.61
Ruminococcus gnavus strain MSK.23.60
Ruminococcus gnavus strain MSK.23.56
Ruminococcus gnavus strain MSK.23.55
Ruminococcus gnavus strain MSK.23.46
Ruminococcus gnavus strain MSK.23.43
Ruminococcus gnavus strain MSK.23.41
Ruminococcus gnavus strain MSK.23.4.7
Ruminococcus gnavus strain MSK.23.27
Ruminococcus gnavus strain MSK.23.20
Ruminococcus gnavus strain MSK.23.18
Ruminococcus gnavus strain MSK.23.17
Ruminococcus gnavus strain MSK.23.10
Ruminococcus gnavus strain MSK.22.96
Ruminococcus gnavus strain MSK.22.91
Ruminococcus gnavus strain MSK.22.53
Ruminococcus gnavus strain MSK.22.24
Ruminococcus gnavus strain MSK.19.38
Ruminococcus gnavus strain MSK.19.33
Ruminococcus gnavus strain MSK.17.62
Ruminococcus gnavus strain MSK.15.9
Ruminococcus gnavus strain MSK.15.77
Ruminococcus gnavus strain MSK.15.69
Ruminococcus gnavus strain MSK.15.58
Ruminococcus gnavus strain MSK.15.56
Ruminococcus gnavus strain MSK.15.54
Ruminococcus gnavus strain MSK.15.32
Ruminococcus gnavus strain MSK.15.18
Ruminococcus gnavus strain MSK.11.9
Ruminococcus gnavus strain MGYG-HGUT-05380
Ruminococcus gnavus strain Map_42_007
Ruminococcus gnavus strain Map_12_010
Ruminococcus gnavus strain Map_12_019
Ruminococcus gnavus strain LMAG.97
Ruminococcus gnavus strain LMAG.9
Ruminococcus gnavus strain JCM6515
Ruminococcus gnavus strain J101312_190322
Ruminococcus gnavus strain J101312_190322
Ruminococcus gnavus strain J101312_190322
Ruminococcus gnavus strain J101312sf1_A9
Ruminococcus gnavus strain J101312sf1_A7
Ruminococcus gnavus strain J101312_190322
Ruminococcus gnavus strain HRGM Genome 0289
Ruminococcus gnavus strain HRGM Genome 0287
Ruminococcus gnavus strain F_DAARGOS_1342
Ruminococcus gnavus strain Firenzuola
Ruminococcus gnavus strain E1_42
Ruminococcus gnavus strain E1_50
Ruminococcus gnavus strain D5sf1_A9
Ruminococcus gnavus strain D5sf1_D8
Ruminococcus gnavus strain D5sf1_E3
Ruminococcus gnavus strain D4sf1_170925_A9
Ruminococcus gnavus strain D3sf1_170926_D8
Ruminococcus gnavus strain D3sf1_170424_E3
Ruminococcus gnavus strain D3sf1_G9

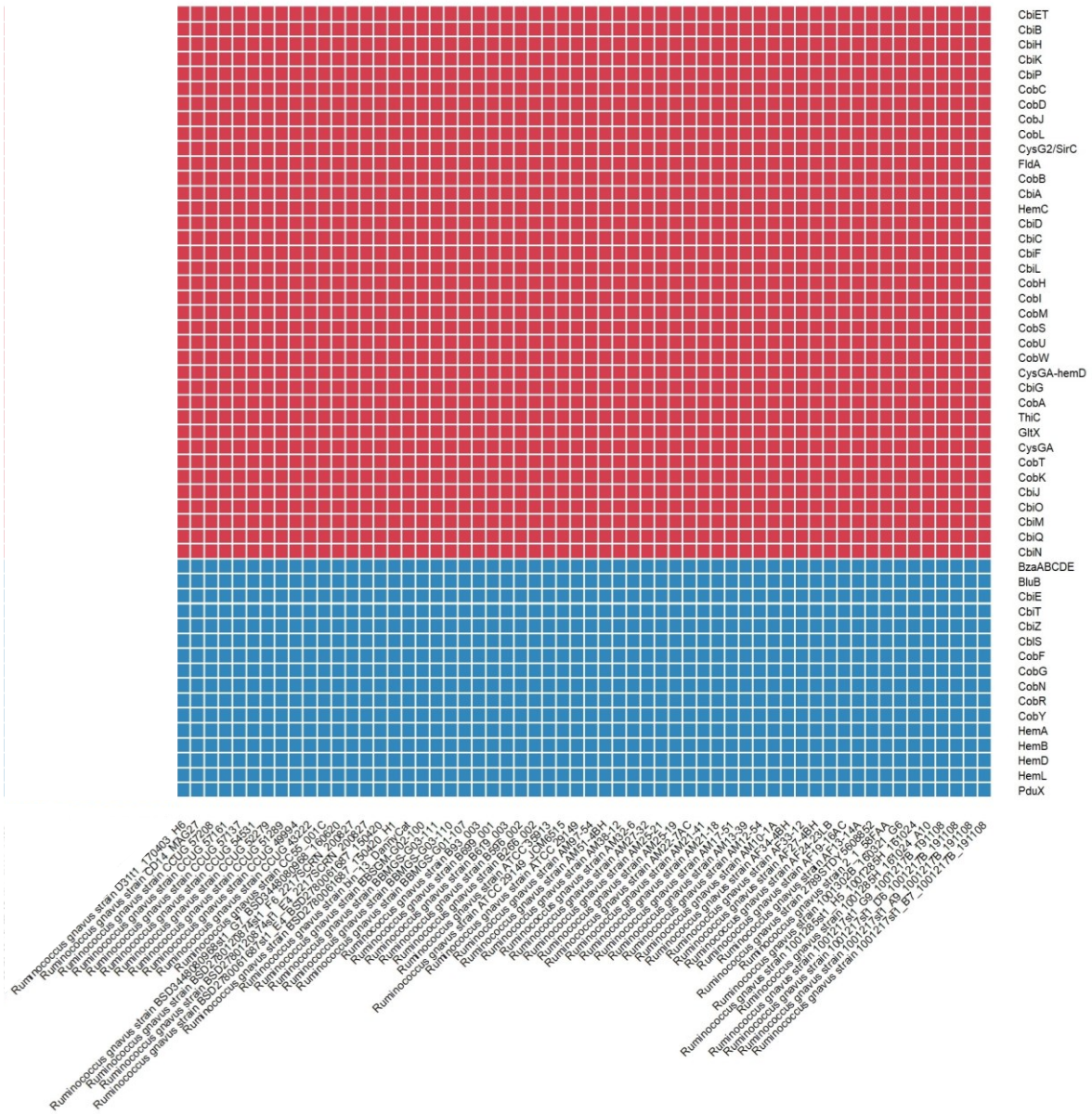
CbiET
CbiB
CbiH
CbiK
CbiP
CobC
CobD
CobJ
CobL
CysG2/SirC
FldA
CobB
CbiA
HemC
CbiD
CbiC
CbiF
CbiL
CobH
CobI
CobM
CobS
CobU
CobW
CysGA-hemD
CbiG
CobA
ThiC
GltX
CysGA
CobT
CobK
CbiJ
CbiO
CbiM
CbiQ
CbiN
BzaABCDE
BluB
CbiE
CbiT
CbiZ
CblS
CobF
CobG
CobN
CobR
CobY
HemA
HemB
HemD
HemL
PduX

Supplementary Figure 5 Comparative genome analysis of cobamide dependent methionine synthase, MetH and cobamide independent methionine synthase, MetE across *R. gnavus* strains. Visual representation of comparative genomics analysis by BLAST in the form of a heat map. Heat map demonstrates the presence or absence of MetH and MetE (y axis) in *R. gnavus* strains (x axis) based on percentage identity. Predicted gene presence is represented by the red colour (percentage identity > 80%) and predicted gene absence is represented by the blue colour indicating a percentage identity less than 80%.

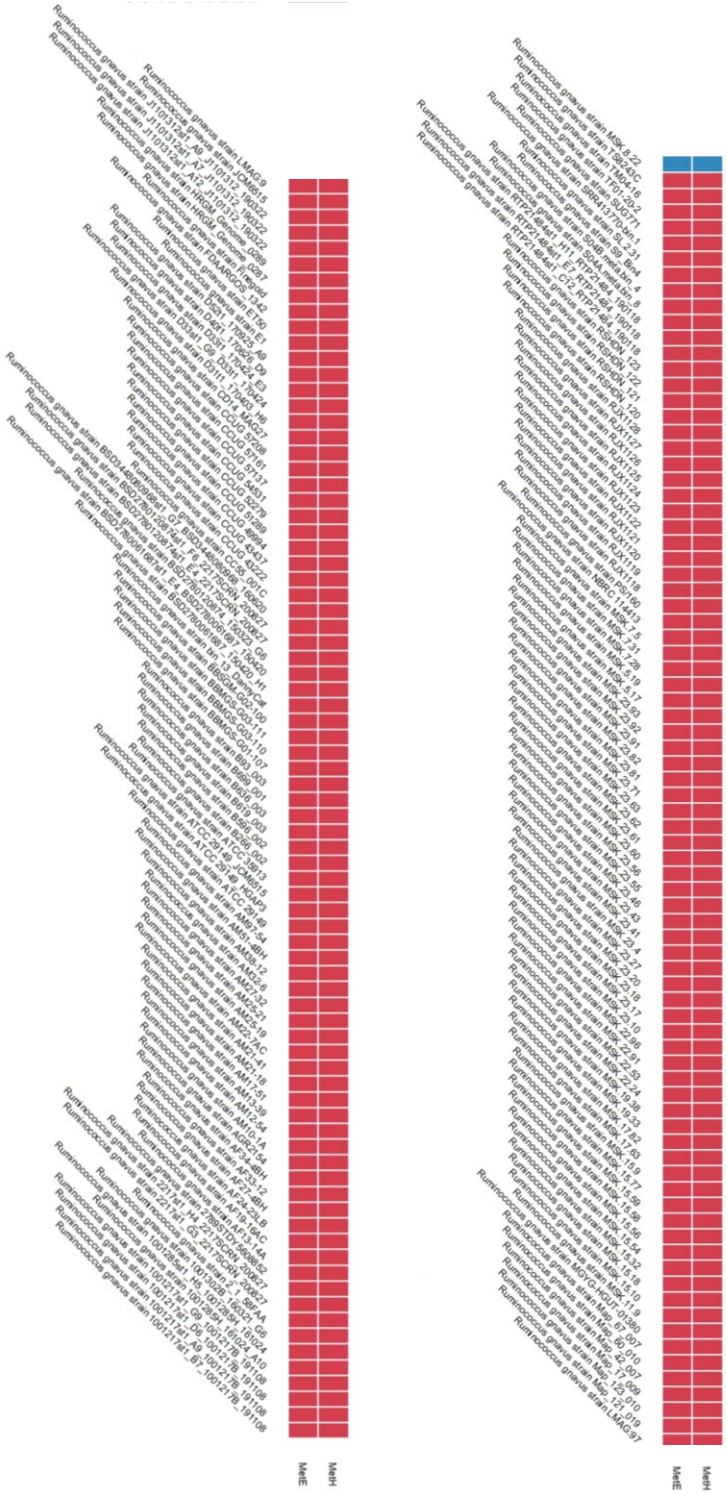

Supplementary Figure 6 Effect of cobamide analogues on growth of *R. gnavus* strains. *R. gnavus* (A) ATCC 29149, (B) ATCC 35913, (C) E1, (D) 2_1_58FAA, (E) CC55_001C and (F) Finegold was grown in Met-deficient LAB medium (LAB(-Met)) with glucose as a sole carbon source alone or supplemented with AdoCbl, MeCbl, OHCbl or CNCbl.

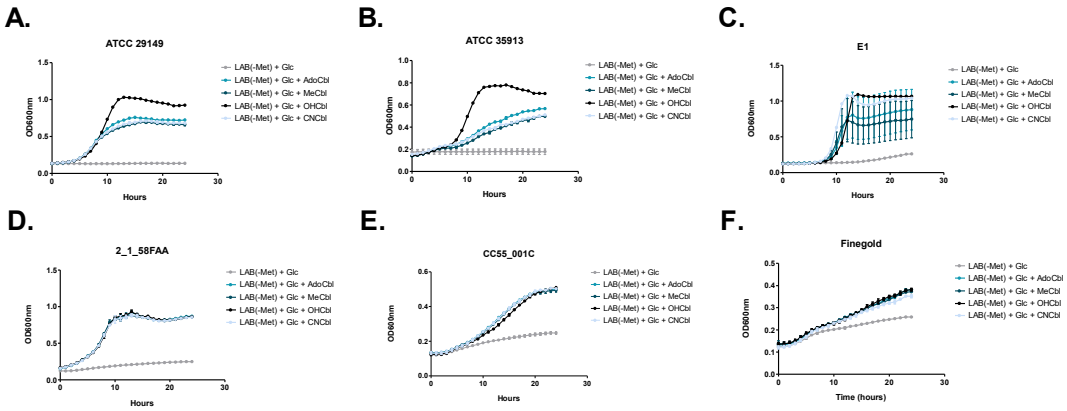

Supplementary Figure 7 Effect of cobamide derivatives on growth of *R. gnavus* strains. *R. gnavus* (A) ATCC 29149, (B) ATCC 35913, (C) E1, (D) 2_1_58FAA, (E) CC55_001C and (F) Finegold was grown in Met-deficient LAB medium (LAB(-Met)) with glucose as a sole carbon source alone or supplemented with PsCbl, Factor III, Factor IIIm, 5MB or Factor A.

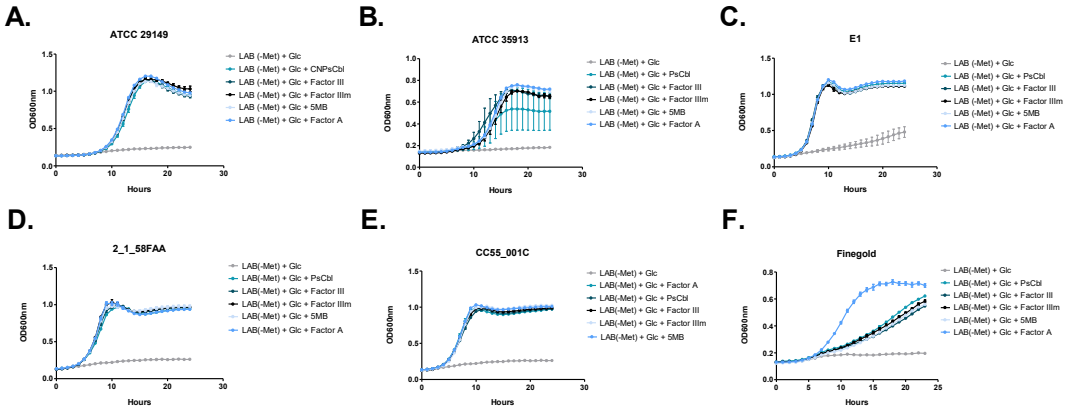

Supplementary Figure 8 Quantification of *L. reuteri* in co-culture with *R. gnavus*. A) Concentration of *L. reuteri* when in co-culture with *R. gnavus* ATCC 29149, determined by qPCR and expressed as 16S rDNA copy number/mL of culture. The values are plot as averages of four replicates. B) Estimated counts of reads from RNA seq performed on *L. reuteri* MM4-1A and *R. gnavus* ATCC 29149 co-cultures grown in LAB(-Met) media. For read count estimation, reads generated from RNA seq were mapped to either a *R. gnavus* ATCC 29149 reference genome or a *L. reuteri* MM4-1A reference genome. The values are plot as averages of three replicates. LR corresponds to *L. reuteri*.

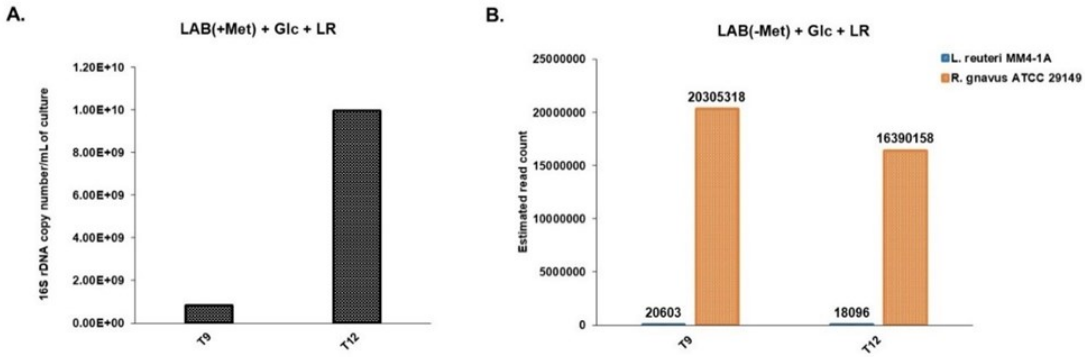

Supplementary Figure 9 Quantification of *R. gnavus* and *L. reuteri* by qPCR in donor faecal sample. The concentrations of *R. gnavus* and *L. reuteri* were determined by qPCR and expressed as 16S rDNA copies number/mL of culture.

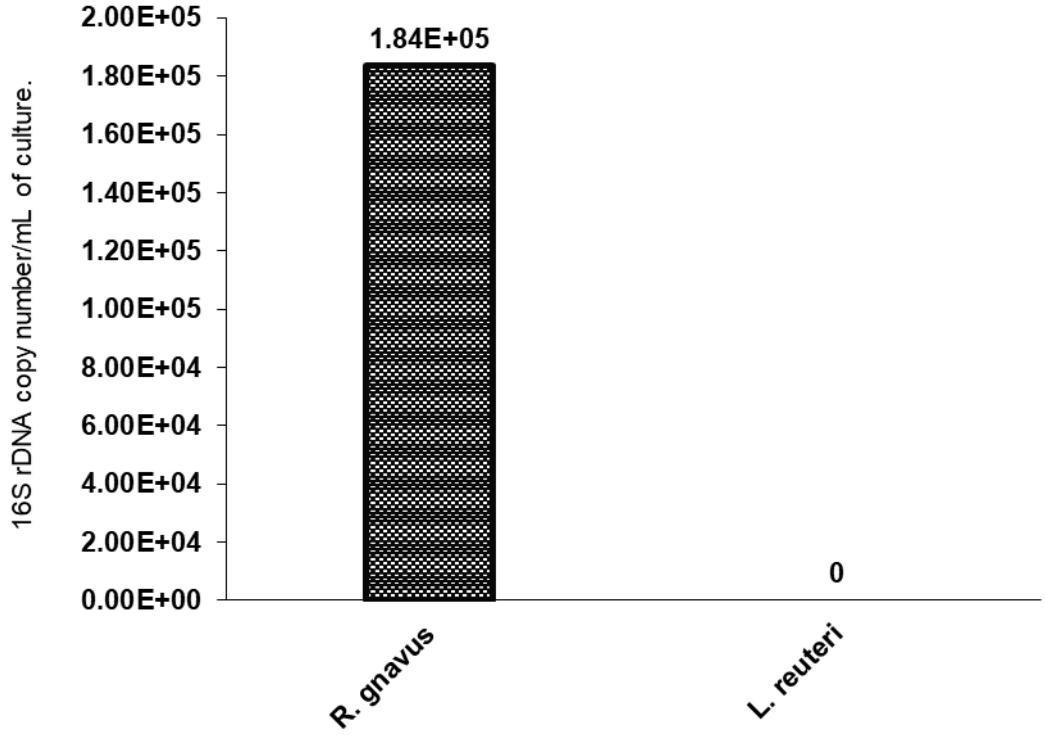

Appendix 2. Supplementary Tables

Supplementary Table 1 Lactobacillus defined medium type 2 (LDMII) composition. Solution needs to be autoclaved at 15 lb/in2 for 15 min in a serum bottle gassed with an N2-H2 (90:10) mixture and sealed with a butyl rubber stopper. Solution was passed through a 0.22-pm pore size membrane filter (Millipore Corp., Bedford, Mass.) and added to sterile basal solution. Solution was autoclaved in a stoppered bottle and added by sterile technique to basal medium (Kotarski and Savage, 1979).

Class	Compound	
Basal	K2HPO4	1.5 g
	KH2PO4	1.5 g
	Vitamin-free Casamino Acic	10 g
	Sodium acetate	15 g
	Sodium citrate	0.22 g
	Sucrose	10 g
	Tryptophane	0.05 g
	Asparagine	0.2 g
	Cysteine-hydrochloride	0.2 g
	Tween 80	1 g
	Water	885 mL
Vitamins	Thiamine hydrochloride	0.02 mg
	ρ-Aminobenzoic acid	0.04 mg
	Calcium panthenic acid	0.40 mg
	Niacin	1.00 mg
	Pyroxidine hydrochloride	0.50 mg
	Biotin	0.8 mg
	Folic acid	2 mg
	Riboflavin	2 mg
	Sodium bicarbonate	5 mg
	Water	50 mL
Biotin	Biotin	0.05 mg
	95% ethanol	0.001 mL
	0.01 N HCl	0.50 mL
Folic acid	Folic acid	0.1 mg
	0.001 N NaOH	5 mL
Riboflavin	Riboflavin	0.4 mg
	0.02 N acetic acid	5 mL
	Adenine sulfate	0.02 g
	Uracil	0.01 g
	Guanine hydrochloride	10 mg
	Cytidylic acid (mixed isome	50 mg
	1N HCl	5 mL
	Water	40 mL
Tween	Tween 80	1.0 g
	Water	9 mL
Thymidine	Thymidine	0.0016 mg
Salts	NaCl	0.2 g
	MgSO4 7H2O	0.1625 g
	MnSO4 H2O	0.0234 g
	FeSO4 7H2O	0.013 g
	Water	6.5 mL
Sucrose	Sucrose	20 g
	Water	60 mL

Supplementary Table 2 LAB medium components. For preparation of 1 L of medium, weigh out 3.1 g KH_2PO_4, 6.48 g K_2HPO_4 and 1.5 g Tricine, then add 600 mL purified water. Add 10 mL ascorbic acid 100X stock solution, 1 mL vitamins and antioxidants 1000X solution, 1 mL nucleotides 1000X stock solution, 100 mL amino acid 10X stock solution, 1 mL salts and minerals + buffer compounds 1000X stock solution and 100 mL salts and minerals 10X stock solution. Check final pH is close to 7 and complete with purified water before filter sterilising.

Class	Compound	
		g/L
Amino acids 10X	l-Histidine	1.7
	l-Isoleucine	2.4
	l-Leucine	10
	l-Methionine	1.25
	l-Valine	7
	l-Arginine	7.2
	l-Cysteine	2
	l-Glutamic acid	6
	l-Phenylalanine	4
	l-Proline	7
	l-Asparagine	5
	l-Aspartic acid	0.5
	l-Glutamine	6
	l-Serine	5
	l-Threonine	5
	l-Alanine	4
	Glycine	3
	l-Lysine	5
	l-Tryptophan	2
	l-Tyrosine	3
		g/100mL
Nucleotides 1000X	Adenine	1.1
	Guanine	0.56
	Uracil	2.3
	Xanthine	0.38
		g/L
Salts & Minerals 10X	KCH_3CO_2 (Potassium acetate)	9
	Ammonium citrate dibasic	17
	$MgCl_2$	3.86
	NaCl	30
	$CaCl_2$ (anhydrous)	0.302
	K_2SO_4	0.23
		g/100mL
Salts & Minerals + buffer compounds 1	$ZnSO_4 * 7 H_2O$	0.5
	$CoCl_2 \cdot 6H_2O$	0.019
	$CuSO_4$ (anhydrous)	0.012
	H_3BO_3	0.075
	KI	0.011
	$MnSO_4 * H_2O$	0.011
	$(NH_4)_6Mo_7O_{24} \cdot 4H_2O$	0.019
	$FeCl_3$	0.3
	$FeSO_4 . 7H_2O$	0.4
	EDTA	0.734
	Nitrilotriacetic acid	0.734
		g/100mL
Vitamins & Antioxidants 1000X	myo-Inositol	0.2
	L-Glutathione reduced	1.5
	Biotin	0.6
	Thiamine HCl	0.056
	Riboflavin	0.09
	Pyridoxamine . 2 HCl	0.5
	Niacin	0.09
	Pyridoxine HCl	0.48
	Calcium Pantothenate	0.12
	Folic acid	0.056
	p-Aminobenzoic acid	0.0056
	Lipoic acid	0.1
		g/100mL
Ascorbic acid 100X	Ascorbic acid	5

Supplementary Table 3 List of *L. reuteri* strains included in comparative genomic analysis. The table provides the name of the strains and the corresponding assembly level of the genome.

L. reuteri strain	Level
JCM 1112	Complete Genome
DSM 20016	Complete Genome
SD2112	Complete Genome
MM4-1A	Contig
CF48-3A	Scaffold
MM2-3	Scaffold
100-23	Contig
mlc3	Contig
lpuph1	Contig
ATCC 53608	Complete Genome
I5007	Complete Genome
TD1	Complete Genome
LTH2584	Scaffold
TMW1.656	Contig
TMW1.112	Contig
LTH5448	Contig
IRT	Complete Genome
DSM 20016	Scaffold
ZLR003	Complete Genome
CRL 1098	Contig
I49	Complete Genome
480_44	Scaffold
482_46	Scaffold
484_32	Scaffold
482_54	Scaffold
484_39	Scaffold
P43	Contig
HI24	Contig
121	Contig
MD IIE-43	Contig
CECT8605	Contig
1366	Scaffold
M27U15	Scaffold
JCM 1081	Scaffold
CSF8	Scaffold
MM34-4A	Scaffold
KLR1001	Contig
KLR2001	Contig
KLR1002	Contig
KLR1004	Contig
KLR2002	Contig
KLR2003	Contig
KLR2007	Contig
KLR3002	Contig
KLR3003	Contig
KLR3004	Contig
KLR3005	Contig
KLR4001	Contig
KLR2004	Contig
KLR2008	Contig
KLR2006	Contig
KLR3006	Contig
LR0	Scaffold
An71	Contig
An166	Contig
I49	Contig
609i	Scaffold
609l	Scaffold

609e	Scaffold
609d	Scaffold
601g	Scaffold
601l	Scaffold
601f	Scaffold
117w	Scaffold
117r	Scaffold
114h	Scaffold
114g	Scaffold
114q	Scaffold
117n	Scaffold
111v	Scaffold
107k	Scaffold
111l	Scaffold
107j	Scaffold
111b	Scaffold
111f	Scaffold
105p	Scaffold
107e	Scaffold
105o	Scaffold
105k	Scaffold
105w	Scaffold
105n	Scaffold
105i	Scaffold
105c	Scaffold
105d	Scaffold
103v	Scaffold
103p	Scaffold
103o	Scaffold
103b	Scaffold
UBA625	Scaffold
RC-14	Contig
20-2	Scaffold
LR5A	Scaffold
E81	Contig
DS12_10	Contig
DS14_10	Contig
DS13_10	Contig
DS22_10	Contig
DS17_10	Contig
WHH1689	Complete Genome
LR18	Scaffold
LR4	Scaffold
LR9	Scaffold
LR8	Scaffold
LR17	Scaffold
LR3	Scaffold
LR13	Scaffold
LR14	Scaffold
LR11	Scaffold
LR2	Scaffold
LR19	Scaffold
LR12	Scaffold
LR10	Scaffold
LR7	Scaffold
LR6	Scaffold
LR1	Scaffold
Byun-re-01	Complete Genome
SKKU-OGDONS-01	Complete Genome
LR CGMCC No.11154	Contig
R2lc	Contig
2010	Contig
UBLRU-87	Scaffold
PNW1	Scaffold
ATG-F4	Complete Genome
C93	Scaffold

C88	Scaffold
W2P31.023	Contig
W1P44.042	Contig
W1P28.032	Contig
I8-5	Scaffold
NM11_1-41	Contig
NM12_1-47	Contig
YSJL-12	Complete Genome
BIO5454	Scaffold
LL7	Complete Genome
reuteri	Complete Genome
PTA6_F8	Scaffold
PTA6_F1	Scaffold
PTA6_F6	Scaffold
PTA6_F2	Scaffold
PTA6_F4	Scaffold
PTA6_C7	Scaffold
PTA6_C2	Scaffold
PTA5_C6B	Scaffold
PTA5_C5	Scaffold
PTA5_C13	Scaffold
PTA5_C4	Scaffold
PTA5_F13	Scaffold
PTA5_F1	Scaffold
PTA5_F11	Scaffold
PTA5_F4	Scaffold
PTA4_C4	Scaffold
PTA4_C2	Scaffold
PTA4_C1	Scaffold
PTA1_F3	Scaffold
PTA2_C2	Scaffold
PTA1_C4	Scaffold
PTA1_C1	Scaffold
PTA1_C3	Scaffold
PTA8_1	Scaffold
PTA5_11	Scaffold
Rat19	Contig
100-93	Contig
L1600-1	Contig
N2J	Contig
Lr4000	Contig
CR	Contig
One-one	Contig
L1604-1	Contig
Lr4020	Contig
AD23	Contig
N4I	Contig
6799jm-1	Contig
G01_USFQ	Contig
G03_USFQ	Contig
G02_USFQ	Contig
SA1427_S38_bin.30	Scaffold
MD207	Contig
D4	Contig
VA24-5	Contig
LMG P-27481	Contig
CNI-KCA2	Chromosome
WCA-386-APC-4I	Contig
Z2	Scaffold
Z5	Scaffold
Z6	Scaffold
Z3	Scaffold
N7	Scaffold
N4	Scaffold
N5	Scaffold
N6	Scaffold

N3	Scaffold
N2	Scaffold
N1	Scaffold
AN417	Complete Genome
1B	Complete Genome
CNEI-KCA3	Complete Genome
AP3	Scaffold
OSU_LbReu_2.2	Contig
COPD095	Contig
TK-F8A	Complete Genome
BSD2780061688_150302_A4	Scaffold
MAG002	Contig
I49	Chromosome
An769	Contig
L3_072_000G1_dasL3_072_000G1_metabat.metabat.69	Contig
YLR001	Complete Genome
N11	Contig
LR1	Contig
E	Contig
Fn041	Scaffold
SD-RD830-FR	Complete Genome
SD-LRE2-IT	Complete Genome
19-E-6	Complete Genome
19-E-3	Complete Genome
ChiSjej1B19-17022	Contig
BHM_Thaddeus_3_1	Scaffold
AG_2_7_1	Scaffold
LTM_Sauna_2_1	Scaffold
2A	Contig
M_81	Scaffold
M_2	Scaffold
M_20	Scaffold
O_Tuki_6_1	Scaffold
S_1_1	Scaffold
R.n.2-A	Scaffold
S_9_1	Scaffold
S_5_1	Scaffold
R.n.1-B	Scaffold
FUA 3048	Scaffold
R.n.3-A	Scaffold
FUA 3043	Scaffold
FUA 3041	Scaffold
3B	Scaffold
D.l.1-B	Scaffold
C.p.1-C	Scaffold
C4	Scaffold
C3	Scaffold
D.l.3-A	Scaffold
CC-AA2-1	Scaffold
CC-AA2-2	Scaffold
WF-AA1-A	Scaffold
O_Tuki_7_1	Scaffold
WF-AA1-C	Scaffold
O_Ruby_9_1	Scaffold
O_Ruby_8_1	Scaffold
apa71	Scaffold
PM_Patrick_6_1	Scaffold
MR6	Scaffold
MR2	Scaffold
PM_Patrick_1_1	Scaffold
PM_Patrick_2_1	Scaffold
M_Angie_4_1	Scaffold
M_Angie_1_1	Scaffold
6C	Scaffold
6B	Scaffold
6A	Scaffold

LTM_Sauna_1_1	Scaffold
SM_1_4_1	Scaffold
LTM_Jesus_5_1	Scaffold
G_6_1	Scaffold
LTM_Jesus_1_1	Scaffold
BHM_Lincecum_1_1	Scaffold
BHM_Lincecum_2_1	Scaffold
BHM_Thaddeus_2_1	Scaffold
AG_2_6_1	Scaffold
AG_3_1_1	Scaffold
21D	Scaffold
21B	Scaffold
PNG008C_M	Scaffold
21A	Scaffold
PB-W2	Scaffold
AG_1_1_1	Scaffold
PNG008A_M	Scaffold
PNG008_ANA	Scaffold
PB-W1	Scaffold
MV4-1a	Scaffold
PNG008_48h	Scaffold
M81-R43	Scaffold
MM36-1a	Scaffold
PNG008_24h	Scaffold
FJ3	Scaffold
ME-261	Scaffold
ME-262	Scaffold
SR14	Scaffold
LMS11-1	Scaffold
LMS11-3	Contig
SR11	Scaffold
Cor137_1_1	Scaffold
Cor124_1_1	Scaffold
T3	Scaffold
T1	Scaffold
tu160	Scaffold
Cor137_3_1	Scaffold
GQ_1_2_1	Contig
GQ_1_7_1	Scaffold
GQ_1_3_1	Scaffold
L3B	Scaffold
GP6	Scaffold
GP1	Scaffold
GP3	Scaffold
EF3_1	Scaffold
EF1_1	Contig
11B	Scaffold
11A	Scaffold
AP5	Scaffold
EF2_1	Scaffold
AP3	Scaffold
4A	Scaffold
AP1	Scaffold
3630	Chromosome
3632	Chromosome
VHProbi E18	Complete Genome
VHProbi M07	Complete Genome
LLR-K67	Scaffold
RTR	Complete Genome
DS0384	Complete Genome
M2021619	Complete Genome
S30_Bin4	Contig
QAULRN18	Scaffold
QAULRN15	Scaffold
BR13-C2	Contig
PB2	Contig

L11	Chromosome
L8	Chromosome
SUG627	Contig
SUG350	Contig
SUG1061	Contig
EFEL6901	Complete Genome
PH-3	Scaffold
DSM 28673	Contig
DSM 100192	Contig
DSM 100191	Contig
FN041	Complete Genome
CIRM-BIA 2122	Contig
CIRM-BIA 1439	Contig
CIRM-BIA 696	Contig
CIRM-BIA 522	Contig
CIRM-BIA 911	Contig
CIRM-BIA 1534	Contig
CIRM-BIA 929	Contig
CIRM-BIA 912	Contig
CIRM-BIA 2121	Contig
AM_LB1	Complete Genome
SRCM210547	Contig
QS01	Chromosome
NPLps08.pb	Contig
NPLps01.et-05	Contig
NPLps02.uf-01	Contig
BRD_L17	Complete Genome
LR6	Scaffold
CML393	Contig
92071	Contig
92126	Contig
92128	Contig
SRCM217616	Contig
SRCM217617	Contig
SRCM217606	Contig
SRCM217608	Contig
SRCM217607	Contig
SRCM217611	Contig
SUG1981	Contig
L6798	Scaffold
Marseille-P4870	Scaffold
Marseille-P5461	Scaffold
Marseille-P5460	Scaffold
Marseille-P4904	Scaffold
INIA P572, INIA P572	Contig
Chicken_14_mag_57	Scaffold
Chicken_19_mag_122	Scaffold
A55_47.LR.DSS	Scaffold
A12_4.LR.DSS	Scaffold
2.LR.Ymh	Scaffold
A33_25_LR_DSS	Scaffold
C31	Scaffold
MGBC110046	Scaffold
IM842	Contig
IM110	Contig
IM566	Contig
AMBV339	Scaffold
BRZ_DH__bin65	Contig
dsm_us_coassembly__bin32	Contig

Supplementary Table 4 Cobamide biosynthetic genes screened against *L. reuteri* genomes in comparative genomic analysis. The table provides the gene name, the origin of the gene sequence and the corresponding reference.

Gene	Gene sequence origin	Reference
BluB	*Pseudomonas denitrificans*	Pollich and Klug, 1995
BzaA	*Eubacterium limosum* ATCC 10825	Hazra *et al.*, 2015
BzaB	*Eubacterium limosum* ATCC 10825	Hazra *et al.*, 2015
BzaC	*Eubacterium limosum* ATCC 10825	Hazra *et al.*, 2015
BzaD	*Eubacterium limosum* ATCC 10825	Hazra *et al.*, 2015
BzaE	*Eubacterium limosum* ATCC 10825	Hazra *et al.*, 2015
BzaF	*Eubacterium limosum* ATCC 10825	Hazra *et al.*, 2015
CbiA	*L. reuteri* DSM20016	
CbiB_CobD	*L. reuteri* DSM20016	
CbiC	*L. reuteri* DSM20016	
CbiD	*L. reuteri* DSM20016	
CbiE	*L. reuteri* DSM20016	
CbiET	*L. reuteri* DSM20016	
CbiF	*L. reuteri* DSM20016	
CbiG	*L. reuteri* DSM20016	
CbiH	*L. reuteri* DSM20016	
CbiJ	*L. reuteri* DSM20016	
CbiK	*L. reuteri* DSM20016	
CbiL	*L. reuteri* DSM20016	
CbiM	*L. reuteri* DSM20016	
CbiN	*L. reuteri* DSM20016	
CbiO	*L. reuteri* DSM20016	
CbiP_CobQ	*L. reuteri* DSM20016	
CbiQ	*L. reuteri* DSM20016	
CbiT	*L. reuteri* DSM20016	
CbiZ	*Halobacterium* sp. strain NRC-1	Woodson and Escalante-Semerena, 2004
CobA	*L. reuteri* DSM20016	
CobB	*L. reuteri* DSM20016	
CobC	*L. reuteri* DSM20016	
CobD	*L. reuteri* DSM20016	
CobF	*Pseudomonas denitrificans* (nom. rej.)	Crouzet *et al.*, 1990
CobG	*Pseudomonas denitrificans* (nom. rej.)	Crouzet *et al.*, 1990
CobH	*L. reuteri* DSM20016	
CobI	*L. reuteri* DSM20016	
CobJ	*L. reuteri* DSM20016	
CobK	*Pseudomonas denitrificans* (nom. rej.)	Crouzet *et al.*, 1990
CobL	*L. reuteri* DSM20016	
CobM	*L. reuteri* DSM20016	
CobN	*Pseudomonas denitrificans* (nom. rej.)	Crouzet *et al.*, 1990
CobR	*Brucella melitensis* (BMEI0709)	Lawrence *et al.*, 2008
CobS	*L. reuteri* DSM20016	
CobS_aerobic	*Pseudomonas denitrificans* (nom. rej.)	Crouzet *et al.*, 1990
CobT	*L. reuteri* DSM20016	
CobT_aerobic	*Pseudomonas denitrificans* (nom. rej.)	Crouzet *et al.*, 1990
CobU	*L. reuteri* DSM20016	
CobW	*Pseudomonas denitrificans* (nom. rej.)	Crouzet *et al.*, 1990
CobY	*Methanocaldococcus jannaschii*	Bult *et al.*, 1996
CysG	*L. reuteri* DSM20016	
CysGA-HemD	*L. reuteri* DSM20016	
FldA	*L. reuteri* DSM20016	
GltX	*L. reuteri* DSM20016	
HemA	*L. reuteri* DSM20016	
HemB	*L. reuteri* DSM20016	
HemC	*L. reuteri* DSM20016	
HemD	*L. reuteri* DSM20016	
HemK	*L. reuteri* DSM20016	
HemL	*L. reuteri* DSM20016	
HemZ	*Bacillus subtilis* strain 168	Homuth *et al.*, 1999
PduX	*Salmonella* Typhimurium (strain LT2 / SGSC1412 / ATCC 700720)	Bobik *et al.*, 1999

SirC	*L. reuteri* DSM20016	

Supplementary Table 5 List of *L. reuteri* strains possessing a cobamide biosynthesis pathway. The table provides the name of the strains, the corresponding assembly level of the genome and the host origin.

Predicted cobamide producing strains	Level	Host
L. reuteri 103b	Scaffold	Mouse
L. reuteri 103o	Scaffold	Mouse
L. reuteri 103p	Scaffold	Mouse
L. reuteri 103v	Scaffold	Mouse
L. reuteri 105p	Scaffold	Mouse
L. reuteri 111b	Scaffold	Mouse
L. reuteri 111f	Scaffold	Mouse
L. reuteri 111l	Scaffold	Mouse
L. reuteri 111v	Scaffold	Mouse
L. reuteri 117n	Scaffold	Mouse
L. reuteri 117r	Scaffold	Mouse
L. reuteri 117w	Scaffold	Mouse
L. reuteri 121	Contig	Pig
L. reuteri 1366	Scaffold	Chicken
L. reuteri 1B	Complete	Horse
L. reuteri 20_2	Scaffold	Pig
L. reuteri 2010	Contig	Rat
L. reuteri 2A	Contig	Rodent
L. reuteri 4A	Scaffold	Bird
L. reuteri 92071	Contig	Food
L. reuteri 92126	Contig	Food
L. reuteri 92128	Contig	Food
L. reuteri AM_LB1	Complete Genome	Bird
L. reuteri An166	Contig	Chicken
L. reuteri An71	Contig	Chicken
L. reuteri AP1	Scaffold	Bird
L. reuteri AP3 (China)	Scaffold	Bird
L. reuteri AP3 (USA)	Scaffold	Bird
L. reuteri AP5	Scaffold	Bird
L. reuteri apa71	Scaffold	Primate
L. reuteri ATCC 53608	Complete	Pig
L. reuteri ATG-F4	Complete	Human
L. reuteri BRZ_DH__bin65	Contig	Chicken
L. reuteri BSD2780061688_150302_A4	Scaffold	Human
L. reuteri C.p.1-C	Scaffold	Rodent
L. reuteri C3	Scaffold	Rodent
L. reuteri C4	Scaffold	Rodent
L. reuteri C88	Scaffold	Human
L. reuteri C93	Scaffold	Human
L. reuteri CC-AA2-1	Scaffold	Mouse
L. reuteri CC-AA2-2	Scaffold	Mouse
L. reuteri CF48-3A	Scaffold	Human
L. reuteri Chicken_19_mag_122	Scaffold	Chicken
L. reuteri CIRM-BIA 1439	Contig	Unknown
L. reuteri CIRM-BIA 2122	Contig	Unknown
L. reuteri CIRM-BIA 522	Contig	Human
L. reuteri CIRM-BIA 911	Contig	Whey
L. reuteri CML393	Contig	Chicken
L. reuteri CNEI-KCA3	Complete	Chicken
L. reuteri COPD095	Contig	Human
L. reuteri Cor137_1_1	Scaffold	Human
L. reuteri Cor137_3_1	Scaffold	Human
L. reuteri CR	Contig	Rat
L. reuteri CRL 1098	Contig	Sourdough
L. reuteri D.l.1-B	Scaffold	Rodent
L. reuteri D.l.3-A	Scaffold	Rodent
L. reuteri DS0384	Complete	Human

L. reuteri DS13_10	Contig	Human
L. reuteri DS14_10	Contig	Human
L. reuteri DS17_10	Contig	Human
L. reuteri DS22_10	Contig	Human
L. reuteri DSM 20016_JGI	Complete Genome	Human
L. reuteri E	Contig	Sheep
L. reuteri E81	Contig	Sourdough
L. reuteri EF1_1	Contig	Bird
L. reuteri EF2_1	Scaffold	Bird
L. reuteri EF3_1	Scaffold	Bird
L. reuteri EFEL6901	Complete Genome	Unknown
L. reuteri FJ3	Scaffold	Human
L. reuteri G01_USFQ	Contig	Mouse
L. reuteri G02_USFQ	Contig	Mouse
L. reuteri G03_USFQ	Contig	Mouse
L. reuteri GP1	Scaffold	Bird
L. reuteri GP3	Scaffold	Bird
L. reuteri GP6	Scaffold	Bird
L. reuteri GQ_1_2_1	Contig	Bird
L. reuteri GQ_1_3_1	Scaffold	Bird
L. reuteri GQ_1_7_1	Scaffold	Bird
L. reuteri HI24	Contig	Curd
L. reuteri I8-5	Scaffold	Mouse
L. reuteri IM566	Contig	Food
L. reuteri IM842	Contig	Human
L. reuteri INIA P572	Contig	Pig
L. reuteri IRT	Complete	Human
L. reuteri JCM 1081	Scaffold	Chicken
L. reuteri JCM 1112	Complete	Human
L. reuteri KLR1004	Contig	Pig
L. reuteri KLR2002	Contig	Pig
L. reuteri KLR2003	Contig	Pig
L. reuteri KLR2007	Contig	Pig
L. reuteri KLR2008	Contig	Pig
L. reuteri KLR3004	Contig	Pig
L. reuteri KLR3005	Contig	Pig
L. reuteri KLR4001	Contig	Pig
L. reuteri L8	Chromosome	Cattle
L. reuteri LLR-K67	Scaffold	Human
L. reuteri LMS11-1	Scaffold	Human
L. reuteri LMS11-3	Contig	Human
L. reuteri LR1 (China)	Scaffold	Goat
L. reuteri LR1 (Russia)	Contig	Human
L. reuteri LR10	Scaffold	Cow
L. reuteri LR13	Scaffold	Cow
L. reuteri LR14	Scaffold	Goat
L. reuteri LR17	Scaffold	Horse
L. reuteri LR18	Scaffold	Horse
L. reuteri LR19	Scaffold	Horse
L. reuteri LR2	Scaffold	Goat
L. reuteri LR3	Scaffold	Goat
L. reuteri LR4	Scaffold	Cow
L. reuteri Lr4000	Contig	Mouse
L. reuteri Lr4020	Contig	Mouse
L. reuteri LR5A	Scaffold	Sourdough
L. reuteri LR6 (India)	Scaffold	Human
L. reuteri LR8	Scaffold	Sheep
L. reuteri LR9	Scaffold	Sheep
L. reuteri LTM_Sauna_1_1	Scaffold	Primate
L. reuteri M2021619	Complete	Human
L. reuteri M27U15	Scaffold	Human
L. reuteri M81-R43	Scaffold	Human
L. reuteri ME-261	Scaffold	Human
L. reuteri ME-262	Scaffold	Human
L. reuteri mlc3	Contig	Rodent
L. reuteri MM2-3	Scaffold	Human

L. reuteri MM34-4A	Scaffold	Human
L. reuteri MM36-1a	Scaffold	Human
L. reuteri MM4-1A	Contig	Human
L. reuteri MR2	Scaffold	Primate
L. reuteri MR6	Scaffold	Primate
L. reuteri MV4-1a	Scaffold	Human
L. reuteri NPLps01.et-05	Contig	Probiotic supplement
L. reuteri NPLps02.uf-01	Contig	Probiotic supplement
L. reuteri NPLps08.pb	Contig	Probiotic supplement
L. reuteri One-one	Contig	Mouse
L. reuteri OSU_LbReu_2.2	Contig	Chicken
L. reuteri PB-W2	Scaffold	Human
L. reuteri PM_Patrick_2_1	Scaffold	Primate
L. reuteri PTA1_C1	Scaffold	Chicken
L. reuteri PTA1_C3	Scaffold	Chicken
L. reuteri PTA1_C4	Scaffold	Chicken
L. reuteri PTA1_F3	Scaffold	Chicken
L. reuteri PTA2_C2	Scaffold	Chicken
L. reuteri PTA4_C1	Scaffold	Chicken
L. reuteri PTA4_C2	Scaffold	Chicken
L. reuteri PTA4_C4	Scaffold	Chicken
L. reuteri PTA5_C13	Scaffold	Chicken
L. reuteri PTA5_C4	Scaffold	Chicken
L. reuteri PTA5_C5	Scaffold	Chicken
L. reuteri PTA5_C6B	Scaffold	Chicken
L. reuteri PTA5_F1	Scaffold	Chicken
L. reuteri PTA5_F11	Scaffold	Chicken
L. reuteri PTA5_F13	Scaffold	Chicken
L. reuteri PTA5_F4	Scaffold	Chicken
L. reuteri PTA6_C2	Scaffold	Chicken
L. reuteri PTA6_C7	Scaffold	Chicken
L. reuteri PTA6_F1	Scaffold	Chicken
L. reuteri PTA6_F2	Scaffold	Chicken
L. reuteri PTA6_F4	Scaffold	Chicken
L. reuteri PTA6_F6	Scaffold	Chicken
L. reuteri PTA6_F8	Scaffold	Chicken
L. reuteri RC-14	Contig	Probiotic Capsule
L. reuteri reuteri	Complete	Human
L. reuteri RTR	Complete	Fermented Fruit
L. reuteri S_1_1	Scaffold	Rodent
L. reuteri S_5_1	Scaffold	Rodent
L. reuteri S_9_1	Scaffold	Rodent
L. reuteri SD2112	Complete	Human
L. reuteri SD-LRE2-IT	Complete	Human
L. reuteri SR11	Scaffold	Human
L. reuteri SR14	Scaffold	Human
L. reuteri SRCM217606	Contig	Cattle
L. reuteri SRCM217607	Contig	Cattle
L. reuteri SRCM217608	Contig	Cattle
L. reuteri SRCM217611	Contig	Cattle
L. reuteri SRCM217616	Contig	Cattle
L. reuteri SRCM217617	Contig	Cattle
L. reuteri subsp. reuteri DSM 20016_Shanghai Majorbio	Scaffold	Human
L. reuteri SUG1061	Contig	Pig
L. reuteri T1	Scaffold	Bird
L. reuteri T3	Scaffold	Bird
L. reuteri TK-F8A	Complete	Probiotic Products
L. reuteri tu160	Scaffold	Bird
L. reuteri VA24-5	Contig	Human
L. reuteri VHProbi E18	Complete	Unknown
L. reuteri VHProbi M07	Complete	Unknown
L. reuteri WCA-386-APC-4I	Contig	Pig
L. reuteri WF-AA1-A	Scaffold	Mouse
L. reuteri WF-AA1-C	Scaffold	Mouse
L. reuteri YLR001	Complete	Yak
L. reuteri Z5	Scaffold	Gruel

L. reuteri Z6	Scaffold	Gruel
L. reuteri ZLR003	Complete	Pig

Supplementary Table 6 List of *R. gnavus* strains included in comparative genomic analysis. The table provides the name of the strains and the corresponding assembly level of the genome.

R. gnauvs strain	Level
CC55_001C	Scaffold
AGR2154	Contig
2789STDY5608852	Scaffold
RJX1128	Scaffold
RJX1126	Scaffold
RJX1124	Scaffold
RJX1125	Scaffold
RJX1123	Scaffold
RJX1127	Scaffold
RJX1120	Scaffold
RJX1122	Scaffold
RJX1119	Scaffold
RJX1121	Scaffold
RJX1118	Scaffold
ATCC 29149_HGAP	Contig
TM04-16	Scaffold
TF01-20-2	Scaffold
AF27-4BH	Scaffold
AF24-23LB	Scaffold
AF19-16AC	Scaffold
AM51-4BH	Scaffold
AF13-14A	Scaffold
AM38-12	Scaffold
AM32-6	Scaffold
AM27-32	Scaffold
AM25-19	Scaffold
AM21-41	Scaffold
AM22-7AC	Scaffold
AM21-18	Scaffold
AM17-51	Scaffold
AM13-39	Scaffold
AM12-54	Scaffold
AF34-4BH	Scaffold
AF33-12	Scaffold
ATCC 29149_JCM6515	Complete Genome
S04B.meta.bin_4	Contig
S04A.meta.bin_8	Contig
LMAG:97	Contig
LMAG:9	Contig
ATCC 29149	Complete Genome
MSK.5.19	Contig
MSK.15.58	Contig
MSK.5.17	Contig
MSK.23.91	Contig
MSK.19.38	Contig
MSK.17.63	Contig
MSK.7.31	Contig
MSK.23.82	Contig
MSK.23.93	Contig
MSK.7.28	Contig
MSK.23.81	Contig
MSK.23.92	Contig
MSK.23.63	Contig
MSK.23.71	Contig
MSK.23.62	Contig
MSK.23.61	Contig

MSK.23.60	Contig
MSK.23.56	Contig
MSK.23.55	Contig
MSK.23.43	Contig
MSK.23.46	Contig
MSK.22.53	Contig
MSK.23.41	Contig
MSK.17.82	Contig
MSK.22.24	Contig
MSK.19.33	Contig
MSK.15.9	Contig
MSK.15.77	Contig
MSK.15.54	Contig
MSK.15.56	Contig
MSK.15.59	Contig
MSK.15.32	Contig
MSK.15.18	Contig
MSK.15.10	Contig
MSK.11.9	Contig
D40t1_170626_D9	Scaffold
1001285H_161024_A10	Scaffold
1001302B_160321_G6	Scaffold
D52t1_170925_A9	Scaffold
BSD2780120874_150323_G6	Scaffold
D31t1_170403_H6	Scaffold
D33t1_170424_E3	Scaffold
BSD2780061687_150420_H1	Scaffold
FDAARGOS_1342	Complete Genome
BBMGS-G03-110	Contig
BBMGS-G03-111	Contig
BBSGM-G02-100	Contig
BBMGS-G01-107	Contig
CD14_MAG27	Contig
HRGM_Genome_0289	Scaffold
HRGM_Genome_0287	Scaffold
NBRC 114413	Complete Genome
MSK.7.5	Contig
MSK.23.4	Contig
MSK.8.22	Contig
MSK.23.20	Contig
MSK.23.17	Contig
MSK.23.18	Contig
MSK.22.96	Contig
MSK.23.10	Contig
MSK.22.91	Contig
ET50	Contig
S9_Bin4	Contig
MSK.23.27	Contig
B93_003	Contig
B699_001	Contig
B636_003	Contig
B619_003	Contig
B266_002	Contig
B596_002	Contig
Map_60_010	Contig
Map_42_007	Contig
Map_67_007	Contig
Map_17_009	Contig
Map_123_010	Contig
Map_121_019	Contig
SUG771	Contig
SL.2.31	Contig
bin_13_DannyCat	Contig
JCM6515	Complete Genome
CCUG 57137	Contig
CCUG 57208	Contig

PS/160	Contig
CCUG 43222	Contig
CCUG 54531	Contig
CCUG 57161	Contig
CCUG 49994	Contig
CCUG 43437	Contig
CCUG 51289	Contig
CCUG 52279	Contig
RSHDN_121	Contig
RSHDN_123	Contig
AM10-1A	Scaffold
AM25-21	Scaffold
AM97-54	Scaffold
RTP21484st1_H11_RTP21484_190118	Scaffold
J1101312st1_A7_J1101312_190322	Scaffold
RTP21484st1_E7_RTP21484_190118	Scaffold
J1101312st1_A12_J1101312_190322	Scaffold
RTP21484st1_C12_RTP21484_190118	Scaffold
J1101312st1_A9_J1101312_190322	Scaffold
D33st1_G9_D33t1_170424	Scaffold
BSD2780120874st1_F6_2217SCRN_200827	Scaffold
BSD2780120874st1_E4_2217SCRN_200827	Scaffold
BSD3448080968st1_G7_BSD3448080968_160620	Scaffold
BSD2780061687st1_E4_BSD2780061687_150420	Scaffold
2217st1_G3_2217SCRN_200827	Scaffold
2217st1_H4_2217SCRN_200827	Scaffold
1001217st1_G9_1001217B_191108	Scaffold
1001217st1_B7_1001217B_191108	Scaffold
1001217st1_D6_1001217B_191108	Scaffold
1001285st1_H5_1001285H_161024	Scaffold
1001217st1_A9_1001217B_191108	Scaffold
RSHDN_122	Contig
RSHDN_120	Contig
TS8243C	Contig
MGYG-HGUT-01380	Scaffold
SRR413770-bin.1	Contig
Finegold	Contig
E1	Complete Genome
ATCC 35913	Scaffold
2_1_58FAA	Complete Genome

Supplementary Table 7 Cobamide biosynthetic genes screened against *R. gnavus* genomes in comparative genomic analysis. The table provides the gene name, the origin of the gene sequence and the corresponding reference.

Gene	Origin	Reference
BluB	*Rhizobium meliloti* strain 1021	(Capela *et al.*, 2001)
BzaABCDE	*Eubacterium limosum* strain ATCC 10825	(Hazra *et al.*, 2015)
CbiA	*R. gnavus* ATCC 29149	
CbiB	*R. gnavus* ATCC 29149	
CbiC	*R. gnavus* ATCC 29149	
CbiD	*R. gnavus* ATCC 29149	
CbiE	*Salmonella* Typhimurium (strain LT2 / SGSC1412 / ATCC 700720)	(Roth *et al.*, 1993)
CbiET	*R. gnavus* ATCC 29149	
CbiF	*R. gnavus* ATCC 29149	
CbiG	*R. gnavus* ATCC 29149	
CbiH	*R. gnavus* ATCC 29149	
CbiJ	*R. gnavus* ATCC 29149	
CbiK	*R. gnavus* ATCC 29149	
CbiL	*R. gnavus* ATCC 29149	

CbiM	*R. gnavus* ATCC 29149	
CbiN	*R. gnavus* ATCC 29149	
CbiO	*R. gnavus* ATCC 29149	
CbiP	*R. gnavus* ATCC 29149	
CbiQ	*R. gnavus* ATCC 29149	
CbiT	*Salmonella* Typhimurium (strain LT2 / SGSC1412 / ATCC 700720)	(Roth *et al.*, 1993)
CbiZ	*Halobacterium salinarum* (strain ATCC 700922 / JCM 11081 / NRC-1)	(Pfeiffer *et al.*, 2008)
CobA	*R. gnavus* ATCC 29149	
CobB	*R. gnavus* ATCC 29149	
CobC	*R. gnavus* ATCC 29149	
CobD	*R. gnavus* ATCC 29149	
CobF	*Pseudomonas denitrificans*	(Crouzet *et al.*, 1990)
CobG	*Pseudomonas denitrificans*	(Crouzet *et al.*, 1990)
CobH	*R. gnavus* ATCC 29149	
CobI	*R. gnavus* ATCC 29149	
CobJ	*R. gnavus* ATCC 29149	
CobK	*R. gnavus* ATCC 29149	
CobL	*R. gnavus* ATCC 29149	
CobM	*R. gnavus* ATCC 29149	
CobN	*Pseudomonas denitrificans*	(Crouzet *et al.*, 1990)
CobR	*Propionibacterium freudenreichii*	(Falentin *et al.*, 2010)
CobS	*R. gnavus* ATCC 29149	
CobS_aerobic	*Pseudomonas denitrificans*	(Crouzet *et al.*, 1990)
CobT	*R. gnavus ATCC 29149*	
CobT_aerobic	*R. gnavus ATCC 29149*	
CobU	*R. gnavus ATCC 29149*	
CobW	*R. gnavus ATCC 29149*	
CobY	*Methanocaldococcus jannaschii* (strain ATCC 43067 / DSM 2661	(Otte and Escalante-Semerena, 2009)
CysG2_SirC	*R. gnavus* ATCC 29149	
CysGA-hemD	*R. gnavus* ATCC 29149	
CysGA	*R. gnavus* ATCC 29149	
FldA	*R. gnavus* ATCC 29149	
GltX	*R. gnavus* ATCC 29149	
HemA	*Salmonella* Typhimurium (strain LT2 / SGSC1412 / ATCC 700720)	(Roth *et al.*, 1993)
HemB	*Salmonella* Typhimurium (strain LT2 / SGSC1412 / ATCC 700720)	(Roth *et al.*, 1993)
HemC	*R. gnavus* ATCC 29149	
HemD	*Salmonella* Typhimurium (strain LT2 / SGSC1412 / ATCC 700720)	(Roth *et al.*, 1993)
HemK	*Salmonella* Typhimurium (strain LT2 / SGSC1412 / ATCC 700720)	(Roth *et al.*, 1993)
HemL	*Salmonella* Typhimurium (strain LT2 / SGSC1412 / ATCC 700720)	(Roth *et al.*, 1993)
HemZ	*R. gnavus* ATCC 29149	
PduX	Salmonella Typhimurium (strain LT2 / SGSC1412 / ATCC 700720)	(Roth *et al.*, 1993)
SmtA	*R. gnavus* ATCC 29149	(Roth *et al.*, 1993)
ThiC	*R. gnavus* ATCC 29149	(Hazra *et al.*, 2015)
CblS	*Burkholderia cenocepacia* J2315	(Holden *et al.*, 2009)

Supplementary Table 8 *Ruminococcus gnavus* strains predicted positive for cobamide synthesis from PBG.

R. gnavus strain
1001217st1_A9_1001217B_191108
1001217st1_B7_1001217B_191108
1001217st1_D6_1001217B_191108
1001217st1_G9_1001217B_191108
1001285H_161024_A10
1001285st1_H5_1001285H_161024
1001302B_160321_G6
2_1_58FAA
2789STDY5608852
AF13-14A
AF19-16AC
AF24-23LB

AF27-4BH
AF33-12
AF34-4BH
AM10-1A
AM12-54
AM13-39
AM17-51
AM21-18
AM21-41
AM22-7AC
AM25-19
AM25-21
AM27-32
AM32-6
AM38-12
AM51-4BH
AM97-54
ATCC 29149
ATCC 29149_HGAP3
ATCC 29149_JCM6515
ATCC 35913
B266_002
B596_002
B619_003
B699_001
B93_003
BBMGS-G01-107
BBMGS-G03-110
BBMGS-G03-111
BBSGM-G02-100
bin_13_DannyCat
BSD2780061687_150420_H1
BSD2780061687st1_E4_BSD2780061687_150420
BSD2780120874st1_E4_2217SCRN_200827
BSD2780120874st1_F6_2217SCRN_200827
BSD3448080968st1_G7_BSD3448080968_160620
CC55_001C
CCUG 43222
CCUG 43437
CCUG 49994
CCUG 51289
CCUG 52279
CCUG 54531
CCUG 57137
CCUG 57161
CCUG 57208
CD14_MAG27
D31t1_170403_H6
D33st1_G9_D33t1_170424
D33t1_170424_E3
D40t1_170626_D9
D52t1_170925_A9
E1
ET50
FDAARGOS_1342
Finegold
HRGM_Genome_0287
HRGM_Genome_0289

J1101312st1_A12_J1101312_190322
J1101312st1_A7_J1101312_190322
J1101312st1_A9_J1101312_190322
JCM6515
LMAG:9
LMAG:97
Map_121_019
Map_123_010
Map_42_007
Map_67_007
MGYG-HGUT-01380
MSK.11.9
MSK.15.10
MSK.15.18
MSK.15.32
MSK.15.54
MSK.15.56
MSK.15.58
MSK.15.59
MSK.15.77
MSK.15.9
MSK.17.63
MSK.17.82
MSK.19.33
MSK.19.38
MSK.22.24
MSK.22.53
MSK.22.91
MSK.22.96
MSK.23.10
MSK.23.17
MSK.23.18
MSK.23.20
MSK.23.27
MSK.23.4
MSK.23.41
MSK.23.43
MSK.23.46
MSK.23.55
MSK.23.56
MSK.23.60
MSK.23.61
MSK.23.62
MSK.23.63
MSK.23.71
MSK.23.81
MSK.23.82
MSK.23.91
MSK.23.92
MSK.23.93
MSK.5.17
MSK.5.19
MSK.7.28
MSK.7.31
MSK.7.5
NBRC 114413
PS/160
RJX1118

RJX1119
RJX1120
RJX1121
RJX1122
RJX1123
RJX1124
RJX1125
RJX1126
RJX1127
RJX1128
RSHDN_120
RSHDN_121
RSHDN_122
RSHDN_123
RTP21484st1_C12_RTP21484_190118
RTP21484st1_E7_RTP21484_190118
RTP21484st1_H11_RTP21484_190118
S9_Bin4
SL.2.31
SRR413770-bin.1
SUG771
TF01-20-2
TM04-16
TS8243C

Supplementary Table 9 *R. gnavus* cobamide specific genes (covering genes encoding cobamide-dependent, biosynthetic or transport proteins), significantly upregulated at 9 hours of growth in response to CNPsCbl supplementation under methionine deficient conditions.

Gene id	L2FC	pvalue	padj	Gene description
RGna_RS04055	0.76	0.001669	0.019383	Vitamin B12 dependent methionine synthase activation subunit && PF02965:Vitamin B12 dependent methionine synthase, activation domain
RGna_RS05485	1.12	0.014073	0.098212	bifunctional adenosylcobinamide kinase/adenosylcobinamide-phosphate guanylyltransferase && PF02283:Cobinamide kinase / cobinamide phosphate guanyltransferase
RGna_RS04050	0.41	0.01834	0.116269	homocysteine S-methyltransferase family protein && PF02607:B12 binding domain|PF02310:B12 binding domain|PF00809:Pterin binding enzyme|PF02574:Homocysteine S-methyltransferase

Supplementary Table 10 *R. gnavus* cobamide specific genes (covering genes encoding cobamide-dependent, biosynthetic or transport proteins), significantly upregulated at 12 hours of growth in response to CNPsCbl supplementation under methionine deficient conditions.

Gene id	L2FC	pvalue	padj	Gene description
RGna_RS03450	0.44	0.00581084	0.03472308	ECF transporter S component && -

Supplementary Table 11 *R. gnavus* cobamide specific genes (covering genes encoding cobamide-dependent, biosynthetic or transport proteins), significantly upregulated at 9 hours of growth in response to *L. reuteri* MM4-1A inoculation under methionine deficient conditions.

Gene id	L2FC	pvalue	padj	Gene description
RGna_RS04055	0.65	0.0009508	0.01173202	Vitamin B12 dependent methionine synthase activation subunit && PF02965:Vitamin B12 dependent methionine synthase, activation domain
RGna_RS05485	1.08	0.00944613	0.06608619	bifunctional adenosylcobinamide kinase/adenosylcobinamide-phosphate guanylyltransferase && PF02283:Cobinamide kinase / cobinamide phosphate guanyltransferase
RGna_RS06665	0.51	0.01710379	0.0993951	propanediol/glycerol family dehydratase large subunit && PF02286:Dehydratase large subunit
RGna_RS04050	0.32	0.02619222	0.13578497	homocysteine S-methyltransferase family protein && PF02607:B12 binding domain|PF02310:B12 binding domain|PF00809:Pterin binding enzyme|PF02574:Homocysteine S-methyltransferase
RGna_RS05510	0.47	0.03295411	0.15768083	uroporphyrinogen-III C-methyltransferase && PF00590:Tetrapyrrole (Corrin/Porphyrin) Methylases|PF02602:Uroporphyrinogen-III synthase HemD
RGna_RS03450	0.33	0.04013776	0.17909059	ECF transporter S component && -
RGna_RS14310	0.45	0.0289267	0.1441535	ECF transporter S component && PF12822:Protein of unknown function (DUF3816)

Supplementary Table 12 *R. gnavus* cobamide specific genes (covering genes encoding cobamide-dependent, biosynthetic or transport proteins), significantly upregulated at 12 hours of growth in response to *L. reuteri* MM4-1A inoculation under methionine deficient conditions.

Gene id	L2FC	pvalue	padj	Gene description
RGna_RS03450	0.77	0.0048551	0.07276888	ECF transporter S component && -
RGna_RS05590	0.95	0.01817584	0.17477532	cobalt ECF transporter T component CbiQ && PF02361:Cobalt transport protein

Supplementary Table 13 *R. gnavus* cobamide specific genes (covering genes encoding cobamide-dependent, biosynthetic or transport proteins), significantly

upregulated at 9 hours of growth in response to PBG supplementation under methionine deficient conditions.

Gene id	L2FC	pvalue	padj	Gene description
RGna_RS04055	0.82	0.026286	0.464782	Vitamin B12 dependent methionine synthase activation subunit && PF02965:Vitamin B12 dependent methionine synthase, activation domain
RGna_RS06655	0.75	0.047599	0.531994	diol dehydratase small subunit && PF02287:Dehydratase small subunit

Supplementary Table 14 Top 35 most dominant species in faecal donor and their relative abundances.

Species	Relative abundance
g__Escherichia;s__Escherichia coli	0.000297
g__Limosilactobacillus;s__Limosilactobacillus reuteri	8.09E-07
g__Streptococcus;s__Streptococcus thermophilus	0.03752
g__Roseburia;s__Roseburia faecis	0.01949
g__Citrobacter;s__Citrobacter farmeri	5.59E-05
g__Eubacterium;s__Eubacterium ventriosum	0.013787
g__Enterobacter;s__Enterobacter hormaechei	2.63E-05
g__Enterococcus;s__Enterococcus faecalis	0.00022
g__Phocaeicola;s__Phocaeicola vulgatus	0.009123
g__Roseburia;s__Roseburia intestinalis	0.0092
g__Faecalibacterium;s__Faecalibacterium prausnitzii	0.005513
g__Fusicatenibacter;s__Fusicatenibacter saccharivorans	0.006423
g__Streptococcus;s__Streptococcus salivarius	0.001679
g__Roseburia;s__Roseburia inulinivorans	0.006296
g__Holdemanella;s__Holdemanella porci	0.005671
g__Unclassified;s__Caudoviricetes sp.	0.005444
g__Bifidobacterium;s__Bifidobacterium longum	0.003796
g__Enterococcus;s__Enterococcus faecium	0.000132
g__Mediterraneibacter;s__[Ruminococcus] lactaris	0.004019
g__Collinsella;s__Collinsella aerofaciens	0.003521
g__Sutterella;s__Sutterella seckii	0.002687
g__Phascolarctobacterium;s__Phascolarctobacterium succinatutens	0.003509
g__Holdemanella;s__Holdemanella biformis	0.003394
g__Bifidobacterium;s__Bifidobacterium adolescentis	0.00105
g__Anaerostipes;s__Anaerostipes hadrus	0.002611
g__Bacteroides;s__Bacteroides ovatus	0.002584
g__Lachnospira;s__Lachnospira pectinoschiza	0.001913
g__Parabacteroides;s__Parabacteroides merdae	0.002326
g__Blautia;s__Blautia sp. KLE 1732	0.002095
g__Slackia;s__Slackia isoflavoniconvertens	0.002242
g__Mediterraneibacter;s__[Ruminococcus] gnavus	0.002031
g__Haemophilus;s__Haemophilus parainfluenzae	0.000861
g__Paratractidigestivibacter;s__Paratractidigestivibacter faecalis	0.001918
g__Klebsiella;s__Klebsiella pneumoniae	9.38E-05
g__Eubacterium;s__Eubacterium sp. CAG:38	0.001465